uOttawa

L'Université canadienne
Canada's university

FACULTÉ DES ÉTUDES SUPÉRIEURES ET POSTOCTORALES

uOttawa

L'Université canadienne
Canada's university

FACULTY OF GRADUATE AND POSDOCTORAL STUDIES

Corrie John Bayley daCosta
AUTEUR DE LA THÈSE / AUTHOR OF THESIS

Ph.D. (Biochemistry)
GRADE / DEGREE

Department of Biochemistry, Microbiology and Immunology
FACULTÉ, ÉCOLE, DÉPARTEMENT / FACULTY, SCHOOL, DEPARTMENT

A Structural Role for Lipids in Coupling Ligand Binding to Channel Gating in a Neurotransmitter Receptor

TITRE DE LA THÈSE / TITLE OF THESIS

John Baenziger
DIRECTEUR (DIRECTRICE) DE LA THÈSE / THESIS SUPERVISOR

CO-DIRECTEUR (CO-DIRECTRICE) DE LA THÈSE / THESIS CO-SUPERVISOR

EXAMINATEURS (EXAMINATRICES) DE LA THÈSE / THESIS EXAMINERS

Natalie Goto

Martin Young

Reinhart Reithmeier

Dan Sparks

Gary W. Slater
Le Doyen de la Faculté des études supérieures et postdoctorales / Dean of the Faculty of Graduate and Postdoctoral Studies

A STRUCTURAL ROLE FOR LIPIDS IN COUPLING LIGAND BINDING TO CHANNEL GATING IN A NEUROTRANSMITTER RECEPTOR

Corrie J.B. daCosta

Thesis submitted to the Department of Biochemistry, Microbiology and Immunology in partial fulfillment of the requirements for the degree of Doctor of Philosophy

University of Ottawa
Ottawa, Ontario, Canada
September, 2006

Your file Votre référence
ISBN: 978-0-494-25864-4
Our file Notre référence
ISBN: 978-0-494-25864-4

To my mother, Jacqueline daCosta. Together we have climbed many mountains...

...Check this one off the list!

Abstract

A simple structure-based mechanism explaining how membrane lipid composition influences the ability of the nicotinic acetylcholine receptor (nAChR) to convert agonist binding into opening of its transmembrane ion channel is proposed. This mechanism is based both on a recent atomic model of the nAChR, as well as extensive characterization of affinity purified nAChRs reconstituted into a number of different model membranes. Biophysical characterization of the nAChR upon reconstitution into membranes of defined lipid composition identifies the receptor's specific lipid requirements, and highlights the structural consequences of its reconstitution into membranes lacking these essential lipids. Infrared measurements show that while membrane lipid composition has no effect on nAChR secondary structure, it influences the ability of the nAChR to undergo agonist induced conformational change. In the absence of specific lipids the nAChR appears locked in a non-conducting conformation in which the binding of agonist fails to trigger a response. Hydrogen-deuterium exchange studies show that these non-functional nAChRs also exhibit increased $^{1}H/^{2}H$ exchange kinetics, while thermal denaturation data shows that they display reduced thermal stability. Interpreted in light of the new nAChR atomic model (PDB ID: 2BG9), these data provide insight into the lipid-dependent structural rearrangements resulting in an uncoupling of the nAChR's ligand binding and channel gating functions.

Acknowledgements

Of course this work could not have been done without the support of many family, friends and colleagues. These people deserve more than the mere "thank you" that they receive here.

- First and foremost I'd like to thank my supervisor Dr. John Baenziger. There are so many things the experience in your lab has given me. The most important of which is the confidence to make my own way in the research world. Your unwavering support, leadership and accessibility (even when at home or the cottage!) has been an important reason for my success. Thanks for everything ("thanks" seems so inadequate). Don't worry... Even when I'm gone I'm sure I'll be calling you every time I get exciting new results.
- To past and present members of my thesis advisory committee (Dr. Carol Huber, Dr. Steven Evans, Dr. Svetlana Borisova, Dr. Natalie Goto and Dr. Mary-Alice Hefford) thank you for your insightful suggestions and comments throughout our many meetings.
- Thanks to the many past and present labmates who have contributed to my experience as part of the Baenziger clan (alphabetically): Mary-Lou Barone, Johnny Bonacci, Casey Carswell, Emilie Chartrand, Jeremy Cheeseman, Veronica Dickson, Daniel Gagné, Mike Goodreid, Danny Hill, Dave Houtman, Yi Huo, Anna Jaszinska, Daniel Kaiser, Prateek Khatri, Roxanne Landry, Nadine Lavinge, Marlene McKay, Sarah Medaglia, Ming Na, Dr. Andrei Ogrel, Marc Rigden, Blair Ritchie, Dr. Steven Ryan, Wajid Sayed, Isabelle Sirois, Michel Sturgeon, Ali Syed, Bridget Thompson, Ngoc Vuong, Ian Wagg and Shuzi Wang.
- Thanks to Dr. Mezl for always reminding me that in order to get a PhD you actually need to write a thesis!
- To Carol Ann (especially you!), Nicole, Lucie, Mireille, Tina, Joanne, and Julie. Thanks for all the help over the years. I would've been lost without you all.
- Thanks to André Bergeron, for always "McGyver-ing" a solution to my many technical problems.

- To Phuc Hoa, Sonia, Lisa, Sheila, Mahmoud, Neil, Nicole, Naveed and all the others who made life as student so enjoyable, I appreciate it.
- Special thanks to Melissa for listening to me moan and grown about how hard it is to write a thesis. Especially considering that yours has been looming large! I know I couldn't have made it through this without our weekly movie hiatuses, or our Tuesday night dinners at your Grandma's.
- Last and certainly not least, thanks to my family. Especially my mother and father... I couldn't have done this without you constantly building me up to feel smarter than actually I am!

My time as a graduate student has also been financially supported through a number of generous scholarships, from several sources. These sources include:

- The Canadian Institutes of Health Research (CIHR).
- The National Science and Engineering Research Council of Canada (NSERC).
- The Government of Ontario (Ontario Graduate Scholoarship, OGS).
- The University of Ottawa for a Strategic Areas of Development award (SAD award), as well as numerous Excellence and Admission Scholarships.
- The Department of Biochemistry, Microbiology and Immunology at the University of Ottawa.

Preface

This thesis is presented as a collection of three manuscripts. The data presented has been published as described below:

Chapter 2

Corrie J.B. daCosta, Andrei A. Ogrel, Elizabeth A. McCardy, Michael P. Blanton and John E. Baenziger. (2002) Lipid-protein interactions at the nicotinic acetylcholine receptor: a functional coupling between nicotinic receptors and phosphatidic acid containing lipid bilayers. *J. Biol. Chem.* **277**, 201-208.

Chapter 3

Corrie J.B. daCosta, Ian D. Wagg, Marlene E. McKay, and John E. Baenziger. (2004) Phosphatidic acid and phosphatidylserine have distinct structural and functional interactions with the nicotinic acetylcholine receptor. *J. Biol. Chem.* **279**, 14967-14974.

Chapter 4

Corrie J.B. daCosta, Daniel E. E. Kaiser, and John E. Baenziger. (2005) Role of glycosylation and membrane environment in nicotinic acetylcholine receptor stability. *Biophys J.* **88(3)**, 1755-1764.

Table of Contents

List of Figures

General Introduction

Chapter 1 - Introduction

Chapter 2 - Phosphatidic Acid/nAChR Interactions

Chapter 3 - Phosphatidylserine/nAChR Interactions

Chapter 4 - Deglycosylation vs. Membrane Environment

Chapter 5 - General Discussion and Conclusions

Appendix

List of Tables

Chapter 1 - Introduction

Chapter 2 - Phosphatidic Acid/nAChR Interactions

Chapter 3 - Phosphatidylserine/nAChR Interactions

List of Abbreviations

α-btx	α-Bungarotoxin
Å	Angstrom
A_{280}	Absorbance at 280nm
ACh	Acetylcholine
AChBP	Acetylcholine binding protein
ATR	Attenuated total reflectance
Ca^{2+}	Calcium ion
Carb	Carbamylcholine
Card	Cardiolipin
Chol	Cholesterol
Cl^-	Cloride ion
C=O	Carbonyl group
COO^-	Carboxyl group
Cryo-EM	Cryo-electron microscopy
D	Desensitized state of the nAChR
DB	Dialysis Buffer
Decylmaltoside	n-Decyl-*β*-D-maltopyranoside
DOPA	Dioleoyl phosphatidic acid
DOPC	Dioleoyl phosphatidylcholine
EC_{50}	Concentration at which ligand is 50% of maximal efficacy
EDTA	Ethylenediaminetetraacetic acid
Endo F1	Endo-β-N-acetylglucosaminidase F1
EPC	Egg phosphatidylcholine
ER	Endoplasmic reticulum
FTIR	Fourier transform infrared
^1H	Hydrogen
^2H	Deuterium
^2H_2O	Deuterium oxide
hrs	Hours
[^{125}I]TID	3-trifluoromethyl-3-(*m*-[^{125}I]iodophenyl)diazirine
IRE	Internal reflection element
K^+	Potassium ion

K_D	Dissociation constant
kDa	KiloDalton
λ	Wavelength
LysoPC	Lysophosphatidylcholine
M	Molarity
M1	1st transmembrane spanning segment of the nAChR
M2	2nd transmembrane spanning segment of the nAChR
M2-M3L	M2-M3 linker
M3	3rd transmembrane spanning segment of the nAChR
M4	4th transmembrane spanning segment of the nAChR
MWCO	Molecular weight cut-off
Na^+	Sodium ion
nAChR	Nicotinic acetylcholine receptor
$N\text{-}^1H$	Peptide hydrogen
$N\text{-}^2H$	Peptide deuterium
NMR	Nuclear magnetic resonance
O	Open/activated state of the nAChR
PA	1,2-Diacyl-*sn*-glycero-3-phosphate
PC	1,2-Diacyl-*sn*-glycero-3-phosphocholine
PE	1,2-Diacyl-*sn*-glycero-3-phosphatidylethanolamine
PI	1,2-Diacyl-*sn*-glycero-3-phosphoinositiDe
PNGase F	Peptide-N^4-(acetyl-β-glucosaminyl)-asparagine amidase
POPA	1-Palmitoyl-2-oleoyl-*sn*-glycero-3-phosphate
POPC	1-PAlmitoyl-2-oleoyl-*sn*-glycero-3-phosphocholine
POPS	1-Palmitoyl-2-oleoyl-*sn*-glycero-3-[phospho-L-serine]
PS	1,2-Diacyl-*sn*-glycero-3-[phospho-L-serine]
P_X/P_{Na}	Permeability of ion "X" relative to the permeability of sodium
R	Resting state of the nAChR
SCAM	Substituted-cysteine-accessibility method
SM	Sphingomyelin
TRB	*Torpedo* ringer buffer
Tris	Tris (hydroxylmethyl)aminomethane
U	Membrane-uncoupled state of the nAChR

GENERAL INTRODUCTION

From Consciousness to Ion Channels

Our ability to perceive, integrate and respond to stimulatory signals in our surrounding environment forms the basis of our consciousness. Ultimately, this consciousness is a result of the complexity of our nervous system. Our ability to see, hear, smell, taste and touch all rely on elements of this nervous system. So does our capacity to move by controlling how and when our muscles contract. Beyond these *simple* perception and locomotion functions, higher brain functions such as thought, memory, and even emotion, are also a product of our nervous system. Understanding how our nervous system works is therefore fundamental for a comprehensive understanding of ourselves.

At its most basic level, our nervous system is a complex circuit of specialized cells called neurons (1). Its capacity to perform such complex functions results from both the functional, structural and organizational diversity of these neurons, as well as the myriad of connections between them. Neurons communicate with one another using electrical signals called action potentials. Action potentials are waves of depolarization that can move along neurons. They are generated and propagated by the controlled diffusion of charged ions, such as sodium and potassium, across the neuronal membrane. Because the neuronal membrane is relatively impermeable to ions, this process relies on a class of specialized proteins called ion channels (1, 2).

Ion channels are integral membrane proteins, which form pores in the neuronal plasma membrane. They permit the passive flow of ions across the membrane, down their electrochemical gradients. There are several classes of ion channels, with many different functions (2). Some are highly specific and only allow the passage of certain ions, while others are less discriminating. Most ion channels are also gated, meaning that they open and

close in response to specific stimuli. Some open in response to the binding of a particular ligand, while others open in response to changes in temperature or pressure. Some ion channels even gate in response to differences in the voltage across their surrounding membrane. As they are the molecules which ultimately generate and perpetuate electrical signals within neurons, ion channels are essential components of our nervous system (1).

The Chemical Synapse and Neurotransmission

The interfacial region connecting two neurons is called a synapse (Figure 0.1). The intervening space between neurons at a synapse presents a physical barrier to the propagation of an action potential. For the action potential to spread from one neuron to the other it must somehow overcome this barrier. In most cases this is accomplished via a chemical intermediate called a neurotransmitter. When an action potential reaches the end of the pre-synaptic neuron, the resulting depolarization causes neurotransmitter filled vesicles to fuse with the plasma membrane. Vesicle fusion releases the neurotransmitter into the synaptic space where it binds to neurotransmitter receptors on the surface of the post-synaptic cell. These neurotransmitter receptors are ligand-gated ion channels that gate open in response to neurotransmitter binding. Ion channel opening generates a new action potential in the post-synaptic neuron. This process of inter-neuronal communication, mediated by a chemical messenger, is called neurotransmission. It is highly analogous to the mechanism by which neurons stimulate muscle cells (1).

Of course this portrayal of neurotransmission is highly simplified. Depending on the neurotransmitter released, post-synaptic effects can be either excitatory or inhibitory. Furthermore, the depolarization resulting from neurotransmission is not always enough to

Figure 0.1

A simplified view of neurotransmission. The steps involved in communicating an action potential from one neuron to another (or to a muscle cell) via a chemical intermediate are labelled and outlined in the figure and text. Note: this figure and all other schematic figures were made with Adobe® Illustrator® CS2.

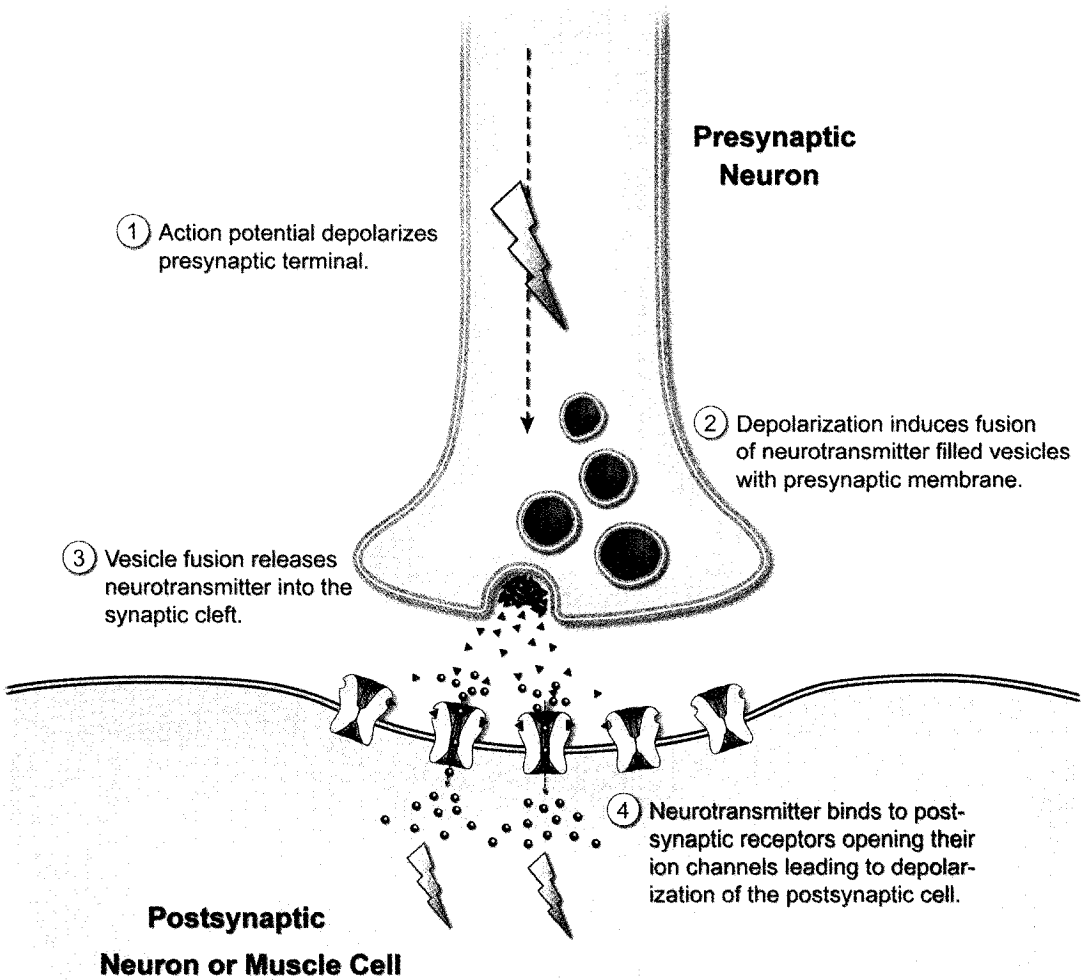
Presynaptic
Neuron
1 Action potential depolarizes presynaptic terminal.
2 Depolarization induces fusion of neurotransmitter filled vesicles with presynaptic membrane.
3 Vesicle fusion releases neurotransmitter into the synaptic cleft.
4 Neurotransmitter binds to post-synaptic receptors opening their ion channels leading to depolar-ization of the postsynaptic cell.
Postsynaptic
Neuron or Muscle Cell

generate a new action potential. Both the density and number of neurotransmitter receptors clustered at the synapse, as well as various factors which influence the ability of the receptor to open in response to neurotransmitter binding can affect the strength of the post-synaptic response. There are also many more proteins involved in the process, including those that are important for vesicle fusion and trafficking. Several other ion channels are also implicated. For example, neurotransmitter receptors are not only found on the post-synaptic membrane, but also on the pre-synaptic membrane. This high level of complexity provides innumerable ways in which neurotransmission can be modulated. Since synaptic plasticity, or changes in the strength of neuronal connections, is thought to underlie fundamental processes such as memory and learning, a molecular interpretation of neurotransmission should help in unraveling higher brain functions.

The work presented in this thesis is based solely on one neurotransmitter receptor isolated from the electric fish *Torpedo californica*. This ligand-gated ion channel is opened by the binding of the endogenous neurotransmitter acetylcholine (ACh) as well as exogenous substances, such as nicotine. Because nicotine was identified as an agonist for this channel before acetylcholine, and because G-protein coupled acetylcholine receptors have also been found within the mammalian nervous system (muscarinic acetylcholine receptors), this neurotransmitter receptor/ion channel is designated the nicotinic acetylcholine receptor (or "nAChR"). The nAChR from *Torpedo* is homologous to both human muscle type and neuronal nAChRs. Due to its high homology with human nAChRs, as well as its natural abundance, the nAChR from *Torpedo* has been extensively studied and is widely regarded as a model for all neurotransmitter receptors (2, 3). It is the prototypical member of a superfamily of highly homologous neurotransmitter receptors found throughout the mammalian peripheral and central nervous systems. Studies involving *Torpedo* nAChRs

have shed light on the mechanism of neurotransmission within the human brain and at the neuromuscular junction.

The Thesis - Statement of Objectives

My research as a PhD student in the Baenziger lab has involved work on mainly two projects. The first project, initiated in September 2000, was to begin examining the physical properties of reconstituted nAChR membranes using infrared spectroscopy. The aim of this work was to look for correlations between the physical properties of reconstituted membranes and their ability to support a functional *Torpedo* nAChR. The ultimate goal of this project has been to shed light on **the mechanisms by which lipids modulate *Torpedo* nAChR structure and function**. Our ability to explain the nAChR's functional reliance on specific lipids has been largely hampered by the lack of a nAChR atomic model. With this in mind, my second project, and the main focus of my PhD research (roughly 60% of my time as a graduate student) has been **to crystallize the nAChR from *Torpedo* with the goal of solving its X-ray crystal structure**. Realizing that this is a very risky and difficult project, and because of its "all-or-none" nature, I have continued working on the nAChR-lipid interactions project. As is often the case in science, two seemingly unrelated phenomena are in fact inextricably linked. Because crystallization of a membrane protein generally requires removal of the protein from its surrounding membrane environment, our inability to crystallize the nAChR may be related to its structural reliance on specific lipids. Understanding how lipids modulate nAChR structure and function may therefore aid in the design of successful crystallization attempts.

In the spring of 2005, the nicotinic acetylcholine receptor field was catapulted into the atomic age by the publishing of a 4Å model of the nAChR from *Torpedo* (4). This model has reinvigorated the nAChR field and already led to a number of mechanistic insights into important aspects of nAChR function (5-12). The model was based on cryo-electron microscopy images of the nAChR in helical membrane tubes. While 4Å resolution data is generally not high enough to build an accurate atomic model, the more than 30 years of extensive biochemical and structural characterization of the nAChR has aided in its construction (3, 13). As a result, to have confidence in the recent atomic model it is necessary to have an intimate knowledge of the various studies that have contributed to it.

The following introduction section of this thesis examines in considerable detail a number of the influential and milestone studies that have contributed to our current understanding of both nAChR structure and function. This in-depth review was undertaken in order to give the reader (and the author!) an intimate understanding of nAChR structure and mechanism, as well as to inspire confidence in the recent atomic model. I have chosen to focus on the exciting biological aspects of my PhD work, rather than the practical and technical aspects. Most of the methodologies used here are either well established, or have been described in detail elsewhere (Note: for a comprehensive discussion of FTIR spectroscopy, and infrared difference spectroscopy, the reader is directed to the Ph.D thesis of Dr. Stephen E. Ryan (307)). The recent breakthrough with regards to receptor structure has allowed me to postulate a simple, structure based mechanism for the modulation of nAChR function by lipids. This novel mechanism is consistent both with the data presented in this thesis, as well as with over thirty years of data examining nAChR-lipid interactions.

CHAPTER 1

INTRODUCTION

1.1 - Nicotinic Acetylcholine Receptors... the beginning

The study of nicotinic acetylcholine receptors actually began in the 19th century when Claude Bernard began investigating the action of the Central American arrow poison, *curare* (14). *Curare* is a poisonous extract from tropical vines which blocks neurotransmission and respiratory muscle contraction (13), ultimately leading to asphyxiation (15). After Bernard's work it was widely held that *curare* acted primarily on motor nerve endings, but by the early 1900's John Newport Langley had proven him wrong and shown that *curare* in fact exerted its effects on the muscle cells themselves. Langley found that treating de-enervated chicken muscle cells with nicotine caused them to contract, and that this contraction could be prevented by prior treatment with Bernard's *curare* (16). Langley also noticed that the inhibited cells were still able to contract when stimulated electrically, suggesting that *curare* did not act directly on the contractile substance, but on some other accessory substance of the muscle. These simple yet elegant experiments led to his hypothesis that the muscle cells contained "a nicotinic receptive substance". Langley later broadened this hypothesis and proposed that bodily tissues bear receptors for drugs (17). At the time this proposal was received with much criticism as it was not in line with current models, however today this concept is widely accepted and is central to modern pharmacology (18).

Langley's experiments showing that a chemical substance was able to cause muscle contraction sparked a debate as to how nerves communicated with muscle cells. The prevailing view had been that neurons exerted their effects directly on muscle cells through some sort of electrical coupling, while an emerging view, more in line with Langley's findings, was that neuronal (or neuromuscular) communication was mediated by a chemical messenger. This chemical messenger could be released from the effector neuron and

received by the affected cell. This idea of transmitting neuronal signals via chemical intermediates was proven in the early 1920's by Sir Henry Hallet Dale and Otto Loewi, work for which they were awarded the 1936 Nobel Prize in Medicine. Many of Dale's experiments were performed on the same nicotinic muscular system that Langley used, but in Dale's case he used the chemical acetylcholine which he found elicited strong responses in many post synaptic cells. In fact, Dale was the first to isolate acetylcholine from mammalian tissue (19), and also showed that it was the most prevalent chemical transmitter in the peripheral nervous system.

In the 1930's there was little discussion as to how acetylcholine actually elicited its effects on post-synaptic cells. This was in large part due to the inability to isolate and study the acetylcholine "receptive substance". Moreover, it was hard to imagine how the binding of acetylcholine to the cell surface could cause intracellular changes. It was not until the 1950's, and the emergence of Hodgkin and Huxley's model explaining the ionic basis of nerve conduction, that the concept of an ion-channel emerged (20-23). At about the same time that Hodgkin and Huxley were being handed their Nobel Prize (1963), Jacques Monod, Francois Jacob, Jeffries Wyman and Jean-Pierre Changeux postulated that certain enzymes may be activated by allosteric or indirect means (24). More specifically, they postulated that the binding of a small molecule could cause a conformational change in a distant region of a protein. Changeux recognized that this model could explain how a chemical transmitter such as acetylcholine was able to alter cell permeability, and postulated that Langley's "nicotinic (or acetylcholine) receptive substance" was a protein in which the binding of acetylcholine is coupled to the opening or gating of an ion channel. To prove his assertion, Changeux needed to find such an ion-channel. The search for the nicotine/acetylcholine gated ion-channel began...

1.2 - Nicotinic Acetylcholine Receptors in Electric Fish

A major breakthrough in the characterization of nicotinic acetylcholine receptors (nAChRs) was their discovery in the electric ray *Torpedo* (*californica*, *marmorata*, and *nobiliana*) and the electric eel *Electrophorus* (25, 26). These fish have highly specialized electric organs called electroplaques which allow them to deliver high current shocks to their prey. The electroplaques are basically a biological "battery" composed of specialized cells called electrocytes (2). Electrocytes develop from muscle cells in embryonic fish (27), and their plasma membranes are modified neuromuscular endplates which contain an extremely high concentration of nicotinic receptors. Electrocytes generate coordinated pulses of current in response to cholinergic neurotransmission analogous to that seen at the mammalian neuromuscular junction. The sum of current generated by each electrocyte, and the organization of electrocytes within the electroplaque tissue, allow *Torpedo* to generate currents large enough to kill their prey (2).

1.3 - Nicotinic Acetylcholine Receptor: Purification and Sequencing

The relative abundance of nicotinic acetylcholine receptors in *Torpedo* has paved the way for their extensive biochemical characterization. By 1974 several groups had succeeded in affinity purifying nicotinic acetylcholine receptors from *Torpedo*, and had shown by SDS-PAGE that the *Torpedo* nAChR was composed of four non-identical polypeptides or subunits (Figure 1.1). The four subunits where named α, β, γ and δ, and have molecular weights of 39, 48, 58 and 64kDa, respectively (28). Early affinity labelling studies suggested that it was the α-subunit which was responsible for ligand binding (28).

Figure 1.1

SDS-PAGE of affinity purified nAChR from *Torpedo californica*. Each of the four nAChR subunits is labelled. Note that the α-subunit band is approximately twice as intense as the bands corresponding to each of the other subunits. This results from the 2:1:1:1 (α:β:γ:δ) stoichiometry of the subunits in the assembled nAChR pentamer. The molecular weights of the standards in the right lane are 116, 80, 51.8 and 34.7 kDa from top to bottom, respectively.

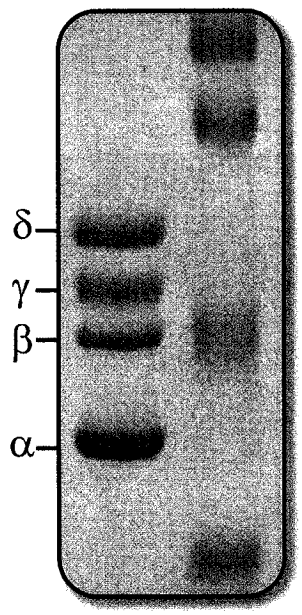
δ
γ
β
α

In 1980 the purification of *Torpedo* nAChR, along with the development of peptide sequencing techniques, allowed Raftery *et al.* to sequence the first fifty-four N-terminal amino acids of each of the four receptor subunits (29). These N-terminal sequences revealed that the four nAChR subunits had a distinct, yet homologous amino acid sequence. Each of the subunits had identical amino acids at a minimum of eleven of the fifty-four positions sequenced, and the overall identity in this region ranged from thirty-five to fifty percent, suggesting that the four subunits descended from a single ancestral gene. On the basis of their sequencing reactions, Raftery *et al.* also showed that the receptor subunits were present in a 2:1:1:1 (α:β:γ:δ) molar ratio, which suggested that the functional form of the receptor was a pentamer with two acetylcholine binding α-subunits.

While the N-terminal sequencing by Raftery *et al.* was informative in its own right, its main contribution was that it was a stepping stone towards the entire receptor sequence. Knowledge of these N-terminal peptide sequences made it possible to synthesize DNA probes which were then used to screen cDNA libraries for clones of each the receptor subunits. By 1983 the complete DNA sequences of all four nAChR subunit genes had been determined (30-33). These DNA sequences yielded predicted primary amino acid sequences which were 43-64% identical and roughly 80% homologous. The length of each subunit ranged from 437 (α) to 501 (δ) amino acids, giving the pentameric receptor complex a predicted (protein only) molecular weight of about 268kDa (32).

The validity of the cloned sequences was verified by heterologous expression of nAChR mRNAs in *Xenopus* oocytes (34). Messenger RNAs encoding each of the nAChR subunits were generated from cloned cDNAs, and co-injected into *Xenopus* oocytes. The expressed receptors were responsive to acetylcholine and inhibited by both *curare* and *α-bungaratoxin*. Omission of the β-, γ-, or δ-subunits resulted in a diminished response to

acetylcholine, while omission of the α-subunit mRNA resulted in a complete loss of acetylcholine sensitivity, further implicating a role for this subunit in agonist binding (34).

1.4 - Nicotinic Acetylcholine Receptor: Topology

Knowledge of nAChR primary sequence allowed for hydropathy plots, which predicted five hydrophobic segments for each of the nAChR subunits (Figure 1.2A)(35). These five hydrophobic segments were interpreted as transmembrane (TM) spanning regions of the protein. The first transmembrane segment corresponds to the signal peptide which is cleaved upon insertion of the polypeptide into the membrane (36). Thus the mature subunit contains only four putative TM segments (designated M1-M4). Given what was known about other membrane proteins at the time, and that each TM is roughly 20-25 amino acids long, it was reasonably assumed that each of the TM segments were transmembrane spanning α-helices (35, 37).

Hydropathy analysis also facilitated the modelling of nAChR subunit topology. During protein synthesis the N-terminal signal peptide guides the large N-terminal domain across the endoplasmic reticulum membrane, meaning that this domain will be on the extracellular side of the cell. Two hundred amino acids into the sequence, hydropathy analysis suggests the polypeptide chain crosses the ER membrane four more times, giving the topology shown in Figure 1.2B. M1-M3 are close in sequence therefore the extramembranous loops connecting them should be relatively small, while the roughly one hundred amino acids between M3-M4 means that this loop will constitute the majority of the receptor's cytoplasmic domain. Chemical labelling studies aimed at pinpointing the location of specific residues (38-43), and the identification of glycosylation sites (44-46) have

Figure 1.2

(A) Hydropathy plot of the nAChR γ-subunit from *Torpedo californica* (based upon the sequence and analysis in Claudio *et al.*)(30). Hydrophobic segments thought to represent transmembrane spanning regions of the nAChR are labelled M1-M4. **(B)** Topology of a single nAChR subunit as predicted by the hydropathy analysis in A). The N-terminal extracellular ligand binding domain (LBD), transmembrane domain (TM), and cytoplasmic domain (CYT) are all labelled. The transmembrane spanning segments are depicted as membrane spanning α-helices (M1-M4). The amphipathic cytoplasmic helix is also labelled (MA). E = extracellular side of the membrane, M = membrane and I = intracellular side of the membrane.

A

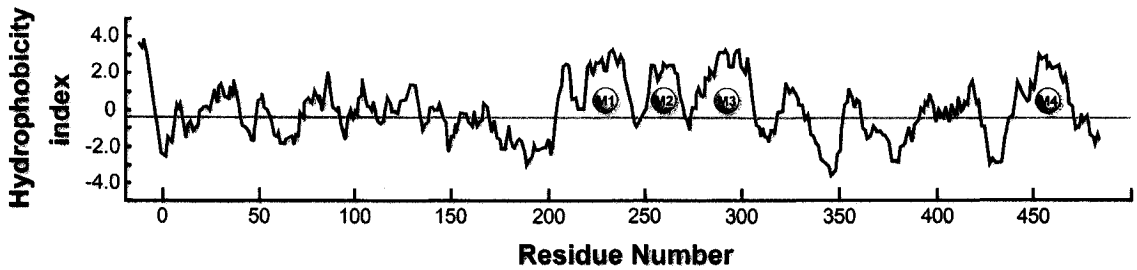
Hydrophobicity index
4.0
2.0
0
-2.0
-4.0
0
50
100
150
200
250
300
350
400
450
Residue Number

B

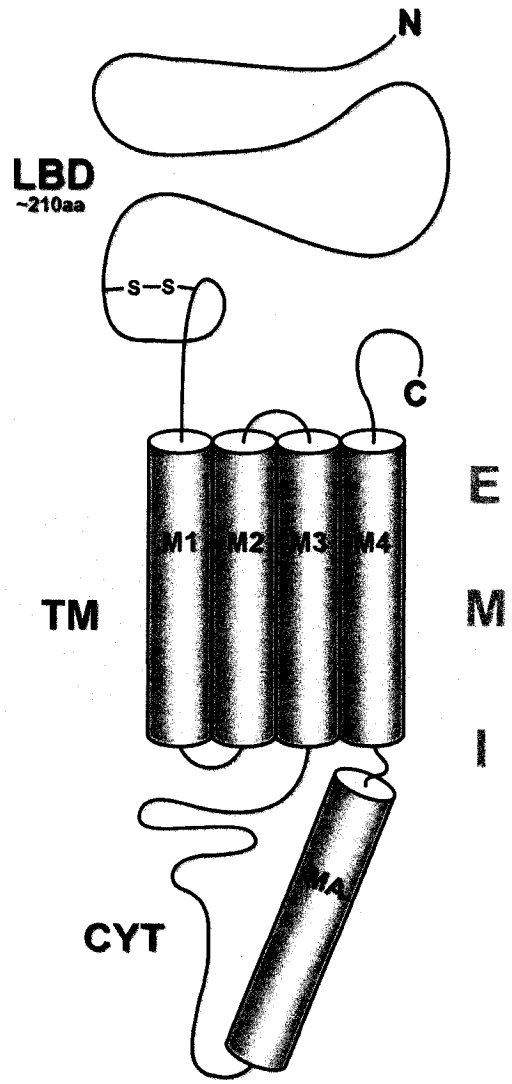
N
LBD
~210aa
S—S
C
E
M1
M2
M3
M4
TM
M
I
MA
CYT

confirmed this proposed topology. In addition, the molecular weights of the extracellular, transmembrane and cytoplasmic domains predicted by this topology were also consistent with early electron microscope images of purified receptors (47).

1.5 - Cys-Loop Receptor Superfamily

With the emergence of gene sequencing techniques in the 1980's, and the subsequent sequencing of several neurotransmitter receptor genes, it quickly became apparent that the nAChR was actually a member of a homologous superfamily of ligand-gated ion channels (35). This superfamily constitutes a major class of both excitatory and inhibitory ligand-gated ion channels found throughout the mammalian central and peripheral nervous systems (3). Sequence analysis revealed that all members of the superfamily contain a pair of cysteines separated by thirteen highly conserved amino acids (nAChR α_1Cys128 and α_1Cys142). Since all known members contain these disulfides, the superfamily has been coined the "Cys-loop" receptors (35).

Members of the Cys-loop receptor superfamily include the acetylcholine, glycine, γ-aminobutyric acid ($GABA_A$), and serotonin ($5\text{-}HT_3$) receptors. All share a common overall architecture, and assemble to form pentameric integral membrane protein complexes, with a central ion conducting pore. Some members, like the nicotinic acetylcholine and $5\text{-}HT_3$ receptors, are cation selective and thus excitatory, while others like the glycine and $GABA_A$ receptors are anion selective and thus inhibitory. Both excitatory and inhibitory Cys-loop receptors can assemble from five identical copies of the same subunit, but more often than not they assemble from several different types of subunit (3). Both the wide variety of

different subunits, as well as the ability to form hetero-pentamers provides a wealth of structural and functional diversity (3).

1.6 - Nicotinic Acetylcholine Receptor Structure

The nicotinic acetylcholine receptor from *Torpedo* contains within it all the parts necessary to translate the binding of acetylcholine into a change in membrane permeability (48). The receptor has both an acetylcholine binding domain, and an ion conducting pore. These two domains are tightly linked so that the binding of acetylcholine can be coupled to ion channel gating. For a detailed understanding of nAChR function and mechanism it is necessary to have an intimate knowledge of nAChR structure. Unfortunately, to date the nAChR has resisted three-dimensional crystallization. As a result there is no high resolution X-ray model of the nAChR. There is, however, thirty years worth of accumulated biochemical data (3, 13) which, in conjunction with homology modelling and moderate resolution (4.0Å) cryo-electron microscopy data, has led to a recent atomic scale model (4). While the limited resolution of this model means that it should be interpreted with caution, it does provide a framework for guiding future experiments and developing hypotheses related to nAChR function. The following is a review of selected biochemical and structural studies which highlight our growing understanding of nAChR structure and mechanism.

Overall nAChR Architecture. The *Torpedo* nAChR is a ~270kDa pentameric integral membrane protein complex, formed from four highly homologous subunits, present in a 2:1:1:1 molar ratio (α:β:γ:δ) (Figure 1.3)(15). Early electron microscopy studies have shown that the five receptor subunits are arranged pseudo-symmetrically around a central,

Figure 1.3

Quaternary organization and overall architecture of the nAChR from *Torpedo*. The five nAChR subunits associate pseudo-symmetrically around a central cation selective pore. The two acetylcholine (red spheres) binding sites are at the interface between the α- and γ/δ-subunits. The relative mass of the extracellular ligand binding, transmembrane and cytoplasmic domains is based upon early electron microscopy images. Reproduced with numerous modifications from Changeux, 1993 (15).

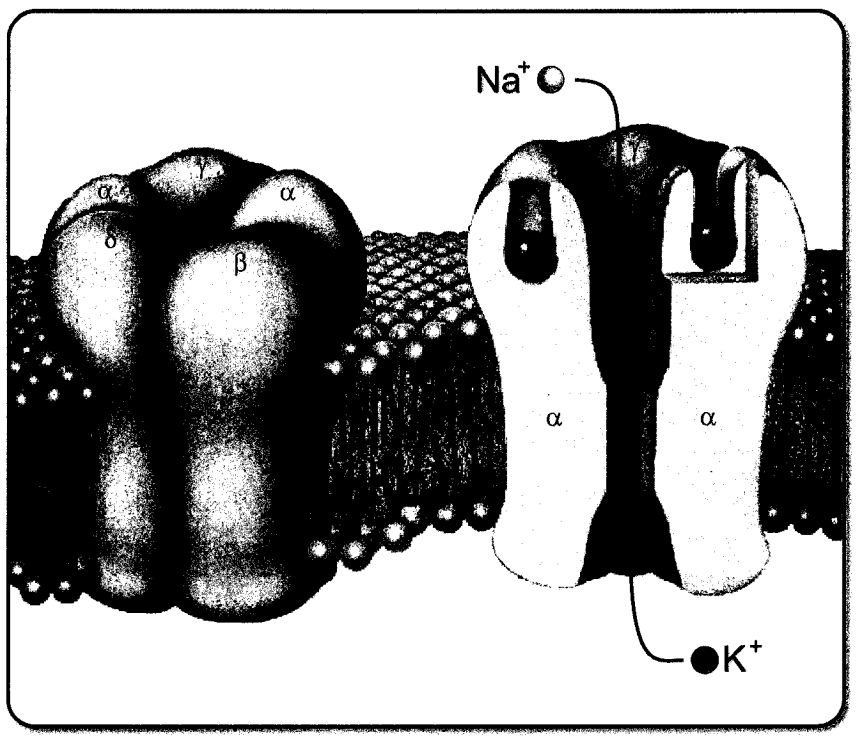
Na+
α
γ
α
δ
β
α
α
K+

cation selective pore. The pore protrudes beyond the membrane and into the synaptic space. The large protruding extracellular domains contain the two neurotransmitter binding sites, which are located at the interfaces between the α-γ and α-δ subunits. The two α-subunits contribute most of the residues involved in ligand binding.

1.6A - Nicotinic Acetylcholine Receptor Structure: Biochemical Studies

Ion Conduction Pathway. Hydropathy plots predicted that each of the receptor's subunits contained four transmembrane (M1-M4) spanning segments (35, 37). Since these four transmembrane segments are the only part of the protein which cross the hydrophobic bilayer, residues in these regions must contribute to the ion conduction pathway.

Identification of pore lining residues began in the mid 1980's with a collaboration between Shosaku Numa's group in Japan and Bert Sakmann in Germany. By combining cDNA expression of recombinant channels with single channel electrophysiological measurements Numa and Sakmann were able to pinpoint a transmembrane segment which affected channel conductance (49). These elegant experiments were made possible by the discovery that bovine nAChRs displayed markedly reduced single channel conductance relative to their *Torpedo* cousins. Single channel conductance measurements of *Torpedo* nAChRs substituted with bovine subunits implicated the bovine δ-subunit. By expressing *Torpedo* α-, β- and γ-subunits with chimaeric (mixed *Torpedo*/bovine) δ-subunits, Imoto *et al.* showed that it was the M2 segments of the bovine δ-subunit which was responsible for the reduced bovine current (49). *Torpedo* nAChRs with the bovine δM2 segment showed reduced single channel conductance, while recombinant *Torpedo* nAChRs, with the bovine δ-subunit in which the M2 region was from *Torpedo*, had conductances similar to that of

wild type *Torpedo* nAChR. While the differences in *Torpedo* and bovine nAChR conductance were ascribed to the δ-subunit, this did not mean that the other subunits did not also form part of the ion conduction pathway. It turns out that the *Torpedo* and bovine α-, β- and γ-subunits are relatively homologous in their M2 regions, so the difference in conductance between the two channels could not be from these subunits, and therefore had to be from the differences in their δM2s.

Given that the four *Torpedo* nAChR subunits are homologous, and that electron microscopy had shown that the nAChR subunits were arranged pseudosymetrically around a putative central ion channel (50), it seemed likely that homologous residues in each subunit would line the pore. This was proven in part by Leonard *et al.* who mutated residues in the M2 region of the α-, β- and δ-subunits, and found that these mutations all altered channel conductance (51). In addition, channel blockers which are thought to enter and block the open pore were found to label a number of subunits at homologous positions (52-54).

The identification of M2 as the ion channel pore was an important step in understanding nAChR function, however at the time it was known from electron microscopic studies (50), that the pore extended beyond the membrane and into both the extra- and intracellular spaces. This raised the possibility that residues outside of the membrane may be important for ion conduction. To test this possibility Numa and colleagues identified charged amino acids in the loops flanking M2 (M1-M2 and M2-M3 loops) which were conserved among subunits, and proposed that these residues formed three concentric rings of negative charge which contributed to ion conduction (55). The three rings were named the extracellular, intermediate and intracellular rings based on their putative positions in the channel as predicted by topology maps. Consistent with a role in ion conduction, mutation of any of the residues within these three rings caused a decrease in single channel

conductance. In addition, the changes observed in rectification upon mutation were consistent with the predicted locations of the rings (55), further supporting the proposed transmembrane topology.

Between 1992 and 2001 Arthur Karlin and coworkers used the substituted-cysteine-accessibility method (or SCAM) to systematically probe the water-accessible regions of the nAChR pore (38, 56-62). This technique involves mutating residues to cysteine and probing their accessibility to aqueous sulfhydryl reagents. Residues both in and around αM2 (αGlu241-αGlu262) and βM2 (βPro248-βAsp273) were mutated to cysteine and probed to see if they lined the ion channel pore (38, 57, 62). A number of residues in M2 were solvent accessible and readily reacted with sulfhydryl reagents, despite being in a predicted transmembrane segment. Furthermore, the observed labelling pattern was not consistent with the periodicity expected for an α-helix. Three consecutive residues in the centre of the αM2 segment: αSer252, αLeu251 and αLeu250 were labelled. If M2 was indeed α-helical, one would expect a single face of the helix to be in contact with solvent, while the opposite face should be buried against the rest of the transmembrane domain (M1-M3). If this were the case, and αM2 was indeed α-helical, then at least one of Ser252, Leu251 and Leu250 should be on the buried face, and not accessible to solvent. To account for this discrepancy, Karlin proposed that the structure of the local region around αSer252, αLeu251 and αLeu250 was not helical, but was instead a loop.

Zhang and Karlin also used SCAM to determine the solvent accessibility of residues in the αM1 (αPro211-αPhe225) and βM1 (βArg219-βPro247) transmembrane segments (60). This work was motivated in part by Karlin's prior finding that the noncompetitive blocker quinacrine azide labelled the αM1 segment, suggesting that M1 could contribute to the ion conduction pore (63). Several residues in the N-terminal third of both αM1 and βM1 reacted

with sulfhydryl reagent and were thus accessible to solvent. Based on these findings Zhang and Karlin suggested that the N-terminal (or extracellular) third of M1 lines the ion channel pore. Again, as in their finding with M2, the labelling pattern of M1 was inconsistent with an α-helical arrangement. Zhang and Karlin did however raise the possibility that the M1 N-terminal region could penetrate beyond the membrane and into solvent. If this were the case, the tip of M1 could be accessible to solvent from both the channel lumen and the protein's exterior surface.

Ion Channel Gate. An essential feature of the receptor is that ligand binding is coupled to the opening of a transmembrane ion channel. The fact that the channel "opens" implies that the channel has both open and closed states, and therefore acts as if it has an acetylcholine controlled gate. Identifying the location of this gate is of elementary importance for a mechanistic description of nAChR function.

The lack of clearly defined density occluding the ion channel pore in cryo-electron microscopy images led to the hypothesis that the channel gate is an energetic barrier to ion flow, instead of a physical one (64). Rather than physically plugging the ion conduction pathway, the gate is a constriction too narrow to allow the passage of a hydrated ion. For ions to pass through this constriction they must shed their hydration shell; a process which is energetically unfavourable if there are no compensatory interactions with the channel wall. Therefore in the gate region one would expect the surrounding channel walls to be relatively inert, and unable to interact with a charged species. A hydrophobic surface would be perfectly suited for this purpose as it would not be able to compensate for the loss of a hydration shell. Using the substituted cysteine accessibility method, Karlin and coworkers found that indeed several hydrophobic residues lined the lumen of the pore (38).

The precise location of the channel gate has been, and to some degree still is, an issue of contention. The reason for this debate is likely related to the nature of the gate. As mentioned above, the gate is not a physical occlusion therefore its location is not obvious. Based on 9Å cryo-EM data, Unwin suggested that the gate was located within M2, towards the centre of the membrane (64). This proposal was based on two observations: a) electron microscopy images suggested that this region was the narrowest part of the pore, and b) this position within M2 was also thought to be the location of a ring of highly conserved leucine residues (αLeu251). Unwin proposed that these leucine residues associated with one another to form a central constriction too narrow to permit the passage of a hydrated ion (Figure 1.4). Through symmetric side to side interactions between their side chains, the leucines stabilized the closed conformation of the pore. Electrophysiology experiments by Labarca *et al.*, and Filatov & White confirmed that these leucine residues were indeed involved in gating (65, 66). Substitution of any of the five leucine residues with either serine or threonine increased mean channel open time in a symmetric fashion. Furthermore, the effects of replacing multiple leucines were additive. These results suggested that symmetric interactions between these conserved leucines contributed to the relative stability of the open and closed states. While these studies did not unequivocally identify this region of the pore as the ion channel gate, they clearly demonstrated the importance of these leucines in channel gating.

One of the advantages of SCAM is that it can be done in the absence or presence of ligand, and can therefore give indications of the relative accessibility of side chains in both the open and closed states. Furthermore, Wilson and Karlin developed methods for introducing sulfhydryl reagents extracellularly, as well as intracellularly (56, 58). This allowed them to probe the accessibility of substituted cysteines from either side of the membrane. Presumably access to particular residues depends upon which side of the gate

Figure 1.4

Two different postulated locations of the nAChR ion-channel gate. Yellow spheres show the location of a highly conserved ring of leucines (αL251) thought to contribute to the narrowest region of the pore, while magenta spheres depict the intracellular location of αG240. 9.0Å Cryo-electron microscopy images (114) and electrophysiological experiments (65, 66) suggested that residues aligning with αL251 constituted the ion channel gate, while data from the substituted cysteine accessibility method (SCAM) suggested that the gate was near αG240 (58). **(A)** Helical representation of αM2 showing the relative position of the residues believed to form the channel gate. Yellow sphere shows the equatorial location of αLeu251 towards the centre of M2, and thus near the middle of the membrane. The magenta sphere shows the position of αG240 in the M1-M2 linker. **(B)** Schematic model of the nAChR pore based upon 9.0Å resolution cryo-electron microscopy images of the nAChR. The model places the ring of conserved leucines in the narrowest region of the pore near the centre of the membrane, and at a kink in the M2 helices. Note that in (B) βM2 and δM2 have been removed for clarity. Concept of figure based upon Unwin, 1995 (114).

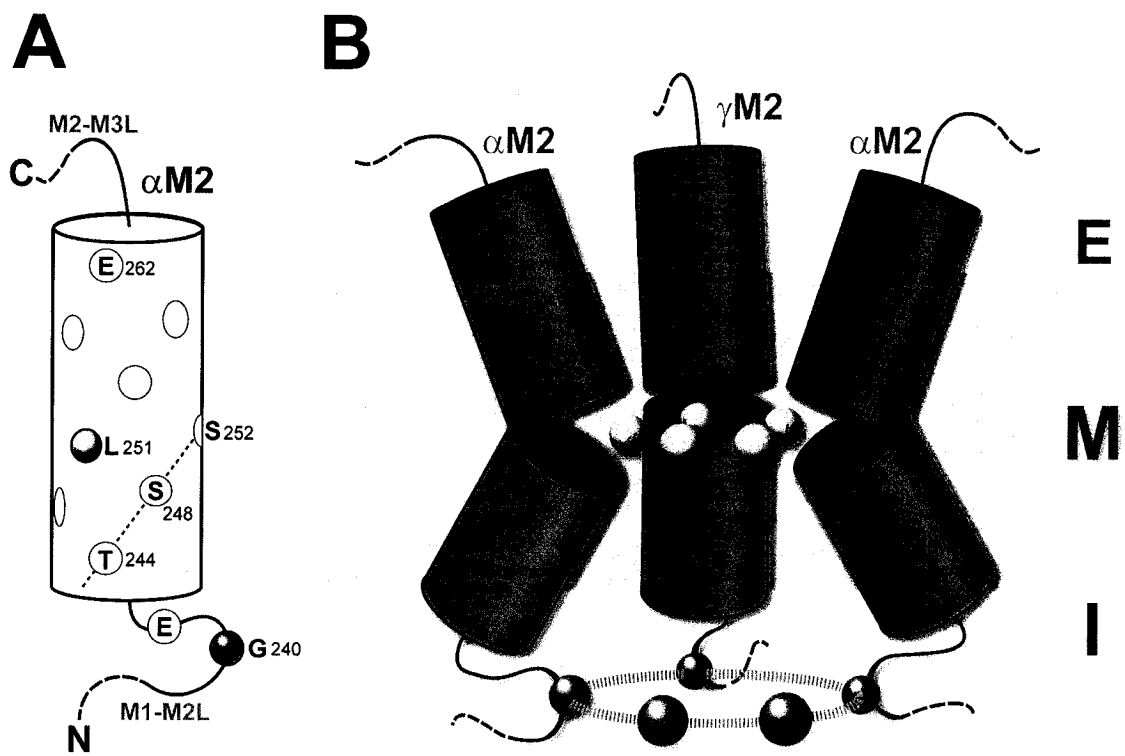
A
M2-M3L
C
αM2
E 262
L 251
S 252
S 248
T 244
E
G 240
M1-M2L
N
B
αM2
γM2
αM2
E
M
I

they are on. When added extracellularly to resting state nAChRs (i.e. channel closed), Wilson & Karlin found that sulfhydryl reagents reacted with residues as far down the pore lumen as αGlu241, well beyond αLeu251. This suggested that the gate was in the vicinity of αGly240 and αThr244 (58). These residues are at the N-terminal end of M2, and form part of the M1-M2 loop, suggesting that the channel gate is on the intracellular side of the membrane (Figure 1.4). This proposed intracellular location of the gate conflicts strongly with Unwin's original proposal based on 9Å electron microscopy data (64). Ultimately a higher resolution structure was needed to settle this debate (67).

nAChR Ion Selectivity. With respect to ion selectivity, the Cys-loop receptors are relatively non-selective in comparison to the highly selective Na^+ and K^+ channels. While the nAChR from *Torpedo* does exclude anions, it does not discriminate well between cations. In fact, the nAChR can conduct all the alkali (Li^+, Na^+, K^+, Rb^+, Cs^+, and Fr^+) and alkaline earth metals (Be^{2+}, Mg^{2+}, Ca^{2+}, Sr^{2+}, Ba^{2+}, Ra^{2+}) (2, 68), as well as numerous organic molecules (Tris, urea, guanidinium, etc) (69). The relative permeability ratios (P_X/P_{Na}) for the more biologically relevant K^+ and Ca^{2+} ions are 1.11 and 0.2, respectively (2).

The relative inability to discriminate between ions is related to the receptor's function. While Na^+ and K^+ channels must be highly selective in order to produce the coordinated changes in membrane permeability necessary for the propagation of an action potential, the primary goal of nicotinic receptors is to bring the post-synaptic cell closer to threshold through depolarization. Ultimately membrane potential is governed primarily by the membrane's relative permeability to both Na^+ and K^+. Under normal steady state conditions, the resting membrane potential is close to the K^+ equilibrium potential ($K_{eq}\cong$-

98mV (2)) since the resting membrane is much more permeable to K^+ than to Na^+. Opening nAChR channels, which are almost as permeable to Na^+ as they are to K^+, increases the membrane's relative Na^+ permeability. This increase in the relative Na^+ permeability drives the membrane potential towards the Na^+ equilibrium potential ($Na_{eq} \cong +67mV$ (2)), depolarizing the cell.

The receptor's low ion selectivity is ultimately a result of its structure. Unlike the high fidelity Na^+ and K^+ channels which have narrow selectivity filters (70-72), the nAChR pore is relatively wide (67). For conduction through K^+ channels, K^+ ions must be dehydrated (70), while the much wider nAChR channel accommodates ions surrounded by their first hydration shell. By allowing ions to remain hydrated, the nAChR is able minimize its physical interactions with conducting ions. Minimizing interactions between the channel and diffusing ions facilitates rapid conduction. Rather than being sorted through physical interactions with the channel, ions and their associated water molecules simply diffuse down their electrochemical gradients.

While the nAChR is selective for cations, the Cys-loop receptor superfamily consists of both cation selective (nAChR and 5-HT_3R) and anion selective (GlyR and $GABA_A$R) channels. In general, the Cys-loop receptor superfamily exhibits poor ion selectivity but good charge selectivity. The structural basis for this charge selectivity remains somewhat unclear. Both cationic and anionic receptors have conserved motifs in their pore lining domains including: a conserved cytoplasmic ring of negatively charged amino acids (55); two polar rings of threonine and/or serines (73); and a hydrophobic ring of leucines (65, 66). Despite these similarities, there is also one very important and conserved difference between cationic and anionic Cys-loop receptors. The M1-M2 linker near the N-terminal,

intracellular side of M2 contains a proline insertion in all anionic channels (2).

Galzi *et al.* determined the minimum set of mutations required to convert the selectivity of neuronal $(\alpha 7)_5$ nAChRs from cationic to anionic (74). Since α7's form homopentamers, single mutations are present in all five channel subunits. To make α7's selective for anions, a minimum of three mutations had to be made. Surprisingly, none of these mutations involved amino acids in the receptors outer, intermediate and inner rings of charge, consistent with other findings (62). Instead the most important mutation was the insertion of a proline between Gly236 and Glu237 (74). This position (designated Pro236') is homologous to the location of the conserved proline in both the GlyR and $GABA_AR$. Corringer *et al.* later found that both the identity and precise position of this insertion was not important (75). The important factor was that the M1-M2 loop had to be lengthened by a single amino acid. Galzi *et al.* also found that it was necessary to mutate Glu237 to alanine and Val251 to threonine. Either of these two latter mutations led to non-functional channels, in which function could only be restored by increasing the length of the M1-M2 linker, or by mutating both Glu237 and Val251. To make the channel anion selective however it was absolutely necessary to lengthen the M1-M2 loop. Since the amino acid insertion in the M1-M2 loop is necessary, it appears that the precise structural arrangement of this region governs charge selectivity.

The ability to convert cation selective channels into anion selective channels reflects the overall similarity in structure of the Cys-loop receptor superfamily (2). It should be mentioned that while it is possible to alter charge selectivity, the resulting channels usually display greatly reduced conductance. In addition, some mutant channels have been shown to retain residual permeability to their original ions (76). So while only a few mutations are required to convert Cys-loop receptor charge selectivity, often these mutant channels do not

display the same highly tuned conductance properties of their wild-types. Clearly charge selectivity is governed by more than a few amino acids, and is most likely a result of the overall structure of the pore.

Ligand Binding Domain. Early affinity labelling experiments suggested that the two nAChR α-subunits were responsible for acetylcholine binding (28). Since the two α-subunits are chemically identical, subsequent studies which showed that the two binding sites exhibited different affinities were somewhat surprising (77-79). To account for this discrepancy, it was suggested that the binding sites were at the interfaces between two subunits. The α-subunit would contribute one side of the interface while either the β-, γ- or δ-subunit would contribute the other. Several other lines of evidence were consistent with this hypothesis. Expression of nAChR α-subunits in oocytes required co-expression with the γ- and δ-subunits in order to recover ACh binding function (80). In addition, further affinity labelling studies using several different competitive antagonists and agonists showed that the α-subunit was not the only subunit labelled (78, 81-84). Both the γ- and δ-subunits were also labelled, suggesting that they were close to, or formed part of the binding site. Because the α-subunit was more strongly labelled than the γ- and δ-subunits, it was called the principle (+) binding subunit and the γ- and δ-subunits were called the complementary (-) binding subunits (85).

To identify the residues important for ligand binding, affinity labelling experiments were followed by proteolysis and Edman degradation. Several residues were identified on both the principle (+, α), and complementary (-, γ/δ) subunits. Some residues were labelled by numerous probes, with different chemical structures suggesting their importance in binding chemically diverse ligands (78, 82, 86-88). On the α-subunit several tyrosines (Y93,

Y190 and Y151, Y198) and two tryptophans (149 and 86) were labelled. In addition to these aromatic residues, numerous acidic residues in and around the binding site have also been identified as important for ligand binding (δD165, δD180 and δE183) (89). The α-subunits also contain a highly conserved cysteine doublet (Cys192/193) which is strongly labelled (13). This unusual cysteine doublet is a defining feature of all α-subunits, but is not conserved in any non-α subunits (85). On the complementary (γ- and δ-) subunits, the agonist nicotine and the antagonist d-tubocurarine both label γTrp55 and δTrp57. Curare also weakly labels γTyr111 and δArg113. Almost all of the residues labelled in both the principle and complementary subunits are in predicted loop structures (85). The sequences of which are relatively conserved, providing further evidence of their functional importance. Because they are highly conserved, and due to their putative role in ligand binding, the loops have all been named (Figure 1.5 – principle subunit loops A, B and C – complementary subunit loops D, E and F).

In general, the acetylcholine binding site is formed by numerous aromatic residues. Their relative abundance suggests that positively charged ligands are stabilized through cation-π interactions, analogous to those seen in the binding site of the soluble enzyme acetylcholine esterase (90). While these two proteins are not homologous, and have very different binding sites, apparently they both take advantage of electron rich aromatic side chains in order to stabilize positively charged ligands. Consistent with this hypothesis is the observation that in the nAChR, mutations of αY93, αY190 and αY198 all affect the apparent affinities of ACh and tetramethylammonium (TMA) in the same way, suggesting that they stabilize the quaternary ammonium portion of ACh (91). Mutating these tyrosines to phenylalanine dramatically lowers the receptor's affinity for agonist, suggesting that the

Figure 1.5

Schematic diagram showing the interfacial location of the acetylcholine (ACh) binding sites within the nAChR. The two ACh binding sites are at the interface between the α/γ and α/δ-subunits. The α subunits provide most of the residues involved in binding and are thus designated the principle (+) binding subunits, while the γ- and δ-subunits are designated the complementary (-) binding subunits. Each subunit provides residues from three conserved loops. The loops from the principle (α-subunits = A, B and C) as well as the loops from the complementary (γ- and δ-subunits = D, E and F) are labelled. Figure concept from Corringer *et al.* (85).

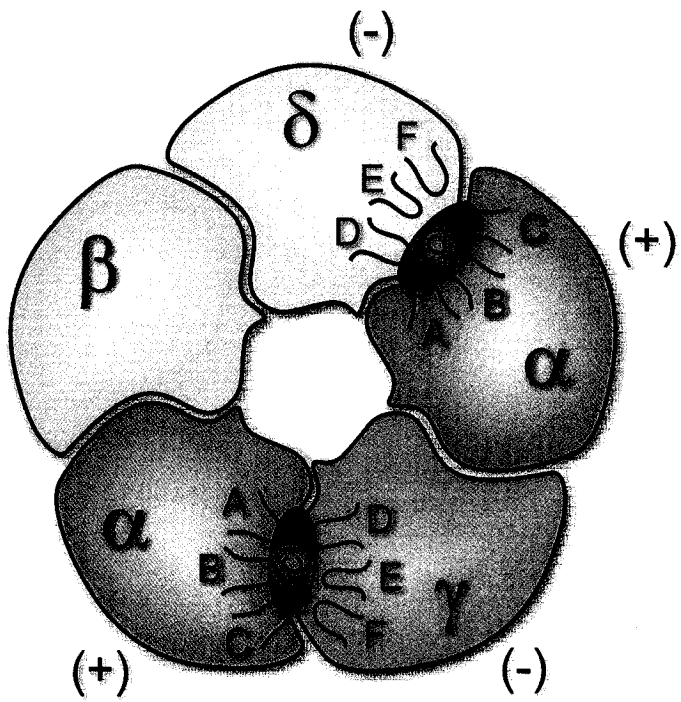
(-)
δ
F
E
D
C
(+)
β
B
A
α
α
A
D
B
E
γ
C
F
(+)
(-)

tyrosine hydroxyl is important for ligand binding. The hydroxyl oxygen would be expected to increase the π-electron density of its adjacent aromatic ring, making it more effective at stabilizing a positively charged ligand (92).

1.6B - Nicotinic Acetylcholine Receptor Structure: Towards an Atomic Model

Cryo-Electron Microscopy. The inability to grow three-dimensional crystals suitable for X-ray crystallographic analysis has, to date, prevented the elucidation of a nAChR X-ray crystal structure (93, 94). These difficulties have inspired the development of other structural methods, such as cryo-electron microscopy (Cryo-EM) pioneered by Richard Henderson and Nigel Unwin at Cambridge University. Given that shorter wavelength radiation permits higher resolution, and since the wavelength of a high energy electron is shorter than that of an X-ray, electron microscopy has the potential to yield resolutions greater than those attainable by X-ray crystallography (i.e. <1.0 Å)(95). Unfortunately matter interacts with electrons about 10,000 times more strongly than it does with X-rays (95). While this strong interaction is precisely what makes electron microscopy so sensitive, an unfortunate consequence is that the irradiating electrons can damage the specimen. Biological samples are particularly sensitive to radiation damage; therefore to collect images of proteins it is necessary to use extremely low electron doses. Images collected with low electron doses usually have poor signal to noise ratio, which has limited the practical resolution attainable by EM to the 5-10.0 Å range (95).

Since 1984, Nigel Unwin has used electron microscopy to image nAChR enriched tubes formed from native *Torpedo* electroplaque membranes (96). These nAChR tubes are

cylindrical arrays of receptor embedded in its native *Torpedo* membrane environment. While preliminary negative staining images were of only modest 30Å resolution, they clearly showed that the tubes exhibited crystalline symmetry and could thus be used for higher resolution analysis. Over the last twenty years, through constant technical improvements, Unwin and coworkers have steadily improved the resolution of their images giving great insight into nAChR structure and mechanism (4, 47, 64, 67, 96-119).

One of the advantages of cryo-electron microscopy is that specimens can be trapped by rapid freezing in different conformational states. In 1988 Unwin imaged both the receptor's resting and desensitized conformations at 18Å resolution, and showed that the conformational changes leading to nAChR desensitization were relatively small (102). In 1993 the resolution of the receptor's resting conformation was improved to 9Å (64). This was followed with a 9Å structure of the ligand-gated open state in 1995 (114). Comparisons between the open and closed states enabled Unwin to propose a rudimentary model for nAChR gating. More recent higher resolution structures have shown that the unliganded conformation of the two α-subunits is different from the β-, γ-, and δ-subunits (117).

While important insight has been gained from Unwin's structures, their limited resolution has also led to incorrect hypotheses. In 1987, Unwin and coworkers used electron microscopy in conjunction with affinity labelling to locate the relative positions of the receptor's five subunits. Based on their results they proposed an anticlockwise α-β-α-δ-γ arrangement (104). Crosslinking (120) and subsequent structural studies (121) have proven this arrangement incorrect. Instead the subunits are arranged in an α-γ-α-δ-β fashion (anticlockwise). In addition, in his 1993 9Å structure, Unwin claimed that the receptors M1, M3 and M4 segments were not α-helical as previously thought, but instead were β-sheet (64). This assertion sparked a heated debate, since at the time there were no other membrane

proteins of known structure with a mixed α/β transmembrane domain. Several reports arose either confirming (122, 123) or refuting (40, 124-130) the existence of nAChR transmembrane β-sheets. In the end, higher resolution data was needed to settle this debate (see below). These incorrect hypotheses serve as vivid reminders that while Unwin's models are informative, their limited resolution means they must be interpreted with a commensurate degree of caution.

Acetylcholine Binding Protein: Homologous to the nAChR Ligand Binding Domain. Structural studies of nicotinic receptors took a giant leap forward in 2001, with the discovery of a soluble protein from *Lymnaea stagnalis* that is homologous to the ligand binding domain of nAChRs (131). The discovery of this protein stemmed from the observation that snail synapses cultured in the absence of supporting glial cells displayed constitutive excitatory postsynaptic potentials, which suggested that under normal physiological conditions glial cells somehow suppressed cholinergic transmission. This surprising finding led to the identification of a glial protein, which when secreted into the synaptic cleft sequesters free ACh, thereby reducing the concentration of ACh available to bind to post-synaptic nAChRs (131). Because of its acetylcholine binding function the protein was called the "acetylcholine binding protein," or AChBP (131). Currently, there are no known mammalian orthologs of AChBP, which basically acts as an ACh buffer capable of modulating cholinergic neurotransmission at the *molluscan* synapse (132).

The AChBP is a 210 amino acid protein, with an apparent molecular weight of 25kDa (SDS-PAGE) (131). Sequence analysis shows that the AChBP is 23.9% identical to the N-terminal 210 amino acids of neuronal α_7 nAChRs. The N-terminal domain of nAChRs corresponds to their ACh binding domain, and the residues directly involved in ACh binding

in nAChRs are conserved in the AChBP. The AChBP has a pharmacological profile similar to that of the α_7 and α_9 nAChRs, and like all nicotinic receptors binds the antagonist α-bungarotoxin with high affinity (131, 132). According to gel filtration chromatography the biologically active form of the AChBP appears to be a pentamer (131), analogous to the Cys-loop superfamily of pentameric ligand gated ion channels. Because of its significant sequence homology and its shared pharmacological profile, the AChBP is thought to be structurally similar to the N-terminal ligand binding domain of nAChRs.

The AChBP has been an attractive candidate for X-ray crystallography because of its presumed structural homology with the ligand binding domain of nicotinic receptors. Furthermore, its solubility makes it much easier to crystallize than an integral membrane protein such as the nAChR. In 2001, Brejc et al. solved the X-ray crystal structure of the AChBP homopentamer at 2.7Å resolution (121). This structure gave the nAChR research community its first atomic level glimpse of the receptor's ligand binding domain. When viewed along its five-fold axis of symmetry the AChBP pentamer is described as a "children's windmill toy" (the authors are from Holland... nice touch!) with each of the five protomers contributing a single petal (Figure 1.6)(121). The pentamer is approximately 80Å wide, and about 63Å tall, which is in good agreement with the dimensions of the nAChR N-terminal domain as determined by electron microscopy (64).

Each AChBP protomer is built around a ten stranded β-sandwich core, with a modified immunoglobulin fold (Figure 1.7). The N-terminus is at one end of the protomer (the top) while the C-terminus is at the other (the bottom) (Figure 1.7A). In nAChRs the C-terminal end of the ligand binding domain would lead directly into the first transmembrane segment (M1), therefore this end of the protomer would be closest to the membrane. The topmost N-terminal segment consists of a short α-helix which packs tightly against the

Figure 1.6

Crystal structure of the Acetylcholine Binding Protein from *Lymnaea stagnalis* (PDB ID: 1I9B)(121). **(A)** The AChBP homopentamer viewed along its five-fold axis. Each protomer (A-E) is coloured differently. **(B)** Side view of the AChBP pentamer upon 90° rotation. The bound HEPES buffer molecule (spheres) depicts the interfacial location of the acetylcholine binding site. Note: all structural figures, including this one, were rendered with PyMol (http://pymol.sourceforge.net).

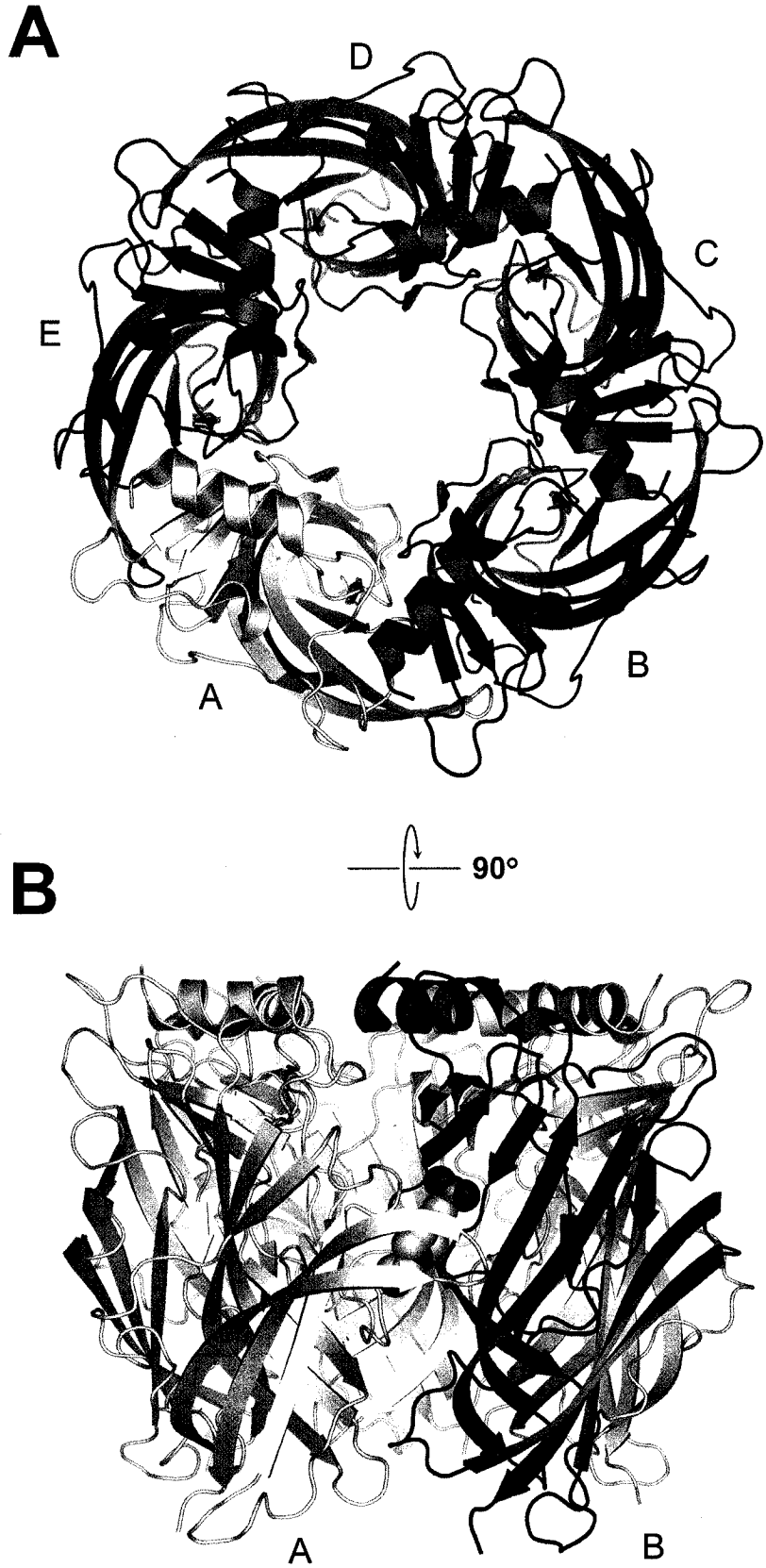
A
D
C
E
B
A
90°
B
A
B

Figure 1.7

(A) Structure of the AChBP protomer (PDB ID: 1I9B)(121). The β-strands comprising the inner and outer β-sheets are blue and red, respectively. The eponymous Cys-loop (L7) is green, while the C-loop (L10) is yellow. The vicinal disulfide bond in the C-loop, and the disulfide bond encircling the Cys-loop have been represented with orange sticks. The N- and C-termini have been denoted by blue and red spheres, respectively. **(B)** Topology map of the AChBP protomer. The colour scheme is the same as in (A). Note that the elements in this schematic are not to scale.

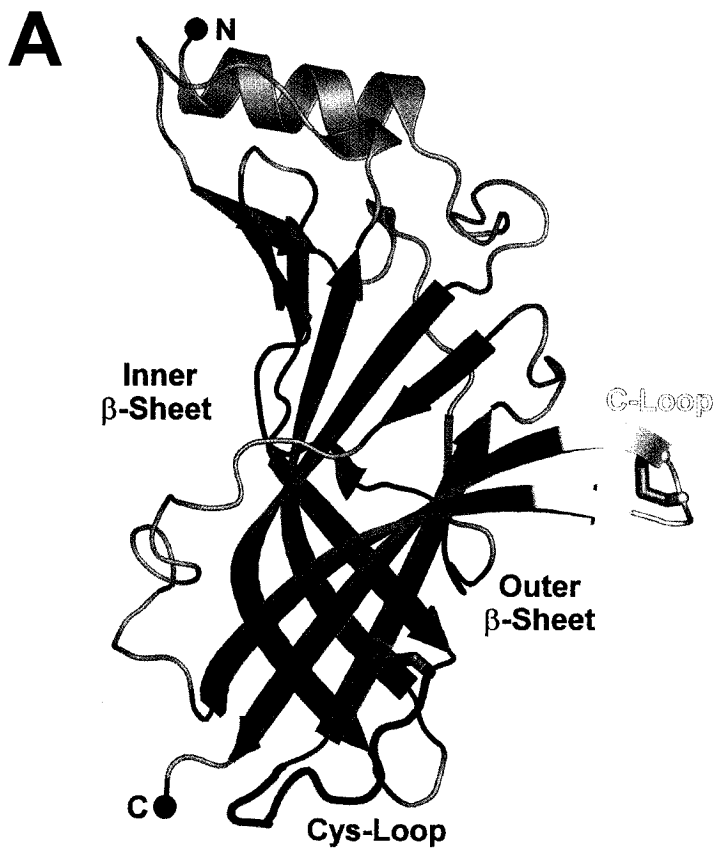
A
N
Inner
β-Sheet
C-Loop
Outer
β-Sheet
C
Cys-Loop
B
L4
L3
α1
L8
L6
L1
L10
S
S
β3
β5
β6
β2
β1
β8
β9
β10
β7
β4
S
S
L2
L9
L7
L5

β-sandwich core. The ten stranded β-sandwich core, though a modified immunoglobulin (Ig) fold does not resemble other Ig-like proteins, or any other known protein structure. It consists of inner and outer β-sheets which each follow a "Greek key" motif (Figure 1.7B). The two sheets twist around each other, and are held together by a hydrophobic core, while their exterior surfaces are covered in several charged residues and are thus relatively hydrophilic. The interface between two subunits is very hydrophobic and convoluted, suggesting that complementarity may be important for stabilizing the pentamer. It should be noted however that the residues lining this interface are not well conserved among the receptor superfamily. Different interactions at this interface could underlie the different allostery observed between members of the Cys-loop superfamily (121).

Several of the loops connecting the individual β-strands are long and extended, presumably because they serve a functional role (121). Of particular note is the large C-loop, which connects the two longest β-strands (β9 and β10) and projects away from the β-sandwich core towards the neighbouring subunit (Figures 1.6 and 1.7). The loop forms a flap around the ligand binding site and is stabilized by a vicinal disulfide bond between Cys187 (α_1-Cys192) and Cys188 (α_1-Cys193). The eponymous Cys loop (Cys123-Cys136/α_1-Cys128-Cys142) in the AChBP consists of only twelve residues rather than the thirteen found in members of the Cys-loop receptor superfamily. Furthermore, the sequence of this loop is not conserved in the AChBP. The loop is primarily hydrophilic in AChBP, while in the Cys-loop receptors it is primarily hydrophobic. Its position at the bottom of the protomer, and its relative hydrophobicity in the Cys-loop receptors suggests that it may interact with the membrane or the receptors transmembrane domain, and could be important for coupling the ion channel domain to the ligand binding domain. This coupling function is

not necessary in the AChBP where instead the loop's hydrophilicity may be important for making the AChBP soluble.

As predicted, the acetylcholine binding site is at the interface between two subunits (Figure 1.6B and 1.8). With respect to each protomer, it is in a roughly equatorial position and is towards the perimeter of the pentameric ring. It is basically a "cleft" surrounded by several loops from the principle face of one subunit (loops A, B and C from the nAChR-α subunit) and several β-strands from the complementary face of an adjacent subunit (strands D, E and F from the nAChR-γ and δ subunits). The interfacial location of the binding site, as well as the relative positions of the principle (+) and complementary (-) faces confirms the proposed α-γ-α-δ-β anticlockwise arrangement of the nAChR.

The original AChBP structure (PDB ID: 1I9B) was supposed to be crystallized in the absence of ligand; however there was unexpected electron density in the binding site (121). This density was attributed to a HEPES buffer molecule. HEPES, like many cholinergic agonists has a quaternary ammonium group and apparently binds weakly to the AChBP (estimated K_D ~100mM). At the ~100-150mM HEPES concentrations used for crystallizing the AChBP, some of the ACh binding sites were occupied by HEPES (Figure 1.6B). Subsequent, higher resolution crystal structures of AChBP in complex with the agonists, nicotine (2.2Å) and carbamylcholine (2.5Å), have given a more descriptive view of ligand binding (Figure 1.8)(133, 134).

The AChBP structure confirms almost 30 years of mutagenesis and chemical labelling studies which have identified residues important for ligand binding (13). In general, the ligands are completely buried by the protein upon binding. Sixty to seventy percent of the ligand is buried by the principle (+) subunit, while the complementary (-) subunit buries the rest. The positively charged nitrogens on HEPES, Carb and nicotine are

Figure 1.8

Structure of the AChBP agonist binding site (PDB ID: 1UV6)(133). **(A)** Location of the acetylcholine binding site at the interface between two AChBP protomers. The subunit which makes most contacts with the bound ligand corresponds to the principle (+, yellow) subunit while the other subunit corresponds to the complementary (-, cobalt) subunit. Residues directly involved in binding the agonist carbamylcholine (Carb, green ball and sticks) are shown (ball and sticks). Carbon atoms are the same colour as the cartoon representations, while oxygens are red, nitrogens blue, and sulfur atoms are orange. **(B)** Close up of the agonist binding site showing residues involved in binding on the principle (left) and complementary (right) subunits. On the principle subunit; Y89 (A-loop), W143 (B-loop), and Y185, Y192, Cys187/188 (C-loop) all form interactions with the bound agonist. **(C)** Surfaces of the principle (left) and complementary (right) subunits. The views in (C) are exactly the same as those in (B).

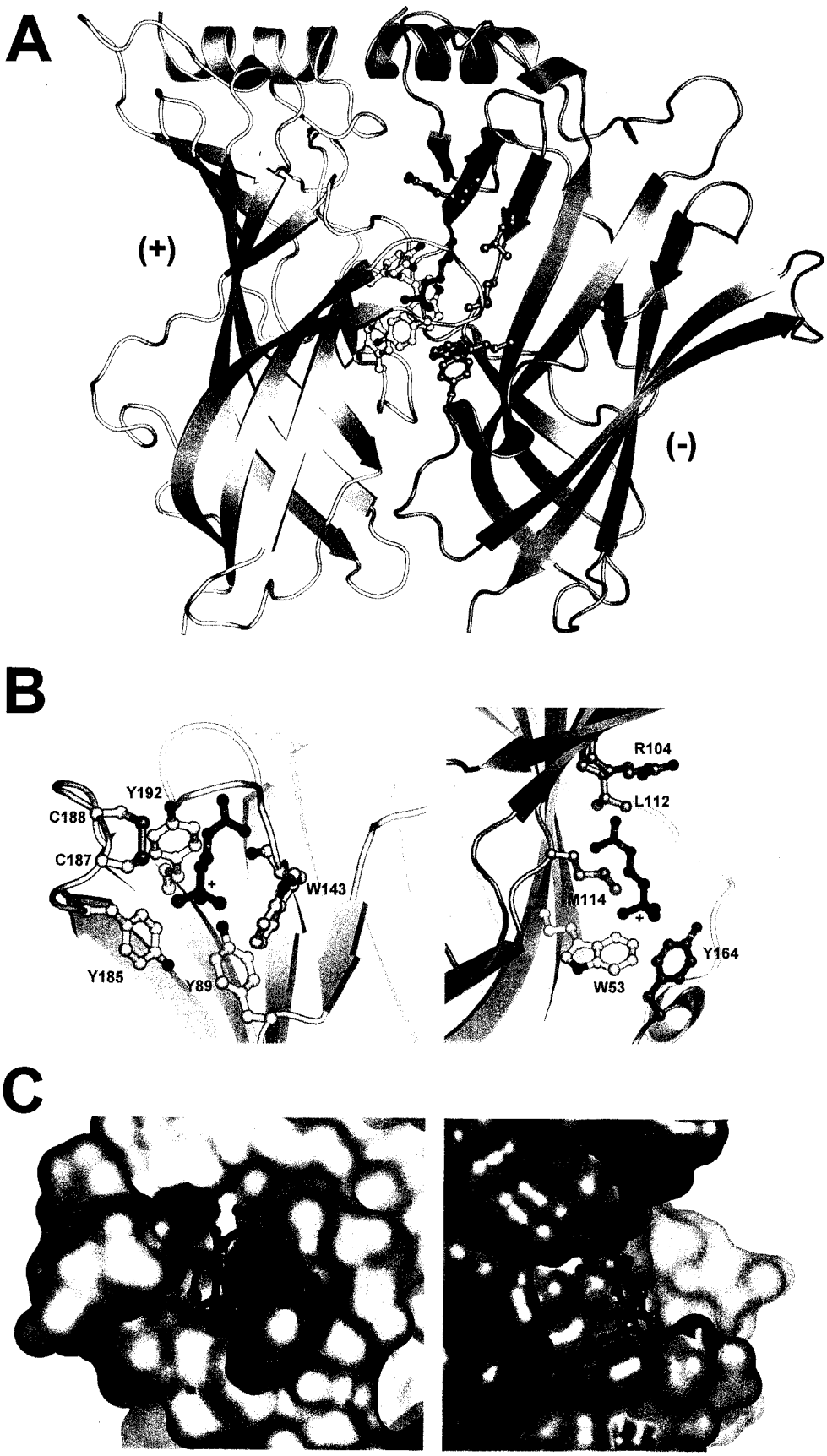
A
(+)
(-)
B
Y192
C188
C187
W143
Y185
Y89
R104
L112
M114
Y164
W53
C

all stabilized through cation-π interactions with Trp143 and Tyr192 on the principle (+) subunit (Figure 1.8B)(133). Tyr89 is also in close proximity to the binding site but is too far to form cation-π interactions and instead contributes a hydrogen bond. Tyr185 only interacts with the choline group on carbamylcholine (and presumably ACh) and not with nicotine (133). This is consistent with the observation that mutation at this site affects carbamylcholine (or ACh) binding much more than nicotine binding (135). The vicinal disulfide between Cys187/188 in the C-loop also contacts bound ligand (Figure 1.8B,C), explaining why it cannot be reduced in the presence of bound agonist (136).

The residues from the neighbouring subunit which form the complementary (-) face of the ligand binding site are less conserved than those from the principle (+) side (121). The variation between the nAChR subunits in this region, likely gives rise to the differences in affinity observed for the various nAChR subtypes. One residue which is conserved in the AChBP and in the nAChR γ- and δ-subunits is Trp53 (γ-Trp54 and δ-Trp57). In the structures of AChBP/agonist complexes, this residue lies under the bound ligand where it presumably forms cation-π interactions which help to stabilize the ligand's positive charge (Figure 1.8B)(133). In the AChBP/agonist structures several other amino acids on the complementary side of the binding site make contact with either nicotine and/or carbamylcholine (Arg104, Leu112 and Met114, see Figure 1.8B) but these residues are not conserved in the nAChR γ- and δ-subunits (133).

AChBP and nAChR Ligand Binding Domain: Homology Modelling. While the atomic model of the AChBP was not a direct model of the nAChR's ligand binding domain, the high sequence homology between the AChBP and the nAChR N-terminal ligand binding domain suggested that they shared the same overall architecture. This allowed Unwin to

model the structure of the nAChR ligand binding domain by forcing homologous residues in each of the four nAChR subunits to adopt an AChBP-like fold. The modelled structures were then fit into the low resolution electron densities determined from EM images of the nAChR in tubular crystals (117). The resulting model is therefore based on the sequence homology between the *molluscan* AChBP and the nAChR ligand binding domain, and assumes that the two domains adopt a similar fold. Because the model is primarily a homology model, it depicts the structure of the polypeptide backbone but does not give precise information about the orientation of amino acid side chains. Furthermore there are regions of the nAChR ligand binding domain, particularly in the non-α-subunits, that are not conserved within the AChBP. Most of these regions are connecting loops between individual β-strands within the domain. As expected, these regions do not overlap as well with the experimental nAChR densities determined by EM, and must be modelled differently from their partners in the AChBP (117).

Once modelled into an AChBP-like fold, the N-terminal domains of the nAChR β-, γ- and δ-subunits all fit reasonably well into their EM electron densities, but in order to fit the α-subunits it was necessary to distort their structures (117). Unwin and coworkers argued that these structural differences were expected since their structure was of the unliganded/resting state, while the AChBP structures were of the ligand bound, and thus activated (117) or desensitized state (137). Unwin proposed that the conformational changes required to relax the nAChR α-subunits back to a AChBP-like (or non-α-subunit-like) conformation were analogous to the structural rearrangements caused by agonist binding, and resulting in channel gating (see below) (117).

4.0Å Structure of the nAChR Pore. While the discovery and subsequent structure determination of the molluscan AChBP may have diminished the potential impact of a nAChR structure, it also allowed Unwin and his group to focus on the remaining unknown regions of nAChR, namely the transmembrane and cytoplasmic domains. In 2003, the continued efforts of Unwin and coworkers to increase the resolution of their nAChR electron diffraction data culminated in a 4.0Å structure of the receptor's transmembrane domain in its closed/resting conformation (67). While 4.0Å resolution generally does not allow for the precise modelling of amino acid side chains, Unwin and colleagues, in conjunction with the thirty years of nAChR biochemical data, were able to define the position and relative orientation of the receptor's transmembrane segments. This structural model, while based largely on modest resolution data, is consistent with numerous chemical labelling studies (39-43, 57, 58, 60-62, 128, 129, 138).

As predicted by hydropathy plots, each of the receptor's five subunits is made up of four transmembrane spanning α-helices designated M1-M4, meaning that the entire transmembrane domain consists of 20 helices. The five groups of four helices, each corresponding to a single subunit, come together with near perfect five-fold symmetry, forming a central ion conducting pore. The overall architecture of the structure is reminiscent of a ship's propeller with each subunit contributing a single blade (Figure 1.9A) (67). Each transmembrane helix is roughly 40Å long, and projects 10Å beyond the ~30Å thick membrane and into the extracellular space (Figure 1.9B). As predicted by electrophysiological (49) and chemical labelling experiments (38, 62), the ion conducting pore is lined with residues from the M2 helices, which tilt radially inwards toward the central pore axis. The M1, M3 and M4 helices also tilt toward the central axis and are notably splayed apart on the extracellular side of the membrane. The centre to centre separation

Figure 1.9

4.0Å structure of the *Torpedo* nAChR transmembrane domain as determined by cryo-electron microscopy (PDB ID: 1OED)(67). **(A)** Structure of the transmembrane region of the pore as viewed from the extracellular side of the membrane. Each subunit is labelled and uniquely coloured (the two α-subunits are both red). The four transmembrane spanning α-helices (M1-M4) in the γ-subunit have been labelled. **(B)** Side view (in the plane of the membrane) of a single nAChR subunit (α). The approximate limits of the hydrophobic core of the membrane are denoted both by the dotted lines as well as the colouring of each helix. Lipid exposed regions are shown in red, and aqueous solvent exposed regions in blue. Note that each helix protrudes approximately 10Å beyond the membrane on its extracellular (E) side (M = membrane, I = intracellular).

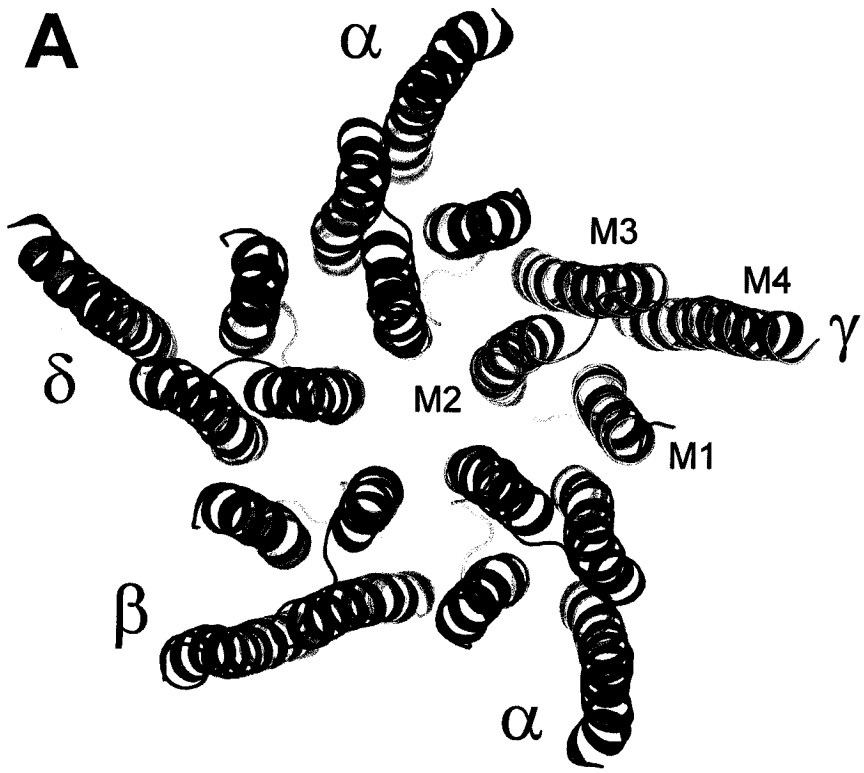
A
α
M3
M4
γ
δ
M2
M1
β
α

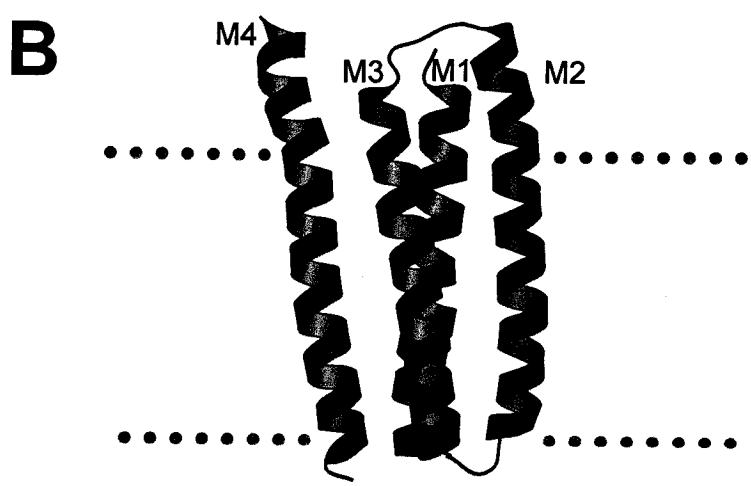
B
M4
M3
M1
M2

between the helices in this region ranges from 12.5-15Å, with the largest separations being between helices from neighbouring subunits (67). These openings are large enough to allow the passage of an ion, suggesting that ions may enter the pore laterally from beside the protein as well as from the large central cavity in the ligand binding domain (see Figure 1.14) (67).

The transmembrane domain (M1-M4) can be subdivided into at least two essential components; an inner ring formed by the M2 helices, and an outer ring formed by the remaining M1, M3 and M4 helices (67) (Figure 1.10). The inner M2 ring forms the ion conducting pore and directly interacts with ions, while the outer ring sequesters this inner ring away from the hydrophobic lipid bilayer. The two rings come together separately, and the distance separating them in the middle of the membrane is comparable to the diameter of the central pore. Separation between M2 and M1/M3 is consistent with the finding that both the Glycine and $GABA_A$ receptors have alcohol binding sites between M2 and M1/M3 (139, 140). Separation between M2 and the remaining helices is also consistent with Karlin's SCAM experiments which showed that positions on both sides of M2 were accessible to small sulfhydryl reagents (38, 62). Karlin and coworkers suggested that the exposure pattern was not consistent with an α-helical structure. This, however, was based on the assumption that M2 was tightly associated with the other TM segments, which we now know is not the case (67). The outer ring (M1, M3 and M4 of each subunit) is stabilized by the clustering of several hydrophobic side chains around a central aromatic residue in M1 (phenylalanine in α, β, δ and tyrosine in γ) (67). M2 makes no extensive van der Waals contacts with either M1 or M3, however there are several hydrophobic residues in M2 in close proximity to hydrophobic residues in both M1 and M3 which could interact upon gating (67).

Figure 1.10

According to Miyazawa *et al.* the nAChR transmembrane domain consists of two distinct rings of α-helices (67). The M2 helices from each subunit associate to form the inner pore ring (blue), which lines the ion conduction pathway. The remaining M1, M3 and M4 helices constitute an outer ring (red) which surrounds and sequesters this inner ring from membrane lipids. Figure adapted from Miyazawa *et al.* (67).

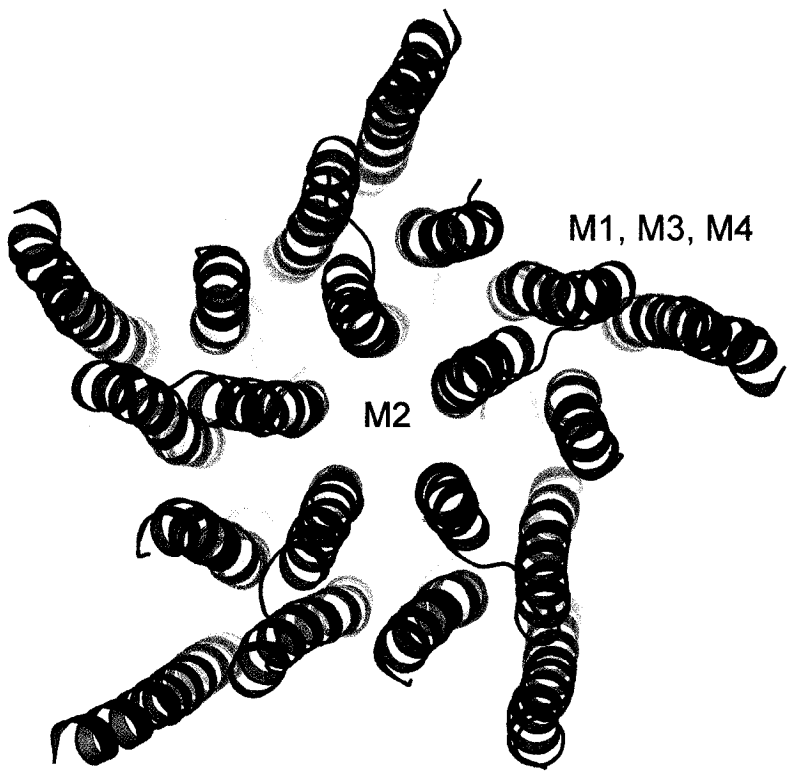
M1, M3, M4
M2

The five M2 helices traverse the bilayer in sync such that sets of homologous residues from each subunit line up to form rings of amino acids with similar physical properties. For the most part these rings are relatively non-polar and thus unlikely to interact strongly with a diffusing ion. However, at αSer266 (Glu in β, γ and δ) and αGlu262 (extracellular ring) there are negatively charged groups which contribute to ion conduction by presumably raising the local cation concentration and lowering the local anion concentration (Figure 1.11)(55, 73). The intermediate ring at αGlu241, which is also important for conduction is not part of the M2 helix but instead is located at the end of the M1-M2 loop and forms a narrow frame around the intracellular pore entryway (Figure 1.11A)(67). The putative cytoplasmic loop (αAsp238) is closer to the C-terminal end of M1 than the N-terminal end of M2 and does not appear to line the pore lumen, at least not in the region which spans the membrane. In addition to the rings of charge there are also conserved rings of polar residues which line the pore near its most constricted region, in particular αThr244 and αSer248. Presumably these residues are also important for ion conduction (67).

Consistent with previous data, Unwin's 4.0Å structure of the closed nAChR pore showed that the ion conduction pathway is a continuous, uninterrupted channel. No region of the protein occludes the channel in its closed state, thus the ion channel gate is indeed an energetic, rather than a physical barrier (67). As mentioned previously, the precise location of the gate has been an issue of some contention (58, 64). This higher resolution data confirms that in the region of the pore corresponding to the middle of the membrane, the pore is maximally constricted. This is a result of small separation between adjacent M2 helices, and the presence of large and bulky hydrophobic side chains. Unwin originally suggested that a ring of highly conserved leucines, including αLeu251, formed the gate (64). With this more recent data, the length of the gate has been extended to include all residues

Figure 1.11

Structure of the *Torpedo* nAChR pore (PDB ID: 1OED)(67). **(A)** Right: Surface diagram of the nAChR transmembrane domain (side view). A single subunit (δ) has been removed to provide an unobstructed view of the ion channel lumen. The M2 helices lining the pore have been coloured cyan, while rings of negative charge formed by homologous residues (see text) are shown in red. The narrowest region of the pore corresponding to the hydrophobic gate is shown in yellow. The ion conduction path is indicated by the central blue "ion" and the dashed line. Left: A ribbon representation of αM2 showing the relative position of highlighted residues lining the pore in the accompanying surface. Dotted lines denote the approximate limits of the membrane. **(B)** View inside the nAChR transmembrane pore from the synaptic space. Hydrophobic residues from each subunit which contribute to the central constriction/gate are shown as transparent spheres and sticks (αVal255: orange, and αLeu251: yellow). Note the "ion" in both figures is not to scale. Figure concept from Miyazawa *et al.* (67).

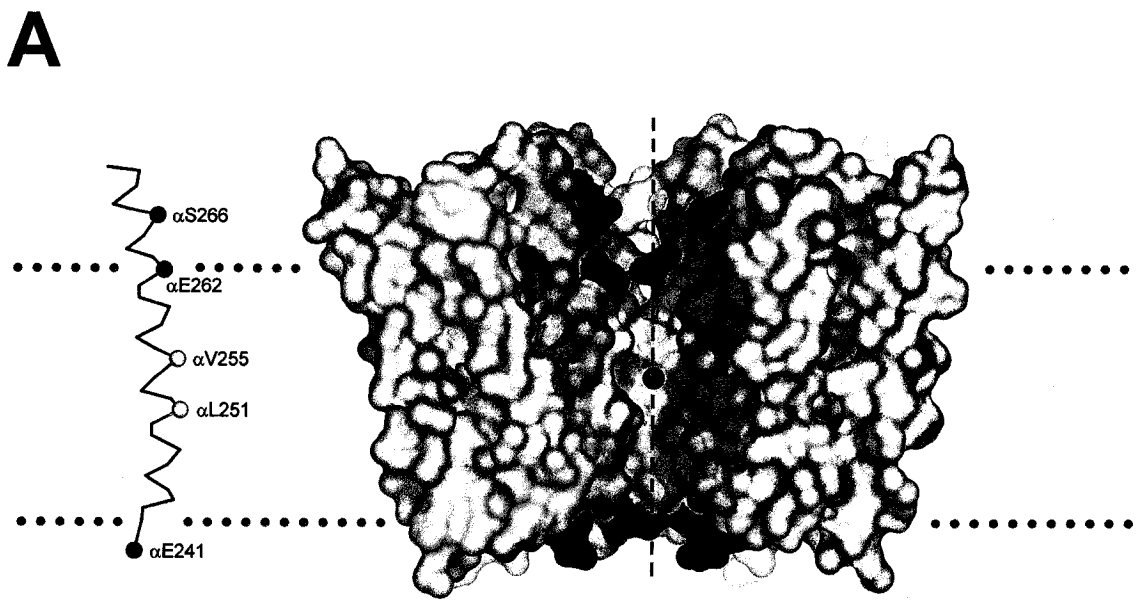
A
αS266
αE262
αV255
αL251
αE241

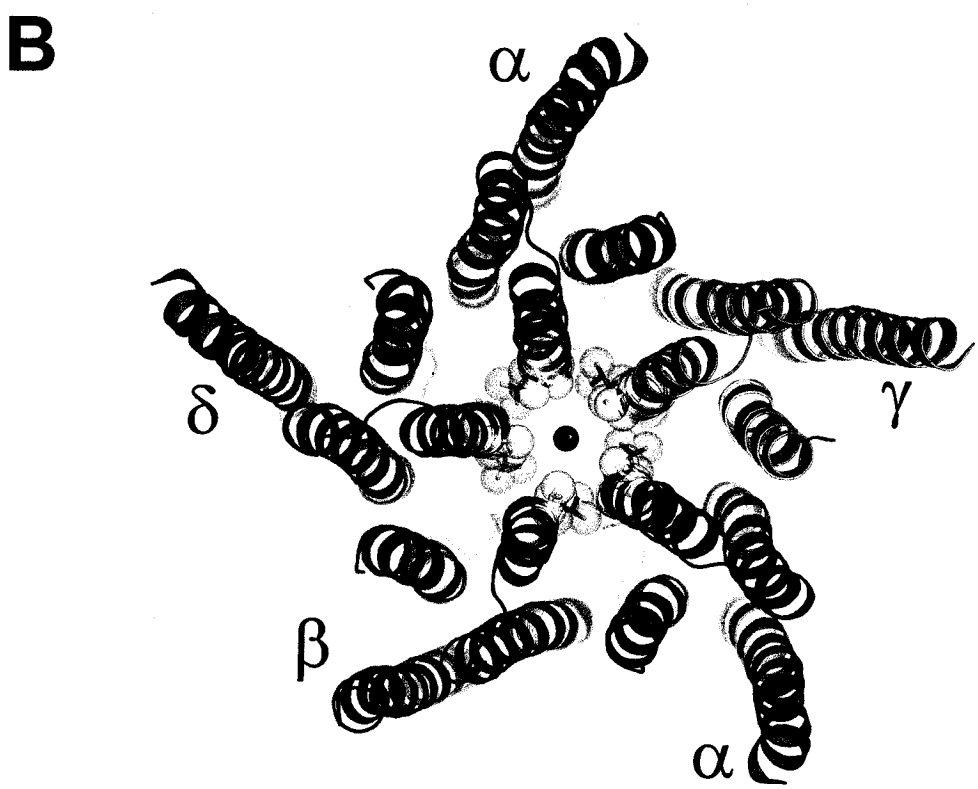
B
α
δ
γ
β
α

between αLeu251 and αVal259. Within this region of M2 a number of highly conserved hydrophobic residues come together through symmetrical side-to-side interactions to form a tight hydrophobic girdle which encircles the pore (67). This hydrophobic girdle extends roughly 8.0Å along the length of the pore, and has an inner diameter less than 7.0Å, which is too narrow to accommodate a hydrated sodium or potassium ion (effective diameter ~8.0Å) (Figure 1.11) (67). Since the pore walls are hydrophobic they are unable to compensate for the loss in energy resulting from ion dehydration. As a result ions retain their hydration shell and are too wide to pass through this barrier. Presumably the binding of acetylcholine triggers a conformational change which ultimately widens the diameter of the channel in this region to greater than 8.0Å (see Figure 1.18B). This larger diameter permits the passage of ions and their associated water molecules (67).

1.6C - A Refined Model of the Full Length nAChR

In general, to build an atomic resolution map of a protein it is necessary to have atomic resolution data. Atomic resolution data is usually obtained in the form of an electron density map, which depicts the precise location of atoms and thus amino acids in the protein. By knowing the position of amino acids, along with a protein's primary structure, it is possible to thread the protein's amino acid sequence into the electron density map and build a chemical model of the protein. Ultimately, the accuracy and reliability of this model is a direct function of the resolution of the electron density map, since higher resolution data allows for a more precise placement of residues.

In early 2005, Unwin published a refined model of the entire nAChR at 4.0Å (4). This model was based on the same images and data used to determine the structure of the

transmembrane domain in 2003 (67). In general, 4.0Å resolution is not high enough to confidently identify amino acid side chains and thus build a reliable atomic resolution model. Unwin's model however is also based on over thirty years of nAChR biochemical and biophysical data. In particular, the acetylcholine binding domain was modelled largely on the X-ray crystal structure of the highly homologous molluscan AChBP (121). By combining previous biochemical studies and homology modelling with the AChBP, Unwin has been able to thread the sequences of each of the four nAChR subunits into his lower resolution (4.0Å) EM data. This resolution is high enough to have confidence in the organization and structure of the polypeptide backbone; however one has to be cautious not to over interpret the precise position of amino acid side chains.

Unwin's model confirms that the nAChR is composed of five elongated subunits which associate in a pseudo-symmetric fashion around a central ion conducting channel (Figure 1.12A)(4). The roughly circular, pentagonal arrangement of the five nAChR subunits is evident when the structure is viewed along its long axis from the synaptic cleft (Figure 1.12A). This view also clearly depicts the central ion conducting path, which in the extracellular synaptic space is relatively wide. If the structure is rotated ninety degrees so that it is viewed perpendicular to the ion channel axis and in the plane of the membrane, it is evident that each of the nAChR subunits adopts a similar fold with three clearly defined domains: a large extracellular ligand binding domain, an α-helical transmembrane spanning domain, and a cytoplasmic domain (Figure 1.12B).

The N-terminal region (~210a.a.) of each subunit, which associates with neighbouring subunits in the synaptic space to form the ligand binding domain, is similar in structure to the AChBP protomer (Figure 1.13). The domain consists of a twisted ten stranded β-sandwich and a short N-terminal helix. The loops connecting several of the

Figure 1.12

Refined model of the *Torpedo* nAChR (PDB ID: 2BG9)(4). **(A)** View inside the nAChR pore, along its central axis, from the extracellular synaptic space. The five nAChR subunits are labelled, and their ligand binding domains are uniquely coloured. The location of the acetylcholine binding site is denoted by the side chain of αW149 (yellow ball and sticks). **(B)** Side view of the *Torpedo* nAChR (in the plane of the membrane) upon 90° rotation of (A). The two front subunits (α and γ) are coloured red and blue. Rear subunits have been coloured grey for clarity. The dotted lines denote the approximate location of the membrane.

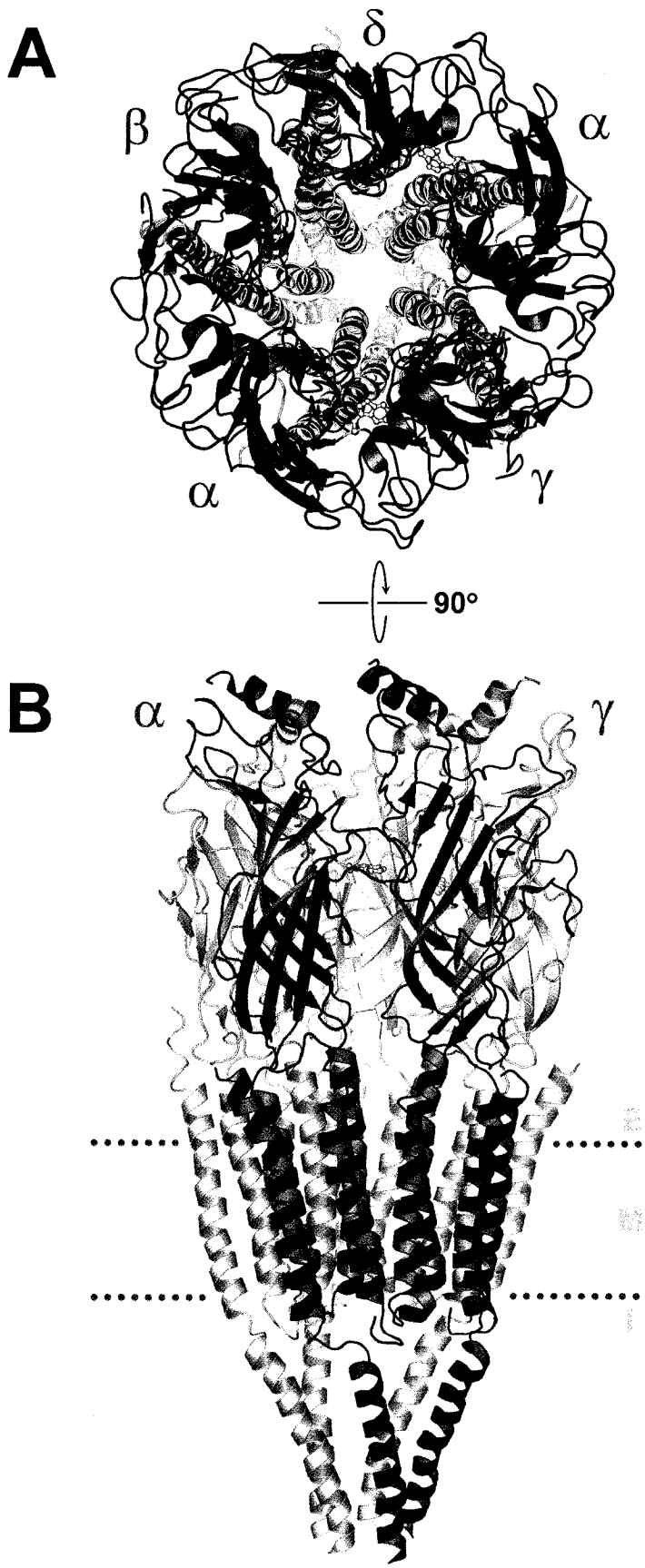
A
δ
β
α
α
γ
90°
B
α
γ

Figure 1.13

Structure of the *Torpedo* nAChR α-subunit (PDB ID: 2BG9)(4). The transmembrane (M1-M4) and cytoplasmic (MA) α-helices are shown in yellow, while the inner and outer β-sheets of the AChBP-like ligand binding domain are blue and red, respectively. The eponymous Cys-loop is green, while the C-loop which caps the binding site is yellow. The vicinal disulfide bridge within the C-loop, and the disulfide encompassing the Cys-loop are shown as orange sticks, while the N- and C-termini are denoted with blue and red spheres, respectively. The approximate location of the central channel axis is shown by the grey line. **(A)** View of the α-subunit from outside the channel. **(B)** View upon 90° rotation (in the plane of the membrane) of A. Figure is based upon Figure 4 in Unwin, 2005(4).

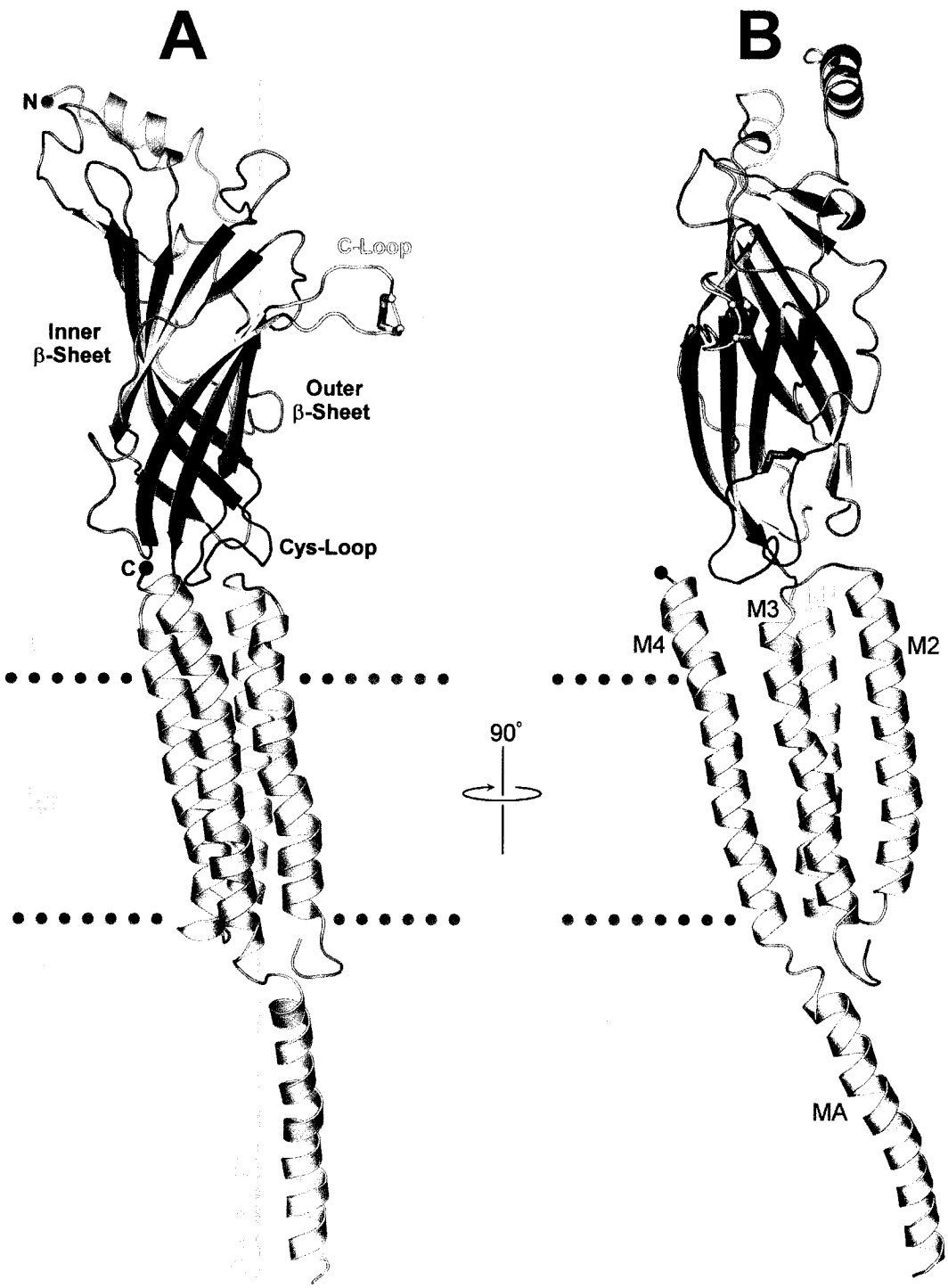
A
B
N
C-Loop
Inner
β-Sheet
Outer
β-Sheet
Cys-Loop
C
90°
M3
M4
M2
MA

strands are extended and thought to be important for function. As described previously, the transmembrane domain of each subunit consists of four transmembrane spanning α-helices (M1-M4) and their connecting loops. The M2s from adjacent subunits form an inner ring of α-helices which line the ion channel, while the M1, M3 and M4 helices surround the inner ring and sequester it from the lipid bilayer (Figure 1.10). Depending on the subunit, the loop connecting M3 and M4 is between sixty and a hundred amino acids long, and constitutes the majority of the cytoplasmic domain. Other than the MA α-helix, most of this domain has not been modelled due to a lack of visible electron density. This suggests that the unmodelled regions of this domain may be quite flexible and thus relatively disordered.

The subunits make extensive contacts with each other in all three of their domains. In the extracellular domain most of these contacts are between polar and charged residues. These interactions, while similar to those found in the highly homologous AChBP, are not as extensive (4). This finding is consistent with the nAChR ligand binding domain being less compact than the AChBP (117). Interestingly, several salt bridges exist between the α-subunits and their neighbours which are not conserved between non-α-subunits, or seen in the AChBP. These interactions could be important for stabilizing the α-subunits resting conformation, a conformation not adopted by the other subunits, and possibly the AChBP (4).

In the transmembrane domain the inter-subunit interactions are mainly a result of hydrophobic side chains projecting out from M1, M2 and M3. The hydrophobic girdle at the centre of M2 is the most obvious inter-subunit interaction (Figure 1.11). In addition to hydrophobic interactions, at least one electrostatic interaction between subunits occurs in the transmembrane region. The α-subunit's Glu262, part of the "extracellular ring", forms salt bridges with δArg277/γLys271. Also of note, most of the interactions between adjacent

subunits in the membrane domain occur on the inner leaflet side of the membrane. This isn't surprising since the tilt of the transmembrane α-helices brings them closest together in this region. The interactions between subunits in the cytoplasmic domain are less well defined since much of this region has not been modelled. The domain consists of five MA helices, one from each subunit, which come together to form an inverted pentagonal cone (4). This cone is held together by inter-subunit interactions at the N-terminal ends of each of the five MA helices.

While there are extensive contacts between the subunits, there are also substantial gaps between them (Figure 1.14). These gaps are found in both the intracellular and extracellular domains/vestibules and are large enough to accommodate a hydrated sodium or potassium ion (4). Furthermore, the walls surrounding the gaps are negatively charged, leading Unwin to propose that they selectively increase the pore's accessibility to cations (Figure 1.14)(4). In the case of the intracellular vestibule there is no large central opening analogous to the one in the extracellular domain, thus ions are forced to pass through these gaps. The gaps, or "windows" (as Unwin calls them), are between the five MA helices and have a maximum diameter of roughly 8.0Å. This is large enough to allow them to accommodate a hydrated sodium or potassium ion, but still small enough to electrostatically repel anions and screen out larger cations (Figure 1.14)(4). The surfaces of the MA helices which frame the intracellular windows are negatively charged in the nAChR and other cation conducting Cys-loop receptors but are positively charged in anion conducting Cys-loop receptors, further highlighting their role in determining charge selectivity (4). In addition, the relatively small diameter of the windows, which is comparable to the most constricted region of the pore, suggests that the windows may in some cases restrict flux and could therefore be important determinants of conductance. Consistent with this are the recent

Figure 1.14

Negatively charged "windows" in the ion-channel wall contribute to nAChR cation selectivity. **(A)** Surface diagram of the entire nAChR (side view). The α- and δ-subunits are red and blue, respectively. Residues framing both the inner and outer windows are shown in yellow. An ion (not to scale) has been placed in the windows to further highlight their locations. **(B)** Enlarged view of the outer window between the α- and δ-subunits. The surface shown is an electrostatic potential surface in which red areas represent regions of relative negative charge, while blue areas represent areas of relative positive charge. **(C)** Enlarged, electrostatic potential surface of the inner window between the δ- and β-subunits. In both (B) and (C) select acidic residues framing the windows have been labelled.

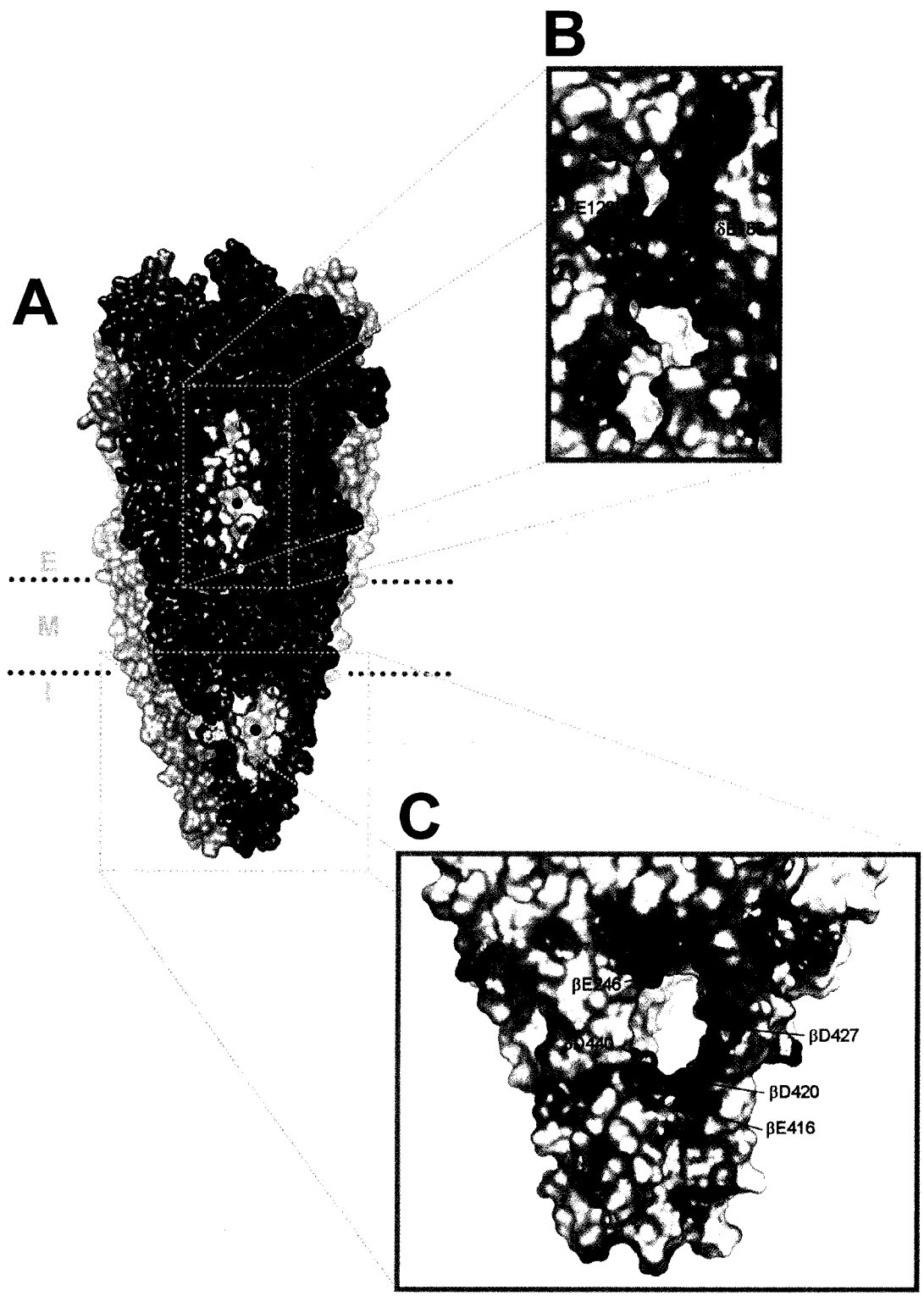
B
A
E
M
T
C
βD427
βD420
βE416

findings that single channel conductance of 5-HT_3 receptors could be dramatically altered by mutating residues which line these window frames (141).

The intracellular and extracellular vestibules which funnel ions into the transmembrane pore are lined with a number of negatively charged residues (4). The dimensions of these vestibules are also narrow enough (~20Å) to ensure that a diffusing ion must interact electrostatically with their surface, yet wide enough to prevent a tight association which would reduce the rate of conduction. Because they are negatively charged they present a cation stabilizing environment while repelling anions, thus they selectively promote cation conduction (Figure 1.15)(4). Mutagenesis studies originally identified specific residues which formed three rings of negative charge (αAsp238, αGlu251 and αGlu262) that were thought to be important for charge selectivity (55). Unwin's structural model shows that while these rings surround the internal and external entrances to the membrane spanning pore and are indeed important for cation conduction, they are supplemented by several negatively charged residues which line the entire walls of the inner and outer vestibules (Figure 1.15). Charge selectivity therefore appears to be a global feature of the pore, rather than the result of a narrow selectivity filter region (4).

1.7 - Current Model of nAChR Gating

The defining feature of the nAChR is its ability to convert a chemical signal into an electrical response. This ability requires two main functions: a specific binding capacity and a controlled ion flux capability. To carry out these two very different functions the nAChR has two discrete structural domains: an extracellular ligand binding domain, and a transmembrane ion channel domain. Understanding how the nAChR couples agonist

Figure 1.15

"Cut-away" views showing the electrostatic potential of the walls lining the *Torpedo* nAChR ion pore. Negatively charged surfaces are shown in red, while positively charged surfaces are blue. Areas that are relatively uncharged are white. Surfaces of both the outer **(A)** and inner **(B)** vestibules are shown. In both (A) and (B), several acidic residues lining the pore are labelled.

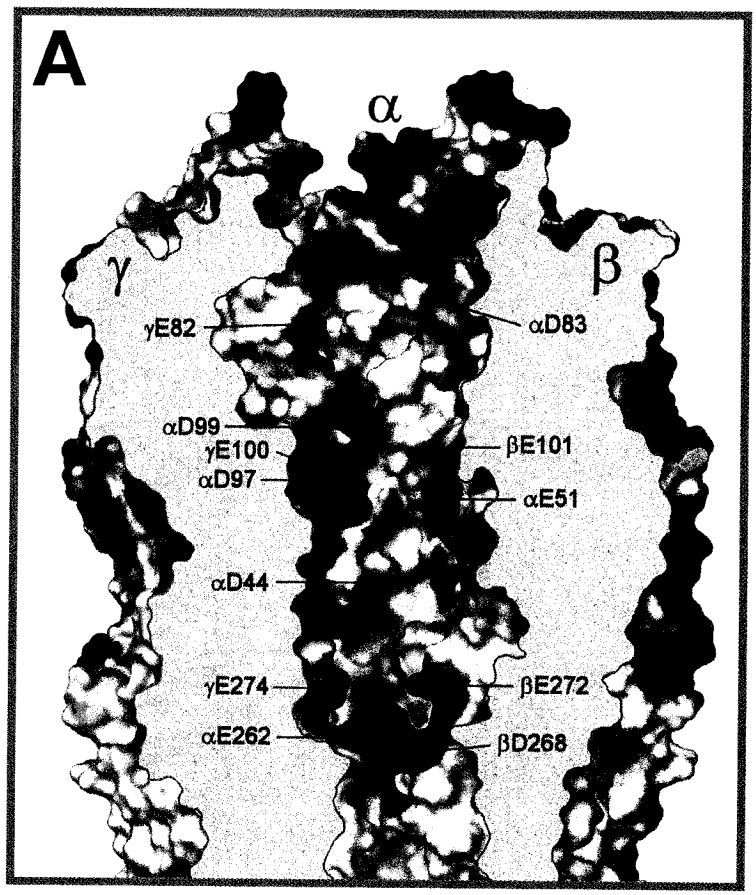
A
α
γ
β
γE82
αD83
αD99
γE100
αD97
βE101
αE51
αD44
γE274
βE272
αE262
βD268

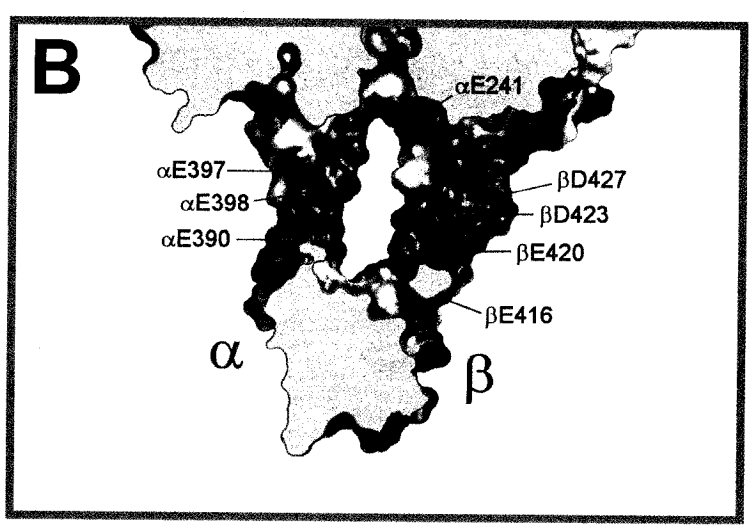
B
αE241
αE397
αE398
αE390
βD427
βD423
βE420
βE416
α
β

binding to channel gating requires a detailed knowledge of the agonist-induced conformational changes in both of these domains.

With regards to the ligand binding domain, the most detailed structural insights have come from recent crystallographic studies involving the AChBP (121, 133, 134, 142). While the AChBP is a soluble protein that is not attached to a transmembrane channel, recent studies in which the AChBP was linked to the transmembrane domain of a 5-HT_3 receptor have confirmed that the AChBP undergoes the conformational changes necessary to gate a Cys-loop receptor pore (7). Crystal structures of the AChBP both in the presence and absence of agonist have shown that the main structural rearrangements resulting from ligand binding involve a repositioning of the C-loop. In the absence of agonist the C-loop extends away from the surface of the protein exposing the binding site to solvent, however upon binding the C-loop closes over the binding site effectively capping it (Figure 1.16)(133, 134). These crystallographic studies are also consistent with AChBP molecular dynamics and fluorescence quenching studies (143). In nAChRs, presumably the conformational changes associated with closing of the C-loop are somehow transferred to the transmembrane pore and result in channel opening.

Unwin has studied the agonist induced structural changes in the nAChR ligand binding domain using cryoelectron microscopy (118). While the cryo-EM data are not of as high resolution as the above AChBP crystallographic studies they have yielded considerable insight. Unlike the AChBP, the nAChR is a heteropentamer formed from four different but highly homologous subunits. In his 4.0Å model of the nAChR's resting state, Unwin noted that within their ligand binding domains, the conformation of the two α-subunit's was different from that of the β-, γ- and δ-subunits (4, 117). Furthermore, the conformation of the non-α-subunits was more similar to that of the liganded AChBP protomer. It appears that

Figure 1.16

Comparison/overlay of the agonist-bound and agonist-free conformations of the AChBP (PDB ID: 1UV6)(133). **(A)** For clarity only two protomers/subunits of the carb-bound and carb-free conformations are shown. The principle (+) subunit is shown in a cartoon representation (green and white), while the complementary (-) subunit is shown as a surface. In the case of the principle subunit, the carb-bound (green) and unbound (white) conformations have been aligned so that the differences resulting from agonist binding can be clearly seen. The conformation of the carb-bound and carb-free structures are almost identical with the exception that the C-loop (thick green and red loop), which is more extended in the agonist-free (red thick loop) conformation than it is in the agonist bound (green thick loop) conformation. **(B)** View of (A) upon ~70° rotation highlighting the changes in conformation of the C-loop upon carb binding (arrow).

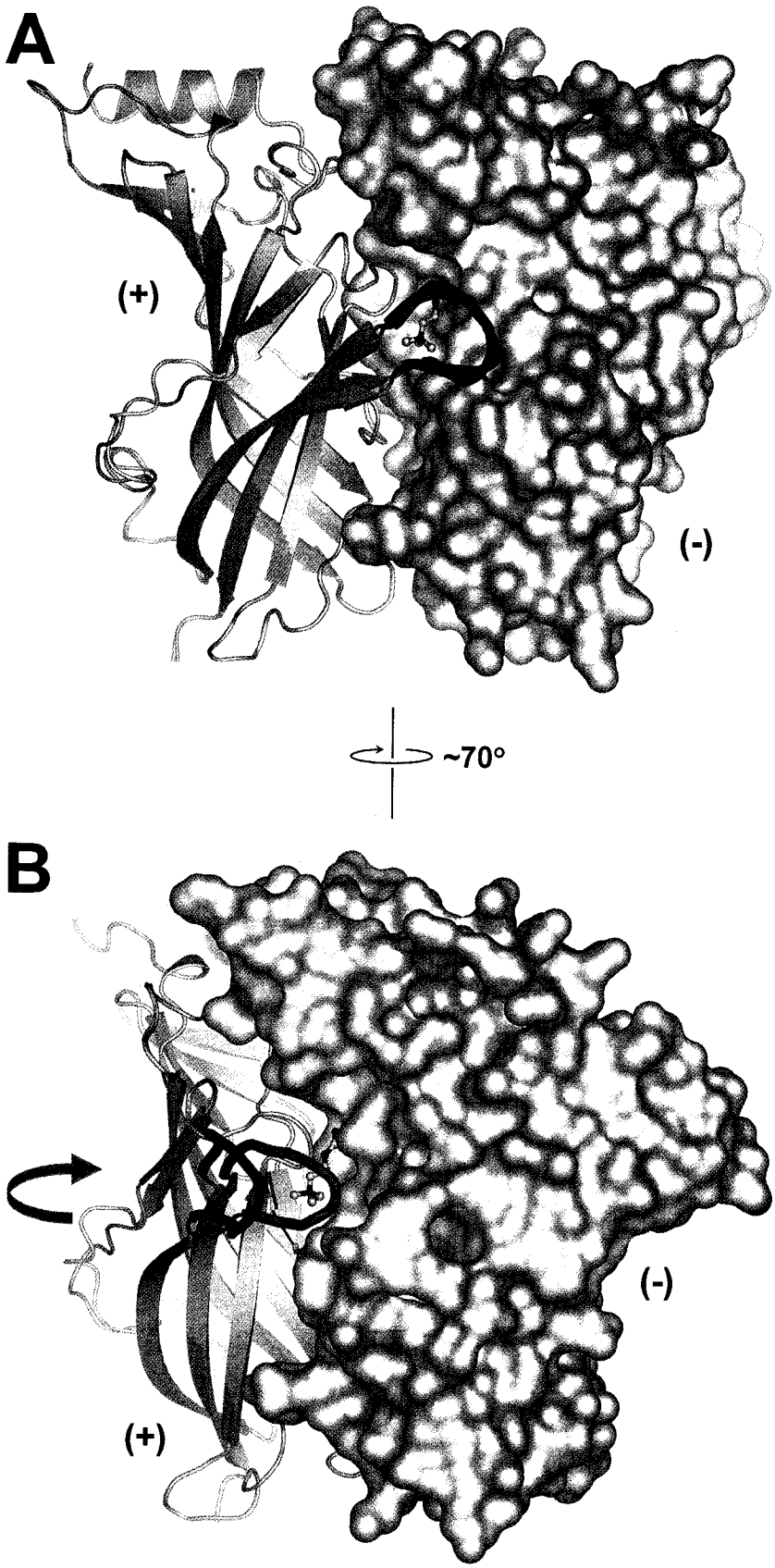
A
(+)
(-)
~70°
B
(-)
(+)

the α-subunits adopt a "strained" conformation in which their inner β-sheets are rotated anticlockwise some 15-16° degrees relative to the other subunits (Figure 1.17). In addition, their C-loops are somewhat extended (117), similar to that seen in the recent unliganded AChBP structures (133, 134). Unwin suggested that the binding of ligand causes the C-loop to be drawn in closer to its location in the non-α/AChBP structures. This movement of the α-subunit C-loop is accompanied by the clockwise relaxation of their inner sheets back to a more non-α/AChBP-like conformation. Since the inner sheet of the ligand binding domain is directly above the channel lining M2 helix of the pore (Figure 1.17), Unwin suggested that the agonist induced relaxation of the α-subunit inner sheets is coupled to movements of α-M2 which open the pore.

In the nAChR's closed conformation, the narrowest region of the pore is formed by a ring of hydrophobic residues contributed from the second transmembrane helix (M2) of each subunit (Figure 1.11). This hydrophobic ring, also referred to as the nAChR's hydrophobic girdle, forms a constriction which is too narrow (diameter ~7.0Å) to allow the passage of a hydrated ion (~8.0Å), thus the structural rearrangements underlying gating of the nAChR's transmembrane ion channel must ultimately involve a widening of the pore within this region. Using cryo-EM Unwin has examined the structure of the nAChR pore in its agonist activated open state (114). The limited (9.0Å) resolution of the current open state model allows for careful speculation as to the conformational changes resulting in opening of the pore. Unwin has suggested that activation forces the five pore lining M2 helices to undergo a clockwise rotation, causing them to collapse back against the outer ring of transmembrane helices (M1, M3 and M4) (Figure 1.18). Such a rotational motion would bring the M2 helices in close apposition with M3. This is consistent with the observation that the relative

Figure 1.17

Superposition of the *Torpedo* α- and δ-subunit ligand binding domains (PDB ID: 2BG9)(4). The two subunits were overlaid by structurally aligning their transmembrane and cytoplasmic domains. The entire ligand binding domain, as well as the top of the transmembrane domain, is shown for the α-subunit. For clarity, only the ligand binding domain is shown for the δ-subunit. Vibrant colours were chosen for the α-subunit, while the corresponding pale colour was used for the δ-subunit. Important regions referred to in the text are coloured differently, and labelled in the figure. In general, the colour scheme is the same as in Figure 1.7. In case of ambiguity, each subunit is labelled in the vicinity of loop 2, the C-loop and the Cys-loop. Arrows represent the approximate movements of the inner and outer β-sheets required to force non-α subunits (β, γ, and δ-subunits) to adopt the "strained"/unliganded α-configuration. Note: the complexity of loop regions has been simplified to allow comparison between the α- and non-α-configurations.

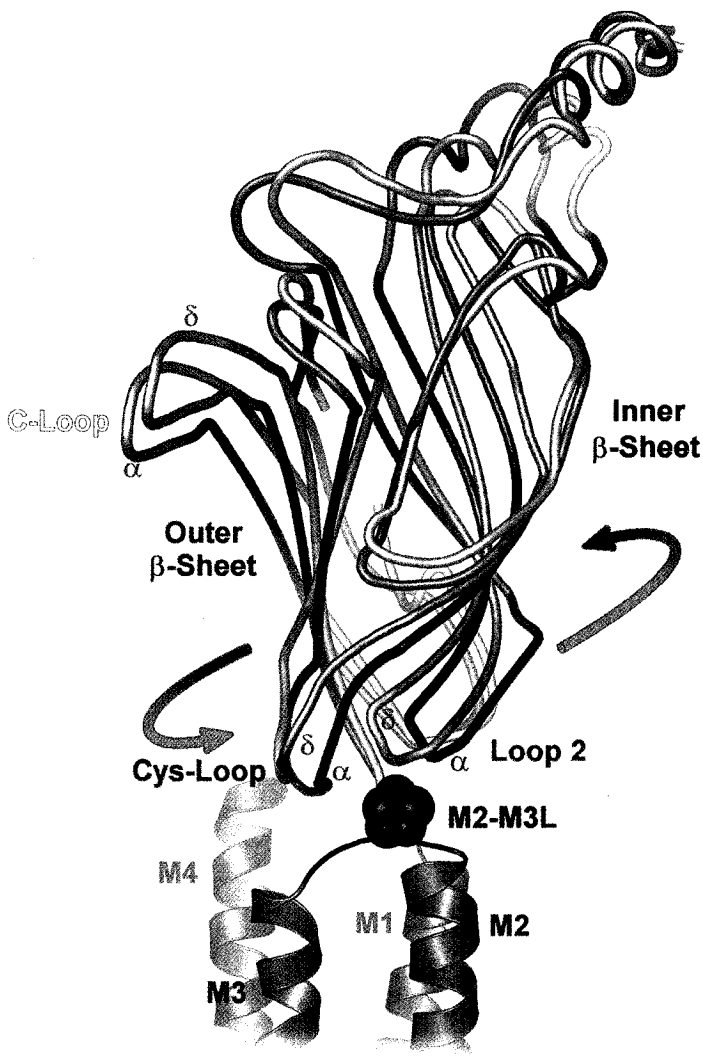
δ
C-Loop
α
Inner
β-Sheet
Outer
β-Sheet
δ
δ
α
α
Loop 2
Cys-Loop
M2-M3L
M4
M1
M2
M3

Figure 1.18

Opening of the ion channel gate involves symmetric motions of the M2 helices towards M3. This movement breaks the hydrophobic gate and increases the inner diameter of the central pore. **(A)** The location of the hydrophobic gate towards the centre of αM2 and the membrane. The yellow spheres represent the position of the two main rings of residues (αL251 and αV255) which associate to form the hydrophobic constriction/gate. **(B)** View of the transmembrane region of the nAChR pore from the synaptic space. The residues in (A) forming the hydrophobic constriction are shown as transparent orange (αL251) and yellow (αV255) spheres. The symmetric clockwise movements of each M2 helix resulting in gating are shown by the green arrows. The red (closed) and green (open) circles show that the diameter of the pore in its narrowest region increases upon gating.

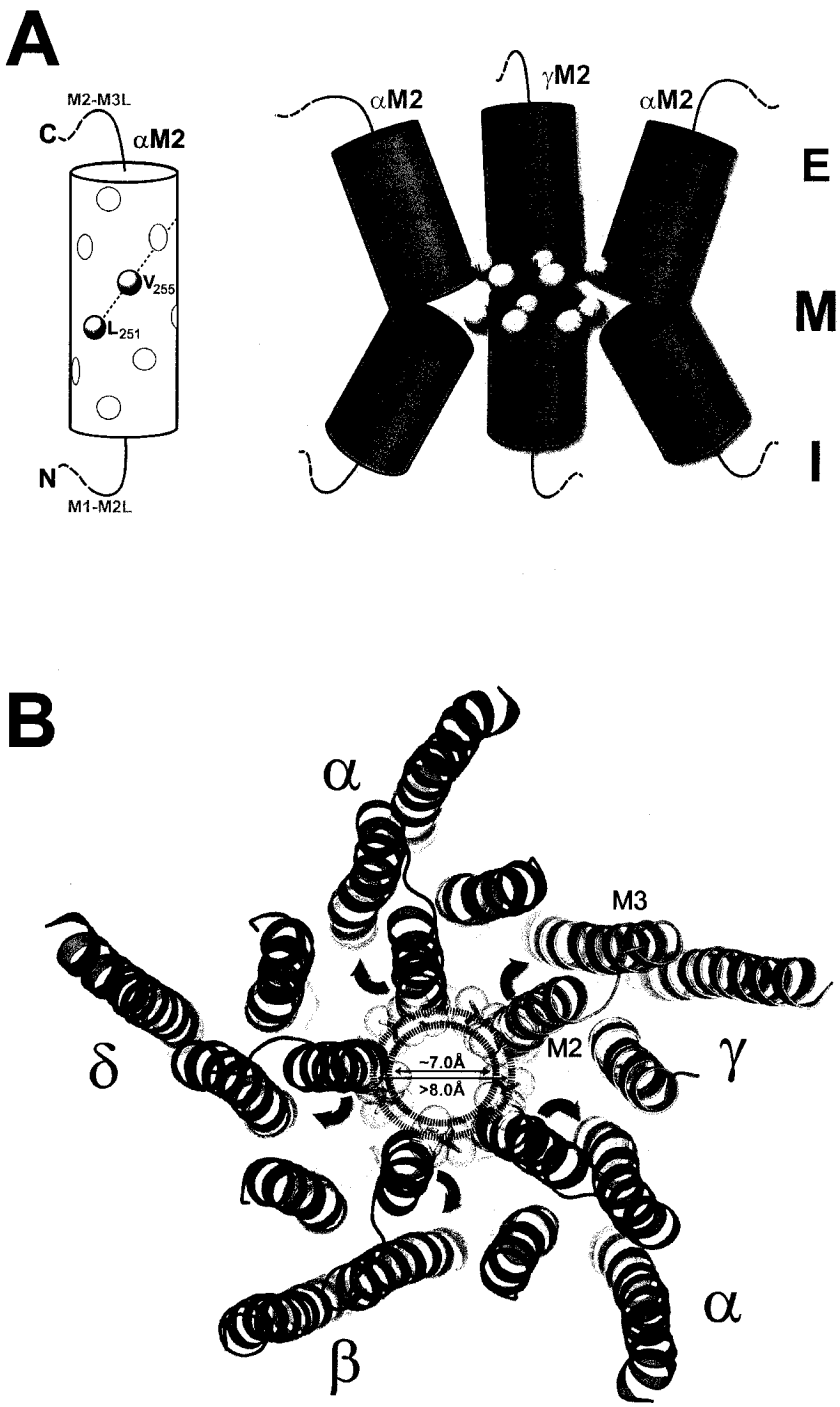
A
M2-M3L
C
αM2
V255
L251
N
M1-M2L
αM2
γM2
αM2
E
M
I
B
α
M3
δ
M2
γ
~7.0Å
>8.0Å
α
β

stability of the open state is dependent upon the volume and stereochemistry of residues within M3 (144).

For the nAChR to convert ligand binding into channel opening, agonist-induced conformational changes in its extracellular ligand binding domain must be communicated to its transmembrane pore, therefore the physical connections between these two distinct structural and functional domains is absolutely essential. Several studies have implicated various structures at the interface between the ligand binding and transmembrane domains as being important for coupling binding to gating. Within the transmembrane domain the short loop connecting M2 and M3 (Figure 1.19), known as the M2-M3 linker, is a well established gating control element (8, 145-149). Mutations within this loop specifically affect nAChR gating kinetics without altering the nAChR's affinity for agonist (147). In particular, a recent study involving unnatural amino acid substitutions has shown that channel opening is directly related to the *cis-trans* conformational preference of a proline residue within the M2-M3 linker (αP272 see Figure 1.19B, top panel)(9).

Within the extracellular ligand binding domain, a number of structures have been implicated in the coupling of agonist binding to channel gating (6-8, 10, 11). Both the eponymous Cys-loop (also known as loop 7) between β-strands β6 and β7, as well as loop 2 between β1 and β2 make direct contacts with the transmembrane domain (Figure 1.19)(4). In order to recover gating in chimaeric receptors formed from the AChBP and the 5-HT_3 receptor transmembrane pore, Bouzat *et al.* found that it was necessary to replace the AChBP Cys-loop and loop 2 with the corresponding 5-HT_3 receptor sequences (7). This directly illustrates that tight association, resulting from structural complementarity between the ligand binding and transmembrane domains is necessary for transmitting conformational changes in the extracellular ligand binding domain to the transmembrane pore. Weak

Figure 1.19

The interface between the extracellular ligand binding domain (LBD) and the transmembrane (TM) pore. **(A)** Ribbon representation of an entire α-subunit. The inner and outer β-sheets of the ligand binding domain are pale blue and pink, respectively, while the transmembrane and cytoplasmic α-helices are yellow. The large dotted lines show the approximate limits of the membrane. Structures at the interface between the two distinct domains have been highlighted and labelled. **(B)** Several enlarged views of the inter-domain interface (boxed region in "A") showing the relative position of residues within the Cys-loop (green) and Loop 2 (cyan) of the ligand binding domain (bottom panel), as well as the M2-M3 linker (M2-M3L, red) from the transmembrane domain (top panel).

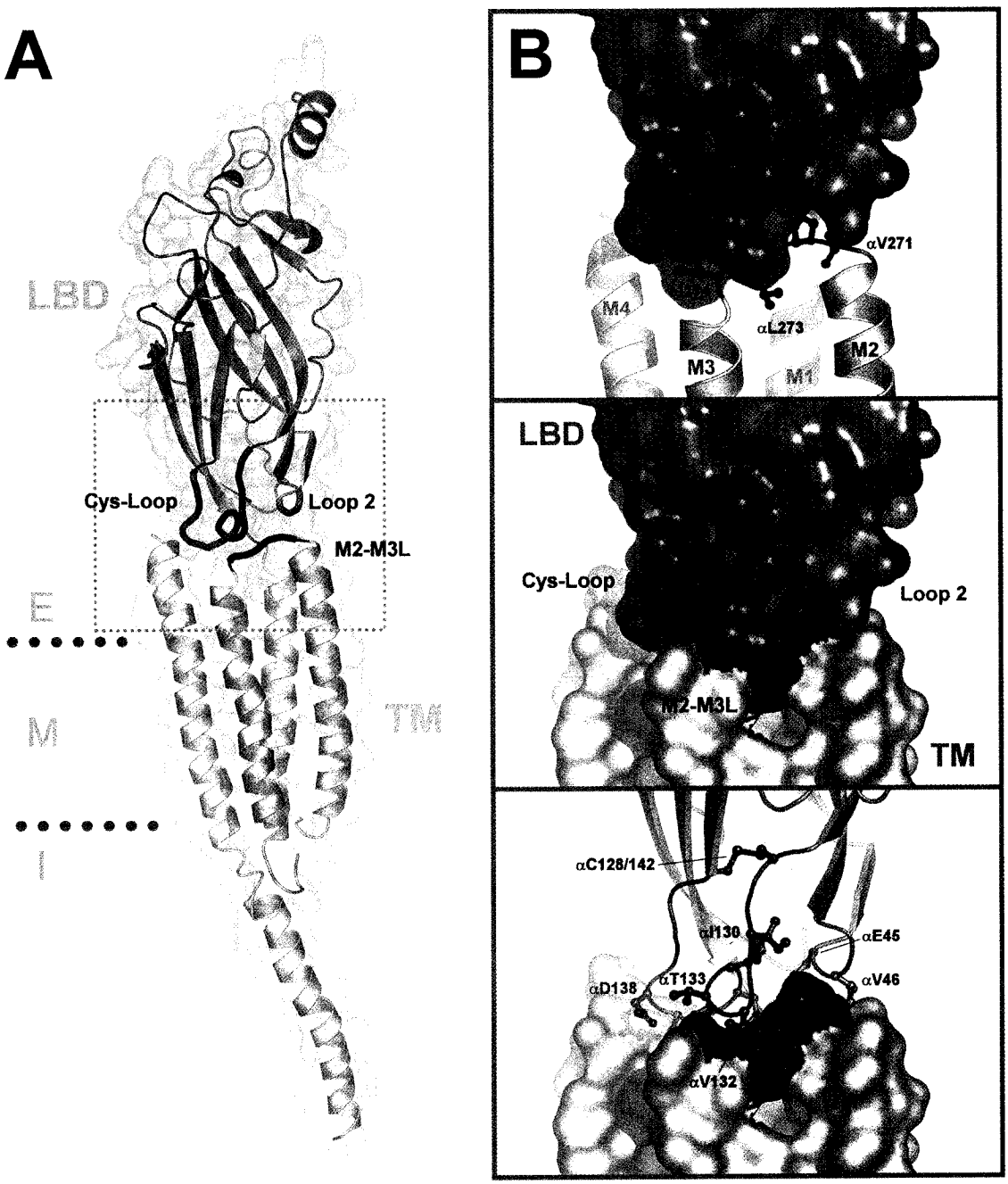
A
LBD
Cys-Loop
Loop 2
M2-M3L
E
M
I
TM
B
αV271
M4
αL273
M3
M2
M1
LBD
Cys-Loop
Loop 2
M2-M3L
TM
αC128/142
αI130
αE45
αD138
αT133
αV46
αV132

interactions between the two domains results in an uncoupling of the nAChR's binding and gating functions (7, 10).

In summary then, the current model for nAChR gating is as follows: agonist binding causes closure of the C-loop, which is accompanied by relaxation of the two α-subunit ligand binding domains back to their non-α conformations (117). Through interactions between loops 2, 7 (Cys-loop) and the M2-M3 linker (6-9, 11), this movement in the α-subunit ligand binding domains is coupled to the clockwise rotation of α-M2 within the transmembrane domain (67). The relative movement of the two α-M2 helices destabilizes the central hydrophobic girdle/gate causing the remaining β, γ and δ-M2 helices to collapse back against the rest of the transmembrane helices (67). The symmetric movement of the five M2 helices widens the inner diameter of the pore to greater than 8Å (114). This diameter is large enough to permit the flow of hydrated sodium and potassium ions. For effective gating to occur there must be a tight coupling between the extracellular ligand binding domain and the transmembrane ion pore(7, 10). This tight association facilitates the transfer of agonist induced conformational changes in the ligand binding domain to the transmembrane pore. Several structures at the interface between the two domains are involved in the gating process (6-11, 150). Some of these structures may be important for ensuring a tight association between the two domains, while others may be directly involved in the conformational changes leading to gating.

1.8 - nAChR-Lipid Interactions

nAChR Purification: A Role for Lipid. Initial studies on the nAChR were performed on receptor rich membranes isolated from the electric organ of electric fish. Because these receptor rich membranes also contained a number of different proteins, there was some debate as to whether the receptor itself contained all the parts necessary for both ligand binding and channel flux properties. As a result there was interest in isolating the nAChR from receptor rich membranes in order to study it in its purified form. Because the nAChR is an integral membrane protein, this required its solubilization and removal from its membrane. Eldefrawi *et al.* solubilized the nAChR from receptor rich membranes using a number of different detergents (151). They found that several of the detergents were able to successfully remove the nAChR from its membrane, however only some detergents were able to retain its ligand binding capabilities. Furthermore, even when solubilized with these detergents the binding properties of the nAChR were different from that of the membrane bound form. These early experiments, while at the time rather puzzling, were the first indication that nAChR function is intimately related to its surrounding membrane.

In the mid to late 1970's there was a race to establish a successful protocol for purifying the nAChR and reconstituting it back into a membrane. For the most part, early attempts were able to recover ligand binding properties (28, 152-157), however ion flux capability proved more problematic. Several reports were published in which despite retaining the ability to bind agonist, recovery of the nAChR's ion flux properties were at best inconsistent (158-161). The irreproducibility of these early attempts was in large part due to a lack of understanding of the parameters necessary for successful nAChR reconstitution. The first reliable protocol leading to successful recovery of both ligand-binding and ion flux,

involved keeping the nAChR in constant contact with solubilized lipids throughout the purification procedure (162). Subsequent reconstitution studies examined in detail the effects of exogenous lipids on nAChR solubilization and function, and optimized the conditions for successful reconstitution (163-165). Jones *et al.* determined the minimum number of lipids required during solubilization and purification in order to retain ion flux capability (166). They found that delipidation to a lipid:protein ratio (LPR) below 45:1 (mol:mol) resulted in irreversible inactivation of the nAChR ion channel. Maintaining a minimum of at least 45 lipids per nAChR during solubilization and purification protected it against inactivation.

The discovery that the addition of exogenous lipids during nAChR purification and solubilization protected its ion flux capability suggested that excessive delipidation could result in inactivation of its ion channel. Interestingly this delipidation did not grossly affect the nAChR's ability to bind agonist, and thus the structure of its ligand binding domain. Given what we now know about nAChR structure, this is perhaps not surprising since the ion channel domain is embedded in the membrane and makes extensive contacts with surrounding lipids (39, 40), while the ligand binding domain is surrounded by solvent and protrudes into the extracellular space (4).

Torpedo nAChR Rich Membranes. The discovery that the nAChR's lipid environment is important for function sparked interest in the composition of the nAChR's surrounding membrane. A number of groups have examined in detail the lipid composition of *Torpedo* nAChR rich membranes (167-169). In general, the membranes are quite diverse both in their lipid head group (Table 1.1) and acyl chain (Table 1.2) compositions. Roughly 25-30% by wt of the *Torpedo* nAChR rich membrane is cholesterol. Of the remaining lipids,

Table 1.1

Lipid head-group composition of *Torpedo* nAChR rich and soybean asolectin membranes . The values are reported as percent by weight (% by wt). PC = phosphatidylcholine, PE = phosphatidylethanolamine, PS = phosphatidylserine, PI = phosphatidylinositol, SM = sphingomyelin and PA = phosphatidic acid. ND = Not detected, (-) = not assayed.

	Approximate percent lipid species by weight (% by wt)			
Reference:	Schiebler & Hucho (167)	Popot *et al.* (169)	Gonzalez-Ros *et al.* (168)	Demel *et al.* (306)
Organism:	*Torpedo californica*	*Torpedo marmorata*	*Torpedo californica*	*Soybean asolectin*
Cholesterol	30	30	25-30	-
PC	32.2	27.3	28.7	24
PE	21.7	27.3	26.8	39
PS	9.8	} 11.9	8.2	19
PI	1.4		ND	1
SM (+ LysoPC)	4.9	0.7	1.7	-
Cardiolipin	-	-	2.5	-
PA	<7	-	2.2	6
Misc.	-	0.7-1	-	11 (Triglycerides Tocopherols, sterols, etc)

Table 1.2

Fatty acid composition of phospholipids in *Torpedo* nAChR rich and soybean asolectin membranes. The values are reported as percent by weight (% by wt).

	Percent fatty acyl chain by weight (% by wt)	
Reference:	Popot *et al.* (169)	Sigma Aldrich (personal communication)
Organism:	*Torpedo marmorata*	*Soybean asolectin*
Myristic ($C_{14:0}$)	0.7	-
Palmitic ($C_{16:0}$)	31	20
Stearic ($C_{18:0}$)	16	4
Oleic ($C_{18:1}$)	12	10
Linoleic ($C_{18:2}$)	-	59
Linolenic ($C_{18:3}$)	-	7
Arachidonic ($C_{20:4}$)	5	-
Icosapentaenoic ($C_{20:5}$)	0.8	-
Docosatetraenoic ($C_{22:4}$)	0.7	-
Docosapentaenoic ($C_{22:5}$)	0.8	-
Docosahexaenoic ($C_{22:6}$)	26	-
Lignoceric ($C_{24:0}$)	5	-

Note: (-) = not assayed.

the vast majority are phospholipids with less than 5% by wt being sphingolipids. The bulk of the phospholipid head groups are either phosphatidylcholine (PC) or phosphatidyl-ethanolamine (PE) moieties, although several other negatively charged phospholipids have been identified, including phosphatidylserine (PS), phosphatidylinositol (PI), phosphatidic acid (PA) and cardiolipin (Card) moieties (Table 1.1). The relative preponderance of anionic headgroups (PS, PA, PI and Card) suggests that the surface of the nAChR rich membranes is somewhat negatively charged. Not only are there diverse lipid head groups, but there are also several different types of acyl chains present (Table 1.2). According to Popot *et al.*, palmitic acid residues are the most common saturated acyl chains, and docosahexaenoic acid residues are the most prevalent unsaturated chains. The complexity and heterogeneity of the nAChR's surrounding lipid environment suggests that nAChR-lipid interactions themselves may be quite complex. In addition, recent studies have shown that homopentameric α7 nAChRs are found in lipid rafts, re-emphasizing the possibility that membrane lipid composition may play a dynamic role in modulating receptor function (218, 219).

Reconstitution into Defined Lipid Mixtures. The finding that in the absence of exogenous lipids the nAChR became inactivated, suggested that lipids somehow stabilized nAChR structure. Whether this effect was a general protective effect of the lipids or the result of a specific interaction between a particular lipid and the nAChR was unclear, largely because the initial lipid mixture used to protect against inactivation (soybean asolectin) contained several different lipid species (Tables 1.1 and 1.2). Subsequent studies examined the nAChR's specific lipid requirements by reconstituting the receptor into vesicles of defined lipid composition and measuring its ability to flux radiolabelled ions (155, 170, 171). Unfortunately, the precise lipid requirements often varied between reports, with some

suggesting that cholesterol was absolutely necessary (155, 171, 172), while others claimed that anionic lipids alone were sufficient (170, 173). These discrepancies could in part be explained by inherent artifacts in the flux measurements stemming from heterogeneity in reconstituted vesicle size and permeability, both parameters which are substantially affected by vesicle lipid composition (163). As a result of the inconsistencies there remains some controversy as to which lipids are absolutely required for flux. In general, early studies highlighted the receptor's rather loose requirement for any one lipid, as several anionic (PS, PA, PG and cardiolipin)(155, 170, 173) and neutral lipids (cholesterol, cholestanol, cholesterol hemisuccinate, vitamin-D3, (±)-α-tocopherol, androstanol and squalene)(173-175) were able to support ion flux. This low chemical specificity argued against a specific cofactor type role for any particular lipid, and instead suggested that nAChR ion channel activity is controlled by a physical property of its surrounding membrane (176).

While there is still some debate as to which lipids the nAChR absolutely requires for function, an emerging consensus is that both phosphatidic acid (anionic) and/or cholesterol (neutral) are particularly good at supporting nAChR function (155, 177). Because both these lipids are known to have membrane ordering effects, it was initially proposed that nAChR function was related to membrane fluidity (155). Subsequent studies however have shown that the presence of anionic and neutral lipids is of utmost importance, and that bulk membrane fluidity plays a minor role (178). Some other physical property of the membrane, imparted by select anionic and neutral lipids must be important for nAChR function.

nAChR-Lipid Affinity: The Lipid Annulus Hypothesis. Even though the nAChR does not exhibit strict specificity for any particular lipid, according to Electron Paramagnetic Resonance (EPR) studies it still discriminates amongst them. EPR, also known as Electron

Spin Resonance (ESR), is a spectroscopic technique particularly suited for the study of biological membranes. Its nanosecond timescale is optimally suited to detect the ultrafast rotational and translational motions of lipids (179). EPR has been used extensively to characterize the interaction of many spin-labelled lipids with a number of different integral membrane proteins, including the nAChR (179-183).

Early EPR studies in which spin labelled lipids were incorporated into native *Torpedo* nAChR-rich membranes showed that the receptor was able to slow both the rotational and translational motions of its surrounding lipids (181). EPR spectra also suggested that a proportion of the lipids were "immobilized", leading to the hypothesis that the nAChR was encircled by a lipid ring or "annulus". The lipids in this ring were thought to have a greater affinity for the receptor's lipid/protein interface. Consistent with this idea was the observation that different spin labelled lipids showed varying proportions of immobilization (180, 182, 183). Amongst the different phospholipid probes tested, spin labelled phosphatidic acid showed the greatest extent of immobilization, suggesting that it had the highest affinity for nAChR (180). A cholesterol-like probe also had a relatively high affinity for nAChR (180), suggesting that the receptor surrounds itself with lipids that are best able to support its ion-channel function.

While the intensity of the perturbed component in the EPR spectra varied from probe to probe (and thus lipid to lipid), its spectral shape remained identical (180). This suggested that even though different amounts of each lipid are immobilized by the receptor, the lipids that are immobilized are all immobilized in an identical way. In other words, while each lipid type interacts with the receptor to a different degree, when they do interact, they interact similarly. Because the lipids were labelled on their acyl chains, and both the labels and the acyl chains were identical for each lipid, the acyl chains of each lipid appear to interact with

the receptor in the same way (180, 184). On the other hand, since there were differences in the amount of lipid immobilized, and the acyl chain portion of the lipids was always the same; the differences in extent immobilized must be due to the variable lipid head groups. Therefore the varying nAChR affinities displayed by different lipids are a result of their head groups and not their acyl chains.

Specific Lipid Binding Sites? While EPR studies showed that the nAChR was surrounded by a lipid annulus, fluorescence quenching studies suggested that there were also "non-annular" sites only accessible to specific lipids (185). Quenching of intrinsic tryptophan fluorescence with brominated phosphatidylcholine (BRPC) moieties could be accounted for by a lipid annulus encircling the perimeter of the nAChR's transmembrane domain, while a mixture of BRPC and brominated cholesterol (BRChol) led to significantly greater quenching (185). This increase in fluorescence quenching in the presence of brominated cholesterol suggested that BRChol was able to access nAChR sites that the BRPC could not. The BRPC quenched annular sites, and the BRChol quenched non-annular sites specific for cholesterol.

These fluorescence quenching studies were consistent with the emerging idea that the receptor contained specific lipid binding sites. Several groups had proposed that interactions between the nAChR and lipids at these sites were important for stabilizing nAChR structure (186-189). In particular, based on a number of early infrared measurements it was thought that the presence of cholesterol in reconstituted nAChR membranes led to an increase in the receptor's α-helical content, while the presence of PA stabilized its β-sheet structures (187-189). While these findings were rather controversial, they could not be discounted given that so little was known about membrane protein structure at the time. Subsequent FTIR studies

by Méthot *et al.* have shown however that reconstituted membrane lipid composition actually has no effect on nAChR secondary structure, but instead modulates nAChR internal dynamics (190). The spectral features originally attributed to differences in nAChR secondary structure could actually be accounted for by artifacts stemming from the lipid-dependent differences in nAChR internal dynamics (see below).

While it has long been proposed that the nAChR transmembrane domain contains specific lipid binding sites, it is important to note that despite substantial effort none have yet been identified (41-43, 175, 191). While "absence of evidence is not evidence of absence", our inability to identify specific lipid binding sites is consistent with the contention that nAChR structure and function is stabilized through some general physical property of its surrounding membrane, rather than a specific molecular interaction between the nAChR and select lipids.

nAChR Structural Effects of Lipids. Given that membrane physical properties modulate nAChR ion channel activity, it has become of particular interest to understand how lipid membranes modulate nAChR structure and function. Early reconstitution experiments showed that despite inactivation of its ion channel, the nAChR retained its pentameric structure as well as its ability to bind agonist (192). This suggested that lipids some how affect the coupling between agonist binding and channel gating (193). Subsequent experiments noted that inactivated receptors were not only unsuccessful in gating, but that they also failed to undergo agonist induced conformational change (155). When reconstituted into a simple dioleoylphosphatidylcholine (DOPC) membrane, the nAChR appeared locked in a non-conducting state in which the binding of agonist no longer elicited a response. Addition of both cholesterol (Chol) and an anionic lipid such as

dioleoylphosphatidic acid (DOPA) restored the nAChR's ability to flux cations and undergo conformational change (155). The recovery of function in the presence of DOPA and Chol was attributed to both the formation of a lipid bilayer with optimal membrane fluidity, as well as a specific structural requirement of the nAChR for each lipid (155). DOPA and Chol were thought to stabilize nAChR secondary structure by binding to specific sites within the receptor's transmembrane domain (186-189).

Subsequent work has led to contradictory conclusions with respect to which lipids are actually required in order to stabilize the nAChR in a functional conformation, as well as what exactly the "non-functional" conformation is. Using chemical labelling techniques and antagonist competition assays, McCarthy & Moore showed that simple mixed membranes composed of egg phosphatidylcholine (EPC) and DOPA were sufficient to stabilize a receptor capable of undergoing conformational change (194). In addition, when the nAChR was reconstituted into mixtures of EPC/Chol or EPC alone it failed to undergo agonist induced conformational change, and displayed a chemical labelling pattern that was essentially identical to that of the agonist-induced desensitized state. This led to the hypothesis that in EPC or EPC/Chol the nAChR adopted the desensitized conformation (194). In contrast, Rankin *et al.* used fluorescence studies involving ethidium bromide to show that mixtures of DOPC/Chol or DOPC/DOPA/Chol support a functional nAChR able to undergo agonist induced activation and subsequent desensitization. However, when the nAChR was reconstituted into DOPC/DOPA or DOPC alone, it failed to undergo conformational change and appeared to be locked in the resting, not the desensitized state (195).

FTIR difference spectroscopy is consistent with the hypothesis that the nAChR adopts a desensitized conformation when reconstituted into a simple phosphatidylcholine

(PC) membrane (177). By taking advantage of the fact that the local anesthetic dibucaine desensitizes the nAChR in the absence of agonist, it is possible to acquire a (±)-agonist difference spectrum from a functional but anesthetic desensitized nAChR (177). Incubation of the nAChR with dibucaine prior to the addition of agonist eliminates the agonist induced conformational changes leading to desensitization. This in turn eliminates the spectral contributions indicative of conformational change, and permits the identification of spectral features resulting solely from agonist binding to a desensitized nAChR. Difference spectra from functional but dibucaine desensitized nAChRs are essentially identical to those from EPC reconstituted nAChRs, which suggests that; a) like desensitized nAChRs the EPC reconstituted nAChRs are unable to undergo conformational change; and b) the EPC reconstituted nAChRs and dibucaine desensitized nAChRs form comparable interactions with agonist, implying a similar structure and conformation of at least their binding sites (177).

While the FTIR difference spectroscopy data was consistent with the hypothesis that PC reconstituted nAChRs are desensitized, it also conflicted with both of the above studies and showed that *either* Chol or DOPA, when incorporated into a PC membrane, was sufficient to stabilize a *proportion* of the nAChRs in a state able to undergo conformational change (177). This led to the hypothesis that lipids modulate the relative number of nAChRs in the resting and desensitized states. This hypothesis was examined in more detail in a subsequent FTIR difference spectroscopy study in which Baenziger *et al.* determined the ability of both Chol and DOPA to independently stabilize a functional, resting state nAChR. The nAChR was reconstituted into EPC membranes with increasing amounts of either Chol or DOPA (176). The relative proportion of nAChRs able to undergo conformational change correlated directly with the amount of either Chol or DOPA added to the EPC membrane.

This further suggested that both of these lipids were able to modulate an equilibrium between the receptor's resting and desensitized states (176). While both lipids could shift this equilibrium towards the resting state, DOPA was far more effective than Chol, and appeared absolutely necessary for stabilizing a fully functional nAChR (176).

nAChR Internal Dynamics and Function: A Correlation? In order to accurately analyze the secondary structure of a protein using infrared spectroscopy it is necessary to acquire protein spectra in ^2H_2O solvent. This is a consequence of extensive overlap between the main protein vibration used for analysis (the amide I band) and solvent ^1H_2O vibrations. As a result protein samples must be exchanged into deuterated buffers. Upon exposure to ^2H_2O, protein peptide hydrogens exchange for deuterons. The rate and extent of peptide $^1H/^2H$ exchange is related to both their exchangeability, and their accessibility. Accessibility is determined not only by the protein's structure, but also by the rates and amplitudes of the protein's internal motions. Protein internal dynamics therefore has the potential to influence the extent of peptide $^1H/^2H$ exchange. Furthermore, since peptide $^1H/^2H$ exchange affects the shape of the amide I band, differences in the extent of peptide $^1H/^2H$ exchange can be erroneously attributed to differences in protein secondary structure. This is precisely the mistake made in early FTIR studies examining nAChR secondary structure upon reconstitution into different membranes. Based on FTIR data, it was originally proposed that cholesterol stabilized the nAChR's α-helical content, while PA stabilized its β-sheet structures (188, 189). Methot *et al.* later showed that membrane lipid composition has no effect on nAChR secondary structure, but instead modulates nAChR internal dynamics and thus $^1H/^2H$ exchange kinetics (190). Subsequent, more in depth studies have shown that increasing levels of either DOPA or Chol in a reconstituted EPC membrane progressively

decreases the rate and extent of nAChR peptide $^{1}H/^{2}H$ exchange. It appears that the addition of either Chol or DOPA to an EPC membrane leads to a slowing of nAChR internal dynamics (196). Since increasing amounts of each of these lipids also increasingly stabilizes a resting state nAChR (176), there appeared to be a link between nAChR internal dynamics and function. Furthermore since both these lipids also decrease membrane fluidity it appeared that fluidity was related to nAChR internal dynamics, which was in turn is related to nAChR function (176, 196).

CHAPTER 2

MANUSCRIPT:

1. **Corrie J.B. daCosta,** Andrei A. Ogrel, Elizabeth A. McCardy, Michael P. Blanton and John E. Baenziger. (2002) **Lipid-protein interactions at the nicotinic acetylcholine receptor: a functional coupling between nicotinic receptors and phosphatidic acid containing lipid bilayers.** *J. Biol. Chem.* **277**, 201-208.

2.1 - Preface

This manuscript is the first of three first author publications presented in this thesis. Originally published in the Journal of Biological Chemistry in January of 2002, this paper is my first publication. The goal of this work was to perform a preliminary biophysical characterization of the physical properties of several model membranes either in the presence or absence of purified nAChR from *Torpedo*. This preliminary characterization was to lay the groundwork for more detailed solid-state NMR studies aimed at correlating membrane physical properties with their ability to stabilize a functional nAChR.

I initiated and performed almost all of the FTIR experiments presented in this manuscript. Dr. Andrei Ogrel collected some of the difference spectra, and also performed the temperature experiments involving the deuterated lipids. The chemical labelling studies were carried out by Elizabeth A. McCardy in the laboratory of Dr. Michael P. Blanton at Texas Tech University.

2.2 - Abstract

The structural and functional properties of reconstituted nicotinic acetylcholine receptor membranes composed of phosphatidylcholine either with or without cholesterol and/or phosphatidic acid have been examined to test the hypothesis that receptor conformational equilibria are modulated by the physical properties of the surrounding lipid environment. Spectroscopic and chemical labelling indicate that the receptor in phosphatidylcholine alone is stabilized in a desensitized-like state, while the presence of either cholesterol or phosphatidic acid favours a resting-like conformation. Membranes that effectively stabilize a resting-like state exhibit a relatively large proportion of non-hydrogen bonded lipid ester carbonyls suggesting a relatively tight packing of the lipid head groups and thus a well ordered membrane. Functional reconstituted membranes also exhibit gel-to-liquid crystal phase transition temperatures that are higher than those of non-functional reconstituted membranes composed of phosphatidylcholine alone. Significantly, incorporation of the receptor into phosphatidic acid containing membranes leads to a dramatic increase in both the lateral packing densities and the gel-to-liquid crystal phase transition temperatures of the reconstituted lipid bilayers. These results suggest a functional link between the nAChR and the physical properties of phosphatidic acid containing membranes that could underlie the mechanism by which this lipid preferentially enhances receptor function.

2.3 - Introduction

Many hypotheses have been suggested to account for the functional sensitivity of the nicotinic acetylcholine receptor (nAChR) from *Torpedo* to the lipid composition of its surrounding environment (197, 198). Roles for bulk membrane fluidity(155), specific lipid binding sites (176, 189), and annular lipids (180, 181) have all been proposed. Despite numerous studies aimed at understanding lipid-protein interactions at the nAChR, however, there is still disagreement even as to which lipids are absolutely required for optimal function. Consequently, the molecular mechanisms by which lipids modulate function remain poorly understood. The lack of definitive insight reflects both the complexities of lipid-protein interactions at the nAChR and the inherent difficulties associated with characterizing the structural and dynamic properties of the nAChR and its surrounding lipids in a membrane environment.

The pioneering work of the Barrantes and McNamee laboratories originally highlighted the requirement for anionic and/or neutral lipids such as phosphatidic acid and cholesterol (Chol), respectively, in reconstituted phosphatidylcholine membranes to stabilize a functional nAChR (153, 155, 172). It was suggested that phosphatidic acid and Chol stabilize distinct β-sheet and α-helix structures, respectively (186-189). In contrast, more recent studies indicate that lipids exert their effects on nAChR function through subtle structural alterations (177, 190). The nAChR in egg phosphatidylcholine (EPC) membranes lacking both neutral and anionic lipids appears to be stabilized in a non-conducting desensitized-like conformation (176, 194). Increasing levels of either Chol or dioleoylphosphatidic acid (DOPA) in EPC membranes stabilize an increasing proportion of nAChRs in a resting-like state that is capable of undergoing agonist induced conformational

change (176). Both lipids also slow nAChR internal motions and increase the lateral packing density of the lipid bilayers (196). These findings were incorporated into the model of lipid action at the nAChR presented in Figure 2.1 (176). A basic tenet of the model is that the equilibrium between the resting and the non-conducting desensitized states is modulated by bulk physical properties of the lipid bilayer. Specific anionic lipid binding sites are also likely important (see (176) for a detailed discussion of the model).

The hypothesis that membrane physical properties influence nAChR function is not new, but there is contradictory evidence both in support of and against such a mechanism of lipid action (155, 178, 188, 196). As we have suggested previously (176), this controversy may stem from the fact that studies testing the link between fluidity and function have generally relied on spin label and fluorescent probes to assess the physical properties of the reconstituted nAChR membranes. Both approaches have characterized the reconstituted membranes in terms of a single parameter, which may not be sufficient considering the complex motional and dynamic properties of lipid bilayers. A combination of solid state ^{2}H NMR spectroscopy and molecular modelling can provide a more comprehensive picture of the motions and dynamics of lipids in a membrane environment and could lead to a more accurate assessment of the link between fluidity and nAChR function (199, 200). ^{2}H NMR spectroscopy requires membrane lipids with either perdeuterated or single-site-deuterium-labelled fatty acyl chains. Lipids such as 1-palmitoyl-2-oleoyl phosphatidylcholine (POPC) and 1-palmitoyl-2-oleoyl phosphatidic acid (POPA) perdeuterated along the saturated palmitoyl chain are commercially available and are ideal for such a study because interpretation of the ^{2}H quadrupolar splittings is not complicated by the orientational constraints of a double bond (201). Unfortunately, ^{2}H NMR/molecular modelling studies are extremely time consuming and require the acquisition and analysis of extensive NMR data.

Figure 2.1

A speculative model of lipid-protein interactions at the nAChR. The model suggests that membrane fluidity modulates nAChR conformational equilibria with a relatively fluid membrane stabilizing a desensitized-like conformation and a membrane of low fluidity stabilizing a resting-like state. Anionic lipids such as DOPA and POPA are required for the nAChR to adopt a fully functional conformation. Conformational states intermediate between the resting and desensitized states are also possible.

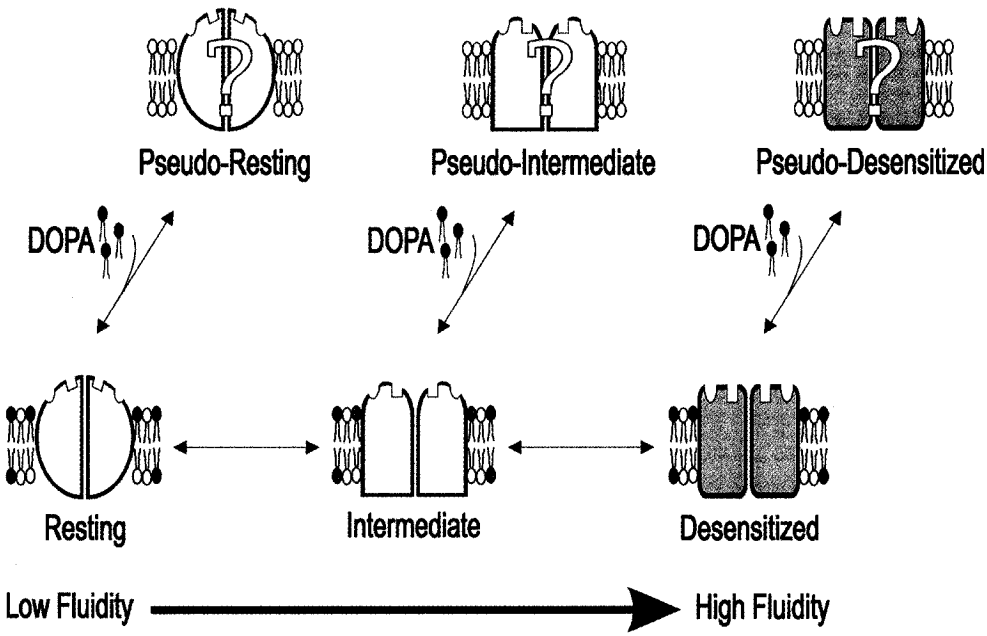
Pseudo-Resting
Pseudo-Intermediate
Pseudo-Desensitized
DOPA
DOPA
DOPA
Resting
Intermediate
Desensitized
Low Fluidity
High Fluidity

The structural and functional properties of the nAChR in mixtures of POPC, POPA, and Chol have also not been defined.

As a first step towards rigorously testing the hypothesized link between nAChR conformational equilibria and the physical properties of the lipid environment surrounding the nAChR, we characterise here the structural and functional properties of reconstituted nAChR membranes composed of POPC, 3:2 POPC/POPA, 3:2 POPC/1,2-dioleoyl phosphatidic acid (DOPA), 3:2 POPC/Chol, and 3:1:1 POPC/POPA/Chol using both Fourier transform infrared (FTIR) spectroscopy and chemical labelling techniques. These lipid mixtures were chosen because each lipid is available in a deuterated form and because preliminary studies suggested that the mixtures should stabilize the nAChR predominantly in either a resting-like (3:2 POPC/POPA, 3:2 POPC/DOPA, 3:2 POPC/Chol, and 3:1:1 POPC/POPA/Chol) or a desensitized-like (POPC) state. As Chol, DOPA, and POPA have distinct structures and likely distinct effects on membrane physical properties, these mixtures provide simple systems in which potential links between the membrane environment and nAChR function can be rigorously tested.

We have characterised the physical properties of the reconstituted nAChR membranes using FTIR spectroscopy, which provides detailed, but qualitative insight into the motional properties of membrane lipids (202). The FTIR data are consistent with a modulation of nAChR conformational equilibria by membrane fluidity, but show that the physical properties of even these simple reconstituted membranes are complex. Significantly, the data indicate that the nAChR selectively influences the physical properties of the lipid environment in which it is imbedded when either DOPA or POPA is present. This novel finding provides direct evidence for a coupling between the physical properties of phosphatidic acid containing membranes and the functional state of the nAChR that could

underlie a mechanism by which lipids modulate nAChR function. The structural and functional characterization of the nAChR in these lipid mixtures also provides a basis for future ^{2}H NMR/molecular modelling studies aimed at further testing the link between fluidity and function.

2.4 - Experimental Procedures

Materials. Frozen *Torpedo californica* electroplax tissue was obtained from either Marinus (Long Beach, CA) or Aquatic Research Consultants (San Pedro, CA). POPC, POPA and DOPA were from Avanti Polar lipids, Inc. (Alabaster, AL) and both cholesterol and carbamylcholine (Carb) were from Sigma (St. Louis, MO). 3-trifluoromethyl-3-(*m*-[^{125}I]iodophenyl) diazirine ([^{125}I]TID; ~10 Ci/mmol) was obtained from Amersham Pharmacia Biotech (Piscataway, NJ) and stored in ethanol at 4°C.

nAChR Purification and Reconstitution. The nAChR was affinity purified on a bromoacetylcholine bromide-derivatized Affi-Gel 102 column (Bio-Rad; Richmond, CA) as described previously (194), but with several modifications. For each reconstitution, crude nAChR membranes from roughly 100 g of *Torpedo* electroplax tissue were solubilized for one hour at 4°C in a total volume of 100 ml dialysis buffer (100 mM NaCl, 10 mM Na_2PO_4, 0.1 mM EDTA, 0.02% w/v NaN_3, pH = 7.8) containing 1% cholate. The solubilized membranes were centrifuged for 30 minutes at 87,000 x g to pellet insoluble material and the supernatants applied to a 10 ml affinity column at a flow rate of 1 ml/min. The column was then washed with 32.5 ml of a 1.3 mM lipid solution in 1% cholate dialysis buffer. This was followed by a 15 ml linear gradient to a 3.2 mM lipid solution in 1% cholate dialysis buffer and an additional 15 ml wash to facilitate complete exchange of endogenous for defined

lipids. A 15 ml linear gradient to a 0.13 mM lipid solution in 0.5% cholate dialysis buffer was followed by a 35 ml wash. The nAChR was then eluted with a 0.13 mM lipid solution in 250 mM NaCl, 0.1 mM EDTA, 0.02% NaN_3, 5 mM phosphate, pH 7.8 with 0.5% cholate and 10 mM Carb. All lipid washes were at 2 ml/min under the control of a Pharmacia FPLC (Uppsala, Sweden). Fractions with an A_{280} greater than 0.05 were pooled in dialysis bags (12-14,000 Daltons cut off) and dialyzed five times against 2 litres of dialysis buffer with buffer change once every 12 hours.

The dialyzed membranes were centrifuged at 120,000 x g for 2 hours to pellet the reconstituted membranes. Yields were typically 6-10 mg of nAChR protein as determined by BCA assay (Pierce; Rockford, Il). The purity of all nAChR samples were analyzed by 12 % SDS PAGE with Coomassie Blue staining. Lipid-protein molar ratios were calculated by FTIR (203) and were generally found to be in the 140-180:1 molar range (Table 2.2). The final lipid composition of each reconstituted membrane was assessed by thin layer chromatography using Silica gel 60 WF_{254} aluminium sheets from Merck (Darmstadt, Germany) in $CHCl_3/CH_3OH/H_2O$, 65/25/5, v/v/v. Lipids were visualized with a 0.05% w/v solution of $FeCl_3 \bullet 6H_2O$ in 90:5 v/v water/glacial acetic acid, followed by heating at 100°C. The final lipid composition of each reconstituted sample did not vary qualitatively from control lipid mixtures. No endogenous lipids were detected.

Transmission FTIR Spectroscopy. All FTIR spectra were recorded on either a Bio-Rad FTS 575 or a FTS 40 spectrometer (Randolph, MA), both equipped with a DTGS detector. For each sample, 250 μg of reconstituted nAChR in 50 μL of 2mM ^1H_2O phosphate buffer (pH 7.0) was centrifuged and the pellet resuspended in 300 - 400 μl of 2 mM ^2H_2O phosphate buffer pH 7.0. After repeating once, the final ^2H_2O suspensions were

incubated at 4°C for precisely 72 hours in order to exchange peptide N-^{1}H for N-^{2}H and then stored at -80°C. Prior to FTIR analysis, samples were individually thawed, centrifuged, and resuspended in 30 μL of ^2H_2O phosphate buffer. After five freeze thaw vortex cycles, each was deposited on a 1 cm diameter CaF_2 window and the excess buffer evaporated with a gentle stream of dry nitrogen. The nAChR film was rehydrated with 8 μL of Torpedo Ringer buffer in ^2H_2O (pD 7.0) and sandwiched between a second CaF_2 window with a 12 μm Teflon spacer. The sandwich was placed in a thermostatically controlled transmission cell from Harrick Scientific (Ossining, New York) and spectra recorded at 2 cm^{-1} resolution signal averaging 4000 scans. Spectra were analysed using GRAMS/32 v.5.01 software (Galactic; Salem, NH) to test for and if necessary subtract uncompensated water vapour (204). Deconvolution of the amide I and lipid carbonyl stretching bands was performed with $\gamma = 10.0$ and a smoothing parameter of 70%.

Thermotropic phase behaviour. Reconstituted nAChR membranes prepared as described above were placed in the thermostatic transmission cell equilibrated with circulating water from a Neslab (Newington, NH) RTE-110 water bath/circulator. Spectra (2 cm^{-1} resolution and 128 scans) were recorded at 1°C intervals as the sample was cooled from 35°C to -10°C using the software program DeltaTemp from Neslab. The actual temperature of the sample cell was monitored using an electronic thermometer (Barnant; Barrington, IL) with a Type J thermocouple probe. A 5 minute time interval was allowed for the water bath to equilibrate at each temperature and then a further 10 minutes for sample equilibration.

FTIR difference spectroscopy. FTIR difference spectra were recorded at 22.5°C using the attenuated total reflectance technique as described in detail elsewhere (205, 206). All spectra were recorded at 8 cm^{-1} resolution signal averaging 512 scans per spectrum.

Each presented spectrum is the average of between 35 and 70 individual difference spectra recorded from at least two different films from at least two separate reconstitutions (see Appendix for a statistical analysis of difference spectra). The difference spectra were baseline corrected between 1800 and 1000 cm^{-1} and were interpolated to an effective resolution of 4 cm^{-1}.

Photolabelling with [^{125}I]TID. nAChR conformation and agonist-induced state transitions were assessed by the technique of hydrophobic photolabelling with 3-trifluoromethyl-3-(*m*-[^{125}I]iodophenyl) diazirine ([^{125}I]TID) as described in detail elsewhere (194, 207-209). Briefly, an aliquot containing 250 μg nAChR protein from each affinity-purified membrane was incubated at a protein concentration of 0.227 mg/ml in a 0.4 μM [^{125}I]TID solution (10 mM MOPS, 100 mM NaCl, 0.1 mM EDTA, and 0.02% NaN_3, pH 7.5) either with or without 400 μM Carb. After 2 hours at room temperature under reduced lighting conditions, each sample was irradiated with a 365 nm UV lamp (Spectroline EN-280L) for 7 minutes at a distance of less than 1 cm. The membranes were centrifuged at 39,000 x g for 1 hour and the resulting pellets solubilized in electrophoresis sample buffer. Individual nAChR subunits were separated by SDS-PAGE using 1.0 mm thick gels. The separating gel was composed of 8% polyacrylamide/0.33% bis-acrylamide. The gels were stained with Coomassie Blue R-250 to visualise nAChR subunit bands and were then dried and exposed to Kodak X-OMAT LS film with an intensifying screen at -80°C (2-18 h exposure). [^{125}I]TID incorporation into each nAChR subunit was quantified by cutting out the receptor bands from the dried 8% acrylamide gel and then assessing the amount of ^{125}I cpm in each band by γ-counting in a Packard Cobra II gamma counter (10 minute counting time/ band).

2.5 - Results

nAChR structure and internal dynamics. FTIR spectra of the nAChR recorded in ^2H_2O buffer exhibit two intense protein bands that are sensitive to protein structure and dynamics (124). The amide I band between 1600 and 1700 cm^{-1} reflects predominantly the carbonyl stretching vibration of the polypeptide backbone and its shape is highly sensitive to protein secondary structure. The amide I band shapes observed in spectra of the nAChR reconstituted into membranes composed of POPC, 3:2 POPC/Chol, 3:2 POPC/POPA, 3:2 POPC/DOPA, and 3:1:1 POPC/POPA/Chol are all similar. Deconvolution shows that each exhibits the same number of component bands with similar frequencies and relative intensities. The similarities of the deconvolved spectra indicate, in contrast to earlier studies (155, 187), that the secondary structure of the nAChR is essentially unaffected by the presence or absence of neutral and anionic lipids.

Close inspection of the resolution enhanced spectra, however, reveals that the presence of Chol and/or either POPA or DOPA in the POPC membranes leads to a subtle increase in intensity of the α-helix component band near 1655 cm^{-1} and a slight decrease in intensity between 1640 and 1650 cm^{-1}. α-Helical vibrations shift down from 1655 cm^{-1} to between 1640 and 1650 cm^{-1} upon peptide $^1H/^2H$ exchange (126, 127). The slight increase in intensity near 1655 cm^{-1} in the presence of Chol and/or POPA or DOPA could reflect a slight increase in the proportion of α-helical peptides that remain in a protiated versus a deuterated form after 3 days exposure to ^2H_2O. In agreement with this interpretation, the residual amide II intensity between 1520 and 1580 cm^{-1}, which is directly related to the number of unexchanged peptide hydrogens, is slightly more intense in spectra of the nAChR reconstituted into POPC membranes containing Chol and/or POPA or DOPA than in spectra

of the nAChR reconstituted into POPC alone (Figure 2.2, right panel). The increased amide II band intensity suggests a slowing of peptide $^{1}H/^{2}H$ exchange in POPC membranes that contain Chol and/or POPA or DOPA (see Discussion).

nAChR Conformational Equilibria. The effect of lipid composition on nAChR conformational equilibria was first examined using FTIR difference spectroscopy. The difference between spectra of the nAChR recorded in the presence and absence of Carb (referred to as a Carb difference spectrum) exhibits five positive marker bands centred near 1663, 1655, 1547, 1430 and 1059 cm^{-1} (the latter two not shown). These marker bands, which reflect vibrational changes associated with the resting to desensitized conformational transition (177, 206), are evident in difference spectra recorded from the nAChR reconstituted into 3:1:1 POPC/POPA/Chol, 3:2 POPC/POPA, and 3:2 POPC/DOPA membranes (Figure 2.3). The positive intensity indicates that each membrane stabilizes a resting-like state that is capable of undergoing agonist induced conformational change. In contrast, positive intensity at each of the five marker frequencies is absent in difference spectra recorded from reconstituted POPC membranes suggesting that the nAChR cannot respond to agonist binding and is likely stabilized in a desensitized state (see below). The nAChR in 3:2 POPC/Chol exhibits some positive intensity at the marker frequencies suggesting that Chol has a limited ability to stabilize a functional nAChR.

The effect of lipid composition on nAChR conformational equilibria was examined further by photolabelling with the conformationally-sensitive probe [^{125}I]TID (194, 207-209). In 3:1:1 POPC/POPA/Chol membranes (as well as native *Torpedo* membranes), [^{125}I]TID photoincorporates into each nAChR subunit with ~4 fold-greater incorporation into the γ-subunit relative to each of the other subunits (Figure 2.4). Addition of agonist and

Figure 2.2

The deconvolved amide I band (left panel) and residual amide II band intensity (right panel) in FTIR spectra recorded from the nAChR reconstituted into A) 3:1:1 POPC/POPA/Chol, B) 3:2 POPC/DOPA, C) 3:2 POPC/POPA, D) 3:2 POPC/Chol, and E) POPC. The amide II bands presented in the right panel are not deconvolved. All samples were exposed to $^{2}H_2O$ buffer for 72 hours at 4°C prior to data acquisition. A spectrum of $^{2}H_2O$ buffer has been subtracted from each.

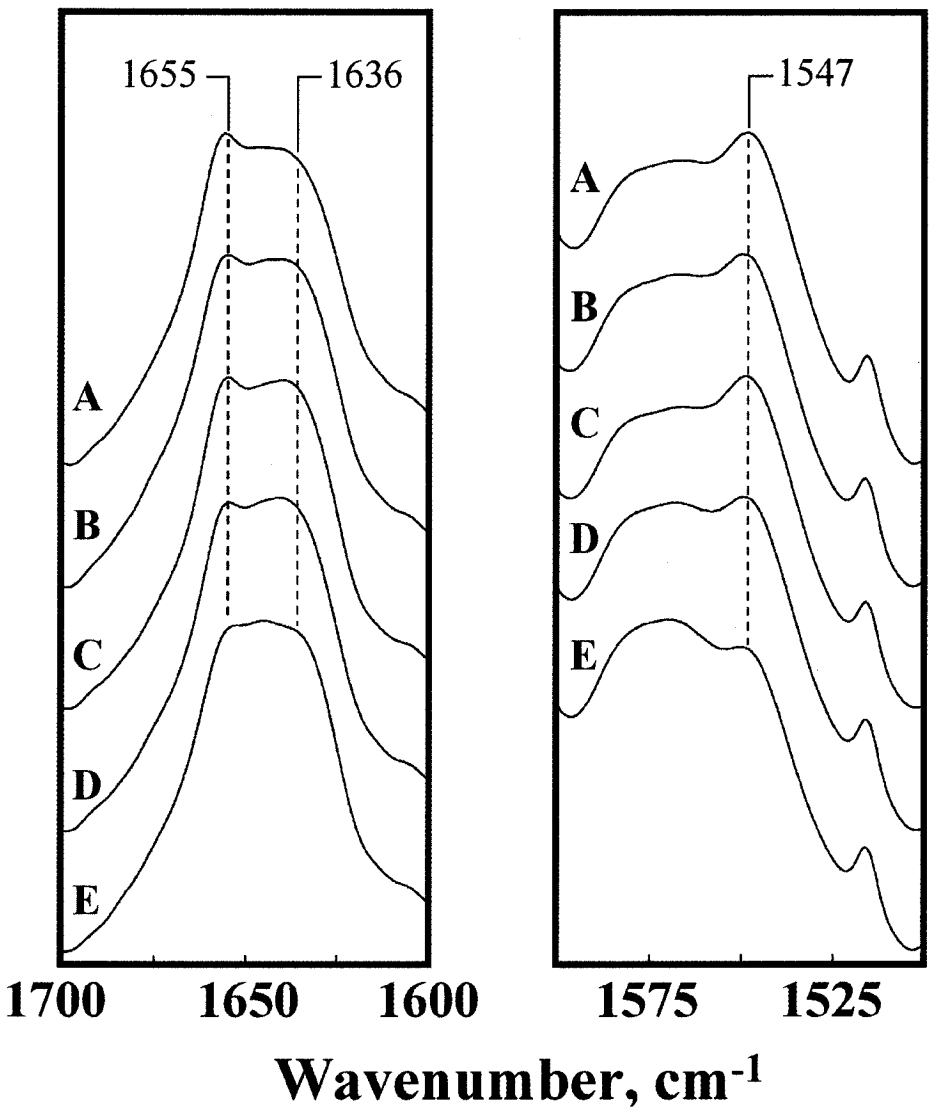
1655
1636
1547
A
B
C
D
E
1700
1650
1600
1575
1525
Wavenumber, cm-1

Figure 2.3

A selected region of Carb difference spectra recorded from the nAChR reconstituted into membranes composed of A) 3:1:1 POPC/POPA/Chol, B) 3:2 POPC/DOPA, C) 3:2 POPC/POPA, D) 3:2 POPC/Chol, and E) POPC. Positive intensity near 1663, 1655, and 1547 cm^{-1} is associated with the resting to desensitized conformational change. Note that a change in intensity near 1663 cm^{-1} is most easily visualised by a change in overlapping negative band intensity near 1668 cm^{-1} (206). Positive intensity at each of these frequencies in traces A to C indicates that the nAChR in 3:1:1 POPC/POPA/Chol, 3:2 POPC/DOPA, and 3:2 POPC/POPA undergoes desensitization upon Carb binding. The absence of positive intensity in trace E indicates that the nAChR in POPC cannot respond to Carb binding and is likely stabilized in a desensitized state. The nAChR in 3:2 POPC/Chol (trace D) exhibits some intensity at each frequency suggesting a limited ability to respond to Carb binding. A small proportion of the nAChRs may be stabilized in a resting-like state in 3:2 POPC/Chol. Both the horizontal line and the shading is included in each spectrum for a visual reference.

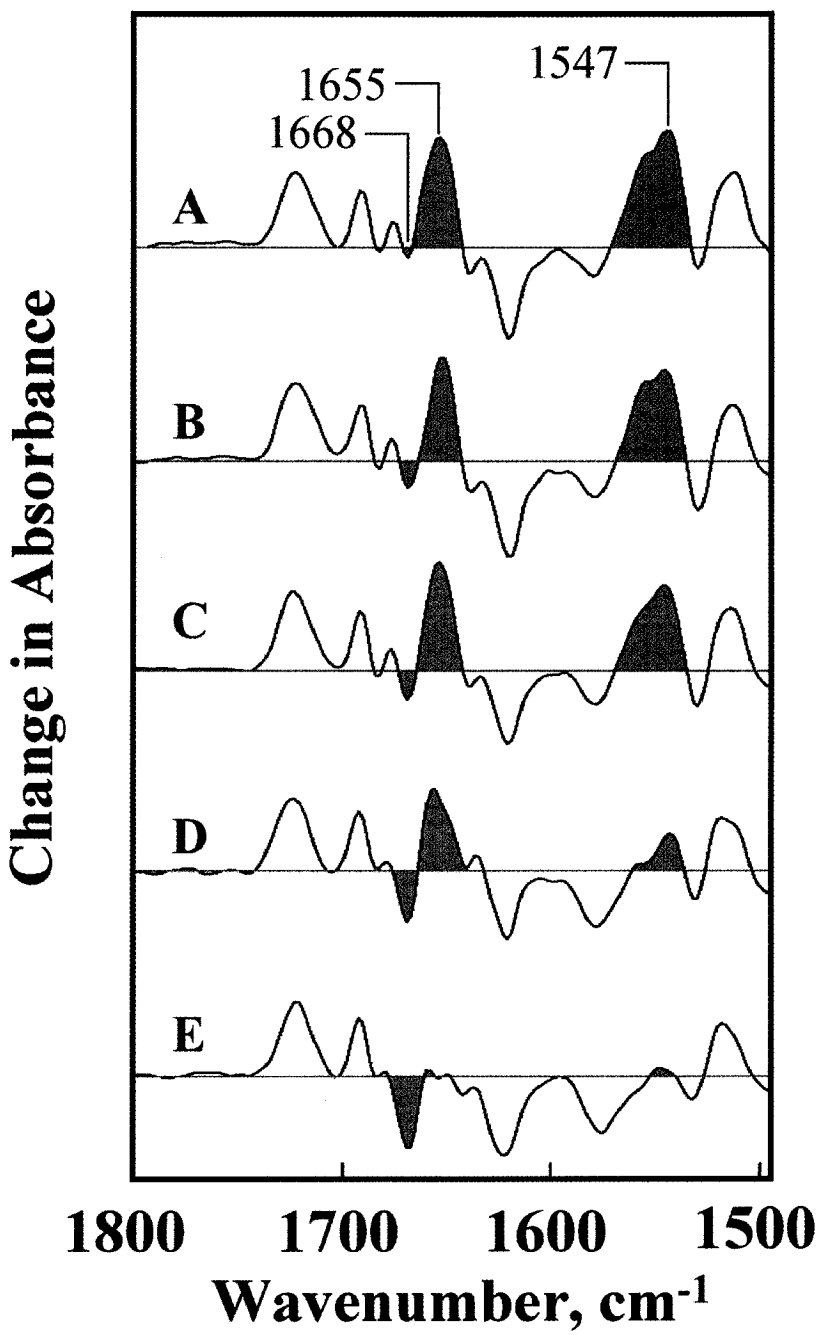
1655
1668
1547
A
B
C
D
E
Change in Absorbance
1800
1700
1600
1500
Wavenumber, cm-1

Figure 2.4

Effects of Carb on the photoincorporation of [^{125}I]TID into the nAChRs reconstituted into defined lipids. Affinity-purified nAChR reconstituted into membranes composed of 3:1:1 POPC/POPA/Chol, 3:2 POPC/POPA, 3:2 POPC/DOPA (data not shown), 3:2 POPC/CH, and POPC was equilibrated 2 hrs with [^{125}I]TID (0.4 μM) in the absence (- lanes) and in the presence (+ lanes) of 400 μM Carb, irradiated at 365 nm for 7 minutes, and the polypeptides resolved by SDS-PAGE. **(A)** Shown is the corresponding autoradiographs of gels containing the [^{125}I]TID labelling experiments for each of the defined lipid environments. The positions of the nAChR subunits are indicated on the left. Note that the autoradiographs for the 3:2 POPC/CH and POPC samples were exposed for much longer times (9 and 6 hours, respectively) than the autoradiographs for the 3:1:1 POPC/POPA/Chol and 3:2 POPC/POPA samples (2 hours each). **(B)** For each [^{125}I]TID labelling experiment, individual nAChR subunit bands were excised from the dried gel and the amount of [^{125}I]TID photoincorporated into each subunit determined by gamma counting (10 minute counting time). Shown are bar graphs of the amount of ^{125}I cpm incorporated into each nAChR subunit in the absence or presence of carbamylcholine (-/+) and presented as the average of triplicate determinations.

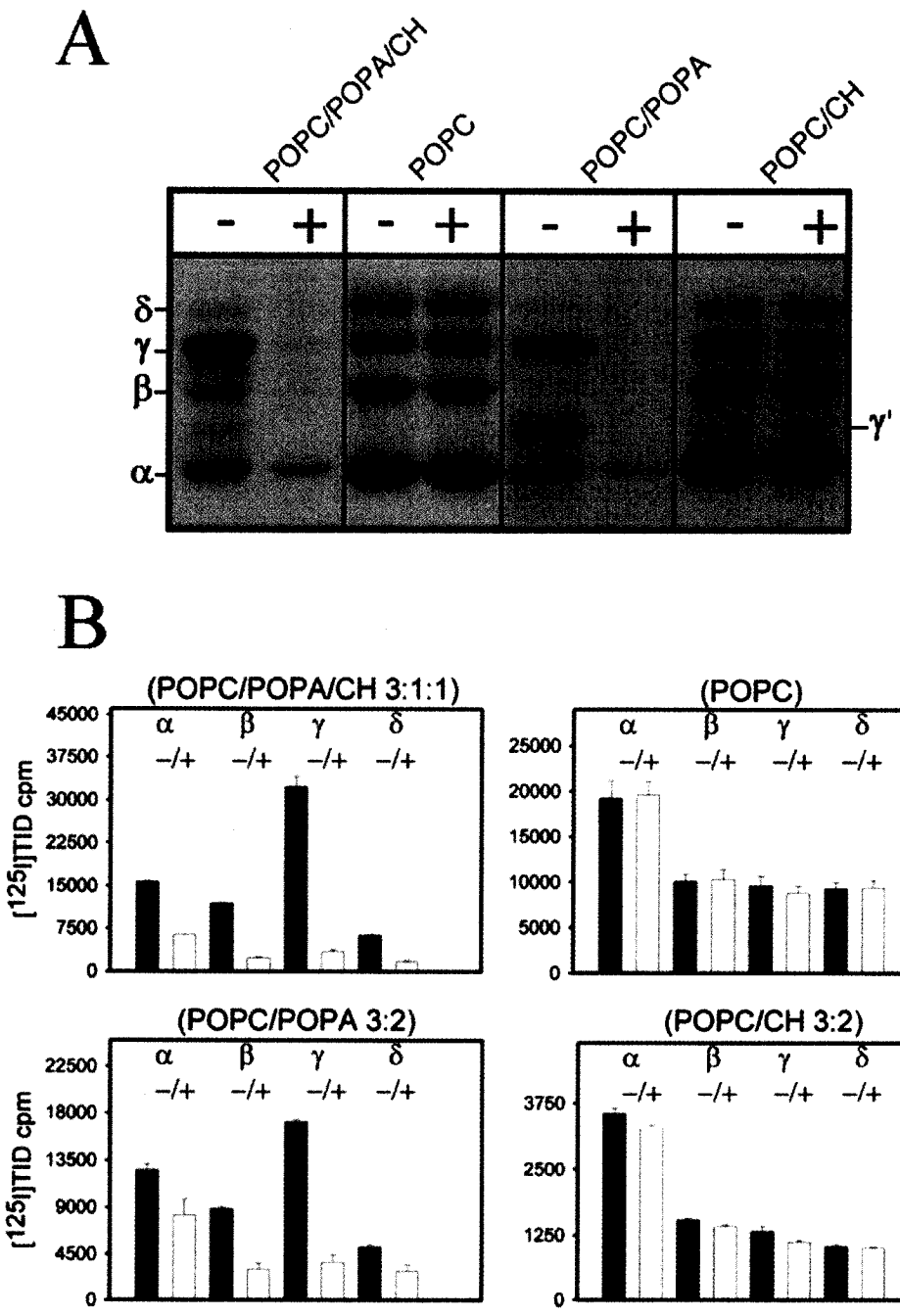
A
POPC/POPA/CH
POPC
POPC/POPA
POPC/CH
- + - + - + - +
δ
γ
β
α
γ'
B
(POPC/POPA/CH 3:1:1)
(POPC)
(POPC/POPA 3:2)
(POPC/CH 3:2)
α β γ δ
–/+ –/+ –/+ –/+
[125]JTID cpm
45000
37500
30000
22500
15000
7500
0
25000
20000
15000
10000
5000
18000
13500
9000
4500
3750
2500
1250

subsequent desensitization of the nAChR results in a dramatic reduction in the extent of [^{125}I]TID incorporation into each subunit. The ratio of the extent of [^{125}I]TID incorporation into the γ and α subunits is a particularly sensitive indicator of the conformational state of the nAChR with a high ratio indicative of a resting conformation (γ/α = 4.11; Table 2.1) and a ratio equal to or less than unity indicative of a desensitized conformation (194, 208).

A similar pattern of [^{125}I]TID labelling in the absence and presence of agonist (Carb) is observed for the nAChR reconstituted into 3:2 POPC/POPA and 3:2 POPC/DOPA membranes (Figure 2.4) showing, in agreement with the FTIR data, that both membranes stabilize a functional receptor that is capable of undergoing agonist induced conformational transitions. In contrast, the nAChR in POPC exhibits much lower levels of [^{125}I]TID incorporation *at equivalent exposures* (see caption of Figure 2.4) to that observed in the 3:1:1 POPC/POPA/Chol membranes in the absence of agonist. The lack of any change in the extent of [^{125}I]TID incorporation upon addition of Carb confirms that the nAChR in POPC is unable to undergo agonist-induced conformational transitions. Both the low overall extent of labelling and the γ/α ratio in the absence and presence of Carb (0.9, 0.84 respectively; Table 2.1) show that the nAChR in POPC is stabilized predominantly in a desensitized-like state. In four out of five reconstitutions, the labelling pattern of the nAChR in 3:2 POPC/Chol was suggestive of a desensitized nAChR. The latter result is in agreement with the limited ability of the nAChR to stabilize a resting-like state in the POPC/Chol membranes as detected by FTIR difference spectroscopy.

Physical Properties of the Reconstituted nAChR Membranes. Two regions of the FTIR spectra exhibit bands that provide qualitative insight into the physical properties of the reconstituted membranes and allow us to make preliminary conclusions regarding the

Table 2.1

Ratio of [^{125}I]TID photoincorporation into the nAChR γ- and α-subunit in the absence and in the presence of Carb. nAChRs reconstituted into lipid vesicles of defined composition were labelled with [^{125}I]TID in the absence (-Carb) or presence (+ Carb) of 400 μM Carb. Following electrophoresis the nAChR subunit bands were excised and the amount of ^{125}I cpm determined by gamma counting (10 min counting time). The γ/α is the ratio of ^{125}I cpm (*i.e.* [^{125}I]TID) incorporation into the γ-subunit relative to the α-subunit. The values in parentheses are the standard error ($n = 3$).

Lipid composition of reconstituted nAChR vesicles.	**γ/α ratio (-Carb)**	**γ/α ratio (+Carb)**
POPC/POPA/CH 3:1:1	4.11 (0.16)	1.06 (0.09)
POPC/DOPA 3:2	2.10 (0.04)	0.67 (0.01)
POPC/POPA 3:2	2.72 (0.11)	0.90 (0.08)
POPC/CH 3:2	0.74 (0.02)	0.68 (0.01)
POPC	0.90 (0.12)	0.84 (0.07)

existence of a correlation between the physical properties of the membranes and their ability to stabilize a functional nAChR. The lipid ester C=O stretching vibration between 1760 and 1700 cm^{-1} is composed of two bands centred near 1740 and 1730 cm^{-1} (Figure 2.5) due to non-hydrogen bonded and hydrogen bonded lipid ester carbonyls, respectively (210, 211). Spectra recorded from reconstituted nAChR membranes composed of 3:1:1 POPC/POPA/Chol, 3:2 POPC/POPA, and 3:2 POPC/DOPA membranes all give rise to similar lipid ester carbonyl stretching band shapes with a relatively large proportion of ester carbonyls in the non-hydrogen bonded state (Figure 2.5, right panel). The large proportion of non-hydrogen bonded lipid ester carbonyls in each case suggests a low degree of water penetration into the interfacial region of the lipid bilayer and thus a high density of head group packing. In contrast, the nAChR in POPC exhibits a much larger proportion of hydrogen bonded lipid ester carbonyls consistent with a greater degree of water penetration into the bilayer and a less ordered membrane. The nAChR in 3:2 POPC/Chol exhibits an intermediate pattern consistent with the relatively weak ability of Chol to stabilize a functional nAChR, although interpretation of the data is likely complicated because the hydroxyl of Chol may hydrogen bond with lipid ester carbonyls altering the shape of the stretching band. Note that within the limits observed in this study, variations in lipid-to-protein ratio had no effect on the interpretation of the data in terms of the relative proportion of hydrogen bonded versus non-hydrogen bonded lipid ester carbonyls in the different membranes.

Surprisingly, we observed substantial differences in the lipid carbonyl ester stretching band shapes in membranes either with or without the nAChR. In all cases, incorporation of the nAChR into the lipid bilayers leads to an increase in the percentage of non-hydrogen bonded lipid ester carbonyls suggesting that the nAChR induces an ordering of the

Figure 2.5

The carbonyl stretching region in deconvolved spectra of lipid membranes composed of A) 3:1:1 POPC/POPA/Chol, B) 3:2 POPC/DOPA, C) 3:2 POPC/POPA, D) 3:2 POPC/Chol, and D) POPC. The left panel shows the deconvolved carbonyl stretching band in spectra of pure lipid membranes. The right panel shows the deconvolved carbonyl stretching band in spectra of the same lipids, but in membranes with the nAChR at the lipid:protein ratios specified in Table 2.2. All spectra were recorded at 22.5 °C. Note that the spectrum of the nAChR in 3:2 POPC/POPA was recorded just below the gel-to-liquid crystal phase transition whereas all other spectra were recorded in the liquid crystal state. Transition from the gel to the liquid crystal phase leads to a slight reduction in the intensity of the 1741 cm^{-1} band due to non-hydrogen bonded lipid ester carbonyls as shown in Figure 2.8. All traces have been baseline corrected between 1770 and 1700 cm^{-1}.

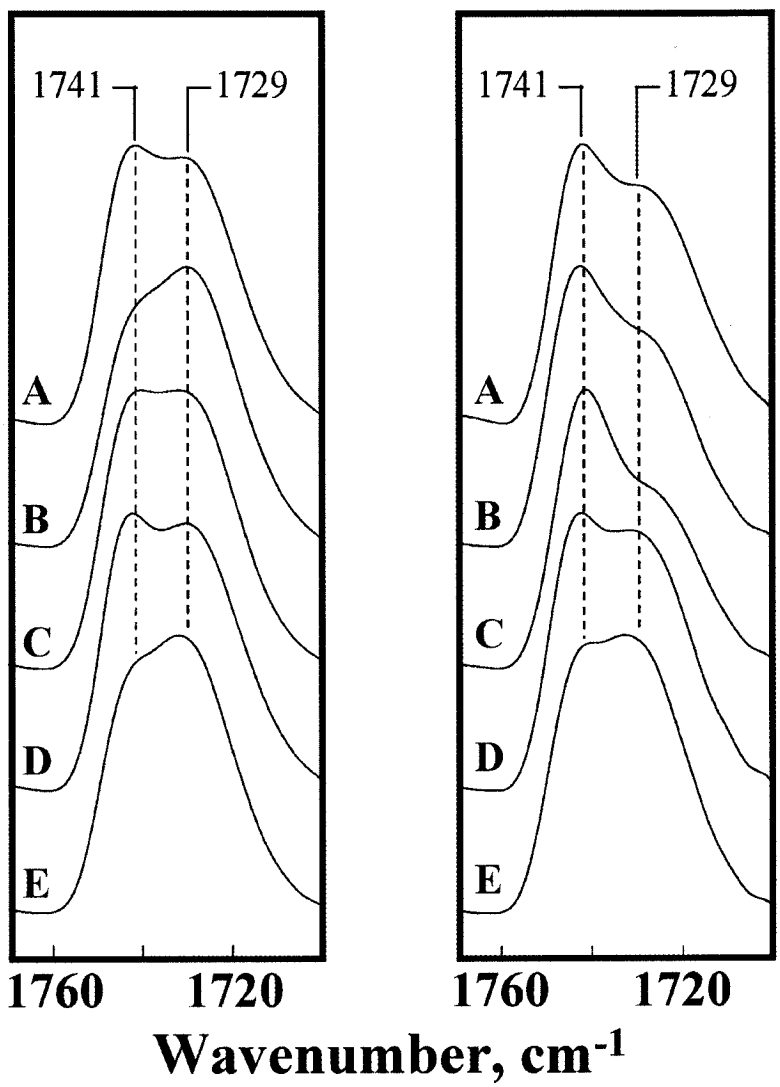
1741
1729
A
B
C
D
E
1760
1720
1741
1729
A
B
C
D
E
1760
1720
Wavenumber, cm-1

membrane. While this is not surprising given the size of the nAChR (~270,000 Daltons), it is significant that the increase in ordering observed upon incorporation of the nAChR into the lipid bilayers is much greater for those membranes that contain the anionic lipids DOPA and POPA. For example, the 3:2 POPC/DOPA and POPC lipid membranes *lacking the nAChR* both exhibit lipid ester carbonyl stretching vibrations at 22.5 °C indicative of a similar high degree of water penetration into the lipid bilayer suggesting a similar degree of membrane order (Figure 2.5). In contrast, the 3:2 POPC/DOPA membranes appear to be substantially more ordered than the POPC membranes, in the presence of the nAChR. This result suggests that the nAChR selectively influences the physical properties of phosphatidic acid containing lipid bilayers.

A similar conclusion was reached upon examination of the gel-to-liquid crystal phase transition temperatures of the various membranes measured in the presence and absence of the nAChR. Gel-to-liquid crystal phase transition temperatures were defined by following the symmetric C-H stretching frequencies of the lipid acyl chains, which decreases by roughly 2 cm^{-1} upon transition from the liquid crystal to the gel state. Cooling curves for the different lipid membranes in the absence of the nAChR (open circles) vary substantially depending on the degree of unsaturation of the lipid bilayers (Figure 2.6). As expected, high levels of Chol abolish the phase transition and order lipids in the liquid crystal state. Incorporation of the nAChR (closed circles) into membranes composed of POPC leads to only a slight broadening of the gel-to-liquid crystal phase transition and very slight shift to higher temperatures. In contrast, incorporation of the nAChR into each membrane that contains either POPA or DOPA leads to a marked increase in the gel-to-liquid crystal phase transition temperature. For example the gel-to-liquid crystal phase transition temperature for the 3:2 POPC/DOPA membranes shifts by roughly 15 °C upon incorporation of the nAChR.

Figure 2.6

Temperature dependence of the C-H symmetric stretching frequencies observed in spectra of membranes composed of A) 3:1:1 POPC/POPA/Chol, B) 3:2 POPC/DOPA, C) 3:2 POPC/POPA, D) 3:2 POPC/Chol, and D) POPC either with (filled circles) or without (clear circles) the nAChR. For more details see Experimental Procedures.

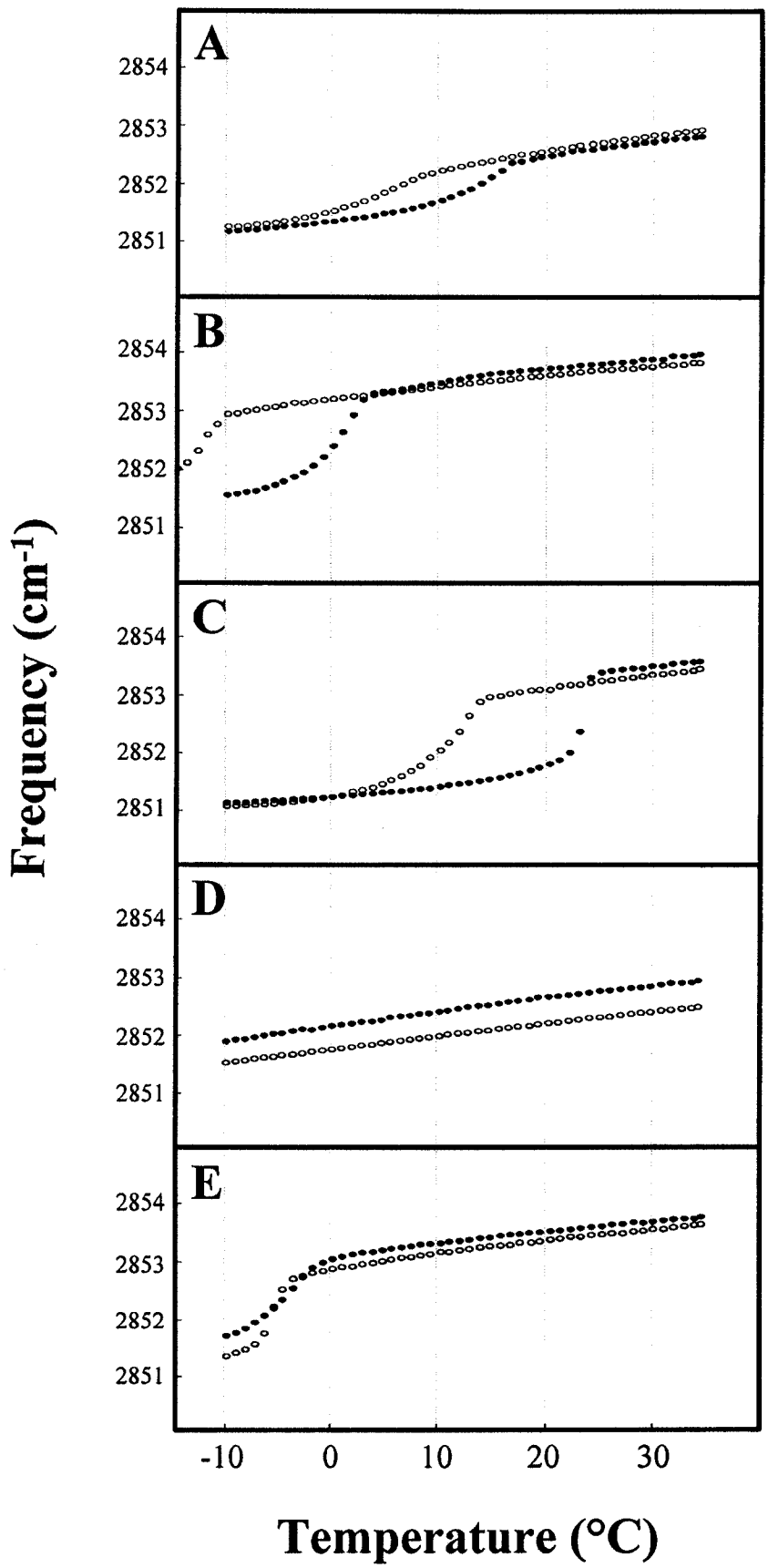
A
B
C
D
E
2854
2853
2852
2851
-10
0
10
20
30
Frequency (cm-1)
Temperature (°C)

This result supports further our conclusion that the nAChR selectively modulates the physical properties of POPC membranes containing the anionic lipids POPA or DOPA.

Does incorporation of the nAChR into 3:2 POPC/POPA membranes lead to a phase separation? The ability of the nAChR to selectively influence the physical properties of POPC membranes containing either DOPA or POPA may reflect a direct interaction between the nAChR and anionic lipids. Such an interaction could lead to a phase separation between POPC and either POPA or DOPA in the presence of the nAChR. Given the roughly 30 °C difference in phase transitions of pure POPC and POPA membranes (Table 2.2), a phase separation of the two lipids in the reconstituted 3:2 POPC/POPA might lead to the formation of lipid environments with distinct phase transition temperatures. While the cooling curves presented in Figure 2.6 show no evidence for two distinct transition temperatures, we tested this possibility further by recording cooling curves for the nAChR reconstituted into 3:2 POPC/POPA membranes where POPA was perdeuterated along the palmitoyl chain. Incorporation of ^{2}H shifts the symmetric C-H stretching frequency of the acyl chain by roughly 800 cm^{-1} allowing for the phase transition of POPA in the reconstituted 3:2 POPC/POPA membranes to be monitored individually. As shown in Figure 2.7, both POPA and POPC in the reconstituted 3:2 POPC/POPA membranes undergo the gel-to-liquid crystal phase transition at roughly the same temperature suggesting that the reconstituted 3:2 POPC/POPA membranes are a homogeneous mixture. Although not definitive, this result argues against a phase separation of zwitterionic and anionic lipids in the presence of the nAChR.

Effect of gel-to-liquid crystal phase transition on the ability of the nAChR to undergo agonist induced conformational change. The nAChR reconstituted 3:2 POPC/POPA membranes have a phase transition temperature that is close to room

Table 2.2

Lipid:protein ratio and gel-to-liquid crystal phase transition temperatures of the lipid membranes measured in the presence and absence of the nAChR. ND = Not determined.

Membrane Lipid Composition	Lipid:protein (mole:mole)	T_M of pure lipid (°C)	T_M of lipid + nAChR (°C)	Change in T_M with nAChR
POPC/POPA/Chol, 3:1:1	330:1	3.8	12.6	+8.8
POPC/DOPA, 3:2	184:1	-12.9	0.5	+13.4
POPC/POPA. 3:2	150:1	10.7	23.7	+13.0
POPC/Chol, 3:2	175:1	ND[a]	ND	ND
POPC	147:1	-6.1	-5.1	+1.0
POPA	ND[b]	27.0	ND	ND

Figure 2.7

Temperature dependence of the C-H (mainly POPC; closed circles, left axis) and C-^{2}H (POPA; open triangles, right axis) symmetric stretching frequencies in spectra of the nAChR reconstituted into membranes composed of 3:2 POPC/ POPA with deuterium labels along the palmitoyl chain of POPA. Note that the sample contains both deuterium-labelled and non-deuterium labelled POPA. The relatively weak C-^{2}H signal also overlapped with the vibration of ^2H_2O leading to a relatively poor signal-to-noise.

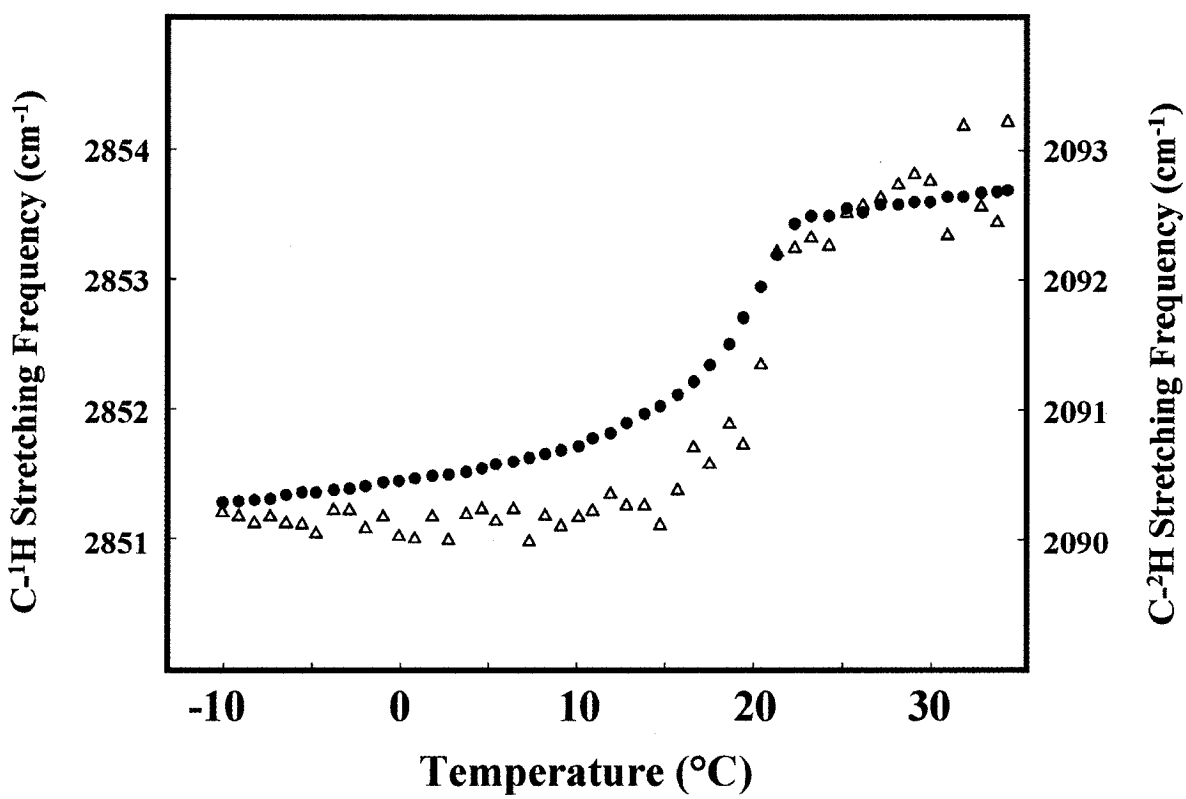
C-1H Stretching Frequency (cm-1)
2854
2853
2852
2851
2093
2092
2091
2090
C-2H Stretching Frequency (cm-1)
-10
0
10
20
30
Temperature (°C)

temperature (Table 2.2). Both the difference spectra and [^{125}I]TID labelling experiments presented in Figures 2.3 and 2.4 were performed at 22.5 °C suggesting that the nAChR may be functional in a membrane that contains a substantial proportion of gel state lipids. To examine in more detail the effects of the gel state on the functional capabilities of the nAChR, Carb difference spectra were recorded above (30 °C) and below (15 °C) the gel-to-liquid crystal phase transition (Figure 2.8). [^{125}I]-TID labelling was also monitored in the gel at 4 °C (data not shown). Both techniques suggest that the nAChR in a gel state membrane retains the ability to undergo agonist induced conformational change. Analysis of the lipid C=O stretching vibration confirms the increased order of the POPC/POPA membranes in the gel state (Figure 2.8). The ability of the nAChR to undergo agonist induced conformational transitions appears to be unaffected by highly rigid gel state lipid bilayers.

2.6 - Discussion

A long term goal of this work is to understand the mechanisms underlying the relative abilities of reconstituted nAChR membranes composed of either POPC alone or POPC with either POPA and/or Chol to stabilize the nAChR in a functional conformation. In this report, we focussed on the link between membrane fluidity and nAChR conformational equilibria proposed in Figure 2.1. Although the results generally support the existence of such a link, the data illustrate the complexity of the physical properties of even these simple reconstituted nAChR membranes and thus the need for more comprehensive ^{2}H NMR/molecular modelling studies to fully test our working model. The data also reveal

Figure 2.8

The left panel is a selected region of Carb difference spectra recorded from the nAChR reconstituted into membranes composed of 3:2 POPC/POPA both above (30 °C) and below (15 °C) the liquid crystal phase transition temperature. The right panel shows the lipid ester carbonyl stretching band of the nAChR membranes at the corresponding temperatures. The photoincorporation of [^{125}I]TID into the nAChR in 3:2 POPC/POPA at 4 °C was indistinguishable from that observed at room temperature both in the presence and absence of Carb (data not shown).

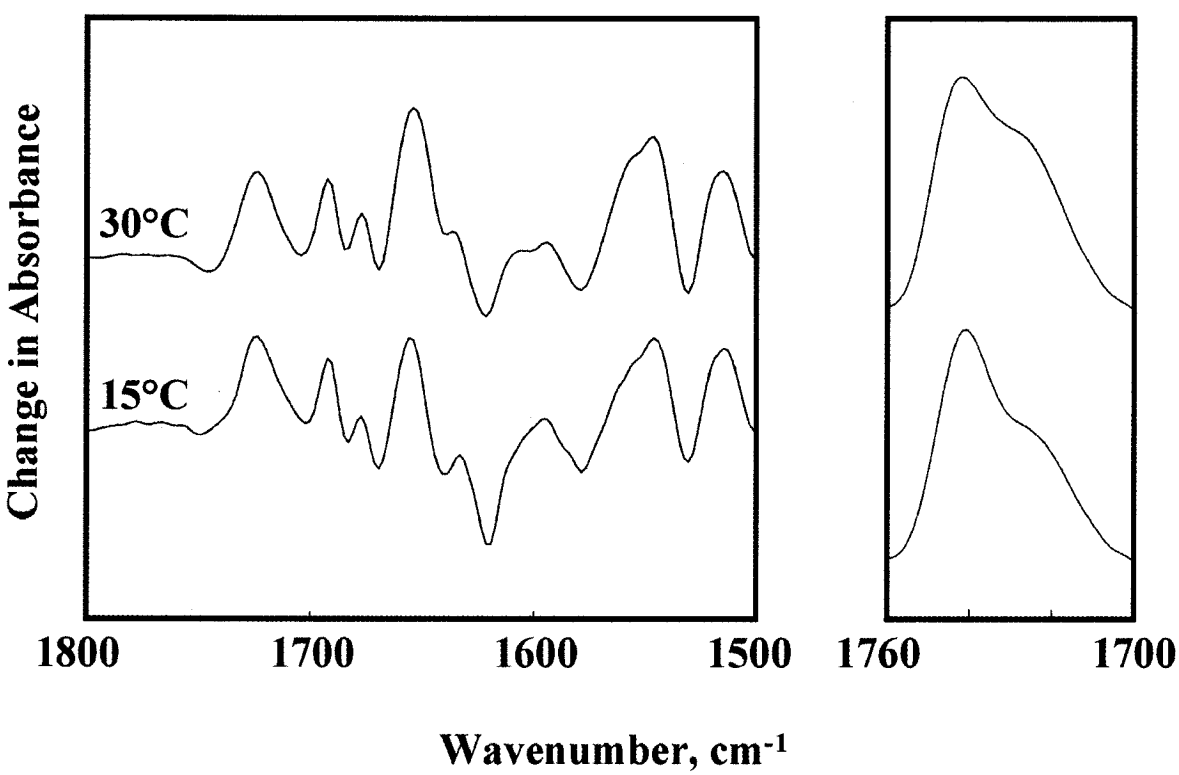
Change in Absorbance
30°C
15°C
1800
1700
1600
1500
1760
1700
Wavenumber, cm-1

several unanticipated features regarding the interactions that occur between the nAChR and lipid bilayers.

FTIR difference spectroscopy and [^{125}I]-TID labelling both indicate, in agreement with previous studies of similar membranes (155, 176, 194, 195), that the nAChR reconstituted into membranes composed of POPC alone is stabilized in a desensitized-like state that does not undergo agonist induced conformational change. The reconstituted POPC membranes have relatively low gel-to-liquid crystal phase transition temperatures and exhibit lipid ester carbonyl stretching band shapes indicative of a high degree of water penetration into the lipid head group region of the bilayer and thus a low lateral lipid packing density. Both are consistent with a relatively disordered or fluid membrane at room temperature.

In contrast, the nAChR in 3:2 POPC/POPA and 3:2 POPC/DOPA membranes is stabilized in a resting-like state that is capable of undergoing agonist induced desensitization. Although the gel-to-liquid crystal phase transition temperatures of the nAChR in 3:2 POPC/POPA and 3:2 POPC/DOPA differ, they are both higher than the phase transition temperature of the reconstituted POPC membranes. The lipid carbonyl ester stretching band shapes suggest a high degree of lateral packing density in the POPA and DOPA containing lipid bilayers reconstituted with the nAChR and thus a higher degree of membrane order. In addition, the presence of phosphatidic acid in phosphatidylcholine membranes appears to slow down nAChR internal motions as monitored by a slowing of exchange kinetics for all nAChR peptide hydrogens (196). Collectively, these results are consistent with the hypothesis that relatively ordered membranes stabilize the receptor in a resting-like state whereas relatively fluid membranes favour a desensitized conformation.

The correlation between fluidity and function is less clear for the reconstituted POPC membranes containing Chol. The nAChR in 3:2 POPC/Chol appears to be predominantly

desensitized, although the FTIR data suggest a limited ability to stabilize receptors in a resting-like state. The lipid ester carbonyl stretching band shape of the reconstituted POPC/Chol membranes is intermediate between that observed in the presence and absence of either POPA or DOPA, consistent with a limited ability to stabilize a functional nAChR. On the other hand, 40 mol% Chol in the POPC membranes abolishes the gel-to-liquid crystal phase transition and, based on the relatively low methylene C-H stretching frequencies, leads to a bilayer with acyl chains that appear be more ordered in the liquid crystal phase than the acyl chains in the reconstituted 3:2 POPC/DOPA and 3:2 POPC/POPA membranes. According to our working model, the latter requires that the 3:2 POPC/Chol membrane should favour the resting state. It is possible, however, that the POPC membranes containing Chol are ordered in a manner that is different from the ordering that occurs in POPC membranes containing either POPA or DOPA.

Note that other studies have reported a greater ability of Chol in either EPC or DOPC membranes to support a functional nAChR that undergoes agonist induced conformational change (176, 195). In EPC and DOPC, 40 and 30 mol% Chol, respectively, are optimal for stabilizing the nAChR in a conformation that is capable of undergoing agonist induced conformational change. The ability of the nAChR to respond to agonist binding in either EPC or DOPC, however, is diminished at both higher and lower levels of Chol (176). Levels of Chol different than those used here in the POPC membranes may be more effective at stabilizing a resting-like state. In addition, it is possible that DOPC or EPC membranes containing Chol are more effective in creating an environment suitable for the nAChR than POPC/Chol mixtures.

Our data also show, in agreement with several other functional studies (155, 177, 194, 195), that the nAChR in 3:1:1 POPC/POPA/Chol membranes is stabilized in a fully

functional state. This result is surprising given our previous work (176), which suggests that either 20% Chol or 20% POPA alone in a POPC membrane is likely to have a very limited ability to stabilize the nAChR in a functional conformation. It appears that Chol and POPA act synergistically in POPC membranes to modulate nAChR conformational equilibria. Unfortunately, the qualitative analysis of membrane physical properties reported here is inadequate to fully understand the unique physical properties of the 3:1:1 POPC/POPA/Chol membrane and why the membrane is particularly effective a stabilizing a functional nAChR. An understanding how this slightly more complex membrane stabilizes a functional nAChR is important given that the physical environment of the 3:1:1 POPC/POPA/Chol membranes is likely more representative of that found in native membranes.

A surprising, but significant finding of this study is that the physical properties of the "functional" POPC membranes containing either DOPA or POPA are strongly influenced by the presence of the nAChR while the physical properties of the "non-functional" pure POPC membranes are relatively unaffected. For all the phosphatidic acid containing membranes, incorporation of the nAChR leads to a large increase in the gel-to-liquid crystal phase transition temperature as well as a large increase in the lateral packing density of the lipid bilayers, the latter reflected by a decrease in water penetration into the bilayer surface and thus a decrease in the number of hydrogen bonded lipid ester carbonyls. Large effects of the nAChR upon the bulk physical properties of any lipid bilayer have not been reported previously. To the best of our knowledge large changes in gel-to-liquid crystal phase transitions have not been reported upon incorporation of any integral membrane protein into a lipid bilayer. The FTIR data, while qualitative, also indicate that the physical properties of some nAChR membranes are not governed by the intrinsic properties of the lipids alone.

The nAChR plays a substantial role in defining the physical characteristics of the reconstituted membranes.

The ability of the nAChR to selectively influence the physical properties of membranes containing POPA or DOPA is particularly intriguing given that both lipids are uniquely effective at stabilizing the nAChR in a functional state. These results suggest the nAChR interacts in a unique fashion with POPA and DOPA containing lipid bilayers. In the reconstituted 3:2 POPC/POPA membranes, this interaction does not likely lead to or result from a lateral phase separation of POPC and POPA because the membranes behave as a homogeneous mixture in terms of the gel-to-liquid crystal phase transition. The ability of the nAChR to modulate the physical properties of the bilayers could stem from hydrophobic mismatching between the nAChR and the fatty acyl chains of the POPC/POPA or POPC/DOPA membranes. A hydrophobic mismatch could lead to large shifts in the gel-to-liquid crystal phase transition temperature upon incorporation of the nAChR (212). Regardless of the precise mechanism, it seems plausible that the unique coupling between the nAChR and the physical properties of the phosphatidic acid containing membrane may play an important role in how phosphatidic acid modulates nAChR function.

Work by others has also suggested a unique role for anionic lipids in modulating nAChR function, although the additional presence of Chol is usually required to stabilize a fully functional nAChR (155, 186, 188, 189). We cannot detect the changes in secondary structure of the nAChR in the presence of either POPA or DOPA that have been detected by others (186, 188, 189) nor do we detect changes in the pKa's of the phosphate stretching vibrations of either POPA or DOPA upon incorporation of the nAChR (data not shown). We are currently trying to define the structural features of phosphatidic acid that make it such an effective determinant of nAChR function. For example, the importance of the negative

charge and/or the small headgroup of phosphatidic acid is being assessed by assessing the structural and functional characteristics of the nAChR in POPC membranes composed of 1-palmitoyl-2-oleoyl phosphatidyl serine and 1-palmitoyl-2-oleoyl phosphatidyl ethanolamine.

We have characterised the structure and conformational states of the nAChR stabilized in POPC, 3:2 POPC/POPA, 3:2 POPC/Chol, and 3:1:1 POPC/POPA/Chol membranes. Each lipid used in these membranes are available in a deuterated form. We are now in a position to rigorously analyze the physical properties of the reconstituted membranes using ^{2}H NMR spectroscopy. These future studies should provide important insight into the mechanisms by which membrane lipids influence integral membrane protein function, in general.

CHAPTER 3

MANUSCRIPT:

2. **Corrie J.B. daCosta**, Ian D. Wagg, Marlene E. McKay, and John E. Baenziger. (2004) **Phosphatidic acid and phosphatidylserine have distinct structural and functional interactions with the nicotinic acetylcholine receptor.** *J. Biol. Chem.* **279**, 14967-14974.

3.1 - Preface

This is the second of three manuscripts included in this thesis. As with the first manuscript, this manuscript was published in the Journal of Biological Chemistry (April, 2004). This paper follows up on the data presented in the last chapter which showed that reconstituted membranes containing lipids with phosphatidic acid headgroups were able to stabilize a functional/resting *Torpedo* nAChR. Using the same FTIR techniques, this work examines whether negative charge is the defining feature of phosphatidic acid moieties that allows them to stabilize a functional nAChR. Instead of reconstituting the nAChR into PA containing membranes, the nAChR was reconstituted into membranes containing lipids with a phosphatidylserine headgroup. Like phosphatidic acid, phosphatidylserine is negatively charged, however phosphatidylserine headgroups are much larger than phosphatidic acid headgroups. Phosphatidylserine moieties also show unique interactions with divalent cations which appear to be enhanced by the presence of the nAChR.

I collected (or supervised the collection of) all FTIR experiments presented in this manuscript. Several experiments were duplicated by both Ian D. Wagg and Marlene E. McKay.

3.2 - Abstract

Bilayers containing phosphatidylcholine (PC) and the anionic lipid phosphatidic acid (PA) are particularly effective at stabilizing the nicotinic acetylcholine receptor (nAChR) in a functional conformation that undergoes agonist induced conformational change. The physical properties of PC membranes containing PA are also substantially altered upon incorporation of the nAChR. To test whether or not the negative charge of PA is responsible for this "bi-directional coupling", the nAChR was reconstituted into membranes composed of PC with varying levels of the net negatively charged lipid, phosphatidylserine (PS). In contrast to PA, increasing levels of PS in PC membranes do not stabilize an increasing proportion of nAChRs in a functional resting conformation nor do they slow nAChR peptide hydrogen exchange kinetics. Incorporation of the nAChR had little effect on the physical properties of the PC/PS membranes, as monitored by the gel to liquid-crystal phase transition temperatures of the bilayers. These results show that a net negative charge alone is not sufficient to account for the unique interactions that occur between the nAChR and PC/PA membranes. Incorporation of the receptor into PC/PS membranes, however, did lead to an altered head group conformation of PS possibly by recruiting divalent cations to the membrane surface. The results show that the nAChR has complex and unique interactions with both PA and PS. The interactions between the nAChR and PS may be bridged by divalent cations, such as calcium.

3.3 - Introduction

The ability of the nicotinic acetylcholine receptor (nAChR) to flux cations across the post-synaptic membrane in response to agonist binding is influenced by the composition of its surrounding lipid environment (197, 198). Although detailed insight into the underlying mechanisms has not yet been achieved, a current model proposes that lipid bilayers modulate nAChR function by altering the natural equilibrium that exists between "functional" resting and "non-functional" desensitized conformational states (176). In native post-synaptic membranes, this equilibrium strongly favours the resting conformation allowing the nAChR to flux cations in response to agonist binding. The equilibrium is maintained in favour of the resting conformation in reconstituted bilayers composed of phosphatidylcholine (PC), an anionic lipid, such as phosphatidic acid (PA), and a neutral lipid, such as cholesterol (Chol) (155, 170, 176). In contrast, the equilibrium shifts in favour of a desensitized, or a desensitized-like state, leading to channel inactivation in pure PC membranes (155, 170, 177, 194, 195). The effects of neutral and anionic lipids on nAChR conformational equilibria are not dependent upon a global change in secondary structure (190). The presence of either or both lipids in a reconstituted PC membrane does slow nAChR peptide hydrogen exchange kinetics, suggesting a decrease in the rates and/or amplitudes of internal nAChR motions (196).

Additional experiments have expanded on this simple model of lipid action, showing that the addition of either PA or Chol alone to a PC membrane is sufficient to shift the conformational equilibrium towards the resting state (176, 177). The degree of the conformational shift depends on both the type and amount of lipid added, with PA being particularly effective at stabilizing a resting conformation (176, 194, 213). As increasing

amounts of either Chol or PA in a PC membrane could lower bilayer fluidity, we suggested that both lipids may shift the conformational equilibrium in favor of the resting state by decreasing the fluidity of the membrane surrounding the nAChR (176, 213). Any links that exist between membrane physical properties and nAChR function, however, are likely complex (213).

A recent study also showed that incorporation of the nAChR into PC membranes containing PA leads to a substantial increase in both the gel to liquid-crystal phase transition temperature and the lateral packing density of the lipids. In contrast, incorporation of the nAChR into membranes composed of either PC or PC/Chol has little effect (213, 214). The ability of the nAChR to selectively modulate the physical properties of PC membranes containing PA is of particular interest given that PC/PA membranes are especially effective at stabilizing a functional nAChR. These results suggest that there is a bi-directional "coupling" between the nAChR and PA-containing lipid bilayers in that the lipids modulate nAChR structure/function while in return the nAChR modulates lipid structure and possibly function. This bi-directional coupling may underlie the unique mechanism by which PA influences nAChR conformational equilibria and thus stabilizes a functional nAChR.

In order to understand the mechanism(s) by which PA modulates nAChR conformational equilibria, it is first necessary to define the structural features of PA that allow it to interact with the nAChR in a unique fashion. To test whether or not a net negative charge is sufficient to account for these interactions, we have reconstituted the nAChR into PC membranes containing varying levels of the lipid phosphatidylserine (PS). PS has a net negative charge and is abundant in *Torpedo* post-synaptic membranes. Surprisingly, our results show that despite its net negative charge, increasing levels of PS in a PC membrane

do not increase the proportion of receptors in the functional resting conformation nor do they slow nAChR peptide hydrogen exchange kinetics. Incorporation of the nAChR into PC/PS membranes also has little effect on the gel to liquid crystal phase transition of the lipid bilayer. Negative charge alone is thus not sufficient to account for the interactions that occur between the nAChR and PA containing lipid bilayers. Incorporation of the nAChR does, however, lead to an altered head group conformation of PS possibly by recruiting divalent cations to the membrane surface. Our results illustrate the complex interactions that can occur between the nAChR and different lipids. The data highlight the unique and possibly essential interactions that occur between the nAChR and PA. Finally, the data suggest that divalent cations play a role in bridging the structural effects that occur between the nAChR and PS containing lipid bilayers.

3.4 - Experimental Procedures

Materials. Frozen *Torpedo californica* electroplax tissue was obtained from either Marinus (Long Beach, CA) or Aquatic Research Consultants (San Pedro, CA). 1-Palmitoyl-2-Oleoyl-*sn*-Glycero-3-Phosphocholine (POPC), 1-Palmitoyl-2-Oleoyl-*sn*-Glycero-3-Phosphate (POPA) and 1-Palmitoyl-2-Oleoyl-*sn*-Glycero-3-[Phospho-L-Serine] (POPS) were from Avanti Polar lipids, Inc. (Alabaster, AL) and both cholesterol and carbamylcholine chloride (Carb) were from Sigma (St. Louis, MO).

nAChR Purification and Reconstitution. The nAChR was solubilized in 1% cholate and affinity purified on a bromoacetylcholine bromide-derivatized Affi-Gel 102 column (Bio-Rad; Richmond, CA) as described in detail elsewhere (194). The column bound nAChR was washed extensively with dialysis buffer (100 mM NaCl, 10 mM Tris-HCl, 0.1

mM EDTA, 0.02% w/v NaN_3, pH = 7.8) containing 1% cholate and a 3.2 mM concentration of the desired lipid. The nAChR was then eluted from the column with a 0.13 mM lipid solution in 250 mM NaCl, 0.1 mM EDTA, 0.02% NaN_3, 5 mM phosphate, pH 7.8 with 0.5% cholate and 10 mM Carb. After elution from the column, the nAChR was dialyzed five times against 2 litres of dialysis buffer with buffer change once every 12 hours.

FTIR Spectroscopy. All FTIR spectra were recorded on either a Digi-Lab FTS 575 or a FTS 40 spectrometer (Randolph, MA) as described by daCosta et al (213). Both spectrometers were equipped with a DTGS detector. For the analysis of protein secondary structure, the extent of peptide hydrogen/deuterium exchange, and lipid thermotropic phase behaviour, each nAChR sample was first incubated at 4°C in ^2H_2O phosphate buffer for precisely 72 hours in order to exchange peptide N-^{1}H for N-^{2}H and then stored at -80°C. Prior to FTIR analysis, samples were individually thawed, centrifuged, resuspended in 30 µl of ^2H_2O phosphate buffer, and subjected to five freeze thaw vortex cycles. Except where noted, all FTIR spectra were recorded in *Torpedo* Ringer buffer (5mM Tris, 250mM NaCl, 5mM KCl, 2mM $MgCl_2$ and 3mM $CaCl_2$, pH = 7).

The POPC/POPS 3:2 samples recorded in the presence of 20mM EDTA (Figure 3.6, right panel, dashed spectrum) were prepared as described above, except that after the 72 hour incubation in ^2H_2O, the membranes were pelleted and resuspended in 20mM EDTA, 5mM Tris ^2H_2O. After fifteen minutes, the samples were pelleted, resuspended in 30µl 2mM ^2H_2O phosphate buffer, and then subjected to freeze-thaw-vortex cycles. Samples deposited on CaF_2 windows were rehydrated with 8µl of 20mM EDTA and 5mM Tris ^2H_2O buffer. All spectral deconvolution was performed using GRAMS/AI v.7.01 software (Galactic; Salem, NH).

The data acquisition protocols for assessing the thermotropic phase behaviour of the membranes have been described previously (213). Briefly, 128 scans at 2 cm^{-1} resolution were acquired at one degree intervals as the sample was cooled from 35°C to -10°C. Note that all of the ^2H_2O buffers were prepared by drying the corresponding ^1H_2O buffers (pH=7.0), and then rehydrating them with the appropriate volume of ^2H_2O. The pD's were then verified with litmus paper.

FTIR difference spectra were recorded at 22.5°C using the attenuated total reflectance technique as described in detail elsewhere (200, 206). Briefly, two spectra were recorded while flowing *Torpedo* Ringer buffer past a nAChR film that was deposited on the surface of a germanium internal reflection element. The flowing buffer was switched to an identical buffer containing 50 μM Carb and a spectrum recorded of the Carb bound state. The nAChR film was then washed with *Torpedo* Ringer buffer for 20 minutes to remove nAChR bound Carb and the data acquisition protocol repeated. All spectra were recorded at 8 cm^{-1} resolution, signal-averaging 512 scans per spectrum, which took approximately 8 minutes per spectrum. Each presented difference spectrum is the average of more than 40 individual difference spectra recorded from at least two different films, from on average four separate reconstitutions (see Appendix). The difference spectra were baseline corrected between 1800 and 1000 cm^{-1} and were interpolated to a resolution of 4 cm^{-1}.

3.5 - Results

FTIR spectra of the nAChR affinity purified and reconstituted into membranes composed of POPC, POPC/POPS 3:1 (mol/mol), POPC/POPS 3:2 (mol/mol), POPC/POPS/Chol 3:1:1 (mol/mol/mol) and POPC/POPA 3:2 (mol/mol) each exhibit four

main features in the 1800 to 1400 cm^{-1} region (Figure 3.1). These four features are mainly attributable to the protein amide I (1700 to 1600 cm^{-1}), amide II (1520 to 1580 cm^{-1}), and amide II' (1500 to 1400 cm^{-1}) vibrations, as well as to the ester carbonyl stretching vibrations of the membrane phospholipid (1750 to 1700 cm^{-1}). The shapes and relative intensities of the three protein bands reflect structural features of the nAChR in each membrane, whereas the shape of the lipid ester carbonyl vibration reflects the structure of the surrounding lipid environment (see below). Subtle differences are observed in each of the vibrational bands between spectra recorded from the nAChR reconstituted into POPC/POPS 3:2 and POPC/POPA 3:2 membranes (Figure 3.1). These variations are typical of the variations observed between spectra recorded from the nAChR in each of the five lipid environments and provide insight into the mechanisms by which the nAChR couples its structure and function to the composition of its surrounding lipid bilayer.

nAChR structure and internal dynamics. The amide I band between 1600 and 1700 cm^{-1} is due predominantly to the peptide carbonyl (C=O) stretching vibration and its shape is sensitive to hydrogen bonding, and thus protein secondary structure. Deconvolution of the amide I band provides a clearer view of the frequencies and relative intensities of the underlying component vibrations and thus permits a qualitative assessment of the secondary structure of the nAChR in each lipid environment (Figure 3.2, left panel) (215). In each case, the deconvolved amide I band exhibits a similar number of underlying components at similar relative intensities including two major peaks of intensity near 1655 cm^{-1} and 1636 cm^{-1} due to α-helical and β-sheet secondary structures, respectively (215). The overall similarities of the deconvolved amide I band shapes indicate that the nAChR has roughly the same mixed α-helix/β-sheet structure in each membrane environment.

Figure 3.1

FTIR spectra of the nAChR reconstituted into POPC/POPA 3:2 (dashed line) and POPC/POPS 3:2 (solid line) membranes. The absorbance axis is shown for the POPC/POPS 3:2 sample (the POPC/POPA 3:2 sample is scaled to the same amide I intensity). All samples had similar amide I intensities that varied by no more than ±5%. Solvent ^2H_2O and atmospheric H_2O vapour have been subtracted from each spectrum. Spectra were baseline corrected and zeroed between 1800 and 1350cm^{-1}.

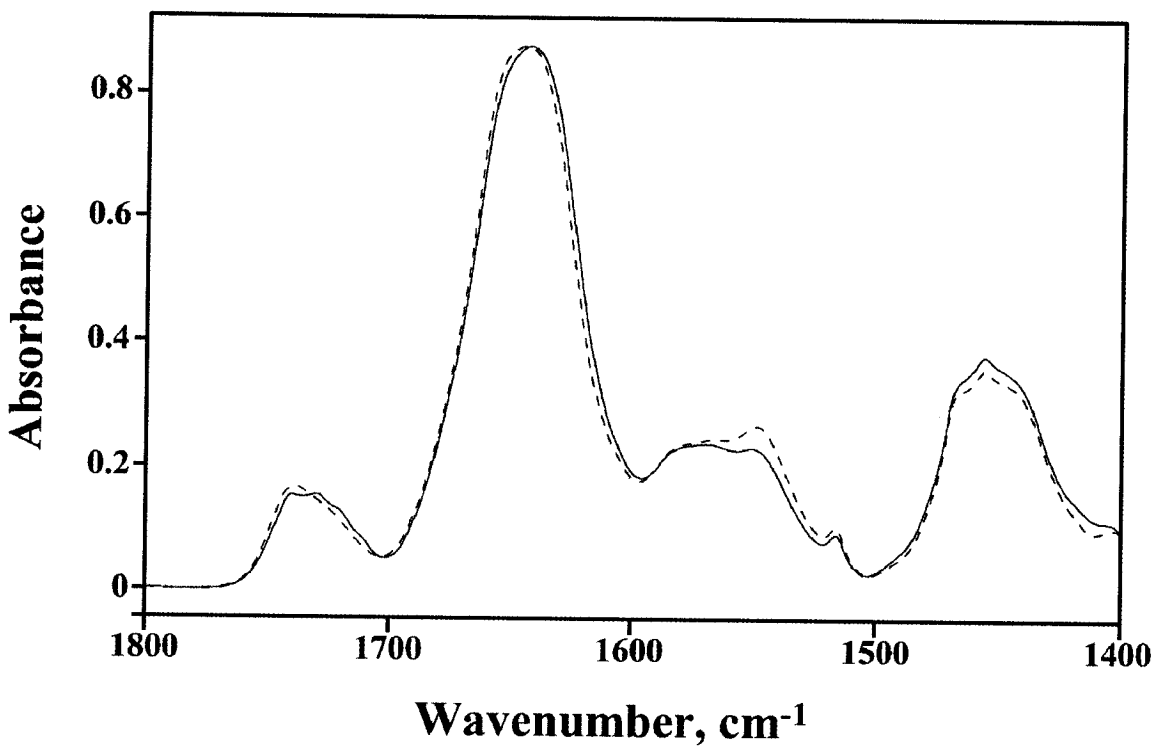
Absorbance
0.8
0.6
0.4
0.2
0
1800
1700
1600
1500
1400
Wavenumber, cm-1

Figure 3.2

The deconvolved amide I band (left panel) and residual amide II band intensity (right panel) in FTIR spectra recorded from the nAChR reconstituted into 3:2 POPC/POPA A), 3:1:1 POPC/POPS/Chol B), 3:2 POPC/POPS C), 3:1 POPC/POPS D), and POPC E) membranes. The amide I bands presented in the left panel were deconvolved between 1900 and 1300 cm^{-1} with a γ factor of 7 and a smoothing parameter of 70%. Amide II bands presented in the right panel are not deconvolved. All samples were exposed to ^2H_2O buffer for 72 h at 4 °C prior to data acquisition and a spectrum of ^2H_2O buffer has been subtracted from each. All samples are hydrated with ^2H_2O *Torpedo* ringer buffer. Spectra were recorded at 22.5 °C.

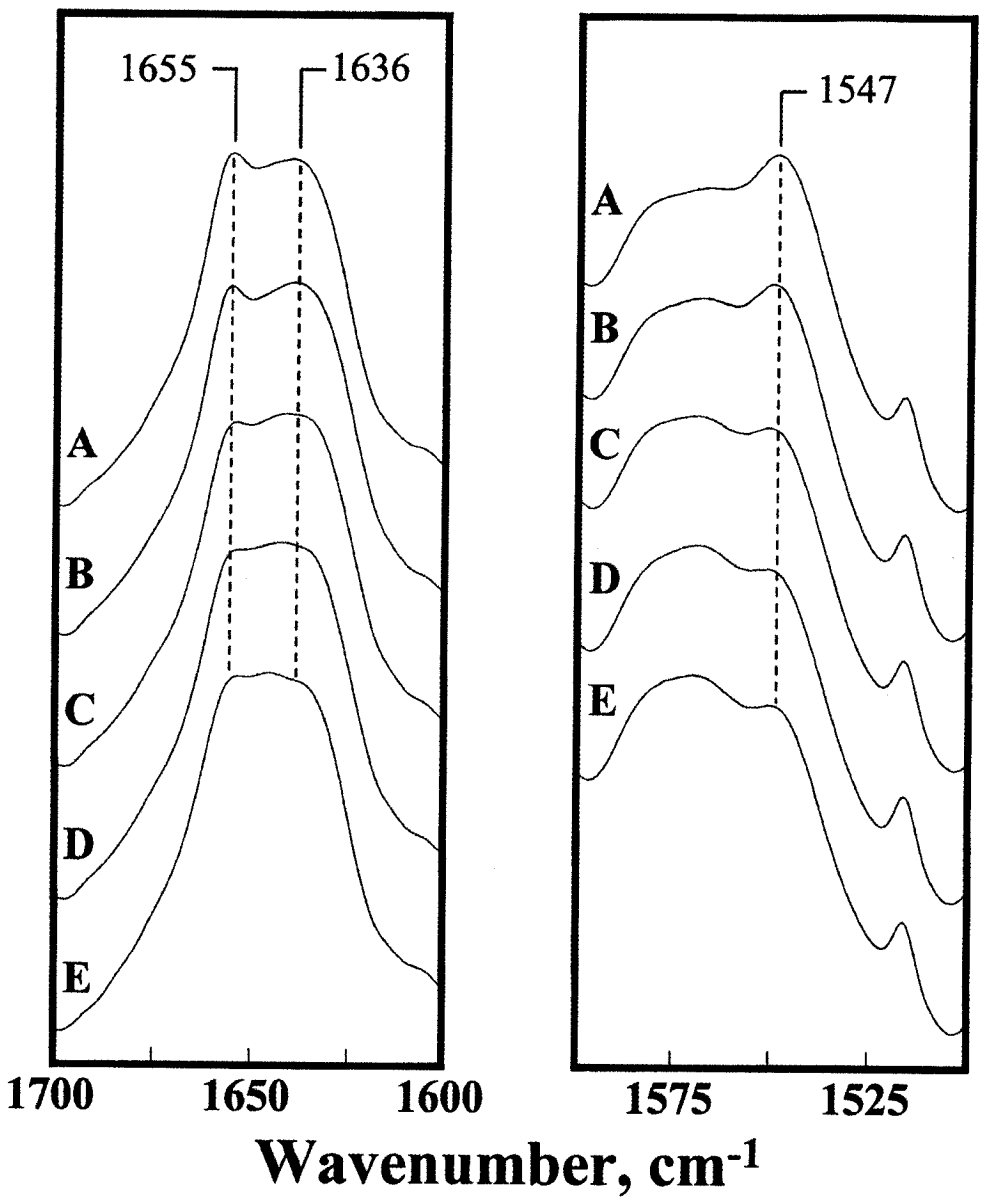
1655
1636
1547
A
B
C
D
E
1700
1650
1600
1575
1525
Wavenumber, cm-1

The non-deconvolved amide I bands in spectra recorded from the nAChR in POPC and mixtures of POPC and POPS, are slightly downshifted in frequency relative to the amide I bands in spectra recorded from the nAChR in either POPC/POPA 3:2 or POPC/POPS/Chol 3:1:1 membranes (Figure 3.1). Deconvolution shows that this downshift in frequency is due to a subtle shift in intensity from 1655 cm^{-1} down to 1645 cm^{-1} (Figure 3.2, left panel). While the decrease in α-helical amide I component band intensity could reflect a minor decrease in α-helical structure, previous studies have shown that the α-helical vibration undergoes a shift in frequency from 1655 cm^{-1} in ^1H_2O down to near 1645 cm^{-1} in ^2H_2O (126, 127). After 72 hours exposure to ^2H_2O, roughly 25% of the nAChR peptide hydrogens remain unexchanged for deuterium, although the extent of peptide hydrogen-deuterium exchange is sensitive to lipid environment (127). The greater intensity near 1655 cm^{-1} in the spectra recorded from the nAChR reconstituted into membranes composed of POPC/POPS/Chol 3:1:1 and POPC/POPA 3:2 could result from a slower rate of peptide hydrogen-deuterium exchange in these two membrane environments relative to that observed in the POPC, POPC/POPS 3:1, and POPC/POPS 3:2 membranes, and thus a greater proportion of unexchanged α-helical structures after three days exposure of the nAChR to ^2H_2O.

A slowing of peptide hydrogen exchange kinetics for the nAChR reconstituted into POPC/POPA 3:2 and POPC/POPS/Chol 3:1:1 versus POPC, POPC/POPS 3:1, and POPC/POPS 3:2 membranes is supported by the relative residual amide II band intensities observed near 1547 cm^{-1} in various spectra (Figure 3.1 and Figure 3.2, right panel). The amide II band is due predominantly to the N-^{1}H in-plane bending vibration of the polypeptide backbone. The vibration shifts down in frequency to near 1450 cm^{-1} (amide II'

band) upon exposure of the nAChR to ^2H_2O and consequent exchange of peptide N-^{1}H for N-^{2}H (126, 127). The residual intensity centred near 1547 cm^{-1}, overlaps with the broad asymmetric stretching vibrations of carboxylic acid side chains (Asp and Glu) between 1560 and 1590 cm^{-1}, and is proportional to the number of unexchanged peptide hydrogens. Spectra of the nAChR in POPC/POPA 3:2 and POPC/POPS/Chol 3:1:1 membranes exhibit an increased residual amide II band intensity near 1547 cm^{-1} and thus a greater proportion of unexchanged peptide hydrogens relative to the nAChR in POPC, POPC/POPS (3:1 and 3:2) membranes. A previous study with the nAChR showed that similar variations in the levels of peptide hydrogen/deuterium exchange lead to similar changes in nAChR amide I band shape (190). These results therefore suggest that the secondary structure of the nAChR is not influenced by the presence of POPA, POPS, or both POPS and Chol in a reconstituted POPC membrane. Instead, these lipids modulate the amplitude and/or rates of nAChR internal motions resulting in differences in the extent of peptide ^{1}H-^{2}H exchange.

Note that the presence of either 25 or 40 mol% POPS in a reconstituted POPC membrane does not lead to a slowing of nAChR peptide hydrogen exchange kinetics and thus a slowing of nAChR internal dynamics (relative to the nAChR in POPC membranes) as seen in the presence of 40 mol% POPA. This shows that negative charge alone is not sufficient to account for the effects of POPA on nAChR structure. The data also support the hypothesis that there is a correlation between the internal dynamics of the nAChR in different membranes and the ability of the membrane to stabilize the nAChR in a functional state (see Discussion).

nAChR Conformational Equilibria. The effects of bilayer lipid composition on nAChR conformational equilibria were examined using FTIR difference spectroscopy

(Figure 3.3). The difference between spectra of the nAChR recorded in the presence and absence of the agonist carbamylcholine (referred to as a Carb difference spectrum) exhibits a complex pattern of positive and negative bands that reflect the vibrational changes in the nAChR that occur upon Carb binding and subsequent desensitization. Positive and negative difference bands in the 1640 to 1670 cm^{-1} (mainly peptide C=O stretching) and 1520 to 1580 cm^{-1} (mainly and peptide N-H bending) regions reflect the structural changes in the polypeptide backbone that occur upon transition from the resting to the desensitized conformational state. The pattern of overlapping difference bands in both regions of spectra recorded from the nAChR in POPC/POPA 3:2 membranes is similar to that observed in difference spectra recorded from the nAChR in native and PC/PA/Chol 3:1:1 membranes (data not shown). This pattern is characteristic of a receptor that is stabilized in a resting conformation that undergoes desensitization upon Carb binding.

Intensity is lost in both the 1640 to 1670 cm^{-1} and 1520 to 1580 cm^{-1} spectral regions of difference spectra recorded from the nAChR reconstituted into POPC, POPC/POPS (3:1 and 3:2) membranes (Figure 3.3, spectra E,D,C). The resulting pattern of bands is similar to that observed in difference spectra recorded from the nAChR reconstituted into PC/PA/Chol 3:1:1 membranes, but while the nAChR is maintained in a desensitized conformation in the presence of a desensitizing local anesthetic, such as dibucaine. The pattern of bands observed in difference spectra recorded from the nAChR in either POPC alone or mixtures of POPC and POPS indicates that the nAChR cannot undergo the resting to desensitized conformational transition upon Carb binding. The spectra suggest that the nAChR is stabilized in a desensitized or desensitized-like conformation (see discussion of reference #176). Based on the FTIR data, it is clear that the presence of POPS alone in a POPC

Figure 3.3

A selected region of Carb difference spectra recorded from the nAChR reconstituted into membranes composed of A) 3:2 POPC/POPA, B) 3:1:1 POPC/POPS/Chol, C) 3:2 POPC/POPS, D) 3:1 POPC/POPS, and E) POPC. Positive intensity near 1663, 1655, and 1547 cm^{-1} is associated with the resting to desensitized conformational change. Note that a change in intensity near 1663 cm^{-1} is most easily visualised by a change in overlapping negative band intensity near 1668 cm^{-1} (206). Positive intensity at each of these frequencies in trace A and B indicates that the nAChR undergoes desensitization upon Carb binding. The absence of positive intensity in traces C, D and E indicates that the nAChR is likely stabilized in a desensitized state. Both the horizontal line and shading have been included in each spectrum as a visual reference.

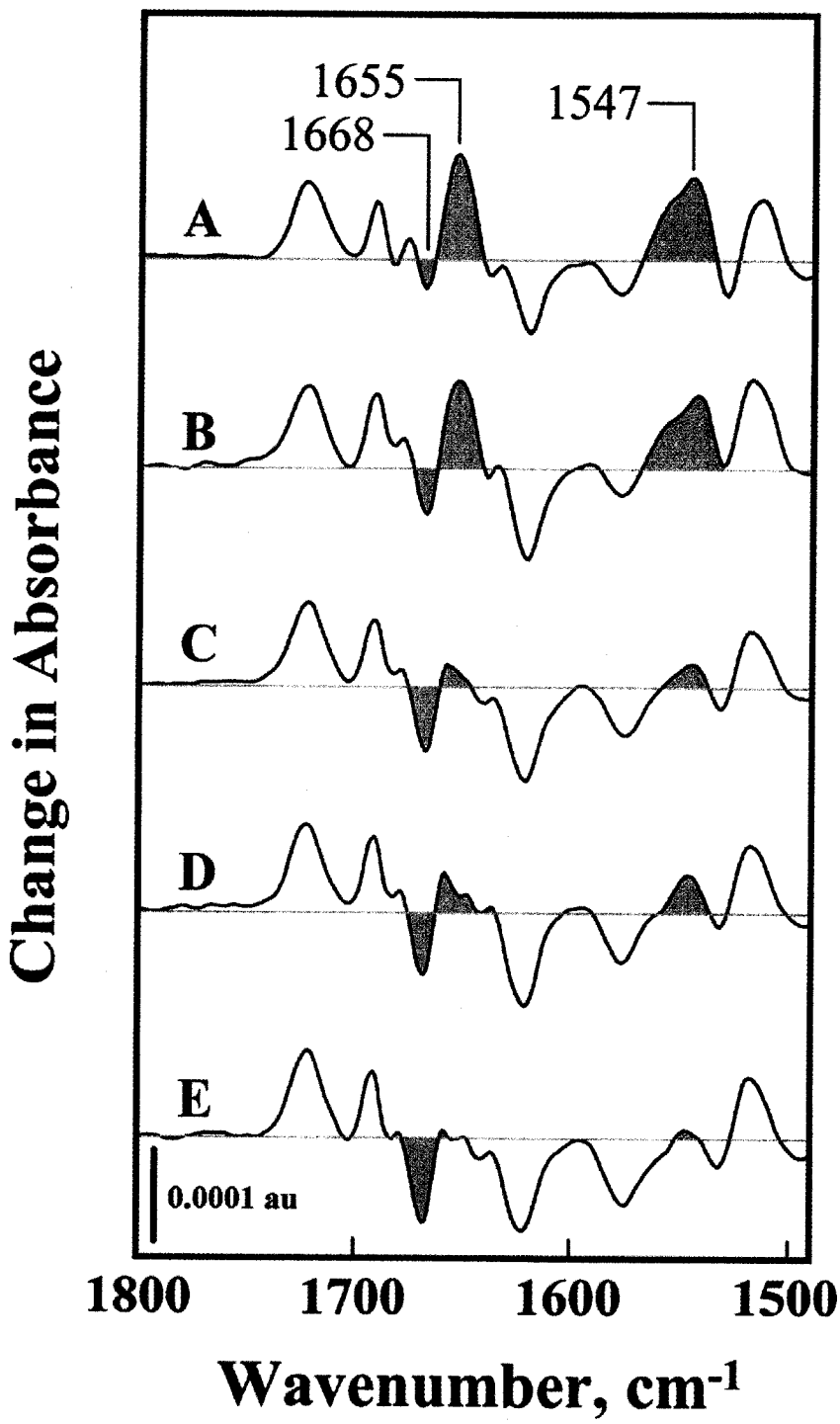
1655
1668
1547
A
B
C
D
E
0.0001 au
Change in Absorbance
1800
1700
1600
1500
Wavenumber, cm-1

membrane is not sufficient to shift the nAChR conformational equilibrium towards the resting state.

In contrast, Carb difference spectra recorded from the nAChR in POPC/POPS/Chol 3:1:1 membranes exhibit a pattern of positive and negative vibrations that is intermediate between that observed in POPC/POPS and POPC/POPA 3:2 membranes. The spectra suggest that mixtures of POPC/POPS and Chol are somewhat effective at stabilizing the nAChR in a resting conformation, although the degree of the conformational shift towards the resting state is not as great as observed in POPC/POPA 3:2 membranes.

Physical Properties of the Reconstituted nAChR Membranes. The effects of nAChR on the physical properties of the reconstituted lipid bilayers was first examined by comparing the gel to liquid crystal phase transition temperatures of the various POPC/POPS membranes in the presence and absence of the nAChR (Figure 3.4). The methylene symmetric C-H stretching frequencies of the fatty acyl chains decreases by roughly 2 cm^{-1} upon transition from the liquid crystal to the gel state and can thus be used to monitor the gel-to-liquid crystal phase transition temperatures of the reconstituted bilayers (202). Cooling curves for the different lipid membranes in the absence of the nAChR (open circles) vary depending on the lipid composition (Figure 3.4). As shown previously, incorporation of the nAChR (closed circles) into membranes composed of POPC (Figure 3.4E) leads to a slight broadening of the gel-to-liquid crystal phase transition and very slight shift to higher temperatures, while incorporation of the nAChR into the 3:2 POPC/POPA membrane (Figure 3.4A) leads to a 15°C increase in the gel-to-liquid crystal phase transition temperature (Table 3.1)(213). In the POPC/POPS 3:1 and 3:2 membranes (Figure 3.4D,C), there is no observed shift in the phase transition temperature, but the difference in frequency

Figure 3.4

Temperature dependence of the C-H symmetric stretching frequency observed in spectra of membranes composed of A) 3:2 POPC/POPA, B) 3:1:1 POPC/POPS/Chol, C) 3:2 POPC/POPS, D) 3:1 POPC/POPS, and E) POPC either with (filled circles) or without (clear circles) incorporated nAChR. All samples are hydrated with ^2H_2O *Torpedo* ringer buffer.

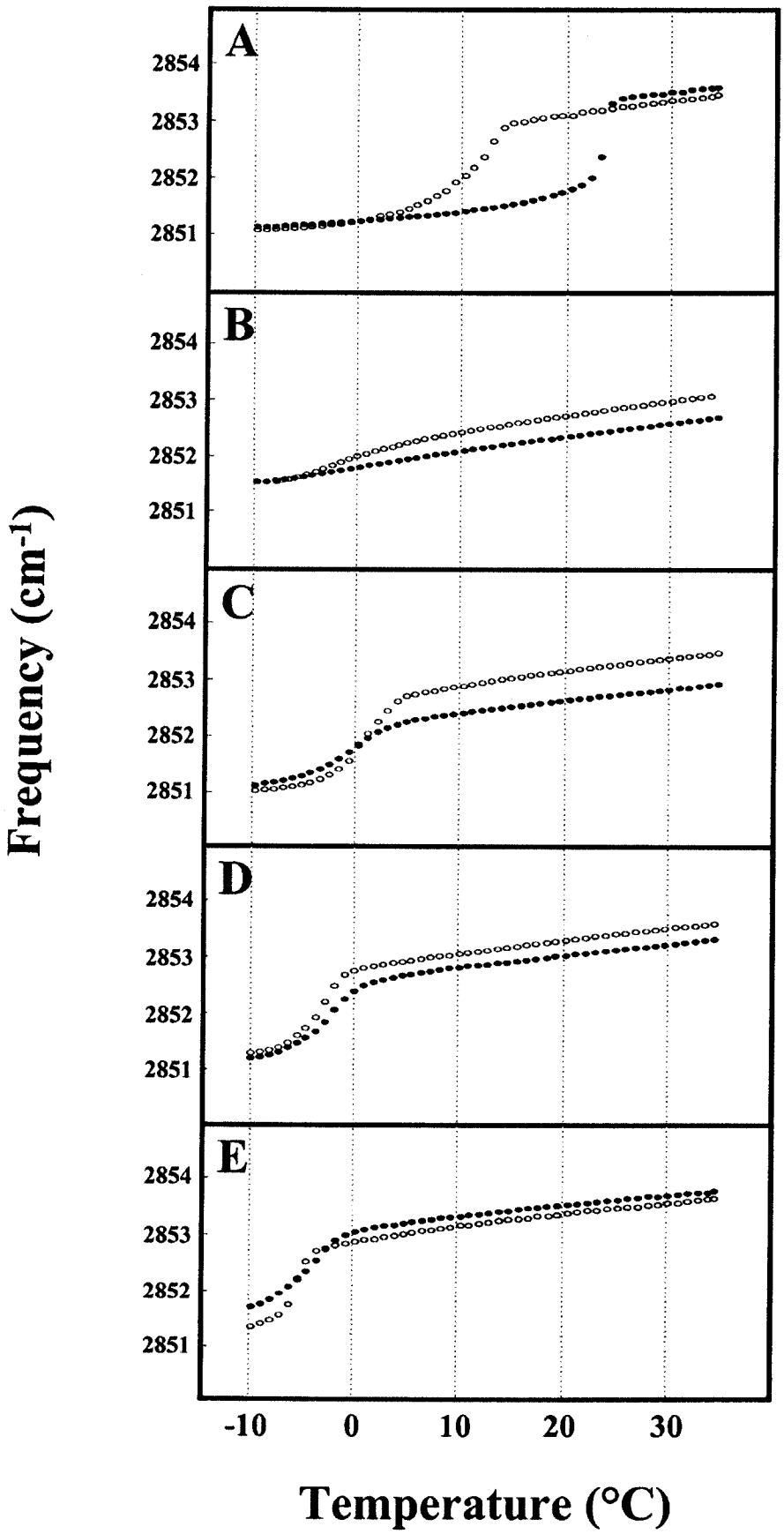
A
B
C
D
E
2854
2853
2852
2851
-10
0
10
20
30
Frequency (cm-1)
Temperature (°C)

Table 3.1

Lipid:protein ratio and gel-to-liquid crystal phase transition temperatures of the lipid membranes measured in the presence and absence of the nAChR. ND = Not determined.

Membrane lipid composition	Lipid:Protein (mole:mole)	T_m of pure lipid (°C)	T_m of lipid + nAChR (°C)	Change in T_m with nAChR (°C)
POPC/POPA 3:2	150:1	11	24	+13
POPC/POPS/Chol 3:1:1	240:1	-2	ND	ND
POPC/POPS 3:2	153:1	+1	-1	-2
POPC/POPS 3:1	152:1	-3	-2	+1
POPC	147:1	-6	-5	+1

between the gel and liquid-crystalline phases is reduced upon nAChR incorporation, possibly due to the presence of calcium (see below)(216). Furthermore, the degree to which the difference in vibrational frequency between the liquid crystalline and gel states is reduced appears to be dependent on the amount of POPS in each membrane. The C-H stretching vibrations of the lipid acyl chains in the liquid crystalline phase of POPC/POPS/Chol 3:1:1 (Figure 3.4B) also vibrate at a slightly lower frequency in the presence of the nAChR essentially eliminating the gel to liquid crystal phase transition. Note that variations in the lipid to protein ratios cannot account for any of the variations in gel to liquid crystal phase transition temperatures (Table 3.1).

The shape of the lipid ester C=O stretching vibration between 1760 and 1700 cm^{-1} is also a qualitative monitor of bilayer physical properties. The band is composed of two components centred near 1741 and 1729 cm^{-1} (Figure 3.5) due to non-hydrogen bonded and hydrogen bonded lipid ester carbonyls, respectively (211). The relative proportion of these two vibrations is a qualitative indicator of the penetration of water into the bilayer interfacial region. A relatively large proportion of non-hydrogen bonded lipid ester carbonyls near 1741 cm^{-1} suggests a low degree of water penetration into the interfacial region of the lipid bilayer and thus a high lateral density of lipid head group packing. Incorporation of the nAChR into POPC/POPA membranes leads to a large increase in the proportion of non-hydrogen bonded lipid ester carbonyls suggesting a substantial ordering of the POPC/POPA membrane. This observations is consistent with the effects of the nAChR on the gel to liquid crystal phase transition temperature of the POPC/POPA membranes (Figure 3.5, right panel, spectrum A). In contrast, reconstitution of the nAChR into POPC has minimal effect on the

Figure 3.5

The carbonyl stretching region in deconvolved spectra of lipid membranes composed of A) 3:2 POPC/POPA, B) 3:1:1 POPC/POPS/Chol, C) 3:2 POPC/POPS, D) 3:1 POPC/POPS, and E) POPC. The left panel shows the deconvolved carbonyl stretching band in spectra of pure lipid membranes. The right panel shows the deconvolved carbonyl stretching region in spectra of the same lipids, but in membranes with the nAChR at the lipid:protein ratios specified in Table 1. All spectra were recorded at 22.5 °C. Note that the spectrum of the nAChR in 3:2 POPC/POPA was recorded just below the gel-to-liquid crystal phase transition whereas all other spectra were recorded in the liquid crystal state. All the spectra have been deconvolved 1900 and 1300 cm^{-1} with a γ factor of 7 and a smoothing parameter of 70%.

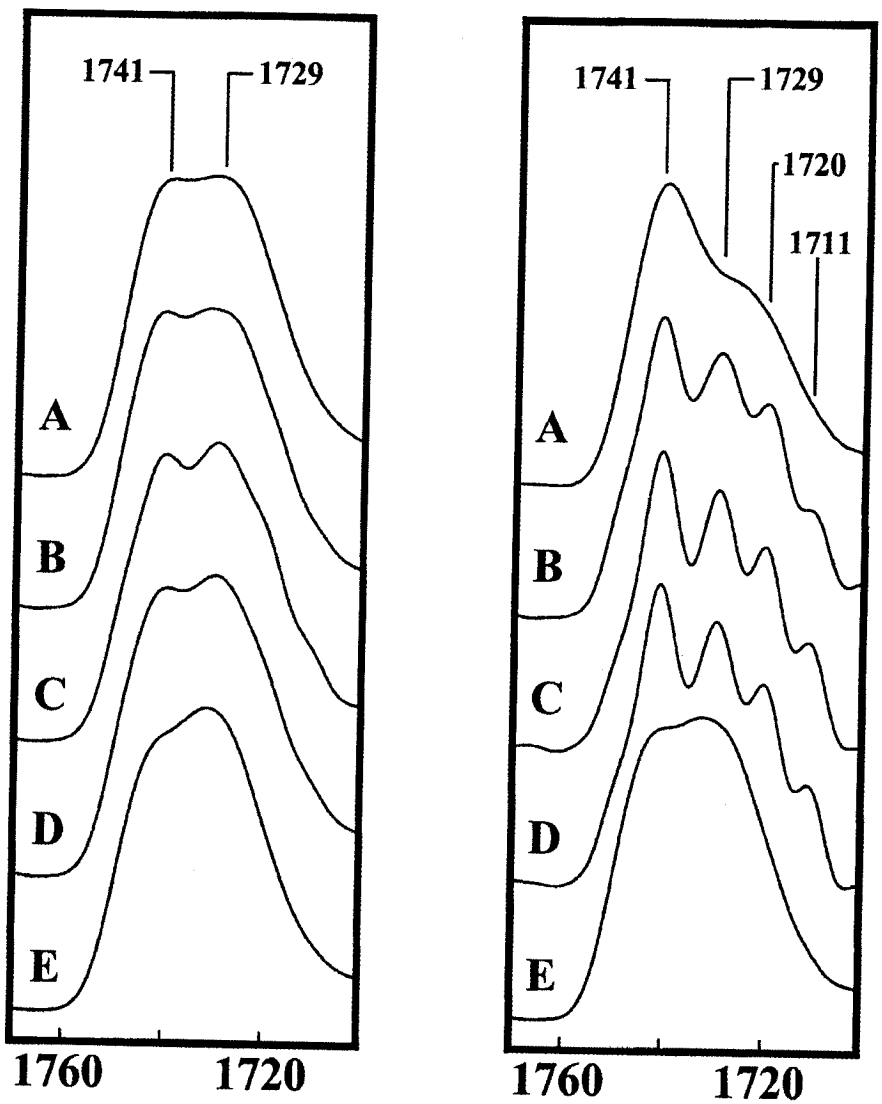
1741
1729
1720
1711
A
B
C
D
E
1760
1720
1760
1720
Wavenumber, cm-1

relative proportion of the two lipid ester carbonyl vibrations suggesting minimal effects on the packing of the bilayer.

Surprisingly, incorporation of the nAChR into membranes composed of either POPC/POPS 3:1, POPC/POPS 3:2, or POPC/POPS/Chol 3:1:1 led to effects on the ester carbonyl stretching vibrations that differ substantially from those observed upon incorporation of the nAChR into either POPC or POPC/POPA 3:2 membranes. For each POPC/POPS membrane, the lipid ester carbonyl stretching band in the presence of the nAChR exhibits four as opposed to two components that are clearly visible in both the deconvolved (Figure 3.5, Right panel, B,C,D) and non-deconvolved (Figure 3.1) spectra at 1741, 1729, 1720, and 1711 cm^{-1}. While not common in FTIR spectra recorded from most lipid membranes, four ester carbonyl stretching vibrations have been detected in spectra of PS bilayers in the presence of calcium (216, 217). In the latter, these vibrations reflect the formation of a complex between Ca^{2+} and the serine carboxylate of PS leading to a reorientation of the glycerol backbone and consequent change in position of the ester carbonyls relative to the polar-apolar lipid interface. Incorporation of the nAChR into POPS containing membranes leads to a dramatic increase in the relative intensity of these four components, suggesting that the presence of the nAChR may lead to the formation of a relatively large proportion of "Ca^{2+}-complexed POPS" (compare Figure 3.5, spectra B,C,D in left vs. right panels).

Role of divalent cations in the interactions between the nAChR and POPS containing bilayers. The altered head group conformation of POPS observed upon incorporation of the nAChR into the POPC/POPS membranes could reflect either an elevated local concentration of Ca^{2+} in the reconstituted versus pure lipid membranes, or a direct

interaction between the nAChR and POPS that mimics the interactions that have been observed by others between Ca^{2+} and PS in pure lipid systems. To distinguish between these two possibilities, we first examined whether or not Ca^{2+} can induce a change in the head group conformation of POPS in a mixed membrane containing both POPS and POPC. In the absence of added divalent cations, spectra of POPC/POPS 3:2 lipid membranes exhibit only two ester carbonyl stretching vibrations (Figure 3.6, Left panel, spectrum A). In *Torpedo* Ringer buffer, which contains 3 mM $CaCl_2$ and 2 mM $MgCl_2$, two main C=O stretching vibrations are observed, but there is subtle intensity in the deconvolved spectra suggesting that a very small proportion of the POPS molecules are complexing with Ca^{2+} (Figure 3.6, left panel, spectrum B). In contrast, four clear ester carbonyl vibrations are observed in spectra of POPC/POPS 3:2 membranes recorded in the presence of 30 mM $CaCl_2$ (Figure 3.6, Left panel, spectrum D) demonstrating that divalent cations form a complex with POPS leading to an alternative head group conformation of POPS in the POPC/POPS 3:2 membranes, even in the absence of the nAChR.

We examined further the involvement of Ca^{2+} by recording FTIR spectra of the reconstituted POPC/POPS 3:2 membranes in buffer lacking divalent cations, as well as in the presence of EDTA. In the absence of added divalent cations, the four intense ester carbonyl vibrations are still evident when the nAChR is present. Addition of 10 mM EDTA led to a reduction in intensity of the four ester carbonyl bands (Figure 3.6, right panel, spectrum C). Interestingly, incubation of the sample in 20 mM EDTA before preparation for FTIR (see methods) completely eliminated the four bands, showing that the altered head group conformation of POPS in the reconstituted nAChR membranes requires the presence of Ca^{2+} and is therefore not likely due to a direct nAChR-POPS interaction (Figure 3.6, right panel,

Figure 3.6

The carbonyl stretching region in deconvolved spectra of 3:2 POPC/POPS membranes hydrated with different ^2H_2O buffers (all pH 7). A) 5mM Tris, B) 5mM Tris, 250mM NaCl, 5mM KCl, 2mM $MgCl_2$ and 3mM $CaCl_2$ (i.e. TRB), C) 5mM Tris, 10mM EDTA *(dashed spectrum incubated in 5mM Tris, 20mM EDTA)*, D) 5mM Tris 30mM $CaCl_2$, and E) 5mM Tris, 250mM NaCl. The left panel shows the deconvolved carbonyl stretching band in spectra of lipid membranes without incorporated nAChR. The right panel shows the deconvolved carbonyl stretching region in spectra of the same buffers, but in the presence of the nAChR. All spectra were recorded at 22.5 °C. All the spectra have been deconvolved 1900 and 1300 cm^{-1} with a γ factor of 7 and a smoothing parameter of 70%.

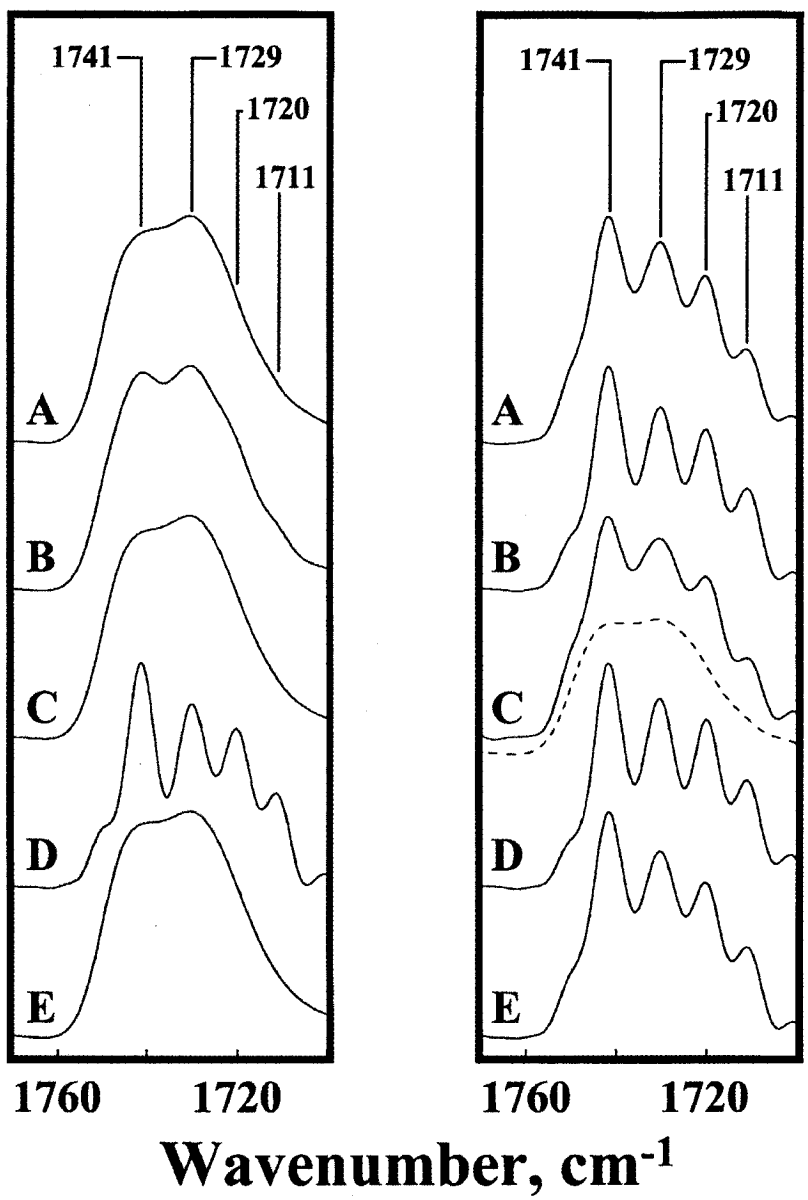
1741
1729
1720
1711
A
B
C
D
E
1760
1720
1741
1729
1720
1711
A
B
C
D
E
1760
1720
Wavenumber, cm-1

dashed spectrum).

Note that the relative amount of Ca^{2+}-complexed versus non-complexed PS molecules in the reconstituted membranes is dependent upon the Ca^{2+} to POPS molar ratio (217). We were initially concerned that the observed increase in Ca^{2+}-complexed POPS in the reconstituted membranes might reflect a greater Ca^{2+} to POPS ratio in the reconstituted samples due to differences in both sample preparation and lipid concentration. To control for this possibility, we prepared FTIR samples using the same protocol for both the reconstituted nAChR and pure lipid membranes using equivalent molar amounts of lipid in each (see methods section). The resulting FTIR spectra are identical to those presented in Figure 3.6 showing that the increase in the amount of Ca^{2+}-complexed POPS in the reconstituted membranes does not reflect an artifact due to variations in sample preparation.

3.6 - Discussion

The main objective of this work was to determine whether or not negative charge is the defining structural feature of PA that makes it such an effective modulator of nAChR function. Reconstituted membranes composed of PC and the anionic lipid PA are particularly effective at stabilizing the nAChR in a conformation that is capable of undergoing agonist-induced conformational change. The nAChR in PC/PA membranes has slower hydrogen exchange kinetics than the nAChR in PC membranes, likely as a result of a slowing of nAChR internal dynamics (196). Incorporation of the nAChR into membranes composed of POPC and POPA also leads to a substantial increase in both the gel to liquid crystal phase transition of the lipid bilayer and the lateral packing density of the lipids (213). In contrast, reconstituted PC or PC/Chol membranes are not as effective at stabilizing the

nAChR in a functional conformation (176) nor does the nAChR have a substantial effect on the physical properties of the lipids upon incorporation into these bilayers (213).

Surprisingly, bilayers composed of POPC with either 25 or 40 mol% POPS are not any more effective at stabilizing the nAChR in a resting state than bilayers composed of POPC alone. FTIR difference spectroscopy shows that neither lipid combination can stabilize the nAChR in a conformation that undergoes agonist induced conformational change. Difference spectra for the nAChR in both POPC/POPS 3:1 and POPC/POPS 3:2 is indicative of a completely desensitized or desensitized-like nAChR. Furthermore, reconstitution of the nAChR into membranes composed of POPC/POPS had little effect on the gel to liquid crystal phase transition of the bilayer and thus on the physical properties of the membrane. In contrast to PA, there is no bi-directional coupling between the structure/function of the nAChR and the structure of its surrounding lipid environment in membranes composed of POPC/POPS.

The inability of PS and the nAChR to interact with each other in a manner that mimics the interactions that occur between the nAChR and PA clearly shows that a net negative charge is not the sole defining structural feature that makes PA an effective modulator of nAChR function. While studies with a wider range of anionic lipids is required for a complete understanding of the role of lipid charge in modulating nAChR function, our data highlight the possibility that PA is unique in its interactions with the receptor. Defining the nature of these interactions is important for understanding the mechanisms of lipid-protein interactions at the nAChR. These interactions could also have broader biological significance. Although PA is found at low levels in *Torpedo* membranes, it is possible that there are high local "concentrations" of PA within the bilayer that influence nAChR function

in a post-synaptic membrane (214). The nAChR in neuronal membranes is targeted to lipid rafts (218-220). It is possible that PA acts within rafts or microdomains to modulate nAChR function *in vivo*. The same mechanisms by which the nAChR influences the physical properties of bilayers containing PA could also allow the nAChR to participate in lipid raft or microdomain formation.

Despite its inability to stabilize a functional nAChR, our data show that POPS interacts with the nAChR in a unique fashion. Reconstitution of the nAChR into membranes composed of POPC/POPS leads to the appearance of four lipid ester carbonyl stretching vibrations near 1741, 1729, 1720, and 1711 cm^{-1} (Figure 3.5, Right panel, B,C,D). Hubner *et al.* have reported that four lipid ester carbonyl stretching vibrations are observed in spectra recorded from PS membranes in the presence of calcium. These four bands reflect the formation of a complex between Ca^{2+} and the serine carboxylate of PS leading to a reorientation of the glycerol backbone and consequent change in position of the ester carbonyls relative to the polar-apolar lipid interface. The different positions of the ester carbonyls in the bilayer gives rise to variations in their extent of hydration, which in turn gives them distinct absorption frequencies in the IR spectrum. In PS-Ca^{2+} membranes, the 1741cm^{-1} and 1720 cm^{-1} peaks originate from the non-hydrogen and hydrogen bonded *sn*-1 ester carbonyl respectively, while the 1729 cm^{-1} and 1711 cm^{-1} peaks originate from the non-hydrogen and hydrogen bonded *sn*-2 ester carbonyl respectively (217). The intensities of the four components reflects the relative proportion of Ca^{2+}-complexed PS.

The altered head group conformation of POPS in the presence of the nAChR is also dependent upon the presence of divalent cations as the spectral features indicative of the formation of this altered conformation are eliminated in the presence of 20 mM EDTA. The

finding that divalent cations are still present in the reconstituted POPC/POPS membranes is surprising. In fact, the altered head group conformation of POPS in the reconstituted POPC/POPS membranes is observed even when divalent cations are not added to the FTIR samples. During affinity purification and reconstitution of the nAChR into the POPC/POPS membranes, neither the lipids nor the nAChR are exposed to buffer containing added Ca^{2+}. In fact, all the solutions used in the reconstitution protocol contain 0.1 mM concentrations of EDTA. The fact that the reconstituted samples exhibit an altered POPS conformation dependent on divalent cations, despite stringent efforts to remove divalent cations (including 5 times dialysis against two litres of divalent cation free buffer with EDTA), shows that either POPS or the nAChR, or a combination of both components have an extremely high affinity for Ca^{2+}. Given that the nAChR is a cation selective ion channel and has a pI of ~5, it is possible the nAChR recruits Ca^{2+} to the bilayer surface in native membranes leading to an elevated local concentration. Ca^{2+} may bridge a direct interaction between negatively charged lipids and the nAChR that is formed in native membranes and maintained throughout the affinity purification protocol. The nAChR and/or POPS must have an extremely high affinity for divalent cations.

A second relevant feature of PS lipid bilayers reported by Hubner *et al.* is that Ca^{2+}-complexation leads to a dramatic increase in the gel-liquid crystal transition temperature. In samples with only a fraction of the PS complexed to Ca^{2+}, two transitions are observed - one transition at the temperature expected for the non-complexed form of PS and the second at a higher temperature due to the Ca^{2+}-complexed PS (217). In our reconstituted POPC/POPS samples containing the nAChR, only one transition is observed, but the C-H stretching frequency of the lipids in the liquid-crystalline phase is always reduced relative to the

frequency of the vibration observed for membranes lacking the nAChR (see in particular Figure 3.4, box C). The degree to which the frequency is depressed may reflect the percentage of complexed PS in the membrane (compare Figure 3.4, boxes C,D). The temperature of the gel to liquid crystal transition of the structurally altered POPS in our reconstituted nAChR membranes may be higher than the temperature range of our experiment. Heating the samples beyond 35°C might induce a second transition bringing the frequency of the C-H stretching vibration closer to that seen for the liquid-crystalline state in membranes without the nAChR.

Our results show that the nAChR can interact with two anioinic lipids, PA and PS, in specific and distinct fashions. The interactions between the nAChR and PA lead to a functional receptor, while the interactions between the nAChR and PS do not. Interactions between the nAChR and PS could, however, still play an important role maintaining membrane structure. The data show that lipid-protein interactions at the nAChR are clearly complex.

Finally, it is interesting to note that mixtures of POPC/POPS/Chol 3:1:1 are effective at modulating nAChR structure and function. The residual amide II intensity observed after exposure of the nAChR in POPC/POPA/Chol 3:1:1 to $^{2}H_{2}O$ suggests that this membrane exhibits peptide hydrogen exchange kinetics that are intermediate between the kinetics observed for the nAChR in POPC/POPA 3:2 and POPC/POPS samples (Figure 3.3, right panel, spectrum B). The nAChR in POPC/POPS/Chol 3:1:1 also exhibits an ability to stabilize the resting conformation of the nAChR that is intermediate between membranes composed of POPC/POPA and those composed of POPC/POPS. The relative proportion of functional receptors is greater than what would be expected for a PC membrane with only

20% Chol (176) or 20% POPS, suggesting that PS and Chol work synergistically to provide a somewhat functional nAChR membrane.

It appears that POPS and Chol act together to create an environment conducive to resting state stabilization. We and others have suggested that membrane fluidity may play a role in modulating the functional state of the nAChR (155, 176, 213). It is possible that the combination of a small headgroup and negative charge on PA allows mixtures of PA and PC to create an ordered, net negatively charged environment that is similar to the environment found in PC/PA/Chol or POPC/POPS/Chol membranes. Further studies should elucidate how interactions between lipids such as PS and PA, as well as bilayer physical properties and divalent cations all work together to create an environment conducive for optimal nAChR function.

CHAPTER 4

MANUSCRIPT:

3. **Corrie J.B. daCosta**, Daniel E. E. Kaiser, and John E. Baenziger. (2005) **Role of glycosylation and membrane environment in nicotinic acetylcholine receptor stability.** *Biophys J.* **88(3)**, 1755-1764.

4.1 - Preface

This, the third and final manuscript presented in this thesis, was published in the spring of 2005 in the Biophysical Journal. The paper is based more on my second research project geared towards crystallizing the nAChR from *Torpedo*. It describes systematic studies exploring the feasibility of enzymatically removing some, or all of the nAChR's extensive glycosylation. Our lack of success with nAChR crystallization led us to believe that this glycosylation may interfere with the formation of nAChR crystals. We hoped that by removing some or all of this sugar we could increase the likelihood of nAChR crystallization, however since the function of this glycosylation was unknown, we were also interested in the effects of glycosylation on nAChR structure and function. We therefore used FTIR spectroscopy to examine in detail the consequences of enzymatically removing the nAChR's glycosylation. We also compared the effects of deglycosylation to those observed upon reconstitution of the nAChR into a simple phosphatidylcholine membrane. This comparison led us to believe that our difficulties with nAChR crystallization are most likely related to its intimate relationship with its surrounding lipids.

I collected all the spectra presented in this manuscript. Dan Kaiser assisted in identifying the conditions for deglycosylation of both membrane bound and detergent solubilized nAChR.

4.2 - Abstract

The effects of glycosylation and membrane environment on the structural stability of the nicotinic acetylcholine receptor (nAChR) from *Torpedo* have been investigated in order to improve our understanding of factors that influence eukaryotic membrane protein crystallization. Gel shift assays and carbohydrate specific staining show that the deglycosylation enzyme, Endo F1, removes at least 50% of membrane reconstituted nAChR glycosylation. The extent of deglycosylation with Endo F1 increases upon detergent solubilization. Removal of between 60-100% of high mannose moieties from the nAChR has no effect on nAChR secondary structure, stability, or flexibility. Deglycosylation does not influence either agonist binding or the ability of the nAChR to undergo agonist induced conformational change. In contrast, nAChR structural stability, flexibility, and function are all negatively influenced by simple changes in reconstituted membrane lipid composition. Our results suggest that deglycosylation may represent a feasible approach for enhancing the crystallizability of the nAChR. Our data also demonstrate that the dependence of nAChR structural stability on lipid environment may represent a significant obstacle to nAChR crystallization. Some membrane proteins may have evolved complex interactions with their lipid environments. Understanding the complexity of these interactions may be essential for devising an appropriate strategy for the crystallization of some membrane proteins.

4.3 - Introduction

Advances in membrane protein crystallography over the past ten years have mainly involved proteins of bacterial as opposed to eukaryotic origin (70, 221-224). While there are several factors that contribute to this discrepancy, the extensive glycosylation found on the extramembranous surfaces of some eukaryotic membrane proteins may play a significant role. Large and highly flexible carbohydrate could form a conformationally-labile shield that hinders the formation of crystal contacts. Heterogeneity of membrane protein glycosylation is also common and could further act as a detriment to crystallization. Although the presence of carbohydrate does not necessarily prevent crystal formation (225-230) carbohydrate removal may, in some cases, increase the likelihood of success.

Removing glycosylation from the surfaces of eukaryotic membrane proteins, however, is problematic. Recombinant approaches, such as the mutagenesis of glycosylation-attachment sites, could in principle be used to completely eliminate carbohydrate. Unfortunately, the expression of recombinant eukaryotic membrane proteins in either bacteria or eukaryotic systems has proven to be either extremely difficult or prohibitively expensive (231).

An alternative approach is to enzymatically remove interfering carbohydrate from naturally abundant eukaryotic membrane proteins. The enzymatic removal of carbohydrate has been successful with soluble proteins (133, 232, 233). Before directly testing the effects of deglycosylation on crystallization, however, there are two additional issues that need to be addressed. First, glycosidase cleavage sites in a natively folded membrane protein may be inaccessible due to the surface topology of the protein (234) and/or steric hinderance from the surrounding membrane. In every case, the feasibility of deglycosylating a native

membrane protein needs to be demonstrated. Second, while the role of glycosylation in membrane protein assembly, recognition and trafficking is well established (235-237), very little is known with respect to its role in protein stability and function. The presence of large glycans on protein loop or turn structures may restrict overall protein flexibility (238) and could be important for the structural stability of a folded membrane protein. As protein stability is particularly critical in membrane protein crystallization (239-241), a legitimate concern is that deglycosylation could increase protein internal dynamics and render a protein less likely to crystallize. The structural and functional ramifications of removing carbohydrate must therefore be assessed.

The nicotinic acetylcholine receptor (nAChR) from *Torpedo californica* is the best characterized member of a superfamily of ligand-gated ion channels, whose members represent the major excitatory and inhibitory neurotransmitter receptors found throughout the mammalian central and peripheral nervous systems. Nicotinic receptors play a central role in intercellular communication within the brain and are the sites of action of numerous pharmaceutical agents (242-244). *Torpedo* nAChR is a 290 kDa pentameric glycoprotein complex composed of four highly homologous subunits ($\alpha_2\beta\gamma\delta$) arranged pseudosymmetrically around a central pore, which functions as a cation-selective channel (13, 97). 75% of the nAChR by mass is extramembranous (67, 110). This relatively large extramembranous region should provide ample surface for the establishment of crystal contacts and thus render the nAChR relatively amenable to crystallization. Despite intense effort, the nAChR has remained refractory to crystallization (93, 94), possibly because of its extensive glycosylation (7.5% by wt). As the composition and structure of the nAChR's

carbohydrate has been characterized (44-46, 245), the nAChR is an ideal candidate for testing the feasibility of deglycosylation as an aid to membrane protein crystallization.

In this report, we examine the feasibility of deglycosylating native nAChR and have characterized both the structural and functional consequences of nAChR deglycosylation. Our results suggest that a substantial proportion (roughly 50% by wt.) of carbohydrate can be successfully removed from natively folded nAChR and that removal of this carbohydrate has no effect on nAChR structural stability, internal dynamics, or function. In fact, the structural and functional consequences of deglycosylation are insignificant compared to the effects of simple changes in membrane lipid composition. Our results support the feasibility of deglycosylation as an approach for enhancing crystallization. Our data also emphasize the key role played by membrane environment in maintaining membrane protein structure and stability.

4.4 - Experimental Procedures

Materials. Frozen *Torpedo californica* electroplax tissue was from either Marinus (Long Beach, CA) or Aquatic Research Consultants (San Pedro, CA). Neuraminidase (Sialidase) from *Vibrio cholerae* was from Roche Applied Science (Laval, Quebec). Recombinant (*E.coli*) GST-Peptide-N^4-(acetyl-*beta*-glucosaminyl)-asparagine amidase (PNGase F) and GST-Endo-β-N-acetylglucosaminidase F1 (Endo F1) from *Chryseobacterium meningosepticum* were from Hampton Research (Laguna Niguel, CA). 1-Palmitoyl-2-oleoyl-*SN*-glycero-3-phosphocholine (POPC) was from Avanti Polar Lipids (Alabaster, AL), while L-α-phosphatidyl-choline (soybean asolectin, Type II-S) was from Sigma (St. Louis, MO), and n-decyl-β-D-maltopyranoside (decylmaltoside) was from

Calbiochem (La Jolla, CA). Low range prestained SDS-PAGE standards were from BioRad (Missassauga, ON). All other reagents were from Sigma or VWR (Missassauga, ON).

nAChR Purification. Crude nAChR membranes from roughly 100 g of *Torpedo* electroplax tissue were solubilized for 1 h at 4°C in a total volume of 100 ml of dialysis buffer (DB = 100 mM NaCl, 10 mM Tris-HCl, 0.1 mM EDTA, 0.02% w/v NaN_3, pH=7.8) containing 1% cholate. Samples for deglycosylation studies were also solubilized in the presence of 100mM β-mercaptoethanol to reduce disulfide linked δ-δ dimers, which leads to the purification of monomeric receptor (i.e. monomers of the $\alpha_2\beta\gamma\delta$ pentamer). Monomerization has no effect on nAChR structure or function (246)(daCosta & Baenziger, unpublished). In all cases, the solubilized nAChR was centrifuged for 30 min at 87,000X*g* to pellet insoluble material and the supernatants applied to a 10-ml affinity column at a flow rate of 1 ml/min.

Decylmaltoside-solubilized nAChR samples for deglycosylation studies were prepared by washing the nAChR on the affinity column with 40ml of 15mM cholate in DB followed by a 7.5ml linear gradient to 2.2mM decylmaltoside in DB. The column was washed with a further 10 ml of 2.2mM decylmaltoside in DB in order to ensure complete exchange of cholate for decylmaltoside and then eluted in 2.2mM decylmaltoside DB containing 10mM Carb. Fractions with an *A*280 greater than 0.05 were pooled and concentrated to 10-30mg/ml by ultrafiltration using a 100kDa MWCO concentrator (Millipore, Ottawa, ON).

nAChR samples for reconstitution into asolectin or POPC were washed on the affinity column with excess, cholate solubilized asolectin or POPC, respectively and then eluted with 10 mM Carb, as described in detail elsewhere (213). Fractions with an A_{280}

greater than 0.05 were pooled in dialysis bags (12–14kDa MWCO) and dialyzed five times against 2 liters of dialysis buffer with buffer change once every 12hrs.

Deglycosylation. Decylmaltoside-solubilized nAChR at a concentration of roughly 20mg/ml was incubated with Endo F1, PNGase F or Sialidase either alone or in various combinations as described in the text. Aliquots were removed at specified times, added directly to SDS-PAGE sample buffer, and stored at -80°C. Each aliquot containing 10-15μg protein was thawed and run on a discontinuous Tris-HCl gel, with a 12% w/v separating and a 4% w/v stacking acrylamide gel. Protein was stained with Coomassie Blue.

The nAChR reconstituted into soybean asolectin (~20mg/ml in 10mM Tris-HCl, pH=7.5) was deglycosylated by incubation on ice for 90 minutes with recombinant Endo F1 (15:2 v/v, nAChR:Endo F1). After incubation, the samples were stored at -80°C. Deglycosylation was again monitored by SDS-PAGE (Figure 4.2A). In addition, residual oligosaccharides were detected directly on the SDS gels by sugar-specific staining using the GelCode® glycoprotein staining kit from Pierce (Rockford, IL). Briefly, the gels were treated with periodic acid to oxidize carbohydrate glycols, and the resulting aldehydes stained with Acidic Fuchsin Sulfite (aldehyde specific stain).

FTIR Spectroscopy. FTIR spectra were recorded on either an FTS 40 or an FTS-575c spectrometer (Digilab; Randolph, MA), equipped with a DTGS detector. Experimental protocols have been described in detail elsewhere (205, 206, 213). Briefly, difference spectra were recorded from a nAChR membrane film deposited on the surface of a germanium attenuated total reflectance element. Carb difference spectra are the difference between spectra of the nAChR recorded in *Torpedo* ringer buffer (TRB=250mM NaCl, 5mM KCl, 2mM $MgCl_2$, 3mM $CaCl_2$, and 10mM Tris, pH=7.0) in the presence or absence of 50

μM carbamylcholine (Carb). Transmission spectra were recorded from the nAChR in ^2H_2O *Torpedo* ringer buffer after precisely 72hr exposure to ^2H_2O (2mM Phosphate, pH=7.0) at 4°C. Spectra were analyzed using GRAMS/AI v.7.01 software (Thermo Galactic; Salem, NH). Solvent ^2H_2O was subtracted from each spectrum and deconvolution of the amide I was performed, where noted, between 1900 and 1300cm^{-1} with $\gamma = 7.0$ and a smoothing parameter of 70%. Spectra were analyzed for residual H_2O vapour, which was subtracted if necessary (204).

$^1H/^2H$ Exchange Kinetics. 250 μg of reconstituted nAChR in 50 μL of 2mM ^1H_2O phosphate buffer (pH=7.0) was dried on a 45 degree, 50x20x2mm germanium total internal reflection element (Harrick Scientific, Ossining, New York). After complete evaporation of ^1H_2O phosphate buffer, as monitored using the OH stretching vibration (approx. 3500cm^{-1}), the nAChR film was rehydrated with 2.9ml of ^2H_2O *Torpedo* Ringer buffer and 2 cm^{-1} resolution IR spectra (86 scans) acquired every 3 minutes for approximately 12hrs (250 total spectra). All spectra were offset corrected at 1900cm^{-1} and the residual amide II intensity (1547cm^{-1}) ratioed against the maximal intensity of the amide I. The t_0 point was calculated from spectra of the dry nAChR film prior to rehydration.

Thermal Denaturation. 250 μg of reconstituted 72hr $^1H/^2H$ exchanged nAChR was placed in a thermostatic transmission cell, the temperature of which was controlled by a circulating water bath. Spectra (2 cm^{-1} resolution and 256 scans) were recorded at 2°C intervals as the sample was heated from 25°C to ~75°C. Five minute intervals were allowed for the water bath to reach each temperature, and then a further fifteen minutes for sample equilibration. The actual temperature of the sample cell was monitored using an electronic thermometer (Barnant; Barrington, IL) with a Type J thermocouple probe. Spectra were

deconvolved between 1800 cm^{-1} and 1300 cm^{-1} with $\gamma = 8.0$ and a smoothing parameter of 80% using GRAMS/AI v.7.01 software (Thermo Galactic; Salem, NH). Percent denaturation was monitored by the percent change in intensity at 1681cm^{-1}. Thermal denaturation is best characterized by the relatively small changes in intensity near 1681 cm^{-1} because changes in intensity near 1623 cm^{-1} are influenced by the spectral changes associated with a gradual increase in peptide hydrogen exchange kinetics with increasing temperature.

4.5 - Results

nAChR Deglycosylation. The ability of three different glycosidase enzymes, Endo F1, PNGase F, and Sialidase, to independently and cooperatively deglycosylate detergent solubilized nAChR was tested under varying conditions of temperature, reaction time and glycosidase/nAChR molar ratio. In each case, the extent and homogeneity of deglycosylation was assessed by SDS-PAGE (Figures 4.1 and 4.2). The presented data are representative of the maximal levels of deglycosylation achieved by each enzyme or enzyme combination under all of the conditions tested. Levels of deglycosylation similar to those observed in Figure 4.1 were subsequently achieved in less than two hours with two to three fold increases in enzyme concentration, as shown for the membrane reconstituted samples in Figure 4.2A. Deglycosylation of the membrane reconstituted samples was also assessed with a carbohydrate specific stain (Figure 4.2B).

Treatment with Endo F1 led to an increase in the electrophoretic mobility (~2kDa) of all four nAChR subunits suggesting deglycosylation (Figure 4.1C). Each of the four nAChR

Figure 4.1

SDS-PAGE of decylmaltoside solubilized nAChR incubated with **(A)** Sialidase, **(B)** PNGase F, **(C)** Endo F1, **(D)** Sialidase and PNGase F, **(E)** Sialidase and Endo F1, **(F)** PNGase F and Endo F1 and **(G)** Sialidase, PNGase F and Endo F1 for 1, 4 and 8 days. For the individual enzyme experiments the nAChR (20 mg/ml) was mixed 75:4 (v/v, nAChR:Endo F1 or Sialidase) or 75:2 (v/v, nAChR:PNGase F) with each enzyme as supplied by the manufacturer. For the combination experiments nAChR was mixed 75:2:2 (v/v/v, nAChR:glycosidase 1:glycosidase 2) or 75:2:2:2 (v/v/v/v, nAChR:glycosidase 1:glycosidase 2:glycosidase 3). The controls on the left of each panel have not been incubated with enzyme. The standards shown correspond to MWs of 116, 80, 51.8, and 34.7kDa from top to bottom respectively. The positions of the nAChR subunits are indicated on the left.

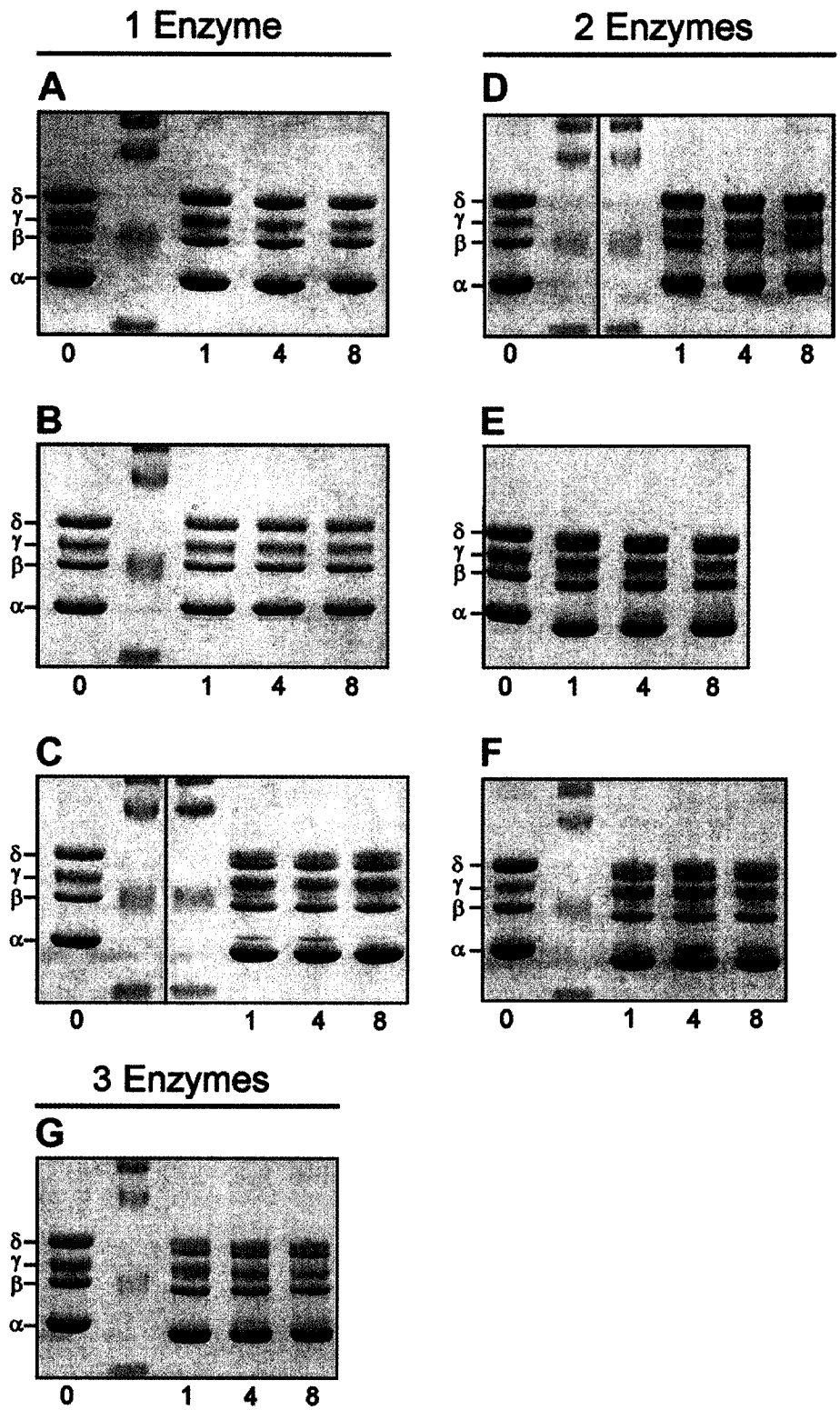
1 Enzyme
2 Enzymes
A
D
δ
γ
β
α
0
1
4
8
B
E
C
F
3 Enzymes
G

Figure 4.2

Deglycosylation of the nAChR reconstituted into soybean asolectin membranes. **(A)** SDS-PAGE of glycosylated (i) and Endo F1 deglycosylated (ii) nAChR. **(B)** SDS gel stained with a carbohydrate specific stain. The leftmost lane in (B) is a glycoprotein positive control (horse radish peroxidase).

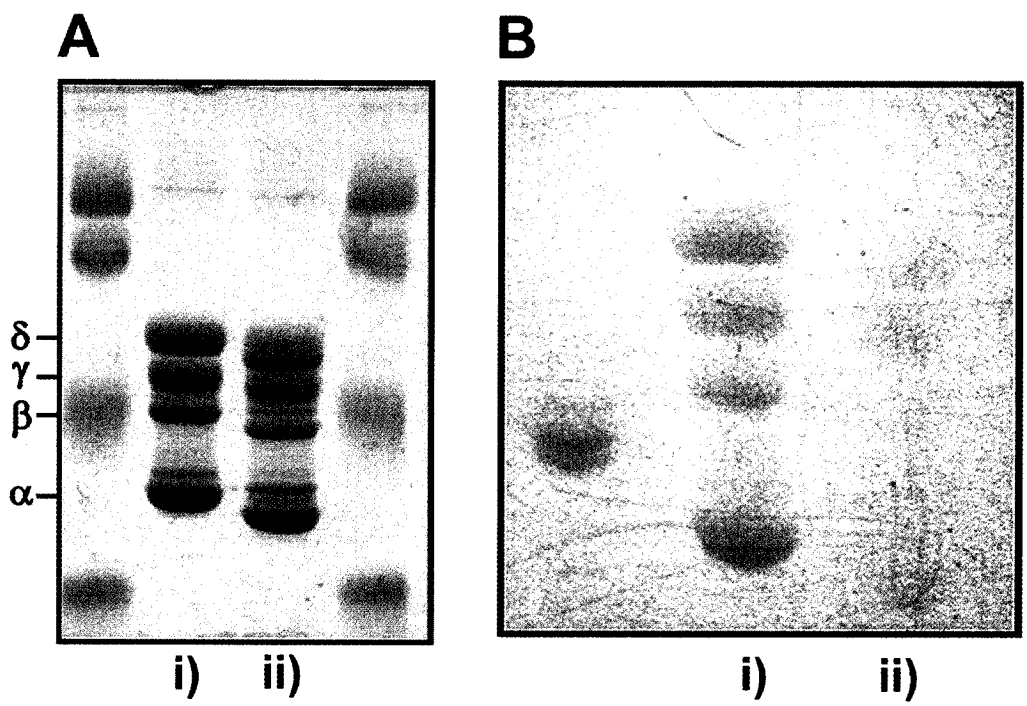
A
B
δ
γ
β
α
i)
ii)
i)
ii)

subunits has one high mannose carbohydrate moiety that is potentially cleaved by Endo F1. In the case of the two α-subunits and the β-subunit, this high mannose glycan is their only carbohydrate (44). The complete and homogenous deglycosylation of these two subunits indicates that their high mannose moiety is accessible and readily cleaved by Endo F1. Carbohydrate specific staining shows essentially complete removal of carbohydrate from the α- and β-subunits (Figure 4.2B).

In contrast, the presence of two δ-subunit bands with distinct electrophoretic mobilities indicates that Endo F1 treatment led to heterogeneous deglycosylation of the δ-subunit (Figure 4.1C). The γ- and δ-subunits are glycosylated with both high mannose and either one or two complex-type carbohydrates, respectively (45, 46, 245). Furthermore, thirty two different varieties of complex carbohydrates have been identified on these subunits, highlighting their overall heterogeneity in terms of complex carbohydrate structure (46). In some cases, particular complex-type structures may sterically restrict the access of Endo F1 to the γ- and δ-subunit's high mannose moiety. Heterogeneity of the γ- and δ-subunit glycosylation may thus account for the observed inability to homogeneously deglycosylate these subunits.

Unlike Endo F1, PNGase F and Sialidase are both capable of removing complex-type carbohydrate, although PNGase F cleaves at the carbohydrate-protein link while Sialidase cleaves terminal sialic acid residues. Under the conditions tested, treatment with PNGase F had essentially no effect on nAChR subunit mobility and thus carbohydrate content, suggesting that the carbohydrate-protein link is inaccessible to PNGase F in a natively folded nAChR (Figure 4.1B). Sialidase led to subtle increases in the electrophoretic mobility of both the γ- and δ-subunits, and thus subtle changes in the levels of their complex-type

carbohydrate (Figure 4.1A). Removal of this small proportion of complex-type carbohydrate did not noticeably enhance the ability of Endo F1 to remove the high mannose glycan on the δ-subunit (Figure 4.1E,G).

We also compared the ability of Endo F1 to deglycosylate detergent solubilized versus membrane reconstituted nAChR. Comparison of Figures 4.1C and 4.2A shows that while Endo F1 is more effective at deglycosylating detergent solubilized nAChR, it is still able to deglycosylate a substantial proportion of membrane reconstituted receptor. Staining for oligosaccharides suggests that the majority of the receptor's carbohydrate has been removed (Figure 4.2B). Consistent with the detergent solubilized nAChR data, the remaining carbohydrate detected by the oligosaccharide stain is located primarily on the γ- and δ-subunits. This ability to partially deglycosylate membrane reconstituted nAChR samples with Endo F1 has allowed us to assess the structural and functional effects of nAChR deglycosylation. All nAChR structural and functional characterization was performed on membrane reconstituted nAChR samples that were deglycosylated with Endo F1 as presented in Figure 4.2. Note that it is of particular interest to test whether or not complete deglycosylation of the ligand-binding α-subunits influences nAChR function.

Effect of Deglycosylation on nAChR Structure. The structural effects of deglycosylation on membrane reconstituted nAChR were assessed using FTIR spectroscopy. The amide I band (1600-1700cm^{-1}) is due predominantly to the peptide carbonyl stretching vibration and its shape is sensitive to protein secondary structure (215). The deconvolved amide I band in spectra of glycosylated and Endo F1 deglycosylated nAChR both exhibit the same number of component bands with similar relative intensities, including two major peaks centered near 1655 cm^{-1} and 1639 cm^{-1} due to α-helical and β-sheet secondary

structures, respectively (Figure 4.3A)(215). The essentially identical amide I band shapes indicates that extensive deglycosylation has no effect on nAChR secondary structure. The two samples also exhibit essentially identical residual amide II band intensity near 1547 cm^{-1} (primarily N-^{1}H bend) (Figure 4.3B). As the amide II vibration shifts down in frequency from 1547 cm^{-1} to 1456 cm^{-1} upon the exchange of peptide N-^{1}H for N-^{2}H (see Figure 4.4), the similar residual amide II intensities indicates that glycosylated and deglycosylated nAChR have essentially identical levels of peptide $^1H/^2H$ exchange after 72hrs exposure to ^2H_2O at 4°C. Note that the relative levels of peptide $^1H/^2H$ exchange in the FTIR spectra can be visually assessed by comparing the residual amide II intensity at 1547 cm^{-1} to that of the adjacent side chain carboxyl stretching vibration centered near 1580 cm^{-1}.

For comparison, we recorded spectra of glycosylated nAChR reconstituted into POPC as opposed to asolectin membranes. The nAChR undergoes more extensive peptide $^1H/^2H$ exchange in POPC, as indicated by the lower residual amide II band intensity near 1547 cm^{-1} (Figure 4.3B). Although nAChR secondary structure is not affected by reconstitution into POPC (190, 213), subtle differences in amide I/I' band shape of 72hr $^1H/^2H$ exchanged samples are observed (Figure 4.3A). These differences in band shape reflect an increased number of α-helical peptide hydrogens that have exchanged for deuterium, which results in a shift in α-helical amide I component band intensity from 1655 cm^{-1} down to 1645 cm^{-1}(190).

Effects of Deglycosylation on nAChR Internal Dynamics. The rate of peptide $^1H/^2H$ exchange is sensitive to protein internal dynamics. As subtle differences in internal dynamics could potentially have dramatic effects on crystallizability, we examined the effects of deglycosylation on the kinetics of nAChR peptide $^1H/^2H$ exchange. Figure 4.4A

Figure 4.3

Effect of deglycosylation and membrane environment on nAChR structure. **(A)** The deconvolved amide I/I' band from glycosylated (i) and Endo F1 deglycosylated (ii) nAChR reconstituted into soybean asolectin membranes, as well as glycosylated nAChR reconstituted into POPC (iii) membranes. The deconvolved spectra show the frequencies and relative intensities of amide I (1655 cm^{-1}, α-helix and 1639 cm^{-1}, β-sheet) and amide I' (1645 cm^{-1}, $^{1}H/^{2}H$ exchanged α-helix) component bands, and thus provide a sensitive measure of nAChR secondary structure. **(B)** Non-deconvolved residual amide II band. Note the amide II vibration (1547 cm^{-1}) partially overlaps with broad bands due to side chain asymmetric COO^{-} stretching vibrations near 1580 and 1560 cm^{-1}. Spectra were recorded at 22.5°C after each sample was exchanged for precisely 72hrs at 4°C. Each spectrum is representative of between four and seven spectra recorded from each sample.

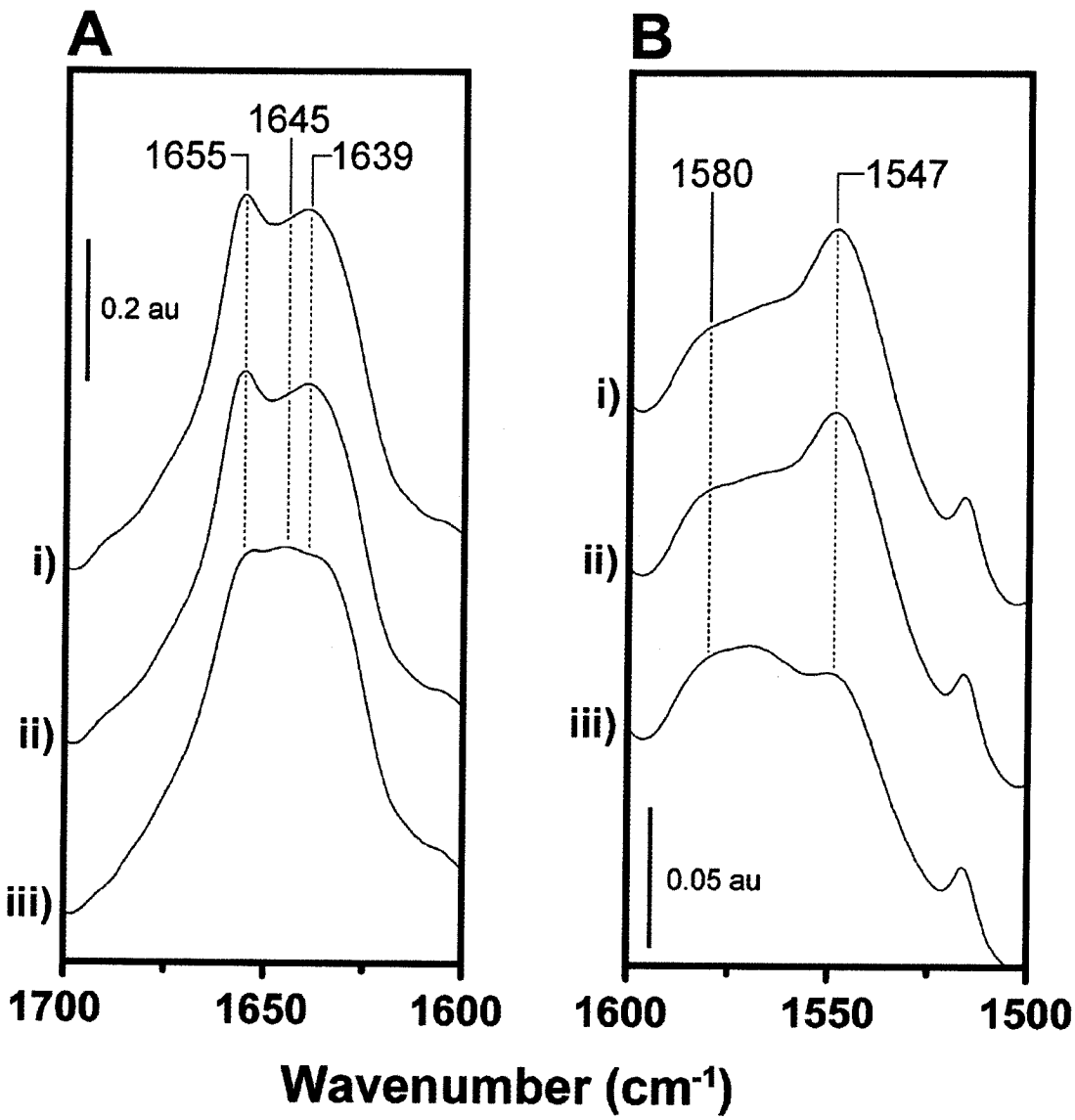
A
1655
1645
1639
0.2 au
i)
ii)
iii)
1700
1650
1600
B
1580
1547
i)
ii)
iii)
0.05 au
1600
1550
1500
Wavenumber (cm-1)

Figure 4.4

Effect of deglycosylation and membrane environment on the kinetics of nAChR peptide $^{1}H/^{2}H$ exchange. **(A)** Non-deconvolved FTIR spectra of glycosylated (i) and Endo F1 deglycosylated (ii) nAChR reconstituted into asolectin membranes as well as POPC reconstituted nAChR (iii). Spectra were recorded after 3 (solid line, top), 24 (dashed line, middle), and 750 (dotted line, bottom) minutes exposure to deuterated buffer at 22.5°C. **(B)** The hydrogen exchange kinetics are plotted as the ratio of residual amide II to amide I band intensity as a function of time after exposure to $^{2}H_2O$ *Torpedo* Ringer buffer for glycosylated (filled circles, n=5), Endo F1 deglycosylated (open circles, n=2), and glycosylated POPC reconstituted nAChR (filled diamonds, n=4). Error bars represent (+) or (-) standard deviation of the mean. Where error bars are not visible they are smaller than the data points. **(C)** Deconvolved lipid ester carbonyl stretching region. Hydrogen bonded ester carbonyls ($1729cm^{-1}$) and non-hydrogen bonded ester carbonyls ($1741cm^{-1}$) are labelled.

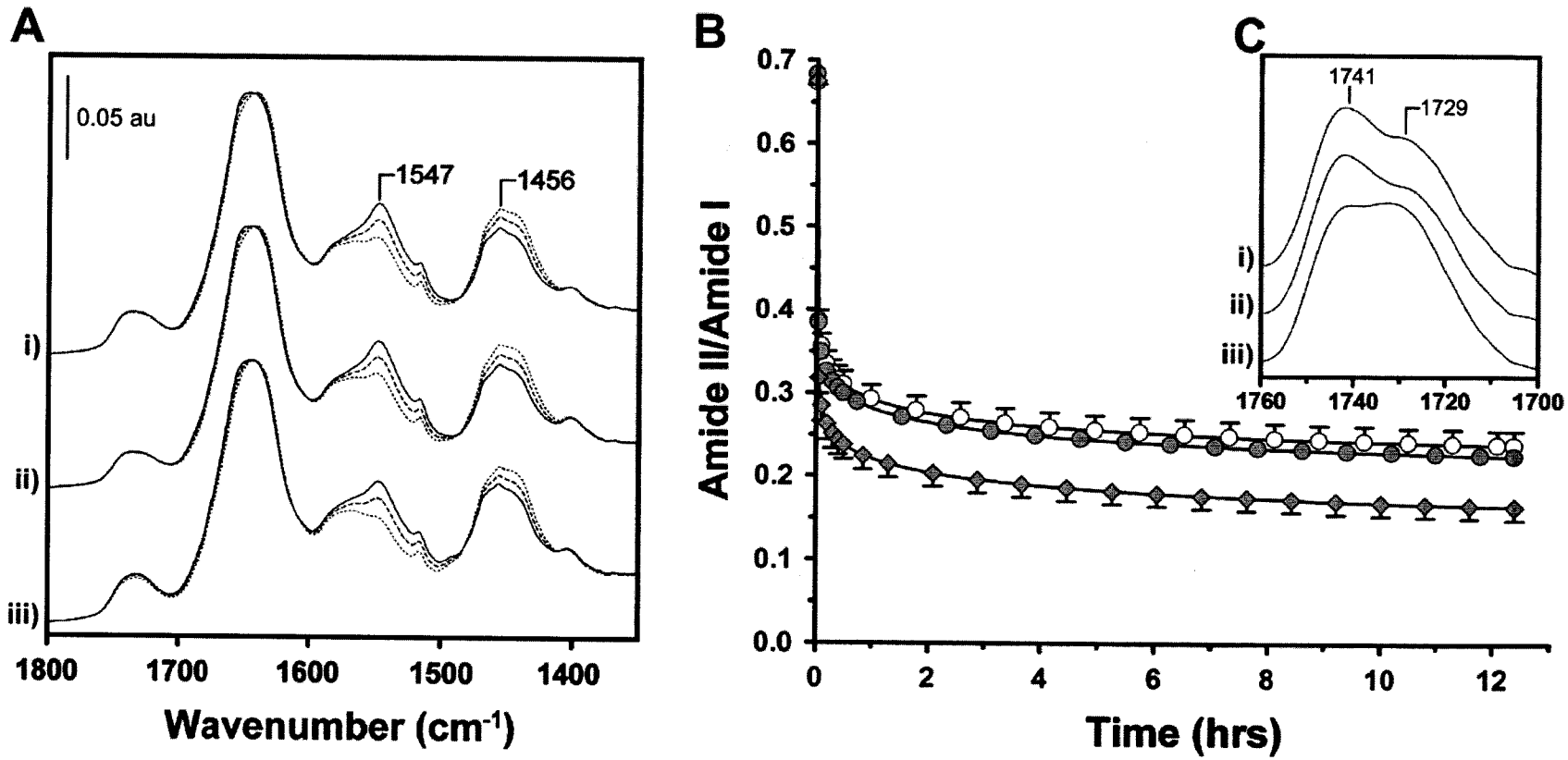
A
0.05 au
1547
1456
i)
ii)
iii)
1800
1700
1600
1500
1400
Wavenumber (cm-1)
B
Amide II/Amide I
0.7
0.6
0.5
0.4
0.3
0.2
0.1
0.0
0
2
4
6
8
10
12
Time (hrs)
C
1741
1729
i)
ii)
iii)
1760
1740
1720
1700

shows spectra from each of the reconstituted nAChR samples acquired at three different times after exposure to ^2H_2O. The $^1H/^2H$ exchange kinetics, presented as a change in the ratio of amide II/amide I band intensity as a function of time are essentially identical for the glycosylated and deglycosylated forms of the asolectin reconstituted nAChR (Figure 4.4B). These results suggest that deglycosylation does not influence nAChR internal dynamics. In contrast, there is a marked increase in the rate of peptide $^1H/^2H$ exchange upon reconstitution of the nAChR into POPC membranes, consistent with the data obtained after 72 hours exposure to ^2H_2O at 4°C (Figure 4.3A,B). Note that the hydrogen exchange data presented in Figure 4.4 was recorded at 22.5°C.

Effect of Deglycosylation on nAChR Thermal Stability. The effect of deglycosylation on nAChR thermal stability was examined by recording infrared spectra as a function of increasing temperature. Thermal denaturation of proteins leads to characteristic changes in amide I band intensity at both 1623 cm^{-1} and 1681 cm^{-1} (Figure 4.5A). Denaturation also leads to increased exposure of peptide N-^1H groups to ^2H_2O solvent and thus a sharp increase in peptide $^1H/^2H$ exchange. Figure 4.5B is a plot of the percent intensity change measured at 1681 cm^{-1} as a function of temperature. The T_d (temperature at 50% denatured) of glycosylated and deglycosylated nAChR are both approximately 55°C, indicating that deglycosylation does not affect nAChR thermal stability. In contrast, the T_d of the nAChR in POPC is slightly lower (~50°C). The cooperativity of thermal denaturation is also decreased upon reconstitution into POPC suggesting a less compact structure.

Effect of Deglycosylation on nAChR Function. The effect of deglycosylation on the ability of the nAChR to undergo agonist induced conformational change was probed by infrared difference spectroscopy (Figure 4.6), which is a sensitive probe of nAChR

Figure 4.5

Effect of deglycosylation and membrane environment on reconstituted nAChR thermal stability. **(A)** 3D Stack plot showing the spectral changes accompanying thermal denaturation of asolectin reconstituted and glycosylated nAChR. Spectra are not $^{2}H_2O$ subtracted. Note: the relative magnitude of change in intensity at 1681 cm^{-1} (and 1623 cm^{-1}) for both the deglycosylated asolectin and POPC samples were similar to those shown above. **(B)** Percent change in intensity at 1681 cm^{-1} as a function of temperature for asolectin reconstituted and glycosylated (filled circles, n=5), Endo F1 deglycosylated (open circles, n=2) and POPC reconstituted (filled diamonds, n=5) nAChR membranes. Error bars represent (+/-) standard deviation of the mean. Where error bars are not visible they are smaller than the data points.

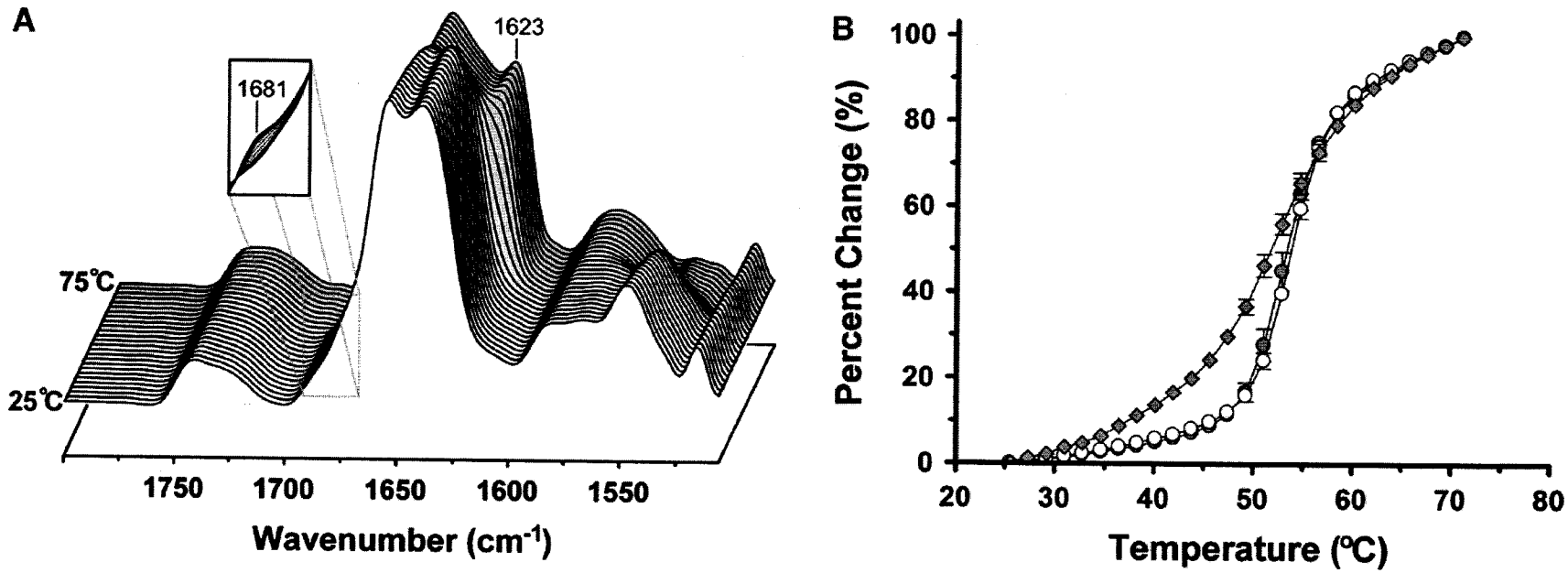
A
1623
1681
75°C
25°C
1750
1700
1650
1600
1550
Wavenumber (cm-1)
B
100
80
60
40
20
0
Percent Change (%)
20
30
40
50
60
70
80
Temperature (°C)

Figure 4.6

Effect of deglycosylation and membrane environment on nAChR function. FTIR difference spectra showing the vibrational shifts occurring in the nAChR upon carbamylcholine binding and subsequent desensitization. The difference spectra were acquired from glycosylated (i) and Endo F1 deglycosylated (ii) nAChR reconstituted into soybean asolectin membranes, as well as glycosylated nAChR reconstituted into POPC membranes (ii). Each presented difference spectrum is the average of at least 30 individual difference measurements.

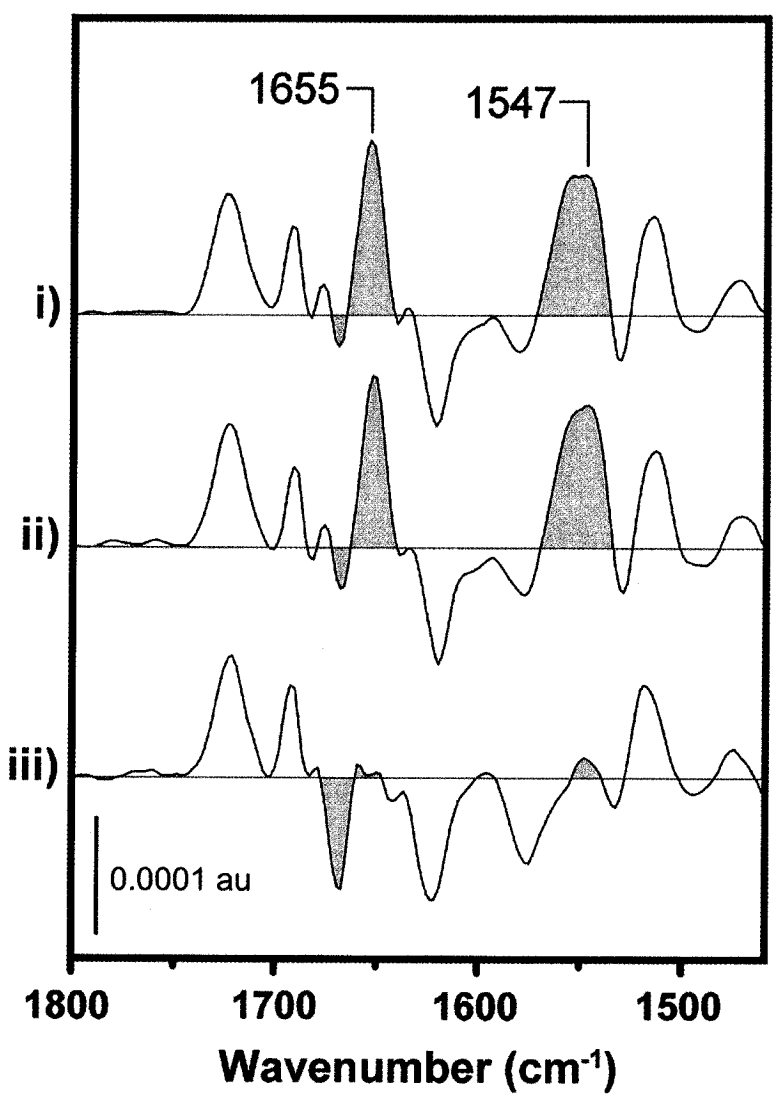
1655
1547
i)
ii)
iii)
0.0001 au
1800
1700
1600
1500
Wavenumber (cm-1)

conformation and function (213, 247). The difference between infrared spectra of the nAChR recorded in the presence and absence of the agonist carbamylcholine (Carb) exhibits a complex pattern of positive and negative bands. Positive intensity in the 1800 cm^{-1} to 1500 cm^{-1} region reflects the vibrational shifts in the polypeptide backbone associated with the resting to desensitized conformational change (177, 248). The pattern of bands in Carb difference spectra recorded from both glycosylated and deglycosylated nAChR is similar to that observed in native membranes (177, 249). Based on the FTIR data, we conclude that the nAChR is stabilized primarily in a functional resting conformation that undergoes Carb induced desensitization (Figure 4.6)(177). Conversely, intensity is lost in the 1800 to 1500 cm^{-1} region of difference spectra recorded from the nAChR reconstituted into POPC membranes. The resulting pattern of difference bands is similar to that observed in Carb difference spectra recorded from functional nAChR membranes in which the nAChR is maintained in the desensitized state by a local anesthetic (206). The difference spectra thus suggest that the nAChR is stabilized in a "desensitized-like" conformation in POPC (176, 213).

Note that the intensity of the Carb bands in Carb difference spectra recorded from the nAChR in POPC versus asolectin membranes are similar. While the affinities of the nAChR for Carb in the two membranes could differ, a similar proportion of nAChRs in each is capable of binding Carb. This observation coupled with the fact there are no significant differences in secondary structure between the nAChR reconstituted into POPC and asolectin membranes, suggests that the proportion of folded nAChRs in each membrane sample is similar. The changes in both the hydrogen exchange kinetics and the thermal denaturation profiles observed between the nAChR reconstituted into membranes composed of POPC and

asolectin are thus not likely due to the presence of a population of improperly folded proteins in POPC.

4.6 - Discussion

The general goal of this work was to determine whether or not deglycosylation is a feasible approach for enhancing the crystallizability of glycosylated integral membrane proteins. Specifically, we were interested in testing whether membrane environment sterically hinders membrane protein deglycosylation. We were also interested in assessing whether carbohydrate removal influences membrane protein structure and/or stability. The latter is of concern because there appears to be a critical link between membrane protein stability and crystallizability (239-241). Deglycosylation could decrease eukaryotic membrane protein stability in a manner that might preclude crystallization, despite the steric benefits of carbohydrate removal.

Gel shift assays show that of the three deglycosidase enzymes tested, Endo F1 is the only one that leads to profound changes in the overall carbohydrate content of the nAChR. Endo F1 is able to cleave high mannose-type carbohydrate from the α- and β-subunits of natively folded nAChR with relative ease. In the case of the γ- and δ-subunits, it appears that a population of these subunits contains complex-type carbohydrate that sterically restricts Endo F1's access to their high mannose moieties. Consequently, on some receptors it is not possible to remove the high mannose moiety from the γ- and δ-subunits. PNGase F and Sialidase were relatively ineffective at removing both high mannose and complex-type carbohydrates from native *Torpedo* nAChR. PNGase F cleaves directly at the protein-

carbohydrate link. The relative inactivity of PNGase F is likely due to its inability to access substrate cleavage sites as a result of nAChR surface topology.

The five receptor subunits have combined a total of eight carbohydrate moieties, each roughly two kilodaltons in size (44, 46). Five of the eight glycans are of the high mannose variety, with there being one high mannose moiety per subunit. The remaining three glycans are of the complex variety, with one chain found on the γ-subunit and two on the δ-subunit. Since Endo F1 is specific for high mannose type carbohydrate, we would expect that at most five of eight glycan chains could be removed with this enzyme (as noted the complex type carbohydrate likely hinders the cleavage of high mannose type carbohydrate from the γ- and δ-subunits). Surprisingly, our carbohydrate-specific staining indicates that more than the expected 60% of the total carbohydrate is removed from the nAChR by Endo F1. This result suggests that either Endo F1 exhibits residual activity for some complex-type carbohydrate or the carbohydrate specific stain is less effective for complex versus high mannose-type sugars. Another possibility is that some of the so called "complex type" carbohydrate may not yet have matured from high mannose to complex-type carbohydrate in our receptor samples, and thus may be removed from the nAChR by Endo F1. Regardless, our results suggest that Endo F1 treatment removes more than 60% (three of five chains) of the high mannose type carbohydrate from the nAChR and therefore likely more than 50% of the total nAChR carbohydrate.

Note that deglycosylation is slightly more effective with detergent-solubilized as opposed to membrane bound nAChR. The reduced efficacy of the enzymes towards reconstituted nAChR could result from steric interference due to the bulky lipid bilayer, and/or adjacent nAChRs in a tightly packed membrane. The glycosylated N-terminal

domain of the nAChR extends roughly 60Å beyond the surface of the membrane (67, 110). Deglycosylation of membrane proteins with relatively small extramembranous domains may be even more sensitive to solubilization. The increased deglycosylation of solubilized samples could also result from increased nAChR internal dynamics brought on by solubilization (see below).

While only partial deglycosylation of the nAChR was achieved, this may be sufficient to improve the likelihood of crystal formation. Partial removal of carbohydrate from individual linkage sites may decrease or eliminate carbohydrate heterogeneity at that site. Removal of any carbohydrate may also free up protein surfaces for the formation of crystal contacts. For example, Endo F1 deglycosylation improved the diffraction quality of crystals formed from the acetylcholine binding protein (133), a soluble protein homologous to the extracellular ligand-binding domain of the *Torpedo* nAChR (121).

It should be noted that not all membrane protein carbohydrate is necessarily detrimental to crystallization. While the large, complex sugars typically found on many membrane proteins (including the nAChR) are more likely to hinder crystallization, relatively small carbohydrate moieties have been shown to participate in membrane protein crystal contacts (228, 250). Clearly, the steric benefits of deglycosylation for membrane protein crystallization need to be assessed on a case by case basis.

A significant result of our study is the demonstration that complete deglycosylation of the α- and β-subunits, and partial deglycosylation of some of the γ- and δ-subunits had no measurable effect on the physical properties of the nAChR. FTIR spectroscopy could not detect any changes in nAChR secondary structure upon deglycosylation. Both the cooperativity and the temperature of thermal denaturation for the nAChR were identical

before and after removal of protein-linked carbohydrate. Peptide hydrogen exchange kinetics, which are sensitive to nAChR internal dynamics and thus protein flexibility, were unaffected by deglycosylation. Carb difference spectra recorded from both glycosylated and deglycosylated nAChR were also essentially identical. Given the above data and the exquisite sensitivity of Carb difference spectra to the nature of both nAChR-agonist interactions and agonist-induced conformational change (177, 248), it can be concluded that removal of high mannose type glycosylation has essentially no effect on nAChR structure or function. More specifically, complete deglycosylation of both the agonist binding α-subunits as well as the β-subunit has no affect on the ability of the nAChR to bind agonist and undergo conformational change. In general, carbohydrate removal from the nAChR, and possibly other integral membrane proteins, may have no detrimental structural/stability effects which could hinder crystallization.

An interesting feature of our study is the demonstration that simple changes in lipid bilayer composition, in contrast to carbohydrate removal, have substantial effects on nAChR structure, function, stability, and flexibility. Reconstitution of the nAChR into POPC versus soybean asolectin membranes leads to the formation of a channel inactive conformation that has both a lower temperature and a decreased cooperativity of thermal denaturation, as well as an increased rate of peptide hydrogen exchange. These physical changes suggest a less compact, more flexible structure. Our data highlight the intimate relationship between lipid bilayer composition and nAChR structure, stability, and function.

The dependence of nAChR structure/stability on membrane environment is significant from a crystallization perspective. The nAChR may require a specific lipid co-factor, which is present in asolectin membranes, to maintain structural integrity. Several

membrane protein structures have been solved in which the protein is complexed with a specific lipid (251-256). Identifying the specific lipids required for structural integrity may be a prerequisite for crystallization of many membrane proteins. Previous studies have shown that the nAChR requires phosphatidic acid and possibly cholesterol in order to adopt a functional resting conformation (176, 189, 213). It is tempting to speculate that these lipids may also be required for nAChR structural integrity and thus crystallization.

Alternatively, nAChR structural stability may be sensitive to a general physical property of the lipid bilayer. While we have not characterized the physical properties in detail, the lipid ester carbonyl stretching vibration provides qualitative insight into the physical packing of the reconstituted POPC and asolectin membranes (Figure 4.4C). The ester carbonyl stretching band consists of two peaks, one due to hydrogen bonded (1729 cm^{-1}) and the other due to non-hydrogen bonded lipid ester carbonyls (1741 cm^{-1})(211). The relative intensities of these two peaks suggest that the reconstituted nAChR/POPC membranes exhibit a greater degree of water penetration into the bilayer interfacial region than in the reconstituted nAChR/asolectin membranes. The increased solvent penetration in POPC is likely a result of decreased lateral bilayer pressure (213, 217, 257). Both the decrease in structural stability and increase in internal dynamics could result from an increase in the fluidity of the reconstituted POPC membranes.

It is important to note that changes in the physical environment surrounding the nAChR upon reconstitution into POPC versus asolectin membranes are relatively small in comparison to the changes in physical environment expected from detergent solubilization. Detergent solubilization should lead to even greater exposure of the transmembrane domain to water and thus an increase in local dielectric constant. The increased dielectric field may reduce the strength of weak polar interactions, such as C_α hydrogen bonds, which may be

important for stabilizing transmembrane domain structure (258). Lateral bilayer pressure will also be absent with a solubilized nAChR. Detergent solubilization may thus have substantial detrimental effects on nAChR structure/stability.

Rosenbusch has suggested that current membrane protein crystallization techniques select for membrane proteins that are particularly stable in the detergent-solubilized state (240, 241). Our previous work has shown an extremely rich complexity to nAChR-lipid interactions (196, 213, 259). It is possible that the nAChR, and some other membrane proteins, have evolved complex interactions with lipid bilayers. These complex lipid-protein interactions may in some cases be essential for membrane protein structure and function, and could underlie the difficulties associated with solubilization and crystallization of these proteins.

4.7 - Conclusions

Our data show that it is possible to enzymatically remove substantial amounts of carbohydrate from a natively-folded integral membrane protein complex, and that extensive removal of protein carbohydrate has no adverse effect on membrane protein structure, function, thermal stability, or flexibility. We show that the overall effects of deglycosylation on nAChR structure and function are insignificant in comparison to those observed upon reconstitution of the nAChR into membranes with a different lipid composition. Although deglycosylation may provide an avenue for increasing nAChR crystallizability, the dependence of nAChR on membrane environment for structural integrity may represent the most significant obstacle in nAChR crystallization.

CHAPTER 5

GENERAL DISCUSSION AND CONCLUSIONS

5.1 - The Old Model: Lipids Modulate and Equlibrium between the Resting and Desensitized States

When I began graduate studies in the year 2000, the prevailing view was that membrane lipid composition controlled a conformational equilibrium between the nAChR's resting and desensitized states (Figure 5.1) (176). The two essential tenets of this model were: a) that lipids modulate a conformational equilibrium, and b) that this equilibrium was between the nAChR's resting and desensitized conformations. The idea of a conformational equilibrium stemmed mainly from difference spectroscopy data in which increasing amounts of either phosphatidic acid (PA) or cholesterol (Chol) were shown to stabilize an increasing proportion of resting state nAChRs (176, 177). Because the proportion of nAChRs able to undergo agonist-induced conformational change correlated directly with the amount of PA or Chol added, the difference spectroscopy data provided compelling evidence that both PA and Chol were able to modulate a nAChR conformational equilibrium. The conformational equilibrium modulated by these lipids was thought to be between the nAChR's resting and desensitized states (176). This hypothesis was based on several key observations including the fact that in the absence of certain lipids, the nAChR adopts a non-conducting, channel inactive conformation in which the binding of agonist no longer elicits a flux response (155). Furthermore, fluorescence studies showed that agonist binding not only failed to promote ion flux, but also failed to induce conformational change (165). Both the non-conducting and unresponsive nature of this state was suggestive of desensitization. These observations, in combination with both chemical labelling and the FTIR difference data suggested that the membrane inactive form of the nAChR was indeed the receptor's desensitized state (176, 177, 194).

Figure 5.1

nAChR-lipid interactions... The Old Model. Lipids, such as phosphatidic acid moieties (PA) and cholesterol (Chol), modulate an equilibrium between the nAChR's resting (R) and desensitized (D) states.

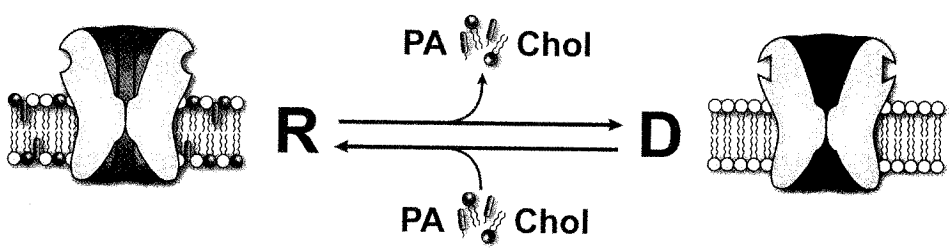
PA
Chol
R
D
PA
Chol

5.2 - "Desensitized" vs. "Desensitized-Like" vs. "Uncoupled"

While at the time it was reasonable to assume that the membrane inactive form of the nAChR was in fact the desensitized state, a growing body of evidence suggests otherwise. Instead, it appears that the membrane inactive form of the nAChR is actually a distinct conformation. While this state shares features in common with the desensitized state, it also exhibits its own unique attributes. For example, early measurements showed that inactive nAChRs exhibit an affinity for agonist that is closer to that of the resting state (i.e. μM), as opposed to the thousand-fold higher affinity indicative of the desensitized state (i.e. nM)(155). In addition, recent structural data, including data presented in this thesis, suggests that despite having the same secondary structure as functional nAChRs, inactive nAChRs exhibit increased internal dynamics (190, 196). Functional, but agonist-desensitized nAChRs do not show increased internal dynamics (190). This is direct evidence that the membrane inactive conformation of the nAChR is structurally different from the agonist-induced desensitized state. This difference in internal dynamics was determined by measuring $^{1}H/^{2}H$ exchange kinetics upon reconstitution of the nAChR into different membranes. While the observed increases in exchange could result from differences in the number of solvent exposed residues arising from variability in reconstituted membrane thickness and permeability, the thermal denaturation data presented here in which a marked decrease in the cooperativity of unfolding is observed also strongly suggests that membrane inactive nAChRs display increased internal dynamics and a less compact structure.

You may have noticed that over the course of the three manuscripts presented in this thesis the nomenclature used to describe the membrane inactive form of the nAChR has changed. Initially this state was referred to as "the desensitized state" and more recently we

have begun calling it "the desensitized-like state". As mentioned above, while having some features indicative of the desensitized state, the membrane inactive conformation of the nAChR appears to be a distinct conformation. The defining feature of this conformation is an uncoupling of the nAChR's two main functions: ligand binding and ion channel gating (154). For this reason, we now refer to this state as the membrane-induced "uncoupled" state.

5.3 - The New Model: Lipids Modulate an Equilibrium between the Resting and Uncoupled States

Because the membrane inactive state of the nAChR is not actually the desensitized state, the current conformational equilibrium model must be refined. A new model which includes the membrane induced "uncoupled" state is presented in Figure 5.2. In this new model, membrane lipid composition modulates a conformational equilibrium between the nAChR's uncoupled and resting states (Figure 5.2, Scheme 1). Note that while this is the primary effect of membrane lipid composition, it is entirely possible that lipids are able to influence other nAChR equilibria. For example, it is conceivable that a physical property of the membrane, such as bulk fluidity, could affect the nAChR's gating and/or desensitization kinetics by altering the rate of receptor conformational change (Figure 5.2- Scheme 2). This would be particularly plausible if the conformational changes upon gating involve large movements in the receptor's transmembrane domain and/or rearrangements of the protein-lipid interface. Until we have a clearer view of the structural rearrangements at the lipid-protein interface upon gating, it is difficult to speculate how lipids modulate channel opening and/or desensitization. For this reason we will restrict our discussion to the influences of

Figure 5.2

nAChR-lipid interactions... The New Model. Scheme 1: Lipids, such as phosphatidic acid moieties (PA) and cholesterol (Chol), modulate a conformational equilibrium between the nAChR's resting (R) state and a unique uncoupled (U) conformation. The defining feature of the nAChR's uncoupled state is a disconnect between its ligand binding and channel gating functions. Sheme 2: Lipids may also influence the thermodynamics and/or kinetics of nAChR activation and desensitization (O = open/activated state, D = desensitized state).

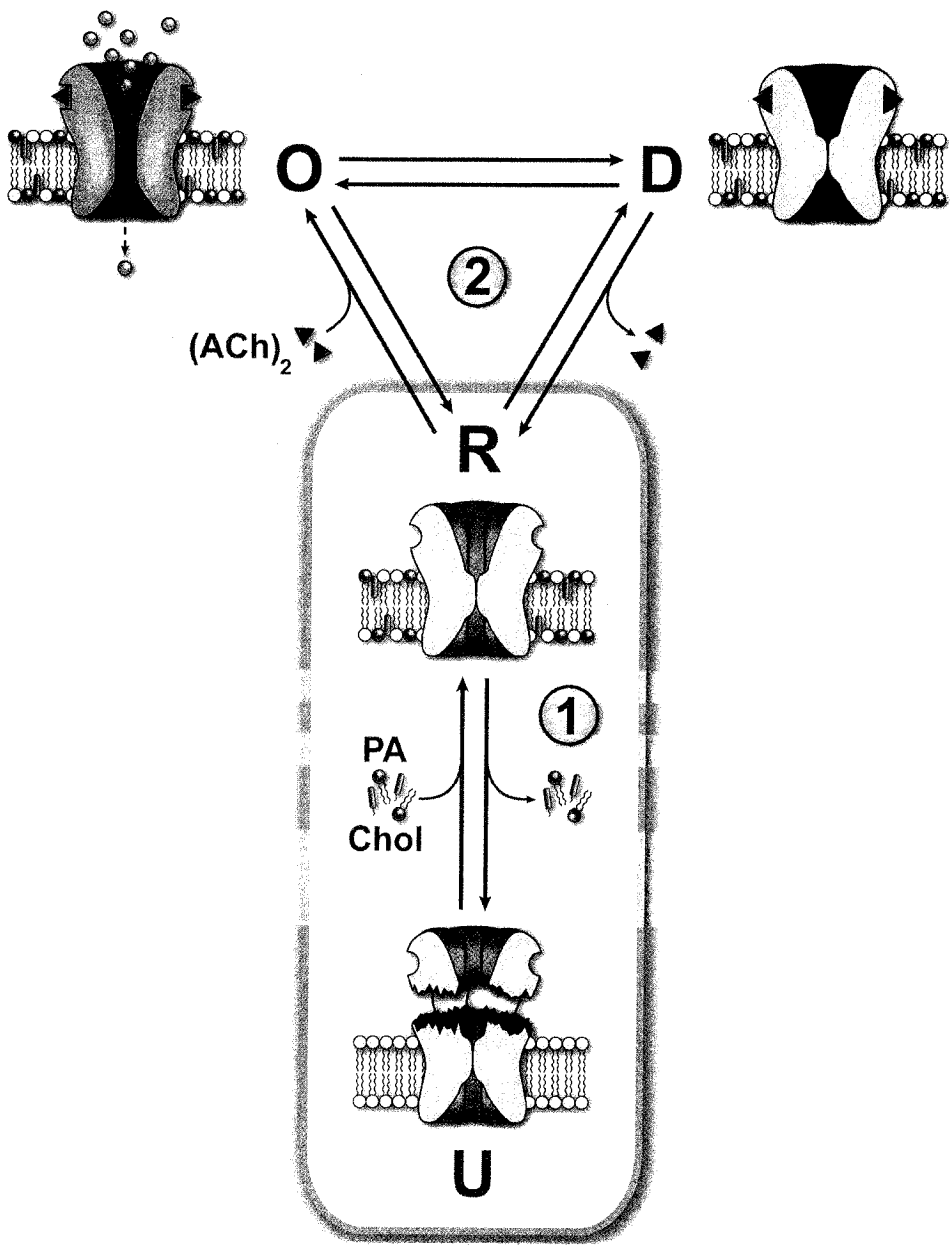
O
D
2
(ACh)2
R
1
PA
Chol
U

lipids on the coupled (resting)-uncoupled conformational equilibrium. Because this equilibrium modulates the proportion of nAChRs able to flux ions in response to agonist, it ultimately affects the strength of the postsynaptic response.

5.4 - A Shift in Paradigm

In April 2005, Nigel Unwin published an atomic model of the nAChR in its resting state (4). This structure (PDB ID: 2BG9) has ushered in a new era in acetylcholine receptor biophysics, and has already led to a number of important mechanistic insights into channel function (8, 9, 11, 260). With this model, we are gaining a detailed knowledge of how agonist binding causes opening of the receptor's transmembrane pore. Several studies have singled out a number of structures at the interface between the ligand binding and ion channel domains as being important for converting agonist binding into ion flux (6-11, 150). This new data, in conjunction with extensive biophysical characterization, affords speculation as to how lipids influence the receptor's ability to convert ligand binding into channel opening.

What follows here is a structure based hypothesis as to how lipids modulate nAChR structure and function. This model draws not only on the data presented in this thesis, but also attempts to reconcile over thirty years of literature examining nAChR-lipid interactions. We start by a) examining the structure of the nAChR with particular emphasis on its implications for nAChR-lipid interactions. We also b) identify regions of the nAChR that both interact strongly with lipids and have the potential to influence nAChR function. We then c) evaluate the structural consequences of nAChR-lipid interactions and postulate a simple structure based mechanism for how lipids influence the coupling between agonist

binding and channel gating. Finally, based on the structural rearrangements thought to give rise to "uncoupling", d) we speculate as to the lipid-specific properties which may be responsible for stabilizing the nAChR's resting/coupled state.

5.5 - nAChR Structure and Implications for nAChR-Lipid Interactions

The nAChR is a ~260kDa pentameric integral membrane protein complex formed from four highly homologous subunits which associate with pseudo five-fold symmetry around a central ion pore (α, γ, α, δ, β)(3). Each of the elongated subunits has a large (~210a.a.), N-terminal domain which protrudes into the synaptic space, projecting away from the membrane surface. This large extramembranous domain contains the neurotransmitter binding sites which are located at the interfaces between the α-γ and α-δ subunits, with the α-subunits providing most of the residues involved in binding. The C-terminal end of the ligand binding domain leads directly into the transmembrane ion channel, which in contrast to the ligand binding domain adopts an entirely α-helical structure. The four transmembrane helices form a four helix bundle motif in which each helix traverses the bilayer and projects roughly 10-15Å beyond the membrane on its extracellular side (67). The second transmembrane helix (M2) of each of the five subunits, come together in the middle of the pentamer to form the central ion conduction pathway. TM helices M1 and M3 encircle the central channel and sequester it from the surrounding lipid, with helix M4 at its periphery where it makes extensive contacts with the surrounding bilayer. The cytoplasmic domain, which lies between M3 and M4 is comprised of an amphipathic helix, and is not as well structurally characterized, since several regions are missing in the current model (4).

Looking at the structure of the transmembrane domain, several important observations with respect to possible lipid-protein interactions can be made. First, the four helices which constitute the membrane spanning portion of each subunit are relatively loosely associated with one another and form several crevices which may be accessed by lipids. In particular, because the helices splay apart towards their extracellular ends, lipids in the outer leaflet may have access to several faces of each of the helices (Figure 5.3). This would explain the relatively large number of residues which have been shown to interact with photoactivatable hydrophobic probes (39, 40, 128, 129, 138, 261), and illustrates that lipid-protein interaction sites need not be limited to the periphery of the protein.

Given that anionic lipids modulate nAChR function, it is interesting to note that a number of basic residues frame several of the transmembrane helices (Figure 5.4). Consistent with the positive inside rule (262-264), the basic residues are more concentrated on the cytoplasmic side of the transmembrane domain. This is in part because the helices funnel together towards the inside of the cell, but also because there are more basic residues on these ends of the helices. This is also significant given that the inner leaflet of the plasma membranes generally contains a greater proportion of anionic lipids.

The current atomic model does not include any modelled lipid molecules, presumably because at 4Å resolution there was no clear electron density attributable to any immobilized lipid. This however does not mean that there are no specific lipid binding sites. Of all the basic residues within the transmembrane domain, αLys242 is the most conserved, being either a lysine or an arginine in all but one of the human Cys-loop receptor subunits (265). In addition to αLys242, several other basic residues including αHis299, αHis300, αArg301 and αHis306 are also relatively well conserved among cationic Cys-loop receptors. These residues are also located in a prime position within the nAChR's transmembrane domain to

Figure 5.4

The location of acidic and basic residues within the nAChR transmembrane domain. **(A)** Cartoon representation of the nAChR transmembrane domain in which basic residues (14 Arg, 17 Lys and 16 His – total 47) are shown as cyan balls and sticks, and acidic residues (11 Asp and 14 Glu – total 25) are shown as magenta balls and sticks. **(B)** Surface representations of (A) where basic residues have been coloured blue, and acidic residues red. Top: view down the pore from the extracellular side of the membrane; middle: side view; bottom: view down the pore from the intracellular side of the membrane. (PDB ID: 2BG9)

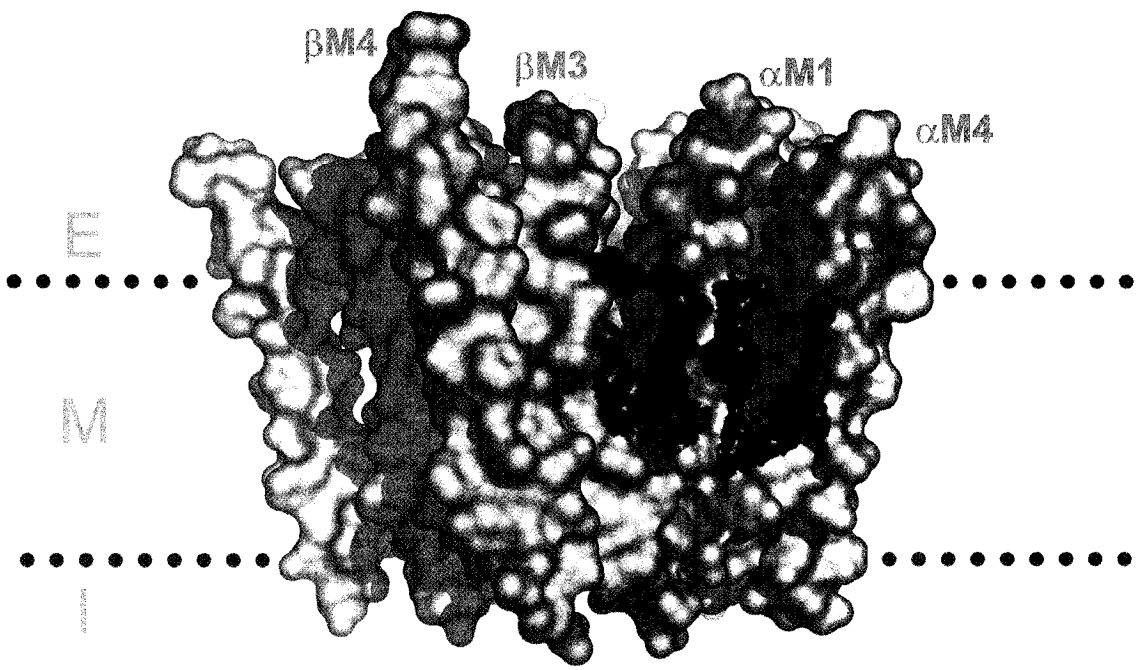
βM4
βM3
αM1
αM4
E
M
I

Figure 5.4

The location of acidic and basic residues within the nAChR transmembrane domain. **(A)** Cartoon representation of the nAChR transmembrane domain in which basic residues (14 Arg, 17 Lys and 16 His – total 47) are shown as cyan balls and sticks, and acidic residues (11 Asp and 14 Glu – total 25) are shown as magenta balls and sticks. **(B)** Surface representations of (A) where basic residues have been coloured blue, and acidic residues red. Top: view down the pore from the extracellular side of the membrane; middle: side view; bottom: view down the pore from the intracellular side of the membrane. (PDB ID: 2BG9)

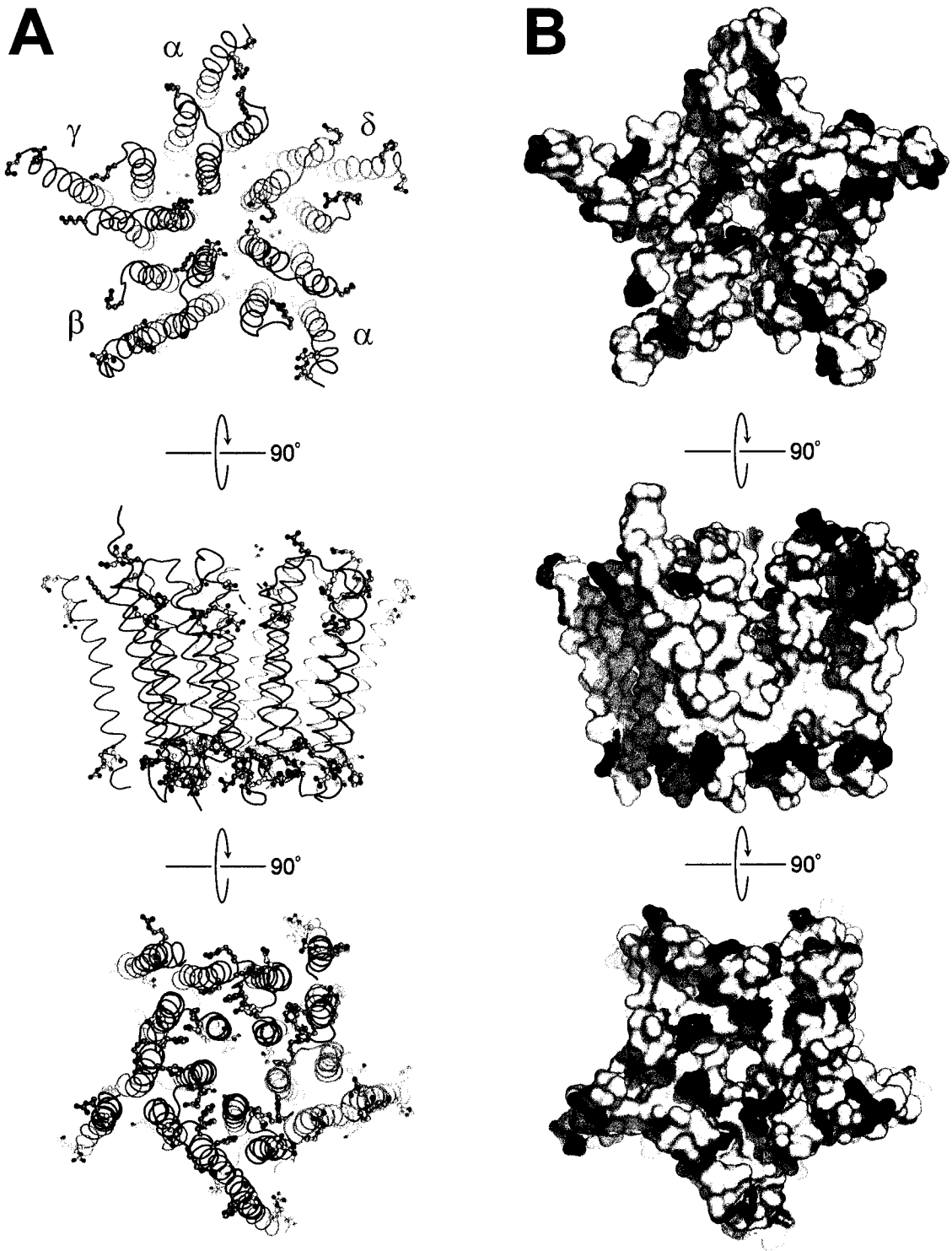
A
α
γ
δ
β
α
90°
90°
90°
B
90°
90°

interact with the interfacial region of the bilayer, and thus lipid headgroups (Figure 5.5). Both the relative conservation, as well as their location suggests that they are the most likely residues to form an anionic lipid binding site. Furthermore, because some of the residues are found at the interface between adjacent subunits, it is tempting to speculate that an anionic lipid bridges an interaction between them, and thus between neighbouring subunits. This hypothetical bridging role for anionic lipid may be required in order to stabilize the quaternary structure of the nAChR. Interestingly, an inter-subunit bridging role for anionic lipids analogous to that proposed here has been observed for the KcsA potassium channel (253, 266-269).

While the possibility of a specific lipid binding site(s) has not been ruled out, it is feasible that the nAChR's apparent affinity for certain lipids is a general property of the channel. For example, Unwin has recently proposed that the receptor's cation selectivity is in large part due to the distribution of negatively charged residues on the surface of the receptor's inner and outer vestibules, which allows it to selectively concentrate cations while repelling anions (4). This hypothesis is consistent with our prior observation (Chapter 3) that the nAChR appears to concentrate Ca^{2+} ions at its surrounding membrane surface. While the large extramembranous domains of the nAChR contain a preponderance of negatively charged residues, it is interesting to note that within the proposed interfacial region of the receptor's transmembrane domain the relative distribution of positively and negatively charged residues is reversed. Within the transmembrane regions of the receptor there is a higher density of positively charged residues (Figure 5.4). This might explain the receptor's apparent ability to selectively enrich its surrounding lipid environment (annulus) with negatively charged lipids. Similar to the case with ions, this enrichment of lipids may be more of an overall electrostatic effect, rather than the result of specific molecular interactions

Figure 5.5

Basic residues within the *Torpedo* nAChR transmembrane domain that potentially form an anionic lipid binding site. The α- and γ-subunits are shown in red and cyan, respectively. **(A)** View of the entire nAChR transmembrane domain showing the clustering of conserved basic residues referred to in the text. The residues are found at the interface between two nAChR subunits and are also located in the interfacial region of the bilayer. **(B)** Close-up view of the boxed area in (A) in which the conserved basic residues and transmembrane helices have been labelled (Note: γK250 aligns with αK242). (PDB ID: 2BG9)

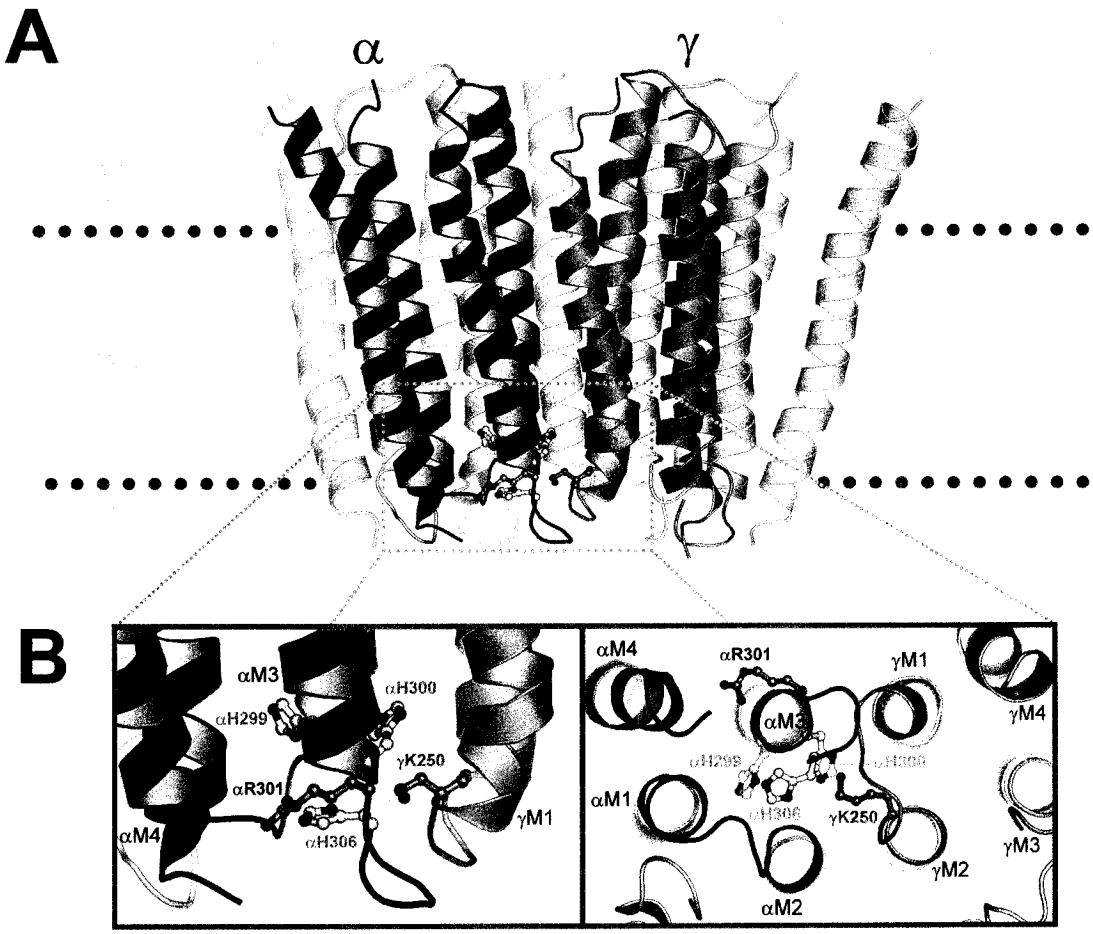
A
α
γ
B
αM3
αH299
αH300
γK250
αR301
αM4
αH306
γM1
αM4
αR301
γM1
αM3
γM4
αH299
αH300
αM1
αH306
γK250
γM3
γM2
αM2

between the receptor and particular lipid head groups. This ability to surround itself with negatively charged lipids is significant from a functional perspective since it would be expected to extend the nAChR's negative electrostatic potential "reach", thereby potentiating its cation concentrating ability. The nAChR may have evolved to specifically concentrate cations directly with the surface charge of its vestibules, and indirectly through its interactions with anionic lipids (Figure 5.6).

In his initial publication of the structure of the nAChR pore, Unwin suggested that the transmembrane domain could be divided into two essential rings with different functions – an inner ring formed by the five M2 helices from each subunit, and a larger outer ring formed by the remaining fifteen M1, M3 and M4 helices (67). The inner M2 ring forms the ion conducting pore and the outer M1, M3 and M4 ring sequesters this inner ring away from the lipid bilayer. Recently, Barrantes has suggested refining this model to include a third, outermost ring comprised of the five M4 helices from each subunit (Figure 5.7)(270). This proposal is based on the hypothesis that M4 may have a unique ability to translate bilayer physical properties into different nAChR gating kinetics. Two lines of evidence support this hypothesis. First the location of M4 on the periphery of the TM domain suggests M4 makes extensive contact with the lipid bilayer, a hypothesis confirmed both by chemical labelling studies (39, 40, 129, 271, 272) and the recent structure (4, 67); and second, several studies have shown that M4 can influence various aspects of nAChR function, including channel gating (273-288).

Several mutagenesis studies have provided strong evidence in support of the hypothesis that M4-lipid interactions modulate nAChR function. Substitution of lipid-exposed residues in the α, β and γM4 segments all alter nAChR gating behaviour (273-282, 285, 286). The effects of multiple mutations are additive, however mutations in αM4 have

Figure 5.6

(A) The preponderance of basic residues within the *Torpedo* nAChR transmembrane domain (blue) may allow the nAChR to selectively enrich its surrounding membrane with negatively charged lipids (PA, red head groups). This enrichment in negatively charged lipids may potentiate the nAChR's ability to concentrate cations, and could thus contribute to the charge selectivity of the channel. In effect, the lipids act as an electrostatic extension of the protein. **(B)** Two-dimensional schematic depicting how the distribution of charge on the surface of the nAChR could allow it to enrich its surrounding membrane environment with negatively charged lipids. Note: in both (A) and (B) red surfaces are negatively charged and blue surfaces are positively charged. (PDB ID: 2BG9)

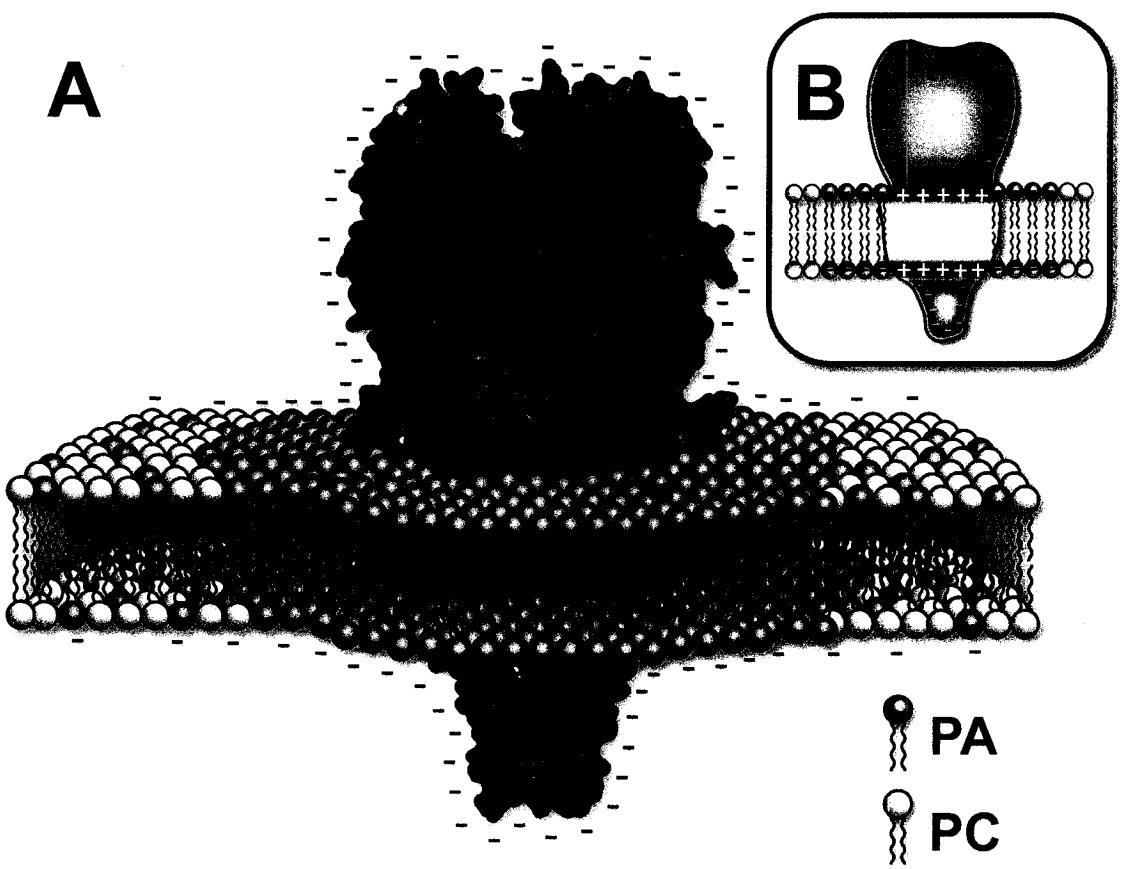
A
B
PA
PC

Figure 5.7

(A) The nAChR transmembrane domain consists of three distinct functional rings. The inner pore ring (blue helices), the middle ring (red helices) and the outer ring (green). The inner ring is formed by the five M2 helices from each subunit and constitutes the ion conduction pathway. The middle ring, which is formed by the M1 and M3 helices, surrounds the inner pore ring and sequesters it from the surrounding membrane. The third and outermost ring is formed from the remaining five M4 helices, and interacts extensively with the lipid membrane. **(B)** Side view of the transmembrane domain of a single nAChR subunit. The helices forming the three rings are shown in blue, red and green. Grey dashed lines demarcate the three distinct functional rings. The inner pore ring forms the ion pore, while the M4 ring interacts extensively with the membrane. (PDB ID: 2BG9)

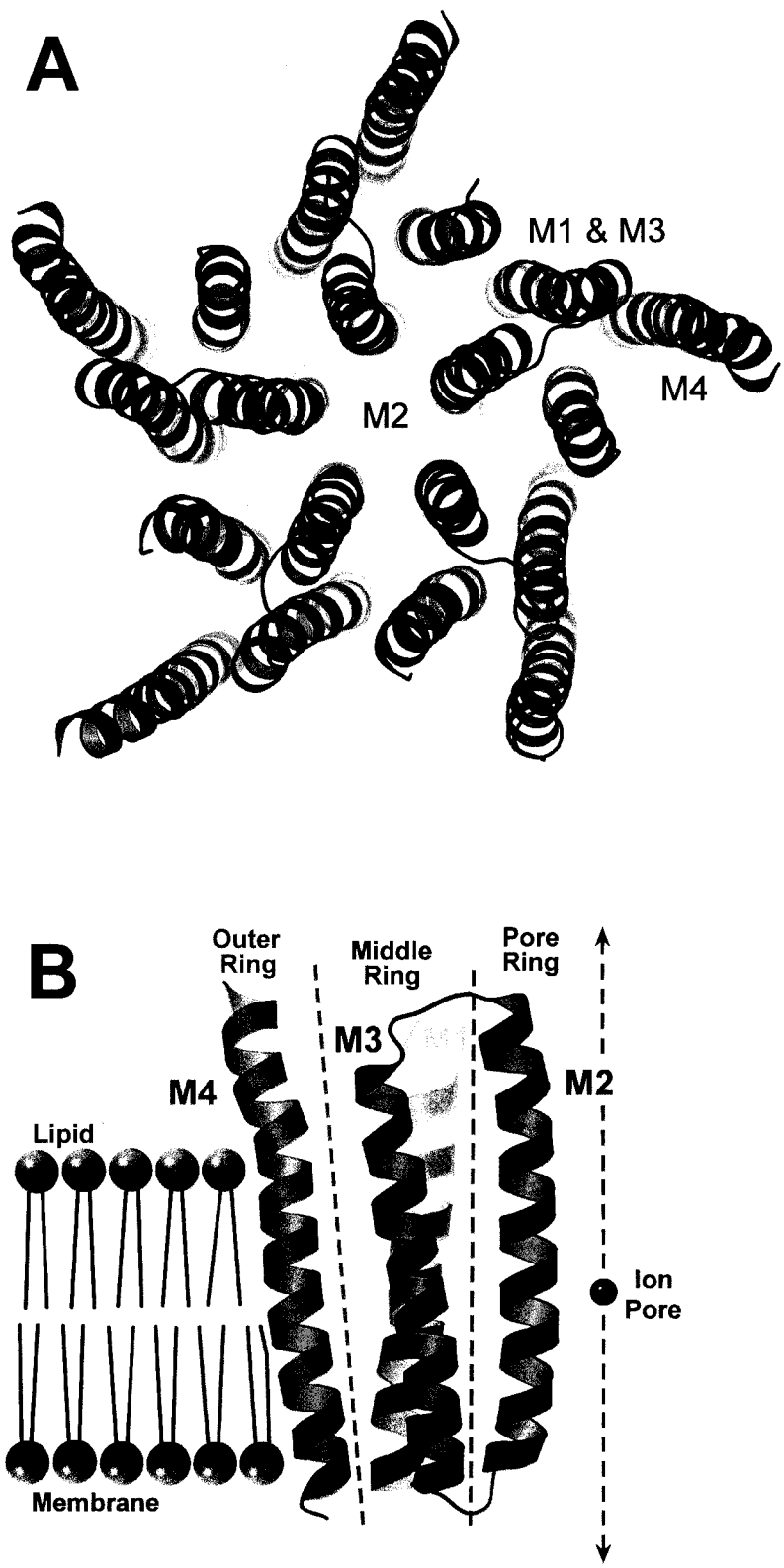
A
M1 & M3
M4
M2
B
Outer Ring
Middle Ring
Pore Ring
M3
M4
M2
Lipid
Ion Pore
Membrane

substantially greater effects than those in either β or γM4, consistent with the fact that it is the α-subunits which are responsible for most of the conformational changes associated with gating (278, 279). In general, mutation to bulkier and more hydrophobic side chains increases nAChR mean channel open time, and reduces agonist EC_{50}. These observations led to the hypothesis that M4 is involved in the nAChR gating mechanism. However, since EC_{50} reflects contributions from both agonist binding and channel gating, decreases in EC_{50} resulting from increases in agonist affinity could not be ruled out. Subsequent kinetic analysis involving select M4 mutants revealed small changes in the rate constants dictating ligand binding, but relatively large differences in those governing channel opening and closing, confirming that M4 influences channel gating (283).

5.6 - M4 and the Cys-Loop

How does M4, which is located at the periphery of the nAChR transmembrane domain, control gating of its central ion channel? Examination of the nAChR structure suggests a possible mechanism. M4, which is >45Å long, is the longest of the four TM helices, and therefore projects the furthest beyond the membrane and into the extracellular space. Unlike the other transmembrane helices, the extracellular end of M4 is not directly under the N-terminal ligand binding domain but instead runs alongside it where its C-terminal end makes contact with the eponymous Cys-loop (Figure 5.8). Mutations in this highly conserved loop alter both nAChR ligand binding and channel gating properties, leading to a severe form of congenital myasthenia gravis (289). Therefore interactions between M4 and the Cys-loop, which affect Cys-loop conformation, have the potential to influence both receptor ligand binding affinity and channel gating kinetics. Furthermore,

Figure 5.8

The C-terminal end of M4 contacts the Cys-loop. **(A)** Structure of the *Torpedo* nAChR α-subunit highlighting structures at the interface between the ligand binding and transmembrane domains. Structures forming physical contacts at the interface between the two domains are labelled (Cys-loop = green, Loop 2 = cyan, M2-M3L = red, and the C-terminal end of M4 = orange). Also shown are the C-loop (yellow), αW149 located in the agonist binding site (orange ball and sticks) as well as αL251 which forms part of the ion channel gate. **(B)** Several close-up views of the boxed interfacial region in (A) showing that the C-terminal end of M4 (orange) interacts with the Cys-loop (green). (PDB ID: 2BG9)

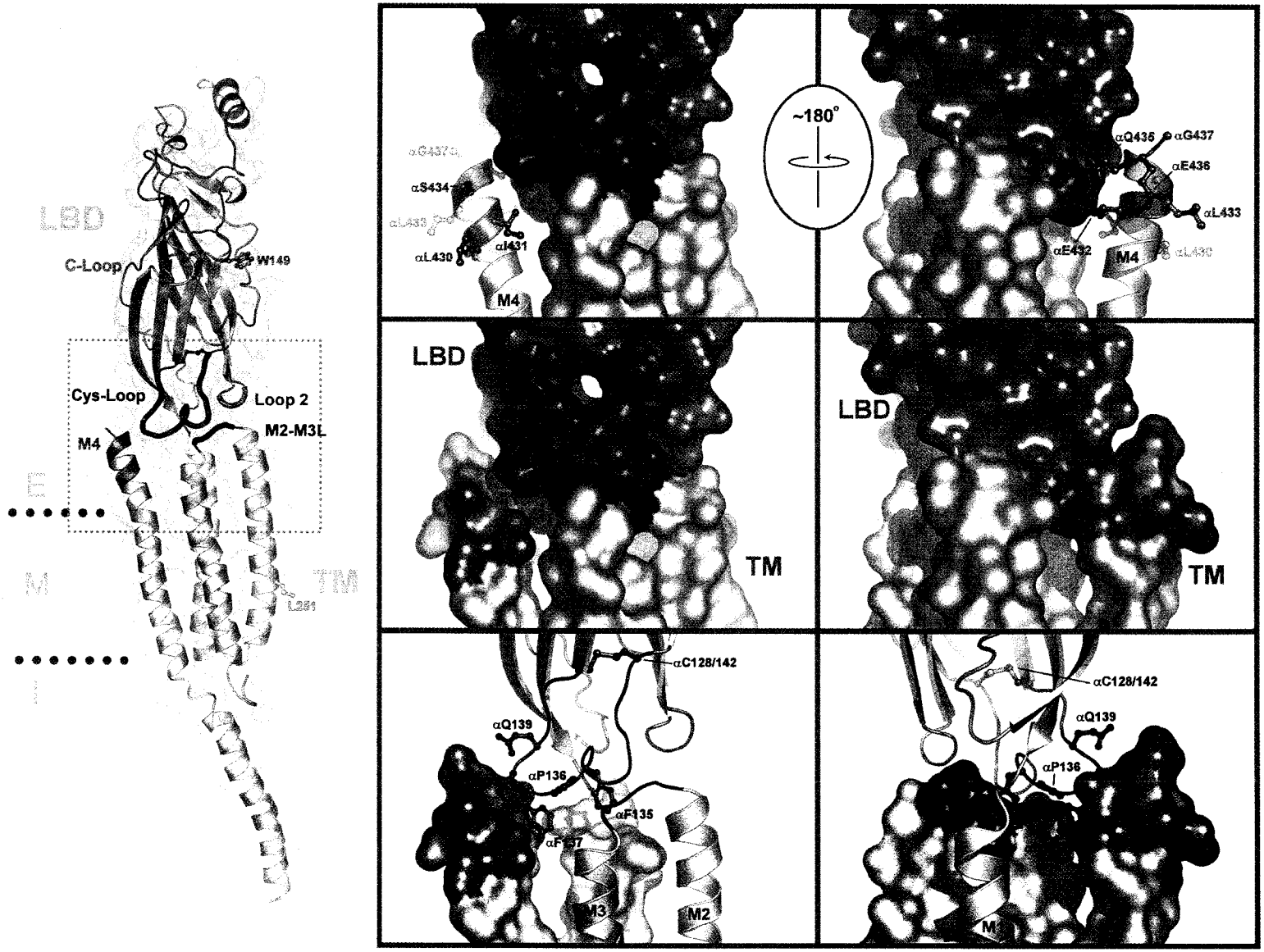
LBD
C-Loop
W149
Cys-Loop
Loop 2
M2-M3L
M4
TM
αG437
αS434
αL433
αI431
αL430
M4
~180°
αQ435
αG437
αE436
αL433
αE432
M4
αL430
LBD
TM
LBD
TM
αC128/142
αQ139
αP136
αF135
αF137
M3
M2
αC128/142
αQ139
αP136
M3

because the Cys-loop has an essential role in relaying the conformational changes in the ligand binding domain to the pore during channel gating (6, 7), interactions between M4 and the Cys-loop might contribute to a tight connection between the nAChR's extramembranous ligand binding domain and its transmembrane pore, thereby influencing the strength of coupling between ligand binding and channel gating.

Several key observations suggest that the Cys-loop plays an indispensable role in connecting the receptor's ligand binding and channel gating functions. Besides being one of the most highly conserved stretches of amino acids in the sequences of all members of the Cys-loop receptor super-family (hence their name!), it is also one of only three structures in the N-terminal ligand binding domain which makes direct contact with the transmembrane pore (the β1-β2 linker and the covalent connection of the polypeptide backbone are the others)(Figure 5.8 and 1.19)(4). Furthermore, some of these contacts are with the M2-M3 linker (6), which is an essential gating control element (8, 145-149). The finding that in order to recover gating in chimaeric AChBP/$5HT_3$ receptors it is necessary to replace the AChBP Cys-loop with that of the $5HT_3$ receptor, directly illustrates that interactions between the Cys-loop and the transmembrane domain are essential for coupling binding to gating (7). The AChBP is a soluble homolog of the nAChR N-terminal ligand binding domain which binds cholinergic agonists/antagonists with similar affinity to that of the nAChR (131, 132). The AChBP however is not connected to a transmembrane ion channel. The fact that the Cys-loop is different in the AChBP, and yet so highly conserved amongst Cys-loop receptor subunits further suggests that it plays an essential role in gating - a role which is relevant to Cys-loop receptor function, but not to AChBP function.

A current model of gating proposes that the Cys-loop (loop 7) and the β1-β2 linker (loop 2) form a clamp which straddles the M2-M3 linker, thereby locking the M2 helix in the

closed/resting conformation (Figures 5.8 and 1.19)(3). The dissociation of M4 from the Cys-loop may increase the dynamics and flexibility of the Cys-loop, allowing it to come away from the M2-M3 linker. Pressure on the M2-M3 linker exerted by residues in the Cys-loop may be important for not only stabilizing the resting closed conformation of the pore, but also for facilitating the conformational changes resulting in repositioning of the M2 helix upon gating. Clearly several residues are involved in gating, however of all the residues within the Cys-loop, αPhe135 appears to be particularly well positioned to interact with the M2-M3 linker. Immediately following αPhe135 in the *Torpedo* α-subunit sequence is αPro136 and αPhe137. Together with αPhe135 these three "FPF" residues are conserved in all human acetylcholine receptor subunits, and highly conserved in all Cys-loop receptor subunits, implying they have an important function (265). While αPhe135 is in the hydrophobic core of the subunit and likely interacts with the M2-M3 linker, αPhe137 projects away from the Cys-loop into solvent, and is well positioned to interact with the C-terminal end of M4 (Figures 5.8 and 5.9). We propose that M4 applies mechanical pressure to the Cys-loop through αPhe137, and in turn this pressure is relayed to the M2-M3 linker via αPhe135. Pro136, which is sandwiched between αPhe135/137, provides rigidity to the polypeptide backbone facilitating the relay of mechanical pressure. This interaction between αPhe137 of the Cys-loop and the C-terminal end of M4 is likely important for stabilizing the channel/closed resting conformation of the nAChR, and may also be critical for facilitating the conformational changes in the M2-M3 linker which are associated with gating.

Figure 5.9

The conserved "FPF" sequence of the Cys-loop (green) interacts with both the C-terminal end of M4 (orange) and the M2-M3 linker (red, M2-M3L). **(A)** and **(C)** αF135 of the Cys-loop makes contact with αP272 of the M2-M3L, while αF137 interacts with αQ435 and αE432 of M4. **(B)** αP272, αF135, αP136, αF137, αE432 and αQ435 line up almost perfectly. This aligned arrangement may permit the relay of mechanical pressure from the end of M4 to αP272 of the M2-M3 linker. (PDB ID: 2BG9)

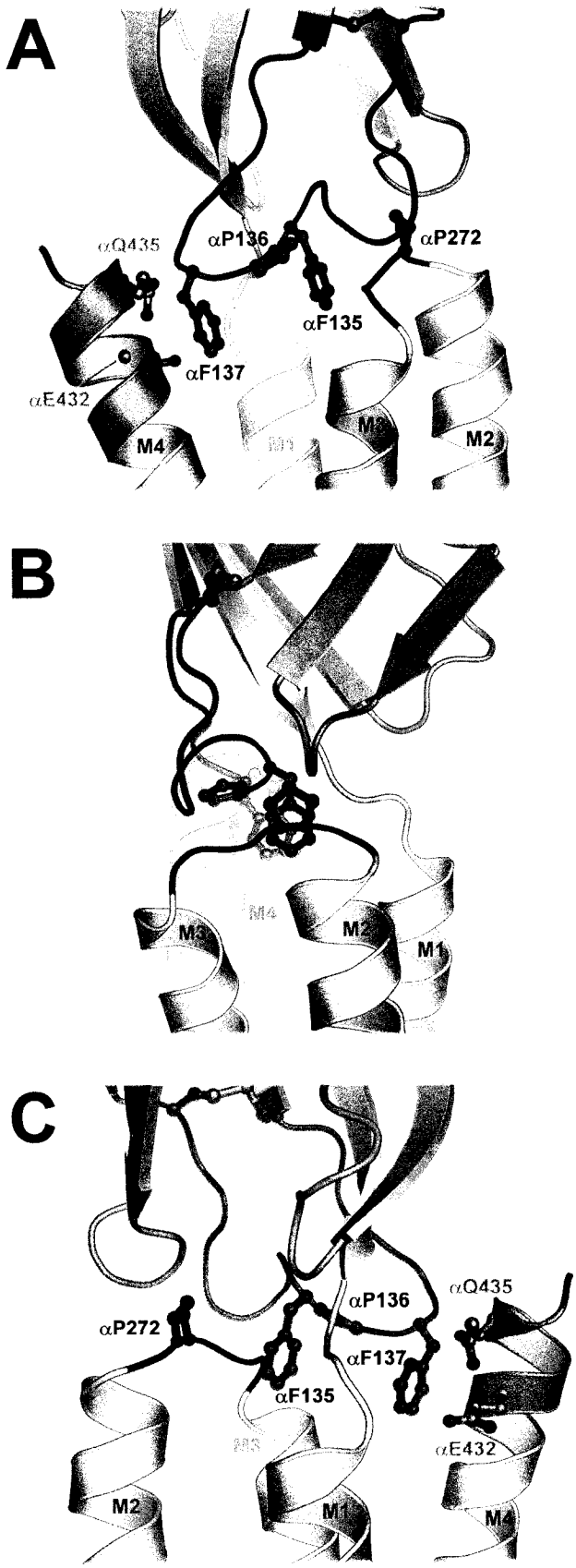
A
αQ435
αP136
αP272
αF135
αF137
αE432
M4
M3
M2
B
M4
M3
M2
M1
C
αP272
αP136
αQ435
αF137
αF135
αE432
M2
M1
M4

5.7 - M4: A Lipid Sensor?

Because M4 makes extensive contacts with the lipid membrane, and at the same time interacts with the Cys-loop, a region which is able to influence both agonist binding affinity and channel gating (289), it is perfectly positioned to translate bilayer physical properties into altered nAChR function. We suggest that the surrounding membrane controls the degree to which the C-terminal end of M4 interacts with the Cys-loop, and that this interaction between M4 and the Cys-loop is necessary for tight association between the extracellular ligand binding domain and the transmembrane pore (Figure 5.10). In effect, the C-terminal M4 segment acts as a "latch", which clamps down on the extracellular N-terminal ligand binding domain, forcing it to interact strongly with the transmembrane pore. The resulting inter-domain interactions stabilize the resting conformation of both the pore and the ligand binding site, and are necessary for coupling agonist binding to channel gating. In membranes which do not support a "functional" resting state nAChR, membrane dependent structural rearrangements of M4 result in loss of this "latching" interaction which weakens the contacts between the ligand binding domain and the transmembrane pore, ultimately causing an uncoupling of ligand binding from channel gating. Because of its ability to influence nAChR function, we call M4 the nAChR's "lipid sensor".

Precisely how loss of interaction between M4 and the Cys-loop results in uncoupling of the receptor's binding and gating functions is not entirely clear. For example, the essential feature of the uncoupled state is that ligand binding fails to trigger channel gating. This could result from a complete lack of conformational change upon agonist binding, or from an inability of the ligand binding domain to communicate its agonist-induced conformational changes to the pore (Figure 5.11). Current data on membrane uncoupled receptors, including

Figure 5.10

Lipids modulate an equilibrium between the nAChR's resting (R) and uncoupled (U) states by influencing the strength of interaction between M4 and the Cys-Loop. The absence of either phosphatidic acid moieties and/or cholesterol in reconstituted nAChR membranes reduces the interaction between the C-terminal end of M4 (orange) and the Cys-loop (green). Loss of this interaction results in weaker association between the extracellular ligand binding domain (purple and blue) and the transmembrane pore (yellow). Reduced interaction between these two functional domains leads to uncoupling of channel gating from ligand binding. Note: the colour scheme used in this figure is the same as in Figures 1.19 and 5.8. A single nAChR subunit is shown for clarity.

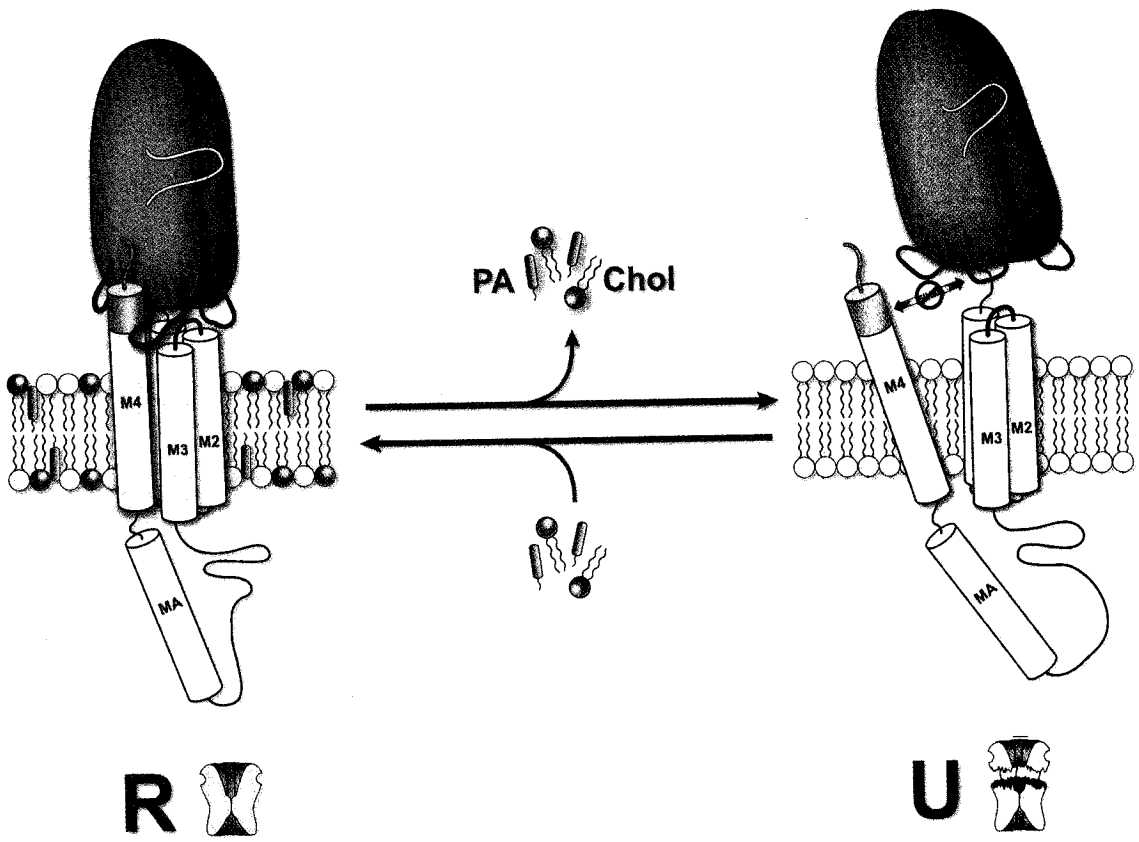
PA
Chol
M4
M3
M2
MA
M4
M3
M2
MA
R
U

Figure 5.11

Schematic diagram depicting some of the possible conformations (U_L, i-iv) of the nAChR upon agonist binding to the uncoupled state (U). Uncoupling, a disconnect between the nAChR's ligand binding and ion-channel functions/domains, ultimately results in a lack of ion flux upon agonist binding. In principle there are a number of ways in which this could happen: i) agonist binding fails to induce conformational change in both the ligand binding and transmembrane domains (i.e. both LBD and TMD remain "R"-like upon agonist binding); ii) ligand induced conformational changes in the ligand binding domain are not transferred to the pore (i.e. despite the LBD being "O"-like upon agonist binding, the TMD remains "R"-like/closed); iii, iv) in the uncoupled state the transmembrane pore adopts a desensitized conformation, therefore whether agonist binding induces conformational change in the ligand binding domain (iv) or not (iii), the channel fails to open. Note that in iii) and iv) the desensitized conformation of the pore also likely exists in the absence of ligand (i.e. ligand binding does not result in desensitization of the pore because the pore is already desensitized). The colour scheme used here is the same as in Figure 5.2 (orange = resting/R-state, green = open/O-state, red = desensitized/D-state). Note: while four possible U_L states are shown here, other combinations likely exist, including novel/not yet characterized conformations of both the ligand binding domain and the pore.

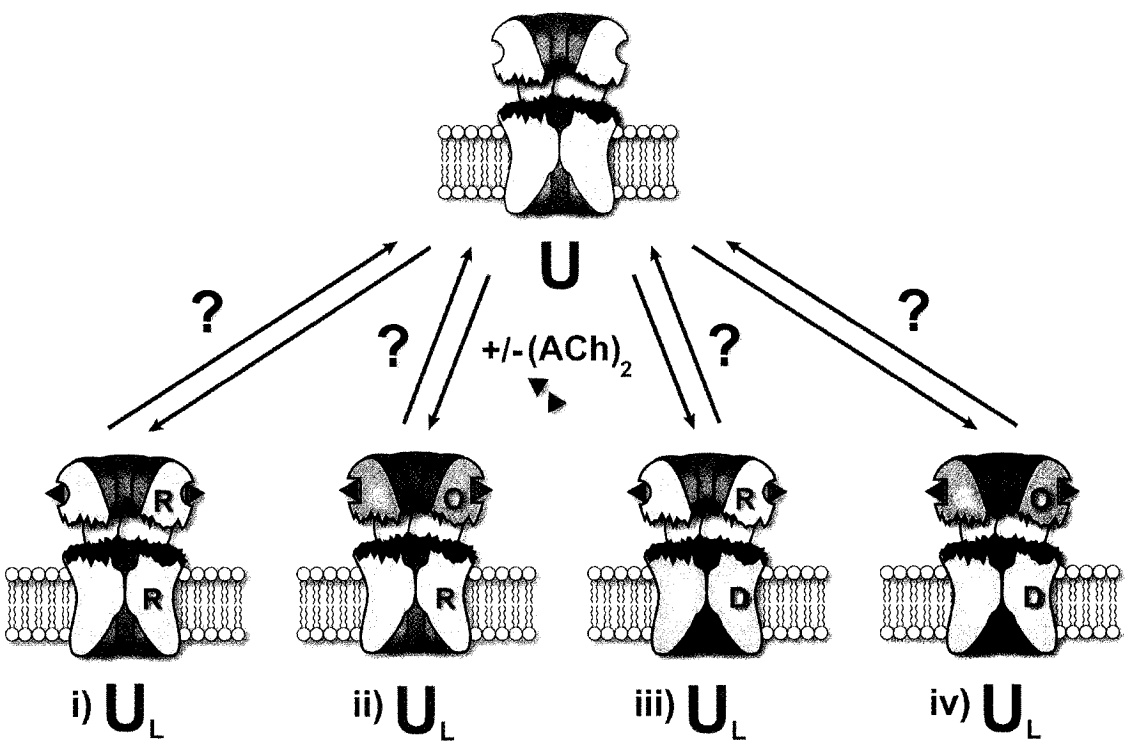
U
?
?
+/-(ACh)2
?
?
R
R
O
R
R
D
O
D
i) UL
ii) UL
iii) UL
iv) UL

the FTIR difference spectroscopy data presented here, suggests that the binding of agonist fails to produce not only the transmembrane domain conformational changes associated with channel gating, but also conformational change within the ligand binding domain (195, 206). Thus the membrane dependent pressure exerted on the Cys-loop by M4 may be important for not only linking the two domains, but also for reducing the energy barrier to conformational change within the ligand binding domain. It appears that unlike the AChBP, the nAChR ligand binding domain cannot undergo conformational change without the stabilizing interactions between its Cys-loop and a transmembrane pore. This is consistent with Unwin's observation that the nAChR's ligand binding domain appears "looser" than that of the AChBP's (117).

The observed biophysical characteristics of membrane uncoupled nAChRs are consistent with the structural perturbations expected from weaker inter-domain interactions as a result of M4 "unlatching". Experiments (including those presented here) have shown that the surrounding membrane influences both nAChR internal dynamics and thermal stability (126, 190, 196). When reconstituted into membranes supporting ion flux capability, the nAChR's internal dynamics are slowed (190, 196), and its thermal stability greater than when reconstituted into membranes that are not capable of supporting ion channel function (126). These observations are also consistent with the early proposal that membrane reconstituted nAChRs are "tighter" than those solubilized in detergents (290). Presumably, like reconstitution into "nonfunctional" membranes, detergent solubilization leads to "unlatching" of the M4 C-terminal segment and reduced association between the nAChR's extracellular and transmembrane domains. The reduced interactions result in increased nAChR flexibility/internal dynamics and reduced thermal stability.

5.8 - Further Evidence of the Functional Importance of M4/Cys-loop Interactions

In addition to its role in coupling ligand binding to gating, there is also evidence that the C-terminal end of M4 (also subunit C-terminus) is required for the allosteric activation of some Cys-loop receptors. For example, the agonist induced response of human α4β2 nAChRs is potentiated by the estrogenic steroid 17β-estradiol (291), and this potentiation is mediated by the receptor's C-terminus (287). Co-application of agonist and 17β-estradiol to *Xenopus* oocytes expressing human α4β2 nAChRs increases the magnitude of whole cell currents relative to cells incubated with agonist alone. This steroid induced potentiation is critically dependent on both the sequence and length of the α4 C-terminus. In particular, the terminal four amino acid "AGMI" sequence is particularly sensitive to both frame shift and substitution mutations (287). Deletion of the terminal isoleucine, as well as internal deletions which shorten M4 by a single amino acid are enough to eliminate potentiation, suggesting that the precise positioning of the terminal M4 sequence is critical. Interestingly, the essential isoleucine in the human α4-subunit aligns with αGln435 in the Torpedo α-subunit, which in the current model makes direct contact with αPhe137 of the conserved Cys-loop "FPF" sequence (Figure 5.9). Presumably, the presence of 17β-estradiol increases the pressure exerted on the Cys-loop by the C-terminal end of M4. This increased pressure, or "latching", results in an increased coupling between ligand binding and channel gating, and explains the observed potentiation. While 17β-estradiol may cause M4 to interact more strongly with the Cys-loop, there is also evidence that the C-terminal end of M4 forms a 17β-estradiol binding site, thus it is also possible that the steroid wedges in between the Cys-loop and M4 (287). In either case the result is greater pressure on the Cys-loop leading to better

coupling between ligand binding and channel gating. The finding that the C-terminus (M4) of human α4β2 nAChRs is involved in modulating receptor function, and that the implicated residues map to *Torpedo* nAChR sites making direct contacts with the Cys-loop, is strong evidence that the interactions between M4 and the Cys-loop are able to influence nAChR gating. These observations also directly demonstrate that M4/Cys-loop interactions are relevant *in vivo*.

The C-terminus of Cys-loop receptors has also been shown to influence their trafficking (288). Export of receptors to the plasma membrane is related to the relative exposure of a conserved motif in M1 (292). Burial of this motif, resulting from proper folding and assembly, promotes transport of the receptor to the cell surface (292). The location of this motif at the interface between the receptor's ligand binding and transmembrane domains suggests that its relative exposure is dependent upon a tight association between the two domains. Weaker inter-domain interactions resulting from M4 "unlatching" may give rise to a greater separation of the two domains and therefore increase the accessibility of the trafficking motif. Recent mutagenesis work has shown that in chimeric α7/5HT$_3$ receptors the length of the C-terminal M4 segment is a critical determinant of receptor trafficking (288). Deletion of the final residue in chimeric α7/5HT$_3$ receptors (Ser449 in murine 5HT$_3$ receptors) reduced their transport to the cell surface by 70%, which led to the hypothesis that somehow the C-terminus locks the receptor in a conformation which masks the conserved trafficking motif in M1. Similar to the above mechanism proposed for the modulation of receptor gating by lipids, it was suggested that through interactions with the highly conserved "FPF" residues in the Cys-loop, M4 acts as a "conformational locker" stabilizing the receptor in its native conformation required for efficient trafficking to the cell surface (288). The final, critical residue of the 5HT$_3$ receptor

(Ser449) aligns with αGln435 in the C-terminal end of αM4, which as already mentioned is in close apposition to αPhe137 of the Cys-loop. This work highlights the importance of the interaction between M4 and Cys-loop, and indicates that the resulting structural stabilization is not only important for coupling the receptor's two main functions (binding and gating), but is also essential for its trafficking and export to the cell surface.

While we have concentrated on the interaction between αGln435 of M4 and αPhe137 of the Cys-loop, it is possible that other residues in the N-terminal ligand binding domain interact with the C-terminal end of M4, and therefore also contribute to coupling. For example, in the current model αLys179 in β-strand 9 points towards the α-subunit's terminal carboxyl (Figure 5.12). A salt bridge between the carboxy terminus and αLys179 would be expected to strengthen the interaction between M4 and the ligand binding domain, thereby increasing coupling. Furthermore, since β-strand 9 leads directly into the C-loop which is an integral part of the agonist binding site, this salt-bridge may be important for stabilizing the conformation of the ligand binding site. This interaction however is highly speculative given the limited resolution of the current model. Furthermore, since αLys179 is not that well conserved amongst Cys-loop receptors (265), it may not be of general importance.

5.9 - Membrane Dependent Conformations of M4

The hypothesis that the membrane modulates the extent of interaction between the C-terminal end of M4 and the Cys-loop implies that M4 adopts different membrane dependent conformations, and thus may be relatively flexible. The current atomic model is consistent with this hypothesis. As noted by Unwin and colleagues when the transmembrane domains of each subunit are aligned by bringing them into strict five fold register, M1, M2, and M3

Figure 5.12

αK179 of β-strand 9 (β9) potentially forms a salt bridge with the C-terminus (C-terminal end of M4) which could also contribute to coupling between the ligand binding and transmembrane domains. The main chain atoms of β9 (αW176-αW187) as well as the side chain of αK179 are shown as balls and sticks. The C-terminus (αG437) is also shown. The distance between the carboxy-terminus and the side chain of αK179 is shown as the yellow dotted line. The colour scheme used here is the same as in Figures 5.8 and 5.9.

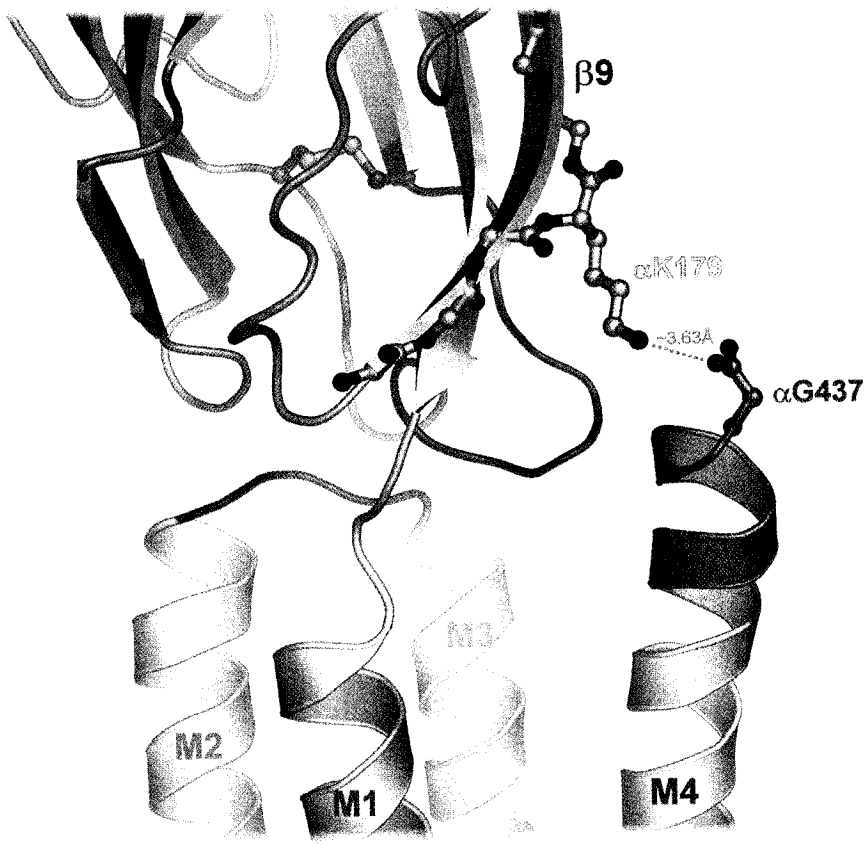
β9
αK175
3.63Å
αG437
M2
M1
M3
M4

superimpose well (RMSD: M1=0.82Å, M2=0.53Å, M3=1.04Å). M4 on the other hand superimposes less precisely (RMSD M4=1.74Å) and comes away from the other helices by variable amounts at its C-terminal extracellular end (Figure 5.13)(67). While this structural heterogeneity may be attributed to sequence variability, it is also possible that it hints at the conformationally dynamic nature of M4, and particularly the flexibility of its C-terminal end. The dynamic nature of M4 could also explain why in earlier low resolution electron microscopy studies the helical nature of M4 was not discernible, while that of the less dynamic M2 was (40, 64).

The essential feature of the membrane-dependent "uncoupled" conformation of the nAChR is that the C-terminal end of M4 does not exert mechanical pressure on the Cys-loop. In principle there are a number of structural rearrangements which could achieve this (Figure 5.14). One possibility is that the C-terminal end of M4 tilts away from the Cys-loop, while its N-terminal end remains in contact with M1 and M3 (Figure 5.14A,B). This would suggest that the C-terminal end of M4 makes fewer protein-protein contacts than its N-terminal end, and therefore is surrounded by either aqueous solvent or lipids in "uncoupled" membranes. Since residues with low conservation are more likely to interact with solvent/lipids (293), the proposed tilt is consistent with the observed pattern of conservation in M4. Furthermore, such a mechanism in which the N-terminal end of M4 remains in contact with M1 and M3 while its C-terminal end tilts away would require a "kink" in the helical nature of M4. Interestingly, the *Torpedo* α-subunit contains a Glycine residue at position 421 in M4, which is highly conserved among nAChR subunits (265). Both the position and high conservation of this residue suggest that it is functionally important. Glycine residues are notoriously flexible, therefore this glycine could act as the proposed tilting pivot point, allowing the C-terminal end of M4 to tilt in response to bilayer forces

Figure 5.13

Overlaid C_α backbone traces of the nAChR transmembrane domain. All five subunits have been overlaid after alignment in order to minimize C_α deviation. The two α-subunits were aligned over their entire sequence since they are supposed to adopt similar conformations. The transmembrane and cytoplasmic domains of the β-, γ- and δ-subunits were aligned with the transmembrane and cytoplasmic domains of the α-subunits (the ligand binding domains of the α-subunits adopt a unique/strained conformation relative to the β-, γ- and δ-subunits (117). **(A)** Each helix of the transmembrane domain (M1-M4) is labelled and coloured differently. **(B)** Each nAChR subunit is labelled and coloured differently. The boxed region highlights the C-terminal end of M4 (referred to in text). (PDB ID: 2BG9).

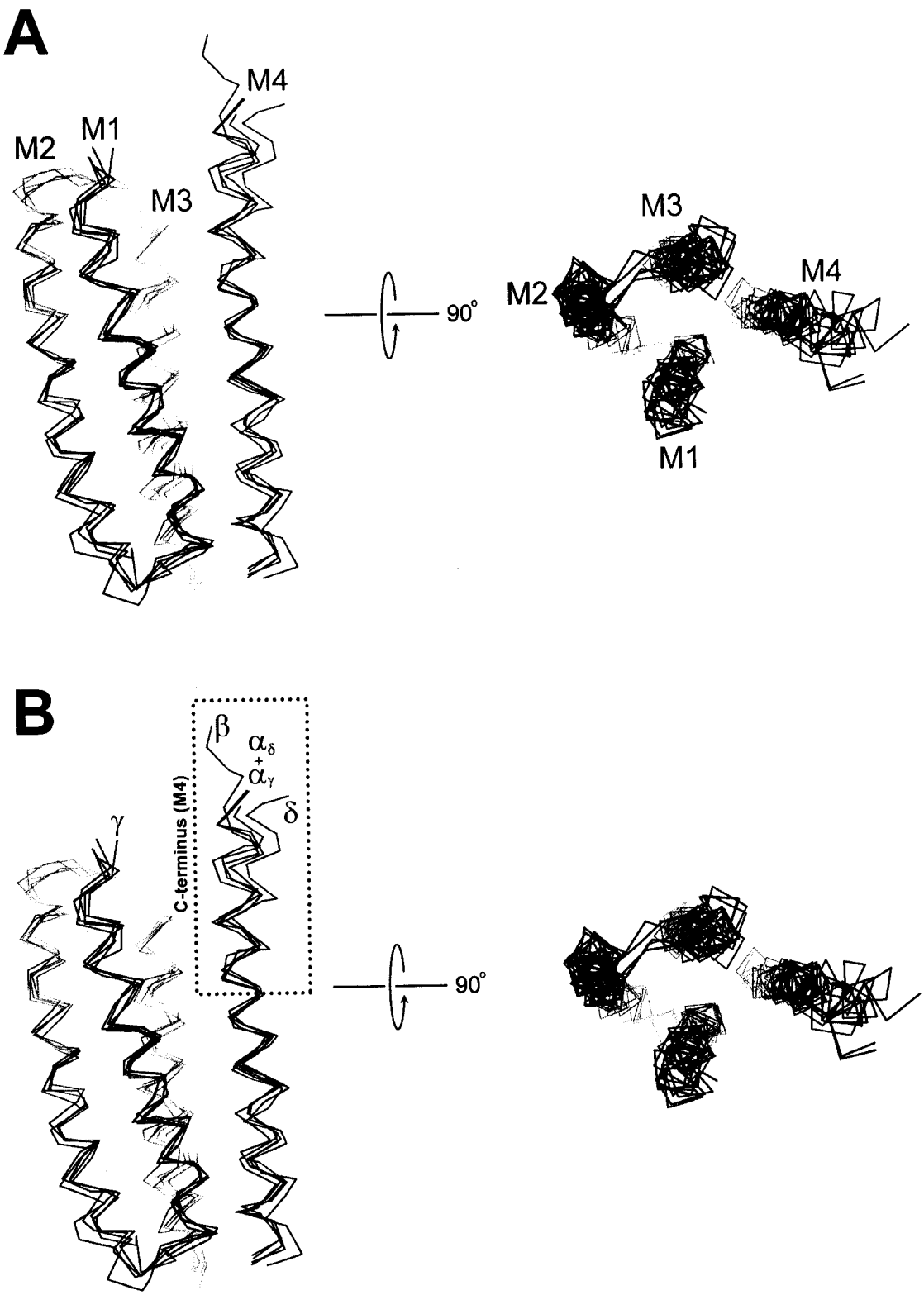
A
M4
M1
M2
M3
90°
M3
M4
M2
M1
B
β
α_δ
+
α_γ
δ
γ
C-terminus (M4)
90°

Figure 5.14

Schematic diagram illustrating the potential lipid-dependent structural rearrangements of M4 leading to uncoupling. Each possibility results in a loss of interaction between the C-terminal end of M4 (orange) and the Cys-loop (green). **(A)** Due to a kink in M4, as a result of a highly conserved glycine (αG421), the C-terminal end of M4 tilts away from the Cys-loop while its N-terminal end remains in contact with the rest of the transmembrane domain. **(B)** Lipid-dependent tilting or twisting of the entire length of M4 moves its C-terminal end away from the Cys-loop. **(C)** M4 may completely dissociate from M1-M3 and exist independently in the membrane. Note: In each case a single subunit has been shown for clarity.

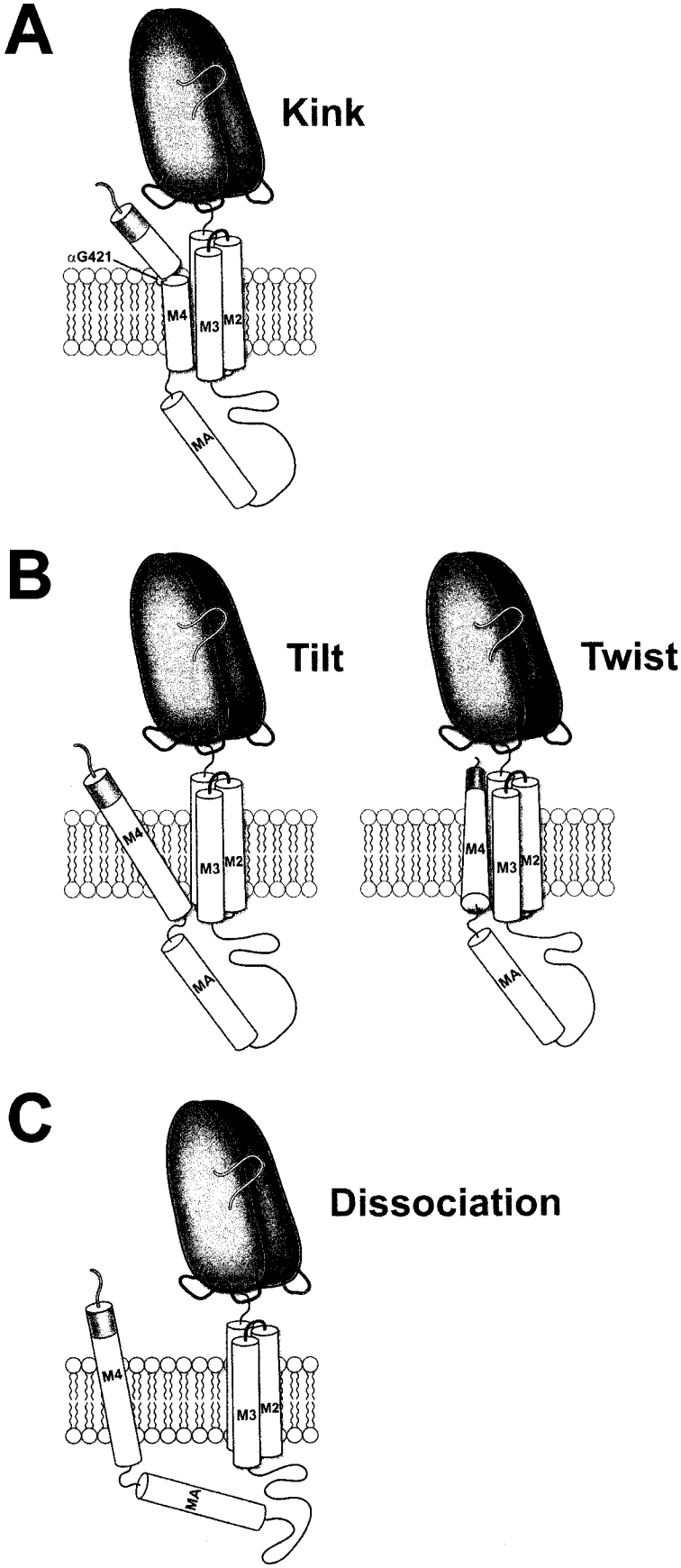
A
Kink
αG421
M4
M3
M2
MA
B
Tilt
M4
M3
M2
MA
Twist
M4
M3
M2
MA
C
Dissociation
M4
M3
M2
MA

(Figure 5.14A). In functional/coupled membranes the end of M4 tilts towards the Cys-loop while in non-functional/uncoupled membranes the C-terminal end of M4 tilts away from the Cys-loop.

Additional evidence for a proposed tilting of M4 comes from a number of recent molecular dynamics simulations. During a recent simulation of a modelled α7 homopentamer in a POPC membrane, the extracellular half of M4 bent outwards, away from the Cys-loop (12). While in another simulation, involving the *Torpedo* nAChR's isolated transmembrane domain in DPPC, M4 of the α, γ and δ-subunits all underwent ~10° clockwise tilts/rotations about their central axes and equilibrated in a new conformation in which M4/Cys-loop interactions would be lost (294). Since both these simulations were performed in membranes not expected to support function, the final conformations of M4 may be similar to that expected for the membrane dependent uncoupled state.

While the tilting of M4 could explain its reduced interaction the Cys-loop, a less conventional, but more intriguing possibility is that M4 is able to dissociate from the rest of the transmembrane domain (M1-M3) and exist independently in the membrane (Figure 5.14C). Despite being a rather radical hypothesis, several lines of evidence are consistent with this proposal: 1) M4 is the least conserved of the transmembrane helices (265), suggesting that it makes few important protein-protein contacts and instead interacts extensively with solvent/lipid (293). 2) Early mutagenesis studies found that substitutions of M4 were much better tolerated than in M1, M2 or M3, suggesting a weak requirement for complementarity between M4 and the rest of the TM domain. Amazingly, substitution of M4 with entire transmembrane helices from other proteins did not result in loss of function, and in some cases actually increased agonist induced responses (i.e. coupling)(273). 3) Fluorescence data of synthesized γM4 peptides reconstituted into liposomes suggests that

lipid composition can modulate the aggregation state of M4. In POPC membranes, γM4 is stable as an isolated peptide, while in POPC/Chol mixtures it self-associates forming homo-oligomers (295). 4) When the nAChR TM domain is proteolyzed by *S.aureus* V8 protease, peptides corresponding to M1, M2 and M3 tend to aggregate with each other both in SDS and organic solvents, while M4 peptides do not (39). This illustrates that M1, M2 and M3 have an intrinsic propensity to associate, while M4 does not. 5) Recent normal mode analysis of homopentameric α7 nAChR's suggests a natural tendency for the M4 helices to move away from the rest of the protein, suggesting that M4 is loosely associated with the rest of the transmembrane domain (260). 6) Helices M1, M2 and M3 are all attached at one end by a relatively small extramembranous linker, which presumably puts restraints on their diffusion in the plane of the membrane relative to one another. M4 on the other hand is covalently attached by a large cytoplasmic domain. This large cytoplasmic linker might allow M4 to diffuse several angstroms away from the other transmembrane helices. 7) In the current atomic model M4 is less precisely positioned than the other transmembrane helices, suggesting that it has a higher degree of conformational freedom (67). While greatest at its C-terminal end, this conformational variability extends the entire length of M4 (Figure 5.13). And finally, 8) recent structural studies involving voltage gated potassium channels, have illustrated the potential for loosely associated transmembrane domains within the same polypeptide (296, 297).

5.10 - M4-Lipid vs. M4-Protein Interactions

In a mechanism where uncoupling results from the dissociation of all, or part of M4, the interplay between M4-protein and M4-lipid interactions is of utmost importance. The

composition of the surrounding membrane may be able to modulate the free energy of transmembrane helix association by controlling the relative affinity of M4 for lipid vs. protein. In certain membranes M4 may prefer to associate with lipids (Figure 5.15, left), while in others it may favour protein-protein interactions with M1-M3 (Figure 5.15, right). Recent fluorescence experiments on synthesized γM4 peptides showed that when reconstituted into POPC, γM4 remained monomeric, but upon reconstitution into POPC/cholesterol it formed oligomers (295). These results directly demonstrate that simple changes in membrane lipid composition can influence the propensity of M4 to form protein-protein contacts. Whether this is a result of interactions between specific lipid molecules and either M4 or M1-M3 is not entirely clear. As mentioned previously, specific lipids may be required to bridge helix-helix interactions (e.g. between M4 and M1-M3) as is observed with the KcsA potassium channel (Figure 5.15A) (253, 266-269).

Instead of specific lipid interactions, a general property of the membrane such as its hydrophobic thickness may drive helix-helix associations (298). For example, hydrophobic mismatch may force M4 to interact with M1-M3 in order to minimize mismatch (Figure 5.15B). The data presented here (Chapter 2) showed that incorporation of the nAChR into POPC bilayers containing POPA caused a dramatic increase in the membrane's gel to liquid crystalline phase transition temperature, as well as a significant decrease in the amount of water penetration into the bilayer's interfacial region. Both these observations are consistent with the expected ordering effect resulting from positive hydrophobic mismatch (212, 299). Interestingly, incorporation of the nAChR into plain POPC membranes resulted in no shift in gel-liquid crystalline phase transition temperature, and no decrease in lipid interfacial hydrogen bonding, suggesting a lack of hydrophobic mismatch. Since only the membranes containing POPA supported nAChR function, there appeared to be a correlation between

Figure 5.15

Schematic diagram illustrating possible lipid properties influencing transmembrane helix association. The composition and physical properties of the surrounding membrane may control the relative affinity of M4 for lipid (left) vs. protein (right). **(A)** Specific lipids are required in order to bridge an interaction between M4 and the rest of the transmembrane domain (M1-M3). **(B)** Hydrophobic thickness of the membrane drives transmembrane helix association. If the hydrophobic thickness of the transmembrane helices (grey region) differs from the hydrophobic thickness of the membrane (grey area), transmembrane helices associate with one another in order to minimize hydrophobic mismatch (right). Conversely, lack of hydrophobic mismatch results in loss of the driving force for transmembrane helix association, and thus dissociation of M4 from M1-M3 (left). **(C)** Top: Incorporation of lipids with a negative spontaneous curvature into planar bilayers results in curvature frustration, a form of potential energy. Bottom: The fully associated form of the nAChR transmembrane domain relieves curvature frustration by surrounding itself with areas of local membrane curvature (right). The release of this potential energy drives transmembrane helix association. In the absence of this stored curvature frustration energy (left) there is no driving force for transmembrane helix association.

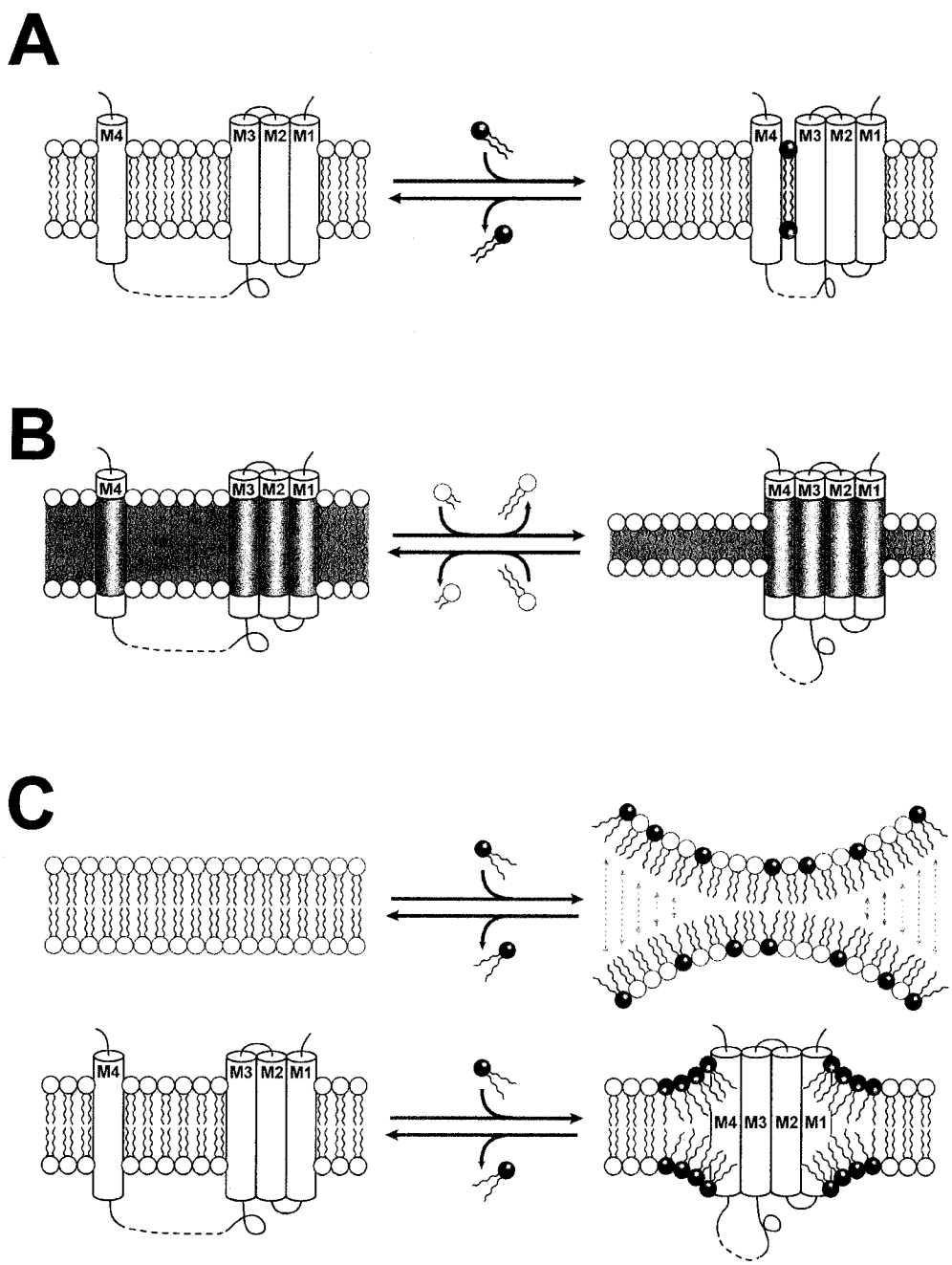
A
M4
M3
M2
M1
B
C

membranes exhibiting hydrophobic mismatch and their ability to stabilize a functional nAChR. Hydrophobic mismatch on its own however does not appear to be sufficient to stabilize a functional nAChR, since incorporation of the nAChR into a number of different PC membranes, with presumably different hydrophobic thicknesses, does not support nAChR function (172, 173, 177, 178, 300). Instead anionic lipids and/or cholesterol appear to be of utmost importance.

An interesting property of the lipids which support nAChR function is their propensity to form negatively curved, non-bilayer structures. Phosphatidic acid, phosphatidylglycerol, phosphatidylethanolamine and cholesterol all have intrinsic negative spontaneous curvatures, and all to some degree support nAChR function. Because these lipids all have intrinsic negative spontaneous curvatures, planar bilayers containing them will all have stored potential energy in the form of curvature frustration (Figure 5.15C) (301). This energy may be released by allowing the bilayer to adopt local regions of negative curvature. The nAChR, by surrounding itself with lipids favouring negative curvature, may be able to relieve some of the stored curvature frustration, thereby lowering the free energy of the entire system. This mechanism of relieving curvature stress may underlie the ability of these negative curvature forming lipids to stabilize the nAChR's coupled resting conformation (Figure 5.15C). The resting state of the nAChR with M4 tightly associated with M1-M3 may represent the best possible conformation for relieving curvature frustration. It is reasonable to envisage a situation where the larger perimeter of the entire 20 helix transmembrane complex facilitates more release of curvature frustration than the combination of five individual M4 helices and the single $(M1\text{-}M3)_5$ complex. This assumes that the isolated M4 helix is unable to relieve significant curvature stress on its own, which is consistent with the recent observation that the isolated γM4 helix adjusts its tilt angle in a

membrane dependent fashion (302, 303). This tilting presumably minimizes hydrophobic mismatch and thus induces minimal, if any, membrane curvature.

The proposal put forth here that the nAChR takes advantage of stored bilayer energy in the form of curvature frustration to drive its transmembrane helix association may be a relatively general mechanism by which integral membrane proteins couple bilayer thermodynamics to their structural stabilization. It has already been proposed that the relief of curvature stress underlies the docking of peripheral proteins to membrane surfaces (304). Curvature stress may also influence the light induced conformational transitions of rhodopsin (305). It is therefore tempting to speculate that integral membrane proteins may make use of this stored curvature frustration energy as a means of assisting membrane protein folding and oligomerization.

5.11 - Summary and Conclusions

In the structure based model presented here we assign a "lipid-sensing" role to the receptor's fourth transmembrane domain (M4), and propose that bilayer physical properties, through M4 and its contacts with the highly conserved Cys-loop, modulate the strength of interaction between the nAChR's extramembranous ligand binding domain and its transmembrane pore (Figure 5.16). Ultimately, effective coupling between the receptor's ligand binding and channel gating functions is dependent upon a tight association between these two distinct domains. The precise structural rearrangements of the M4 "lipid sensor" which lead to uncoupling remain to be established. However, the end result is proposed to be a reduced interaction between the C-terminal end of M4 and the Cys-loop. This reduced association results in weaker inter-domain interactions and forces the nAChR to adopt a

Figure 5.16

M4: a "Lipid Sensor". Membrane physical properties, through M4 and its contacts with the highly conserved Cys-loop, modulate the strength of interaction between the nAChR's extramembranous ligand binding and transmembrane domains. In effect, the C-terminal M4 segment acts as a "latch", which in membrane-dependent manner, clamps down on the extracellular N-terminal ligand binding domain, forcing it to interact with the transmembrane pore. Tight association between these two independent domains is necessary for a coupling of their distinct functions (i.e. ligand binding and channel gating).

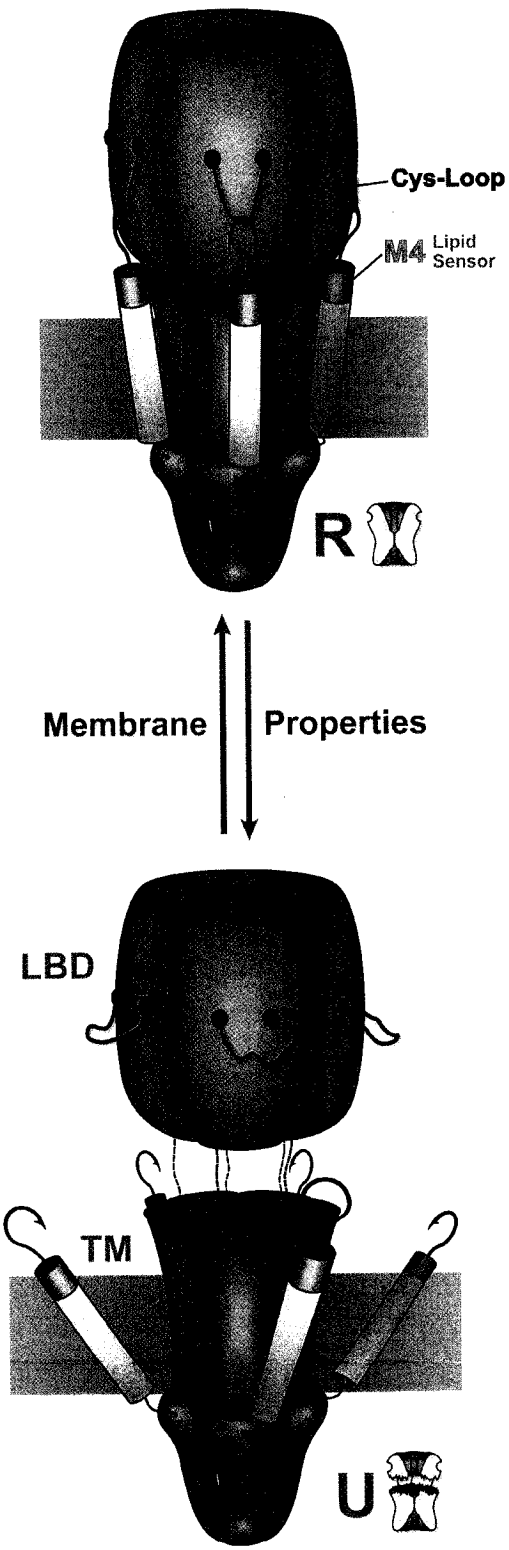
Cys-Loop
M4 Lipid Sensor
R
Membrane
Properties
LBD
TM
U

unique, uncoupled conformation in which the binding of agonist no longer elicits conformational change. Based on the affinity of this uncoupled state for agonist, it appears as though the nAChR's ligand binding domain adopts a conformation resembling the resting state, while chemical labelling studies suggest that the transmembrane pore adopts a conformation similar to the desensitized state (194).

This structure based model incorporates over thirty years of nAChR-lipid data, and explains at the structural level how lipids modulate the receptor's ability to convert agonist binding into channel gating. The model specifically explains the data presented in this thesis by providing a structural explanation as to why uncoupled nAChRs exhibit increased $^{1}H/^{2}H$ exchange kinetics/internal dynamics, as well as a reduced cooperativity of thermal denaturation. The data presented here examining the physical properties of nAChR reconstituted membranes also takes an important step towards understanding the physical properties of membranes that are important for stabilizing the nAChR's resting conformation. Membrane ordering resulting from either hydrophobic mismatch or the nAChR induced relief of curvature stress suggests that one (or both) of these properties could be related to nAChR resting state stabilization.

The data presented in this thesis also highlight the nAChR's functional requirement and relative affinity for phosphatidic acid moieties. This intimate relationship between the nAChR and phosphatidic acid moieties makes evolutionary sense. Lipids with phophatidic acid (PA) headgroups have a natural tendency to form curved bilayer structures, which means that bilayers containing significant amounts of these lipids hold potential energy stored within them in the form of curvature frustration. This energy could be used to drive both the association of transmembrane helices, as well as the formation of the undulating membrane structures found at synaptic junctions (1). Furthermore, because PA is negatively

charged, the nAChR's ability to surround itself with PA will increase its negative electrostatic reach, thereby potentiating its ability to selectively concentrate cations. In effect, the lipids become an electrostatic extension of the ion channel (Figure 5.6).

The interactions between the nAChR and its surrounding lipids illustrate an emerging concept in membrane protein structural biology – that in order to gain a detailed understanding of the mechanism and function of some membrane proteins, an intimate knowledge of their interactions with their surrounding membrane environment is paramount. Lipid-protein interactions, like those described here for the nAChR, represent a novel and relatively underappreciated way of modulating the strength of the post-synaptic response. Given that the Cys-loop receptor superfamily forms the largest family of both excitatory and inhibitory neurotransmitter receptors found throughout the mammalian central and peripheral nervous systems (3), the implications of these lipid-protein interactions with respect to fine-tuning higher brain functions should not be underestimated.

References

1. Nicholls, J.G., R.A. Martin, B.G. Wallace, and P.A. Fuchs. 2001. From Neuron to Brain. Sinauer Associates, Inc., Sunderland, Massachusetts, U.S.A. 580 pp.

2. Hille, B. 2001. Ion Channels of Excitable Membranes. Sinauer Associates, Inc., Sunderland, Massachusetts U.S.A. 814 pp.

3. Sine, S.M., and A.G. Engel. 2006. Recent advances in Cys-loop receptor structure and function. *Nature* 440:448-455.

4. Unwin, N. 2005. Refined structure of the nicotinic acetylcholine receptor at 4Å resolution. *J Mol Biol* 346:967-989.

5. Lester, H.A., M.I. Dibas, D.S. Dahan, J.F. Leite, and D.A. Dougherty. 2004. Cys-loop receptors: new twists and turns. *Trends Neurosci* 27:329-336.

6. Kash, T.L., A. Jenkins, J.C. Kelley, J.R. Trudell, and N.L. Harrison. 2003. Coupling of agonist binding to channel gating in the $GABA_A$ receptor. *Nature* 421:272-275.

7. Bouzat, C., F. Gumilar, G. Spitzmaul, H.L. Wang, D. Rayes, S.B. Hansen, P. Taylor, and S.M. Sine. 2004. Coupling of agonist binding to channel gating in an ACh-binding protein linked to an ion channel. *Nature* 430:896-900.

8. Lee, W.Y., and S.M. Sine. 2005. Principal pathway coupling agonist binding to channel gating in nicotinic receptors. *Nature* 438:243-247.

9. Lummis, S.C., D.L. Beene, L.W. Lee, H.A. Lester, R.W. Broadhurst, and D.A. Dougherty. 2005. Cis-trans isomerization at a proline opens the pore of a neurotransmitter-gated ion channel. *Nature* 438:248-252.

10. Xiu, X., A.P. Hanek, J. Wang, H.A. Lester, and D.A. Dougherty. 2005. A unified view of the role of electrostatic interactions in modulating the gating of Cys-loop receptors. *J Biol Chem* 280:41655-41666.

11. Grutter, T., L.P. de Carvalho, V. Dufresne, A. Taly, S.J. Edelstein, and J.P. Changeux. 2005. Molecular tuning of fast gating in pentameric ligand-gated ion channels. *Proc Natl Acad Sci U S A* 102:18207-18212.

12. Law, R.J., R.H. Henchman, and J.A. McCammon. 2005. A gating mechanism proposed from a simulation of a human α7 nicotinic acetylcholine receptor. *Proc Natl Acad Sci U S A* 102:6813-6818.

13. Karlin, A. 2002. Emerging structure of the nicotinic acetylcholine receptors. *Nat Rev Neurosci* 3:102-114.

14. Bernard, C. 1865. An Introduction to the Study of Experimental Medicine. Dover Publications, New York. 226 pp.

15. Changeux, J.P. 1993. Chemical signaling in the brain. *Sci Am* 269:58-62.

16. Langley, J.N. 1907. On the contraction of muscle chiefly in relation to the presence of receptive substances. Part 1. *J Physiol (Lond)* 36:347–384

17. Maehle, A.H. 2004. "Receptive substances": John Newport Langley (1852-1925) and his path to a receptor theory of drug action. *Med Hist* 48:153-174.

18. Maehle, A.H., C.R. Prull, and R.F. Halliwell. 2002. The emergence of the drug receptor theory. *Nat Rev Drug Discov* 1:637-641.

19. Dale, H.H., and H.W. Dudley. 1929. The presence of histamine and acetylcholine in the spleen of the ox and the horse. II. *J Physiol (Lond)* 68:97-123.

20. Hodgkin, A.L., and A.F. Huxley. 1952. The dual effect of membrane potential on sodium conductance in the giant axon of Loligo. *J Physiol* 116:497-506.

21. Hodgkin, A.L., and A.F. Huxley. 1952. Propagation of electrical signals along giant nerve fibers. *Proc R Soc Lond B Biol Sci* 140:177-183.

22. Hodgkin, A.L., and A.F. Huxley. 1952. A quantitative description of membrane current and its application to conduction and excitation in nerve. *J Physiol* 117:500-544.

23. Hodgkin, A.L., A.F. Huxley, and B. Katz. 1952. Measurement of current-voltage relations in the membrane of the giant axon of Loligo. *J Physiol* 116:424-448.

24. Monod, J., J. Wyman, and J.P. Changeux. 1965. On the Nature of Allosteric Transitions: a Plausible Model. *J Mol Biol* 12:88-118.

25. Changeux, J.P., M. Kasai, and C.Y. Lee. 1970. Use of a snake venom toxin to characterize the cholinergic receptor protein. *Proc Natl Acad Sci U S A* 67:1241-1247.

26. Miledi, R., P. Molinoff, and L.T. Potter. 1971. Isolation of the cholinergic receptor protein of Torpedo electric tissue. *Nature* 229:554-557.

27. Conti-Tronconi, B.M., and M.A. Raftery. 1982. The nicotinic cholinergic receptor: correlation of molecular structure with functional properties. *Annu Rev Biochem* 51:491-530.

28. Weill, C.L., M.G. McNamee, and A. Karlin. 1974. Affinity-labeling of purified acetylcholine receptor from Torpedo californica. *Biochem Biophys Res Commun* 61:997-1003.

29. Raftery, M.A., M.W. Hunkapiller, C.D. Strader, and L.E. Hood. 1980. Acetylcholine receptor: complex of homologous subunits. *Science* 208:1454-1456.

30. Claudio, T., M. Ballivet, J. Patrick, and S. Heinemann. 1983. Nucleotide and deduced amino acid sequences of Torpedo californica acetylcholine receptor γ-subunit. *Proc Natl Acad Sci U S A* 80:1111-1115.

31. Noda, M., H. Takahashi, T. Tanabe, M. Toyosato, Y. Furutani, T. Hirose, M. Asai, S. Inayama, T. Miyata, and S. Numa. 1982. Primary structure of α-subunit precursor of Torpedo californica acetylcholine receptor deduced from cDNA sequence. *Nature* 299:793-797.

32. Noda, M., H. Takahashi, T. Tanabe, M. Toyosato, S. Kikyotani, Y. Furutani, T. Hirose, H. Takashima, S. Inayama, T. Miyata, and S. Numa. 1983. Structural homology of Torpedo californica acetylcholine receptor subunits. *Nature* 302:528-532.

33. Noda, M., H. Takahashi, T. Tanabe, M. Toyosato, S. Kikyotani, T. Hirose, M. Asai, H. Takashima, S. Inayama, T. Miyata, and S. Numa. 1983. Primary structures of β- and δ-subunit precursors of Torpedo californica acetylcholine receptor deduced from cDNA sequences. *Nature* 301:251-255.

34. Mishina, M., T. Kurosaki, T. Tobimatsu, Y. Morimoto, M. Noda, T. Yamamoto, M. Terao, J. Lindstrom, T. Takahashi, M. Kuno, and et al. 1984. Expression of functional acetylcholine receptor from cloned cDNAs. *Nature* 307:604-608.

35. Schofield, P.R., M.G. Darlison, N. Fujita, D.R. Burt, F.A. Stephenson, H. Rodriguez, L.M. Rhee, J. Ramachandran, V. Reale, T.A. Glencorse, and et al. 1987. Sequence and functional expression of the GABA A receptor shows a ligand-gated receptor super-family. *Nature* 328:221-227.

36. Anderson, D.J., P. Walter, and G. Blobel. 1982. Signal recognition protein is required for the integration of acetylcholine receptor δ-subunit, a transmembrane glycoprotein, into the endoplasmic reticulum membrane. *J Cell Biol* 93:501-506.

37. Numa, S. 1987. A molecular view of neurotransmitter receptors and ionic channels. *Harvey Lect* 83:121-165.

38. Akabas, M.H., D.A. Stauffer, M. Xu, and A. Karlin. 1992. Acetylcholine receptor channel structure probed in cysteine-substitution mutants. *Science* 258:307-310.

39. Blanton, M.P., and J.B. Cohen. 1992. Mapping the lipid-exposed regions in the Torpedo californica nicotinic acetylcholine receptor. *Biochemistry* 31:3738-3750.

40. Blanton, M.P., and J.B. Cohen. 1994. Identifying the lipid-protein interface of the Torpedo nicotinic acetylcholine receptor: secondary structure implications. *Biochemistry* 33:2859-2872.

41. Blanton, M.P., and H.H. Wang. 1990. Photoaffinity labeling of the Torpedo californica nicotinic acetylcholine receptor with an aryl azide derivative of phosphatidylserine. *Biochemistry* 29:1186-1194.

42. Blanton, M.P., and H.H. Wang. 1991. Localization of regions of the Torpedo californica nicotinic acetylcholine receptor labeled with an aryl azide derivative of phosphatidylserine. *Biochim Biophys Acta* 1067:1-8.

43. Giraudat, J., C. Montecucco, R. Bisson, and J.P. Changeux. 1985. Transmembrane topology of acetylcholine receptor subunits probed with photoreactive phospholipids. *Biochemistry* 24:3121-3127.

44. Poulter, L., J.P. Earnest, R.M. Stroud, and A.L. Burlingame. 1989. Structure, oligosaccharide structures, and posttranslationally modified sites of the nicotinic acetylcholine receptor. *Proc Natl Acad Sci U S A* 86:6645-6649.

45. Strecker, A., P. Franke, C. Weise, and F. Hucho. 1994. All potential glycosylation sites of the nicotinic acetylcholine receptor δ-subunit from Torpedo californica are utilized. *Eur J Biochem* 220:1005-1011.

46. Shoji, H., N. Takahashi, H. Nomoto, M. Ishikawa, I. Shimada, Y. Arata, and K. Hayashi. 1992. Detailed structural analysis of asparagine-linked oligosaccharides of the nicotinic acetylcholine receptor from Torpedo californica. *Eur J Biochem* 207:631-641.

47. Mitra, A.K., M.P. McCarthy, and R.M. Stroud. 1989. Three-dimensional structure of the nicotinic acetylcholine receptor and location of the major associated 43-kD cytoskeletal protein, determined at 22 A by low dose electron microscopy and x-ray diffraction to 12.5 A [published erratum appears in J Cell Biol 1989 Oct;109 (4 Pt 1):1185]. *J Cell Biol* 109:755-774.

48. Changeux, J.P., A. Devillers-Thiery, and P. Chemouilli. 1984. Acetylcholine receptor: an allosteric protein. *Science* 225:1335-1345.

49. Imoto, K., C. Methfessel, B. Sakmann, M. Mishina, Y. Mori, T. Konno, K. Fukuda, M. Kurasaki, H. Bujo, Y. Fujita, and et al. 1986. Location of a δ-subunit region determining ion transport through the acetylcholine receptor channel. *Nature* 324:670-674.

50. Kistler, J., and R.M. Stroud. 1981. Crystalline arrays of membrane-bound acetylcholine receptor. *Proc Natl Acad Sci U S A* 78:3678-3682.

51. Leonard, R.J., C.G. Labarca, P. Charnet, N. Davidson, and H.A. Lester. 1988. Evidence that the M2 membrane-spanning region lines the ion channel pore of the nicotinic receptor. *Science* 242:1578-1581.

52. Giraudat, J., M. Dennis, T. Heidmann, J.Y. Chang, and J.P. Changeux. 1986. Structure of the high-affinity binding site for noncompetitive blockers of the acetylcholine receptor: serine-262 of the δ-subunit is labeled by [^{3}H]chlorpromazine. *Proc Natl Acad Sci U S A* 83:2719-2723.

53. Giraudat, J., M. Dennis, T. Heidmann, P.Y. Haumont, F. Lederer, and J.P. Changeux. 1987. Structure of the high-affinity binding site for noncompetitive blockers of the acetylcholine receptor: [^{3}H]chlorpromazine labels homologous residues in the β and δ chains. *Biochemistry* 26:2410-2418.

54. Hucho, F., W. Oberthur, and F. Lottspeich. 1986. The ion channel of the nicotinic acetylcholine receptor is formed by the homologous helices M II of the receptor subunits. *FEBS Lett* 205:137-142.

55. Imoto, K., C. Busch, B. Sakmann, M. Mishina, T. Konno, J. Nakai, H. Bujo, Y. Mori, K. Fukuda, and S. Numa. 1988. Rings of negatively charged amino acids determine the acetylcholine receptor channel conductance. *Nature* 335:645-648.

56. Wilson, G., and A. Karlin. 2001. Acetylcholine receptor channel structure in the resting, open, and desensitized states probed with the substituted-cysteine-accessibility method. *Proc Natl Acad Sci U S A* 98:1241-1248.

57. Zhang, H., and A. Karlin. 1998. Contribution of the β-subunit M2 segment to the ion-conducting pathway of the acetylcholine receptor. *Biochemistry* 37:7952-7964.

58. Wilson, G.G., and A. Karlin. 1998. The location of the gate in the acetylcholine receptor channel. *Neuron* 20:1269-1281.

59. Karlin, A., and M.H. Akabas. 1998. Substituted-cysteine accessibility method. *Methods Enzymol* 293:123-145.

60. Zhang, H., and A. Karlin. 1997. Identification of acetylcholine receptor channel-lining residues in the M1 segment of the β-subunit. *Biochemistry* 36:15856-15864.

61. Akabas, M.H., and A. Karlin. 1995. Identification of acetylcholine receptor channel-lining residues in the M1 segment of the α-subunit. *Biochemistry* 34:12496-12500.

62. Akabas, M.H., C. Kaufmann, P. Archdeacon, and A. Karlin. 1994. Identification of acetylcholine receptor channel-lining residues in the entire M2 segment of the α-subunit. *Neuron* 13:919-927.

63. DiPaola, M., P.N. Kao, and A. Karlin. 1990. Mapping the alpha-subunit site photolabeled by the noncompetitive inhibitor [^{3}H]quinacrine azide in the active state of the nicotinic acetylcholine receptor. *J Biol Chem* 265:11017-11029.

64. Unwin, N. 1993. Nicotinic acetylcholine receptor at 9Å resolution. *J Mol Biol* 229:1101-1124.

65. Filatov, G.N., and M.M. White. 1995. The role of conserved leucines in the M2 domain of the acetylcholine receptor in channel gating. *Mol Pharmacol* 48:379-384.

66. Labarca, C., M.W. Nowak, H. Zhang, L. Tang, P. Deshpande, and H.A. Lester. 1995. Channel gating governed symmetrically by conserved leucine residues in the M2 domain of nicotinic receptors. *Nature* 376:514-516.

67. Miyazawa, A., Y. Fujiyoshi, and N. Unwin. 2003. Structure and gating mechanism of the acetylcholine receptor pore. *Nature* 424:949-955.

68. Dwyer, T.M., D.J. Adams, and B. Hille. 1980. The permeability of the endplate channel to organic cations in frog muscle. *J Gen Physiol* 75:469-492.

69. Huang, L.Y., W.A. Catterall, and G. Ehrenstein. 1978. Selectivity of cations and nonelectrolytes for acetylcholine-activated channels in cultured muscle cells. *J Gen Physiol* 71:397-410.

70. Doyle, D.A., J. Morais Cabral, R.A. Pfuetzner, A. Kuo, J.M. Gulbis, S.L. Cohen, B.T. Chait, and R. MacKinnon. 1998. The structure of the potassium channel: molecular basis of K^+ conduction and selectivity. *Science* 280:69-77.

71. Zhou, Y., J.H. Morais-Cabral, A. Kaufman, and R. MacKinnon. 2001. Chemistry of ion coordination and hydration revealed by a K^+ channel-Fab complex at 2.0Å resolution. *Nature* 414:43-48.

72. Sato, C., Y. Ueno, K. Asai, K. Takahashi, M. Sato, A. Engel, and Y. Fujiyoshi. 2001. The voltage-sensitive sodium channel is a bell-shaped molecule with several cavities. *Nature* 409:1047-1051.

73. Imoto, K., T. Konno, J. Nakai, F. Wang, M. Mishina, and S. Numa. 1991. A ring of uncharged polar amino acids as a component of channel constriction in the nicotinic acetylcholine receptor. *FEBS Lett* 289:193-200.

74. Galzi, J.L., A. Devillers-Thiery, N. Hussy, S. Bertrand, J.P. Changeux, and D. Bertrand. 1992. Mutations in the channel domain of a neuronal nicotinic receptor convert ion selectivity from cationic to anionic. *Nature* 359:500-505.

75. Corringer, P.J., S. Bertrand, J.L. Galzi, A. Devillers-Thiery, J.P. Changeux, and D. Bertrand. 1999. Mutational analysis of the charge selectivity filter of the α7 nicotinic acetylcholine receptor. *Neuron* 22:831-843.

76. Keramidas, A., A.J. Moorhouse, C.R. French, P.R. Schofield, and P.H. Barry. 2000. M2 pore mutations convert the glycine receptor channel from being anion- to cation-selective. *Biophys J* 79:247-259.

77. Sine, S.M., H.J. Kreienkamp, N. Bren, R. Maeda, and P. Taylor. 1995. Molecular dissection of subunit interfaces in the acetylcholine receptor: identification of determinants of α-conotoxin M1 selectivity. *Neuron* 15:205-211.

78. Pedersen, S.E., and J.B. Cohen. 1990. d-Tubocurarine binding sites are located at α-γ and α-δ subunit interfaces of the nicotinic acetylcholine receptor. *Proc Natl Acad Sci U S A* 87:2785-2789.

79. Sine, S.M. 1993. Molecular dissection of subunit interfaces in the acetylcholine receptor: identification of residues that determine curare selectivity. *Proc Natl Acad Sci U S A* 90:9436-9440.

80. Blount, P., and J.P. Merlie. 1989. Molecular basis of the two nonequivalent ligand binding sites of the muscle nicotinic acetylcholine receptor. *Neuron* 3:349-357.

81. Dennis, M., J. Giraudat, F. Kotzyba-Hibert, M. Goeldner, C. Hirth, J.Y. Chang, C. Lazure, M. Chretien, and J.P. Changeux. 1988. Amino acids of the Torpedo marmorata acetylcholine receptor α-subunit labeled by a photoaffinity ligand for the acetylcholine binding site. *Biochemistry* 27:2346-2357.

82. Middleton, R.E., and J.B. Cohen. 1991. Mapping of the acetylcholine binding site of the nicotinic acetylcholine receptor: [^{3}H]nicotine as an agonist photoaffinity label. *Biochemistry* 30:6987-6997.

83. Langenbuch-Cachat, J., C. Bon, C. Mulle, M. Goeldner, C. Hirth, and J.P. Changeux. 1988. Photoaffinity labeling of the acetylcholine binding sites on the nicotinic receptor by an aryldiazonium derivative. *Biochemistry* 27:2337-2345.

84. Oswald, R.E., and J.P. Changeux. 1982. Crosslinking of alpha-bungarotoxin to the acetylcholine receptor from Torpedo marmorata by ultraviolet light irradiation. *FEBS Lett* 139:225-229.

85. Corringer, P.J., N. Le Novere, and J.P. Changeux. 2000. Nicotinic receptors at the amino acid level. *Annu Rev Pharmacol Toxicol* 40:431-458.

86. Kao, P.N., A.J. Dwork, R.R. Kaldany, M.L. Silver, J. Wideman, S. Stein, and A. Karlin. 1984. Identification of the alpha subunit half-cystine specifically labeled by an affinity reagent for the acetylcholine receptor binding site. *J Biol Chem* 259:11662-11665.

87. Abramson, S.N., Y. Li, P. Culver, and P. Taylor. 1989. An analog of lophotoxin reacts covalently with Tyr190 in the α-subunit of the nicotinic acetylcholine receptor. *J Biol Chem* 264:12666-12672.

88. Cohen, J.B., S.D. Sharp, and W.S. Liu. 1991. Structure of the agonist-binding site of the nicotinic acetylcholine receptor. *J Biol Chem* 266:23354-23364.

89. Czajkowski, C., and A. Karlin. 1995. Structure of the nicotinic receptor acetylcholine-binding site. Identification of acidic residues in the delta subunit within 0.9 nm of the 5 α-subunit-binding. *J Biol Chem* 270:3160-3164.

90. Sussman, J.L., M. Harel, F. Frolow, C. Oefner, A. Goldman, L. Toker, and I. Silman. 1991. Atomic structure of acetylcholinesterase from Torpedo californica: a prototypic acetylcholine-binding protein. *Science* 253:872-879.

91. Sine, S.M., P. Quiram, F. Papanikolaou, H.J. Kreienkamp, and P. Taylor. 1994. Conserved tyrosines in the α-subunit of the nicotinic acetylcholine receptor stabilize quaternary ammonium groups of agonists and curariform antagonists. *J Biol Chem* 269:8808-8816.

92. Nowak, M.W., P.C. Kearney, J.R. Sampson, M.E. Saks, C.G. Labarca, S.K. Silverman, W. Zhong, J. Thorson, J.N. Abelson, N. Davidson, and et al. 1995. Nicotinic receptor binding site probed with unnatural amino acid incorporation in intact cells. *Science* 268:439-442.

93. Paas, Y., J. Cartaud, M. Recouvreur, R. Grailhe, V. Dufresne, E. Pebay-Peyroula, E.M. Landau, and J.P. Changeux. 2003. Electron microscopic evidence for nucleation and growth of 3D acetylcholine receptor microcrystals in structured lipid-detergent matrices. *Proc Natl Acad Sci U S A* 100:11309-11314.

94. Hertling-Jaweed, S., G. Bandini, A. Muller-Fahrnow, V. Dommes, and F. Hucho. 1988. Rapid preparation of the nicotinic acetylcholine receptor for crystallization in detergent solution. *FEBS Lett* 241:29-32.

95. Fujiyoshi, Y. 1998. The structural study of membrane proteins by electron crystallography. *Adv Biophys* 35:25-80.

96. Brisson, A., and P.N. Unwin. 1984. Tubular crystals of acetylcholine receptor. *J Cell Biol* 99:1202-1211.

97. Unwin, N. 2003. Structure and action of the nicotinic acetylcholine receptor explored by electron microscopy. *FEBS Lett* 555:91-95.

98. Stauffer, K.A., N.M. Kumar, N.B. Gilula, and N. Unwin. 1991. Isolation and purification of gap junction channels. *J Cell Biol* 115:141-150.

99. Toyoshima, C., and N. Unwin. 1990. Three-dimensional structure of the acetylcholine receptor by cryoelectron microscopy and helical image reconstruction. *J Cell Biol* 111:2623-2635.

100. Unwin, N. 1989. The structure of ion channels in membranes of excitable cells. *Neuron* 3:665-676.

101. Toyoshima, C., and N. Unwin. 1988. Ion channel of acetylcholine receptor reconstructed from images of postsynaptic membranes. *Nature* 336:247-250.

102. Unwin, N., C. Toyoshima, and E. Kubalek. 1988. Arrangement of the acetylcholine receptor subunits in the resting and desensitized states, determined by cryoelectron microscopy of crystallized Torpedo postsynaptic membranes. *J Cell Biol* 107:1123-1138.

103. Toyoshima, C., and N. Unwin. 1988. Contrast transfer for frozen-hydrated specimens: determination from pairs of defocused images. *Ultramicroscopy* 25:279-291.

104. Kubalek, E., S. Ralston, J. Lindstrom, and N. Unwin. 1987. Location of subunits within the acetylcholine receptor by electron image analysis of tubular crystals from Torpedo marmorata. *J Cell Biol* 105:9-18.

105. Unwin, N. 1986. The use of cryoelectron microscopy in elucidating molecular design and mechanisms. *Ann N Y Acad Sci* 483:1-4.

106. Unwin, N., and R. Henderson. 1984. The structure of proteins in biological membranes. *Sci Am* 250:78-94.

107. Unwin, N. 1980. Electron diffraction and membrane proteins. *Prog Clin Biol Res* 40:335-336.

108. Unwin, N. 2000. The Croonian Lecture 2000. Nicotinic acetylcholine receptor and the structural basis of fast synaptic transmission. *Philos Trans R Soc Lond B Biol Sci* 355:1813-1829.

109. Tierney, M.L., and N. Unwin. 2000. Electron microscopic evidence for the assembly of soluble pentameric extracellular domains of the nicotinic acetylcholine receptor. *J Mol Biol* 303:185-196.

110. Miyazawa, A., Y. Fujiyoshi, M. Stowell, and N. Unwin. 1999. Nicotinic acetylcholine receptor at 4.6Å resolution: transverse tunnels in the channel wall. *J Mol Biol* 288:765-786.

111. Unwin, N. 1998. The nicotinic acetylcholine receptor of the Torpedo electric ray. *J Struct Biol* 121:181-190.

112. Beroukhim, R., and N. Unwin. 1997. Distortion correction of tubular crystals: improvements in the acetylcholine receptor structure. *Ultramicroscopy* 70:57-81.

113. Beroukhim, R., and N. Unwin. 1995. Three-dimensional location of the main immunogenic region of the acetylcholine receptor. *Neuron* 15:323-331.

114. Unwin, N. 1995. Acetylcholine receptor channel imaged in the open state. *Nature* 373:37-43.

115. Berriman, J., and N. Unwin. 1994. Analysis of transient structures by cryo-microscopy combined with rapid mixing of spray droplets. *Ultramicroscopy* 56:241-252.

116. Unwin, N. 1993. Neurotransmitter action: opening of ligand-gated ion channels. *Cell* 72 Suppl:31-41.

117. Unwin, N., A. Miyazawa, J. Li, and Y. Fujiyoshi. 2002. Activation of the nicotinic acetylcholine receptor involves a switch in conformation of the alpha subunits. *J Mol Biol* 319:1165-1176.

118. Unwin, N. 2002. Structure of the acetylcholine-gated channel. *Novartis Found Symp* 245:5-15; discussion 15-21, 165-168.

119. Valenzuela, C.F., P. Weign, J. Yguerabide, and D.A. Johnson. 1994. Transverse distance between the membrane and the agonist binding sites on the Torpedo acetylcholine receptor: a fluorescence study. *Biophys J* 66:674-682.

120. Karlin, A., E. Holtzman, N. Yodh, P. Lobel, J. Wall, and J. Hainfeld. 1983. The arrangement of the subunits of the acetylcholine receptor of Torpedo californica. *J Biol Chem* 258:6678-6681.

121. Brejc, K., W.J. van Dijk, R.V. Klaassen, M. Schuurmans, J. van Der Oost, A.B. Smit, and T.K. Sixma. 2001. Crystal structure of an ACh-binding protein reveals the ligand-binding domain of nicotinic receptors. *Nature* 411:269-276.

122. Gorne-Tschelnokow, U., A. Strecker, C. Kaduk, D. Naumann, and F. Hucho. 1994. The transmembrane domains of the nicotinic acetylcholine receptor contain α-helical and β-structures. *Embo J* 13:338-341.

123. Ortells, M.O., and G.G. Lunt. 1996. A mixed helix-β-sheet model of the transmembrane region of the nicotinic acetylcholine receptor. *Protein Eng* 9:51-59.

124. Methot, N., M.P. McCarthy, and J.E. Baenziger. 1994. Secondary structure of the nicotinic acetylcholine receptor: implications for structural models of a ligand-gated ion channel. *Biochemistry* 33:7709-7717.

125. Methot, N., B.D. Ritchie, M.P. Blanton, and J.E. Baenziger. 2001. Structure of the pore-forming transmembrane domain of a ligand-gated ion channel. *J Biol Chem* 276:23726-23732.

126. Methot, N., and J.E. Baenziger. 1998. Secondary structure of the exchange-resistant core from the nicotinic acetylcholine receptor probed directly by infrared spectroscopy and Hydrogen/Deuterium exchange. *Biochemistry* 37:14815-14822.

127. Baenziger, J.E., and N. Methot. 1995. Fourier transform infrared and hydrogen/deuterium exchange reveal an exchange-resistant core of α-helical peptide hydrogens in the nicotinic acetylcholine receptor. *J Biol Chem* 270:29129-29137.

128. Blanton, M.P., E.A. McCardy, A. Huggins, and D. Parikh. 1998. Probing the structure of the nicotinic acetylcholine receptor with the hydrophobic photoreactive probes [^{125}I]TID-BE and [^{125}I]TIDPC/16. *Biochemistry* 37:14545-14555.

129. Blanton, M.P., L.J. Dangott, S.K. Raja, A.K. Lala, and J.B. Cohen. 1998. Probing the structure of the nicotinic acetylcholine receptor ion channel with the uncharged photoactivable compound -^{3}H-diazofluorene. *J Biol Chem* 273:8659-8668.

130. Corbin, J., N. Methot, H.H. Wang, J.E. Baenziger, and M.P. Blanton. 1998. Secondary structure analysis of individual transmembrane segments of the nicotinic acetylcholine receptor by circular dichroism and Fourier transform infrared spectroscopy. *J Biol Chem* 273:771-777.

131. Smit, A.B., N.I. Syed, D. Schaap, J. van Minnen, J. Klumperman, K.S. Kits, H. Lodder, R.C. van der Schors, R. van Elk, B. Sorgedrager, K. Brejc, T.K. Sixma, and W.P. Geraerts. 2001. A glia-derived acetylcholine-binding protein that modulates synaptic transmission. *Nature* 411:261-268.

132. Smit, A.B., K. Brejc, N. Syed, and T.K. Sixma. 2003. Structure and function of AChBP, homologue of the ligand-binding domain of the nicotinic acetylcholine receptor. *Ann N Y Acad Sci* 998:81-92.

133. Celie, P.H., S.E. van Rossum-Fikkert, W.J. van Dijk, K. Brejc, A.B. Smit, and T.K. Sixma. 2004. Nicotine and carbamylcholine binding to nicotinic acetylcholine receptors as studied in AChBP crystal structures. *Neuron* 41:907-914.

134. Hansen, S.B., G. Sulzenbacher, T. Huxford, P. Marchot, P. Taylor, and Y. Bourne. 2005. Structures of Aplysia AChBP complexes with nicotinic agonists and antagonists reveal distinctive binding interfaces and conformations. *Embo J* 24:3635-3646.

135. Galzi, J.L., D. Bertrand, A. Devillers-Thiery, F. Revah, S. Bertrand, and J.P. Changeux. 1991. Functional significance of aromatic amino acids from three peptide loops of the α7 neuronal nicotinic receptor site investigated by site-directed mutagenesis. *FEBS Lett* 294:198-202.

136. Damle, V.N., and A. Karlin. 1980. Effects of agonists and antagonists on the reactivity of the binding site disulfide in acetylcholine receptor from Torpedo californica. *Biochemistry* 19:3924-3932.

137. Le Novere, N., T. Grutter, and J.P. Changeux. 2002. Models of the extracellular domain of the nicotinic receptors and of agonist- and Ca^{2+}-binding sites. *Proc Natl Acad Sci U S A* 99:3210-3215.

138. Blanton, M.P., Y. Xie, L.J. Dangott, and J.B. Cohen. 1999. The steroid promegestone is a noncompetitive antagonist of the Torpedo nicotinic acetylcholine receptor that interacts with the lipid-protein interface. *Mol Pharmacol* 55:269-278.

139. Mascia, M.P., J.R. Trudell, and R.A. Harris. 2000. Specific binding sites for alcohols and anesthetics on ligand-gated ion channels. *Proc Natl Acad Sci U S A* 97:9305-9310.

140. Wick, M.J., S.J. Mihic, S. Ueno, M.P. Mascia, J.R. Trudell, S.J. Brozowski, Q. Ye, N.L. Harrison, and R.A. Harris. 1998. Mutations of gamma-aminobutyric acid and glycine receptors change alcohol cutoff: evidence for an alcohol receptor? *Proc Natl Acad Sci U S A* 95:6504-6509.

141. Kelley, S.P., J.I. Dunlop, E.F. Kirkness, J.J. Lambert, and J.A. Peters. 2003. A cytoplasmic region determines single-channel conductance in 5-HT_3 receptors. *Nature* 424:321-324.

142. Celie, P.H., I.E. Kasheverov, D.Y. Mordvintsev, R.C. Hogg, P. van Nierop, R. van Elk, S.E. van Rossum-Fikkert, M.N. Zhmak, D. Bertrand, V. Tsetlin, T.K. Sixma, and A.B. Smit. 2005. Crystal structure of nicotinic acetylcholine receptor homolog AChBP in complex with an α-conotoxin PnIA variant. *Nat Struct Mol Biol* 12:582-588.

143. Gao, F., N. Bren, T.P. Burghardt, S. Hansen, R.H. Henchman, P. Taylor, J.A. McCammon, and S.M. Sine. 2005. Agonist-mediated conformational changes in acetylcholine-binding protein revealed by simulation and intrinsic tryptophan fluorescence. *J Biol Chem* 280:8443-8451.

144. Wang, H.L., M. Milone, K. Ohno, X.M. Shen, A. Tsujino, A.P. Batocchi, P. Tonali, J. Brengman, A.G. Engel, and S.M. Sine. 1999. Acetylcholine receptor M3 domain: stereochemical and volume contributions to channel gating. *Nat Neurosci* 2:226-233.

145. Lynch, J.W., S. Rajendra, K.D. Pierce, C.A. Handford, P.H. Barry, and P.R. Schofield. 1997. Identification of intracellular and extracellular domains mediating signal transduction in the inhibitory glycine receptor chloride channel. *Embo J* 16:110-120.

146. Rovira, J.C., J.J. Ballesta, F. Vicente-Agullo, A. Campos-Caro, M. Criado, F. Sala, and S. Sala. 1998. A residue in the middle of the M2-M3 loop of the β4 subunit specifically affects gating of neuronal nicotinic receptors. *FEBS Lett* 433:89-92.

147. Grosman, C., F.N. Salamone, S.M. Sine, and A. Auerbach. 2000. The extracellular linker of muscle acetylcholine receptor channels is a gating control element. *J Gen Physiol* 116:327-340.

148. Rovira, J.C., F. Vicente-Agullo, A. Campos-Caro, M. Criado, F. Sala, S. Sala, and J.J. Ballesta. 1999. Gating of α3β4 neuronal nicotinic receptor can be controlled by the loop M2-M3 of both α3 and β4 subunits. *Pflugers Arch* 439:86-92.

149. Campos-Caro, A., S. Sala, J.J. Ballesta, F. Vicente-Agullo, M. Criado, and F. Sala. 1996. A single residue in the M2-M3 loop is a major determinant of coupling between binding and gating in neuronal nicotinic receptors. *Proc Natl Acad Sci U S A* 93:6118-6123.

150. Kash, T.L., M.J. Dizon, J.R. Trudell, and N.L. Harrison. 2004. Charged residues in the β2 subunit involved in $GABA_A$ receptor activation. *J Biol Chem* 279:4887-4893.

151. Eldefrawi, M.E., A.T. Eldefrawi, S. Seifert, and R.D. O'Brien. 1972. Properties of lubrol-solubilized acetylcholine receptor from Torpedo electroplax. *Arch Biochem Biophys* 150:210-218.

152. Lindstrom, J., R. Anholt, B. Einarson, A. Engel, M. Osame, and M. Montal. 1980. Purification of acetylcholine receptors, reconstitution into lipid vesicles, and study of agonist-induced cation channel regulation. *J Biol Chem* 255:8340-8350.

153. Criado, M., H. Eibl, and F.J. Barrantes. 1984. Functional properties of the acetylcholine receptor incorporated in model lipid membranes. Differential effects of chain length and head group of phospholipids on receptor affinity states and receptor-mediated ion translocation. *J Biol Chem* 259:9188-9198.

154. Andreasen, T.J., and M.G. McNamee. 1980. Inhibition of ion permeability control properties of acetylcholine receptor from Torpedo californica by long-chain fatty acids. *Biochemistry* 19:4719-4726.

155. Fong, T.M., and M.G. McNamee. 1986. Correlation between acetylcholine receptor function and structural properties of membranes. *Biochemistry* 25:830-840.

156. Huganir, R.L., M.A. Schell, and E. Racker. 1979. Reconstitution of the purified acetylcholine receptor from Torpedo californica. *FEBS Lett* 108:155-160.

157. Karlin, A., and D. Cowburn. 1973. The affinity-labeling of partially purified acetylcholine receptor from electric tissue of Electrophorus. *Proc Natl Acad Sci U S A* 70:3636-3640.

158. Briley, M.S., and J.P. Changeux. 1978. Recovery of some functional properties of the detergent-extracted cholinergic receptor protein from Torpedo marmorata after reintegration into a membrane environment. *Eur J Biochem* 84:429-439.

159. Hazelbauer, G.L., and J.P. Changeux. 1974. Reconstitution of a chemically excitable membrane. *Proc Natl Acad Sci U S A* 71:1479-1483.

160. Michaelson, D.M., and M.A. Raftery. 1974. Purified acetylcholine receptor: its reconstitution to a chemically excitable membrane. *Proc Natl Acad Sci U S A* 71:4768-4772.

161. Briley, M.S., and J.P. Changeux. 1977. Isolation and purification of the nicotinic acetylcholine receptor and its functional reconstitution into a membrane environment. *Int Rev Neurobiol* 20:31-63.

162. Epstein, M., and E. Racker. 1978. Reconstitution of carbamylcholine-dependent sodium ion flux and desensitization of the acetylcholine receptor from Torpedo californica. *J Biol Chem* 253:6660-6662.

163. Anholt, R., D.R. Fredkin, T. Deerinck, M. Ellisman, M. Montal, and J. Lindstrom. 1982. Incorporation of acetylcholine receptors into liposomes. Vesicle structure and acetylcholine receptor function. *J Biol Chem* 257:7122-7134.

164. Anholt, R., J. Lindstrom, and M. Montal. 1981. Stabilization of acetylcholine receptor channels by lipids in cholate solution and during reconstitution in vesicles. *J Biol Chem* 256:4377-4387.

165. Heidmann, T., A. Sobel, J.L. Popot, and J.P. Changeux. 1980. Reconstitution of a functional acetylcholine receptor. Conservation of the conformational and allosteric transitions and recovery of the permeability response; role of lipids. *Eur J Biochem* 110:35-55.

166. Jones, O.T., J.H. Eubanks, J.P. Earnest, and M.G. McNamee. 1988. A minimum number of lipids are required to support the functional properties of the nicotinic acetylcholine receptor. *Biochemistry* 27:3733-3742.

167. Schiebler, W., and F. Hucho. 1978. Membranes rich in acetylcholine receptor: characterization and reconstitution to excitable membranes from exogenous lipids. *Eur J Biochem* 85:55-63.

168. Gonzalez-Ros, J.M., M. Llanillo, A. Paraschos, and M. Martinez-Carrion. 1982. Lipid environment of acetylcholine receptor from Torpedo californica. *Biochemistry* 21:3467-3474.

169. Popot, J.L., R.A. Demel, A. Sobel, L.L. Van Deenen, and J.P. Changeux. 1978. Interaction of the acetylcholine (nicotinic) receptor protein from Torpedo marmorata electric organ with monolayers of pure lipids. *Eur J Biochem* 85:27-42.

170. Ochoa, E.L., A.W. Dalziel, and M.G. McNamee. 1983. Reconstitution of acetylcholine receptor function in lipid vesicles of defined composition. *Biochim Biophys Acta* 727:151-162.

171. Dalziel, A.W., E.S. Rollins, and M.G. McNamee. 1980. The effect of cholesterol on agonist-induced flux in reconstituted acetylcholine receptor vesicles. *FEBS Lett* 122:193-196.

172. Criado, M., H. Eibl, and F.J. Barrantes. 1982. Effects of lipids on acetylcholine receptor. Essential need of cholesterol for maintenance of agonist-induced state transitions in lipid vesicles. *Biochemistry* 21:3622-3629.

173. Sunshine, C., and M.G. McNamee. 1992. Lipid modulation of nicotinic acetylcholine receptor function: the role of neutral and negatively charged lipids. *Biochim Biophys Acta* 1108:240-246.

174. Criado, M., and F.J. Barrantes. 1984. Conversion of acetylcholine receptor dimers to monomers upon depletion of non-receptor peripheral proteins. *Biochim Biophys Acta* 798:374-381.

175. Addona, G.H., H. Sandermann, Jr., M.A. Kloczewiak, S.S. Husain, and K.W. Miller. 1998. Where does cholesterol act during activation of the nicotinic acetylcholine receptor? *Biochim Biophys Acta* 1370:299-309.

176. Baenziger, J.E., M.L. Morris, T.E. Darsaut, and S.E. Ryan. 2000. Effect of membrane lipid composition on the conformational equilibria of the nicotinic acetylcholine receptor. *J Biol Chem* 275:777-784.

177. Ryan, S.E., C.N. Demers, J.P. Chew, and J.E. Baenziger. 1996. Structural effects of neutral and anionic lipids on the nicotinic acetylcholine receptor. An infrared difference spectroscopy study. *J Biol Chem* 271:24590-24597.

178. Sunshine, C., and M.G. McNamee. 1994. Lipid modulation of nicotinic acetylcholine receptor function: the role of membrane lipid composition and fluidity. *Biochim Biophys Acta* 1191:59-64.

179. Marsh, D., and L.I. Horvath. 1998. Structure, dynamics and composition of the lipid-protein interface. Perspectives from spin-labelling. *Biochim Biophys Acta* 1376:267-296.

180. Ellena, J.F., M.A. Blazing, and M.G. McNamee. 1983. Lipid-protein interactions in reconstituted membranes containing acetylcholine receptor. *Biochemistry* 22:5523-5535.

181. Marsh, D., and F.J. Barrantes. 1978. Immobilized lipid in acetylcholine receptor-rich membranes from Torpedo marmorata. *Proc Natl Acad Sci U S A* 75:4329-4333.

182. Marsh, D., A. Watts, and F.J. Barrantes. 1981. Phospholipid chain immobilization and steroid rotational immobilization in acetylcholine receptor-rich membranes from Torpedo marmorata. *Biochim Biophys Acta* 645:97-101.

183. Rousselet, A., P.F. Devaux, and K.W. Wirtz. 1979. Free fatty acids and esters can be immobilized by receptor rich membranes from Torpedo marmorata but not phospholipid acyl chains. *Biochem Biophys Res Commun* 90:871-877.

184. Mantipragada, S.B., L.I. Horvath, H.R. Arias, G. Schwarzmann, K. Sandhoff, F.J. Barrantes, and D. Marsh. 2003. Lipid-protein interactions and effect of local anesthetics in acetylcholine receptor-rich membranes from Torpedo marmorata electric organ. *Biochemistry* 42:9167-9175.

185. Jones, O.T., and M.G. McNamee. 1988. Annular and nonannular binding sites for cholesterol associated with the nicotinic acetylcholine receptor. *Biochemistry* 27:2364-2374.

186. Bhushan, A., and M.G. McNamee. 1993. Correlation of phospholipid structure with functional effects on the nicotinic acetylcholine receptor. A modulatory role for phosphatidic acid. *Biophys J* 64:716-723.

187. Butler, D.H., and M.G. McNamee. 1993. FTIR analysis of nicotinic acetylcholine receptor secondary structure in reconstituted membranes. *Biochim Biophys Acta* 1150:17-24.

188. Fernandez-Ballester, G., J. Castresana, A.M. Fernandez, J.L. Arrondo, J.A. Ferragut, and J.M. Gonzalez-Ros. 1994. A role for cholesterol as a structural effector of the nicotinic acetylcholine receptor. *Biochemistry* 33:4065-4071.

189. Fong, T.M., and M.G. McNamee. 1987. Stabilization of acetylcholine receptor secondary structure by cholesterol and negatively charged phospholipids in membranes. *Biochemistry* 26:3871-3880.

190. Methot, N., C.N. Demers, and J.E. Baenziger. 1995. Structure of both the ligand- and lipid-dependent channel-inactive states of the nicotinic acetylcholine receptor probed by FTIR spectroscopy and hydrogen exchange. *Biochemistry* 34:15142-15149.

191. Middlemas, D.S., and M.A. Raftery. 1987. Identification of subunits of acetylcholine receptor that interact with a cholesterol photoaffinity probe. *Biochemistry* 26:1219-1223.

192. Heidmann, T., A. Sobel, and J.P. Changeux. 1980. Conservation of the kinetic and allosteric properties of the acetylcholine receptor in its Na cholate soluble 9 S form: effect of lipids. *Biochem Biophys Res Commun* 93:127-133.

193. Andreasen, T.J., D.R. Doerge, and M.G. McNamee. 1979. Effects of phospholipase A2 on the binding and ion permeability control properties of the acetylcholine receptor. *Arch Biochem Biophys* 194:468-480.

194. McCarthy, M.P., and M.A. Moore. 1992. Effects of lipids and detergents on the conformation of the nicotinic acetylcholine receptor from Torpedo californica. *J Biol Chem* 267:7655-7663.

195. Rankin, S.E., G.H. Addona, M.A. Kloczewiak, B. Bugge, and K.W. Miller. 1997. The cholesterol dependence of activation and fast desensitization of the nicotinic acetylcholine receptor. *Biophys J* 73:2446-2455.

196. Baenziger, J.E., T.E. Darsaut, and M.L. Morris. 1999. Internal dynamics of the nicotinic acetylcholine receptor in reconstituted membranes. *Biochemistry* 38:4905-4911.

197. Barrantes, F.J. 1989. The lipid environment of the nicotinic acetylcholine receptor in native and reconstituted membranes. *Crit Rev Biochem Mol Biol* 24:437-478.

198. McNamee, M.G., and T.M. Fong. 1988. Effects of Membrane Lipids and Fluidity on Acetylcholine Receptor Function. In Lipid Domains and the Relationship to Membrane Function. R.C. Aloia, C.C. Curtain, and L.M. Gordon, editors. Alan R. Liss, Inc., New York. 43-62.

199. Auger, M., D. Carrier, I.C.P. Smith, and H.C. Jarrell. 1990. Elucidation of motional modes in glycoglycerolipid bilayers. A ^{2}H NMR relaxation and line-shape study. *J Am Chem Soc* 112:1373-1381.

200. Baenziger, J.E., H.C. Jarrell, and I.C. Smith. 1992. Molecular motions and dynamics of a diunsaturated acyl chain in a lipid bilayer: implications for the role of polyunsaturation in biological membranes. *Biochemistry* 31:3377-3385.

201. Seelig, J., and N. Waespe-Sarcevic. 1978. Molecular order in cis and trans unsaturated phospholipid bilayers. *Biochemistry* 17:3310-3315.

202. Mendelsohn, R., and H.H. Mantsch. 1986. Fourier transform infrared studies of lipid-protein interaction. In Progress in Protein-Lipid Interactions 2. W.D. Pont, editor Elsevier Science Publishers BV (Biomedical Division), 103-224.

203. Goormaghtigh, E., V. Cabiaux, and J.M. Ruysschaert. 1990. Secondary structure and dosage of soluble and membrane proteins by attenuated total reflection Fourier-transform infrared spectroscopy on hydrated films. *Eur J Biochem* 193:409-420.

204. Reid, S.E., D.J. Moffat, and J.E. Baenziger. 1996. The selective enhancement and subsequent subtraction of atmospheric water vapour contributions from Fourier transform infrared spectra of proteins. *Spectrochimica Acta, Part A* 52:1347-1356.

205. Baenziger, J.E., K.W. Miller, and K.J. Rothschild. 1992. Incorporation of the nicotinic acetylcholine receptor into planar multilamellar films: characterization by fluorescence and Fourier transform infrared difference spectroscopy. *Biophys J* 61:983-992.

206. Ryan, S.E., and J.E. Baenziger. 1999. A structure-based approach to nicotinic receptor pharmacology. *Mol Pharmacol* 55:348-355.

207. White, B.H., and J.B. Cohen. 1992. Agonist-induced changes in the structure of the acetylcholine receptor M2 regions revealed by photoincorporation of an uncharged nicotinic noncompetitive antagonist. *J Biol Chem* 267:15770-15783.

208. Blanton, M.P., E.A. McCardy, and M.J. Gallagher. 2000. Examining the noncompetitive antagonist-binding site in the ion channel of the nicotinic acetylcholine receptor in the resting state. *J Biol Chem* 275:3469-3478.

209. Chiara, D.C., M.A. Kloczewiak, G.H. Addona, J.A. Yu, J.B. Cohen, and K.W. Miller. 2001. Site of resting state inhibition of the nicotinic acetylcholine receptor by a hydrophobic inhibitor. *Biochemistry* 40:296-304.

210. Hubner, W., and H.H. Mantsch. 1991. Orientation of specifically ^{13}C=O labelled phosphatidylcholine multilayers from polarized attenuated total reflection FT-IR spectroscopy. *Biophys J* 59:1261-1272.

211. Blume, A., W. Hubner, and G. Messner. 1988. Fourier transform infrared spectroscopy of ^{13}C = O-labeled phospholipids hydrogen bonding to carbonyl groups. *Biochemistry* 27:8239-8249.

212. Gil, T., J.H. Ipsen, O.G. Mouritsen, M.C. Sabra, M.M. Sperotto, and M.J. Zuckermann. 1998. Theoretical analysis of protein organization in lipid membranes. *Biochim Biophys Acta* 1376:245-266.

213. daCosta, C.J., A.A. Ogrel, E.A. McCardy, M.P. Blanton, and J.E. Baenziger. 2002. Lipid-protein interactions at the nicotinic acetylcholine receptor. A functional coupling between nicotinic receptors and phosphatidic acid-containing lipid bilayers. *J Biol Chem* 277:201-208.

214. Poveda, J.A., J.A. Encinar, A.M. Fernandez, C.R. Mateo, J.A. Ferragut, and J.M. Gonzalez-Ros. 2002. Segregation of phosphatidic acid-rich domains in reconstituted acetylcholine receptor membranes. *Biochemistry* 41:12253-12262.

215. Jackson, M., and H.H. Mantsch. 1995. The use and misuse of FTIR spectroscopy in the determination of protein structure. *Crit Rev Biochem Mol Biol* 30:95-120.

216. Casal, H.L., A. Martin, H.H. Mantsch, F. Paltauf, and H. Hauser. 1987. Infrared studies of fully hydrated unsaturated phosphatidylserine bilayers. Effect of Li^+ and Ca^{2+}. *Biochemistry* 26:7395-7401.

217. Hubner, W., H.H. Mantsch, F. Paltauf, and H. Hauser. 1994. Conformation of phosphatidylserine in bilayers as studied by Fourier transform infrared spectroscopy. *Biochemistry* 33:320-326.

218. Oshikawa, J., Y. Toya, T. Fujita, M. Egawa, J. Kawabe, S. Umemura, and Y. Ishikawa. 2003. Nicotinic acetylcholine receptor α7 regulates cAMP signal within lipid rafts. *Am J Physiol Cell Physiol* 285:C567-574.

219. Bruses, J.L., N. Chauvet, and U. Rutishauser. 2001. Membrane lipid rafts are necessary for the maintenance of the α7 nicotinic acetylcholine receptor in somatic spines of ciliary neurons. *J Neurosci* 21:504-512.

220. Marchand, S., A. Devillers-Thiery, S. Pons, J.P. Changeux, and J. Cartaud. 2002. Rapsyn escorts the nicotinic acetylcholine receptor along the exocytic pathway via association with lipid rafts. *J Neurosci* 22:8891-8901.

221. Bass, R.B., K.P. Locher, E. Borths, Y. Poon, P. Strop, A. Lee, and D.C. Rees. 2003. The structures of BtuCD and MscS and their implications for transporter and channel function. *FEBS Lett* 555:111-115.

222. Iverson, T.M., C. Luna-Chavez, G. Cecchini, and D.C. Rees. 1999. Structure of the Escherichia coli fumarate reductase respiratory complex. *Science* 284:1961-1966.

223. Iwata, S., J.W. Lee, K. Okada, J.K. Lee, M. Iwata, B. Rasmussen, T.A. Link, S. Ramaswamy, and B.K. Jap. 1998. Complete structure of the 11-subunit bovine mitochondrial cytochrome bc1 complex. *Science* 281:64-71.

224. Dutzler, R., E.B. Campbell, M. Cadene, B.T. Chait, and R. MacKinnon. 2002. X-ray structure of a ClC chloride channel at 3.0Å reveals the molecular basis of anion selectivity. *Nature* 415:287-294.

225. Rowlinson, S.W., J.R. Kiefer, J.J. Prusakiewicz, J.L. Pawlitz, K.R. Kozak, A.S. Kalgutkar, W.C. Stallings, R.G. Kurumbail, and L.J. Marnett. 2003. A novel mechanism of cyclooxygenase-2 inhibition involving interactions with Ser-530 and Tyr-385. *J Biol Chem* 278:45763-45769.

226. Malkowski, M.G., S.L. Ginell, W.L. Smith, and R.M. Garavito. 2000. The productive conformation of arachidonic acid bound to prostaglandin synthase. *Science* 289:1933-1937.

227. Kurumbail, R.G., A.M. Stevens, J.K. Gierse, J.J. McDonald, R.A. Stegeman, J.Y. Pak, D. Gildehaus, J.M. Miyashiro, T.D. Penning, K. Seibert, P.C. Isakson, and W.C. Stallings. 1996. Structural basis for selective inhibition of cyclooxygenase-2 by anti-inflammatory agents. *Nature* 384:644-648.

228. Teller, D.C., T. Okada, C.A. Behnke, K. Palczewski, and R.E. Stenkamp. 2001. Advances in determination of a high-resolution three-dimensional structure of rhodopsin, a model of G-protein-coupled receptors (GPCRs). *Biochemistry* 40:7761-7772.

229. Palczewski, K., T. Kumasaka, T. Hori, C.A. Behnke, H. Motoshima, B.A. Fox, I. Le Trong, D.C. Teller, T. Okada, R.E. Stenkamp, M. Yamamoto, and M. Miyano. 2000. Crystal structure of rhodopsin: A G protein-coupled receptor. *Science* 289:739-745.

230. Li, J., P.C. Edwards, M. Burghammer, C. Villa, and G.F. Schertler. 2004. Structure of bovine rhodopsin in a trigonal crystal form. *J Mol Biol* 343:1409-1438.

231. Loll, P.J. 2003. Membrane protein structural biology: the high throughput challenge. *J Struct Biol* 142:144-153.

232. Grueninger-Leitch, F., A. D'Arcy, B. D'Arcy, and C. Chene. 1996. Deglycosylation of proteins for crystallization using recombinant fusion protein glycosidases. *Protein Sci* 5:2617-2622.

233. Dale, G.E., B. D'Arcy, C. Yuvaniyama, B. Wipf, C. Oefner, and A. D'Arcy. 2000. Purification and crystallization of the extracellular domain of human neutral endopeptidase (neprilysin) expressed in Pichia pastoris. *Acta Crystallogr D Biol Crystallogr* 56 (Pt 7):894-897.

234. Petrescu, A.J., A.L. Milac, S.M. Petrescu, R.A. Dwek, and M.R. Wormald. 2004. Statistical analysis of the protein environment of N-glycosylation sites: implications for occupancy, structure, and folding. *Glycobiology* 14:103-114.

235. Ramanathan, V.K., and Z.W. Hall. 1999. Altered glycosylation sites of the δ-subunit of the acetylcholine receptor (AChR) reduce α-δ association and receptor assembly. *J Biol Chem* 274:20513-20520.

236. Merlie, J.P., R. Sebbane, S. Tzartos, and J. Lindstrom. 1982. Inhibition of glycosylation with tunicamycin blocks assembly of newly synthesized acetylcholine receptor subunits in muscle cells. *J Biol Chem* 257:2694-2701.

237. Rickert, K.W., and B. Imperiali. 1995. Analysis of the conserved glycosylation site in the nicotinic acetylcholine receptor: potential roles in complex assembly. *Chem Biol* 2:751-759.

238. Live, D.H., R.A. Kumar, X. Beebe, and S.J. Danishefsky. 1996. Conformational influences of glycosylation of a peptide: a possible model for the effect of glycosylation on the rate of protein folding. *Proc Natl Acad Sci U S A* 93:12759-12761.

239. Garavito, R.M., and J.P. Rosenbusch. 1980. Three-dimensional crystals of an integral membrane protein: an initial x-ray analysis. *J Cell Biol* 86:327-329.

240. Rosenbusch, J.P. 2001. Stability of membrane proteins: relevance for the selection of appropriate methods for high-resolution structure determinations. *J Struct Biol* 136:144-157.

241. Rosenbusch, J.P., A. Lustig, M. Grabo, M. Zulauf, and M. Regenass. 2001. Approaches to determining membrane protein structures to high resolution: do selections of subpopulations occur? *Micron* 32:75-90.

242. Dani, J.A. 2001. Overview of nicotinic receptors and their roles in the central nervous system. *Biol Psychiatry* 49:166-174.

243. Quick, M.W., and R.A. Lester. 2002. Desensitization of neuronal nicotinic receptors. *J Neurobiol* 53:457-478.

244. Hogg, R.C., M. Raggenbass, and D. Bertrand. 2003. Nicotinic acetylcholine receptors: from structure to brain function. *Rev Physiol Biochem Pharmacol* 147:1-46.

245. Nomoto, H., N. Takahashi, Y. Nagaki, S. Endo, Y. Arata, and K. Hayashi. 1986. Carbohydrate structures of acetylcholine receptor from Torpedo californica and distribution of oligosaccharides among the subunits. *Eur J Biochem* 157:233-242.

246. Anholt, R., J. Lindstrom, and M. Montal. 1980. Functional equivalence of monomeric and dimeric forms of purified acetylcholine receptors from Torpedo californica in reconstituted lipid vesicles. *Eur J Biochem* 109:481-487.

247. Ryan, S.E., M.P. Blanton, and J.E. Baenziger. 2001. A conformational intermediate between the resting and desensitized states of the nicotinic acetylcholine receptor. *J Biol Chem* 276:4796-4803.

248. Ryan, S.E., D.G. Hill, and J.E. Baenziger. 2002. Dissecting the chemistry of nicotinic receptor-ligand interactions with infrared difference spectroscopy. *J Biol Chem* 277:10420-10426.

249. Baenziger, J.E., K.W. Miller, M.P. McCarthy, and K.J. Rothschild. 1992. Probing conformational changes in the nicotinic acetylcholine receptor by Fourier transform infrared difference spectroscopy. *Biophys J* 62:64-66.

250. Fukuda, M.N., D.S. Papermaster, and P.A. Hargrave. 1979. Rhodopsin carbohydrate. Structure of small oligosaccharides attached at two sites near the NH_2 terminus. *J Biol Chem* 254:8201-8207.

251. Kurisu, G., H. Zhang, J.L. Smith, and W.A. Cramer. 2003. Structure of the cytochrome b6f complex of oxygenic photosynthesis: tuning the cavity. *Science* 302:1009-1014.

252. Zhang, H., G. Kurisu, J.L. Smith, and W.A. Cramer. 2003. A defined protein-detergent-lipid complex for crystallization of integral membrane proteins: The cytochrome b6f complex of oxygenic photosynthesis. *Proc Natl Acad Sci U S A* 100:5160-5163.

253. Valiyaveetil, F.I., Y. Zhou, and R. MacKinnon. 2002. Lipids in the structure, folding, and function of the KcsA K^+ channel. *Biochemistry* 41:10771-10777.

254. Belrhali, H., P. Nollert, A. Royant, C. Menzel, J.P. Rosenbusch, E.M. Landau, and E. Pebay-Peyroula. 1999. Protein, lipid and water organization in bacteriorhodopsin crystals: a molecular view of the purple membrane at 1.9Å resolution. *Structure Fold Des* 7:909-917.

255. McAuley, K.E., P.K. Fyfe, J.P. Ridge, N.W. Isaacs, R.J. Cogdell, and M.R. Jones. 1999. Structural details of an interaction between cardiolipin and an integral membrane protein. *Proc Natl Acad Sci U S A* 96:14706-14711.

256. Lee, A.G. 2003. Lipid-protein interactions in biological membranes: a structural perspective. *Biochim Biophys Acta* 1612:1-40.

257. Soderlund, T., J.M. Alakoskela, A.L. Pakkanen, and P.K. Kinnunen. 2003. Comparison of the effects of surface tension and osmotic pressure on the interfacial hydration of a fluid phospholipid bilayer. *Biophys J* 85:2333-2341.

258. Popot, J.L., and D.M. Engelman. 2000. Helical membrane protein folding, stability, and evolution. *Annu Rev Biochem* 69:881-922.

259. daCosta, C.J., I.D. Wagg, M.E. McKay, and J.E. Baenziger. 2004. phosphatidic acid and phosphatidylserine have distinct structural and functional interactions with the nicotinic acetylcholine receptor. *J Biol Chem* 279:14967-14974.

260. Cheng, X., B. Lu, B. Grant, R.J. Law, and J.A. McCammon. 2006. Channel opening motion of α7 nicotinic acetylcholine receptor as suggested by normal mode analysis. *J Mol Biol* 355:310-324.

261. Leite, J.F., M.P. Blanton, M. Shahgholi, D.A. Dougherty, and H.A. Lester. 2003. Conformation-dependent hydrophobic photolabeling of the nicotinic receptor: electrophysiology-coordinated photochemistry and mass spectrometry. *Proc Natl Acad Sci U S A* 100:13054-13059.

262. von Heijne, G. 1984. Analysis of the distribution of charged residues in the N-terminal region of signal sequences: implications for protein export in prokaryotic and eukaryotic cells. *Embo J* 3:2315-2318.

263. von Heijne, G. 1989. Control of topology and mode of assembly of a polytopic membrane protein by positively charged residues. *Nature* 341:456-458.

264. von Heijne, G., and Y. Gavel. 1988. Topogenic signals in integral membrane proteins. *Eur J Biochem* 174:671-678.

265. Le Novere, N., and J.P. Changeux. 1999. The Ligand Gated Ion Channel Database. *Nucleic Acids Res* 27:340-342.

266. Deol, S.S., C. Domene, P.J. Bond, and M.S. Sansom. 2006. Anionic phospholipid interactions with the potassium channel KcsA: simulation studies. *Biophys J* 90:822-830.

267. Alvis, S.J., I.M. Williamson, J.M. East, and A.G. Lee. 2003. Interactions of anionic phospholipids and phosphatidylethanolamine with the potassium channel KcsA. *Biophys J* 85:3828-3838.

268. Marius, P., S.J. Alvis, J.M. East, and A.G. Lee. 2005. The interfacial lipid binding site on the potassium channel KcsA is specific for anionic phospholipids. *Biophys J* 89:4081-4089.

269. Williamson, I.M., S.J. Alvis, J.M. East, and A.G. Lee. 2003. The potassium channel KcsA and its interaction with the lipid bilayer. *Cell Mol Life Sci* 60:1581-1590.

270. Barrantes, F.J. 2004. Structural basis for lipid modulation of nicotinic acetylcholine receptor function. *Brain Res Brain Res Rev* 47:71-95.

271. Blanton, M.P., and E.A. McCardy. 2000. Identifying the lipid-protein interface and transmembrane structural transitions of the Torpedo Na,K-ATPase using hydrophobic photoreactive probes. *Biochemistry* 39:13534-13544.

272. White, B.H., and J.B. Cohen. 1988. Photolabeling of membrane-bound Torpedo nicotinic acetylcholine receptor with the hydrophobic probe 3-trifluoromethyl-3-(m-[^{125}I]iodophenyl)diazirine. *Biochemistry* 27:8741-8751.

273. Tobimatsu, T., Y. Fujita, K. Fukuda, K. Tanaka, Y. Mori, T. Konno, M. Mishina, and S. Numa. 1987. Effects of substitution of putative transmembrane segments on nicotinic acetylcholine receptor function. *FEBS Lett* 222:56-62.

274. Li, L., Y.H. Lee, P. Pappone, A. Palma, and M.G. McNamee. 1992. Site-specific mutations of nicotinic acetylcholine receptor at the lipid-protein interface dramatically alter ion channel gating. *Biophys J* 62:61-63.

275. Li, L., M. Schuchard, A. Palma, L. Pradier, and M.G. McNamee. 1990. Functional role of the cysteine 451 thiol group in the M4 helix of the γ-subunit of Torpedo californica acetylcholine receptor. *Biochemistry* 29:5428-5436.

276. Lee, Y.H., L. Li, J. Lasalde, L. Rojas, M. McNamee, S.I. Ortiz-Miranda, and P. Pappone. 1994. Mutations in the M4 domain of Torpedo californica acetylcholine receptor dramatically alter ion channel function. *Biophys J* 66:646-653.

277. Bouzat, C., N. Bren, and S.M. Sine. 1994. Structural basis of the different gating kinetics of fetal and adult acetylcholine receptors. *Neuron* 13:1395-1402.

278. Lasalde, J.A., S. Tamamizu, D.H. Butler, C.R. Vibat, B. Hung, and M.G. McNamee. 1996. Tryptophan substitutions at the lipid-exposed transmembrane segment M4 of Torpedo californica acetylcholine receptor govern channel gating. *Biochemistry* 35:14139-14148.

279. Ortiz-Miranda, S.I., J.A. Lasalde, P.A. Pappone, and M.G. McNamee. 1997. Mutations in the M4 domain of the Torpedo californica nicotinic acetylcholine receptor alter channel opening and closing. *J Membr Biol* 158:17-30.

280. Bouzat, C., A.M. Roccamo, I. Garbus, and F.J. Barrantes. 1998. Mutations at lipid-exposed residues of the acetylcholine receptor affect its gating kinetics. *Mol Pharmacol* 54:146-153.

281. Tamamizu, S., G.R. Guzman, J. Santiago, L.V. Rojas, M.G. McNamee, and J.A. Lasalde-Dominicci. 2000. Functional effects of periodic tryptophan substitutions in the αM4 transmembrane domain of the Torpedo californica nicotinic acetylcholine receptor. *Biochemistry* 39:4666-4673.

282. Tamamizu, S., Y. Lee, B. Hung, M.G. McNamee, and J.A. Lasalde-Dominicci. 1999. Alteration in ion channel function of mouse nicotinic acetylcholine receptor by mutations in the M4 transmembrane domain. *J Membr Biol* 170:157-164.

283. Bouzat, C., F. Barrantes, and S. Sine. 2000. Nicotinic receptor fourth transmembrane domain: hydrogen bonding by conserved threonine contributes to channel gating kinetics. *J Gen Physiol* 115:663-672.

284. Santiago, J., G.R. Guzman, L.V. Rojas, R. Marti, G.A. Asmar-Rovira, L.F. Santana, M. McNamee, and J.A. Lasalde-Dominicci. 2001. Probing the effects of membrane cholesterol in the Torpedo californica acetylcholine receptor and the novel lipid-exposed mutation αC418W in Xenopus oocytes. *J Biol Chem* 276:46523-46532.

285. Garbus, I., A.M. Roccamo, and F.J. Barrantes. 2002. Identification of threonine 422 in transmembrane domain alpha M4 of the nicotinic acetylcholine receptor as a possible site of interaction with hydrocortisone. *Neuropharmacology* 43:65-73.

286. Ortiz-Acevedo, A., M. Melendez, A.M. Asseo, N. Biaggi, L.V. Rojas, and J.A. Lasalde-Dominicci. 2004. Tryptophan scanning mutagenesis of the γM4 transmembrane domain of the acetylcholine receptor from Torpedo californica. *J Biol Chem* 279:42250-42257.

287. Paradiso, K., J. Zhang, and J.H. Steinbach. 2001. The C-terminus of the human nicotinic α4β2 receptor forms a binding site required for potentiation by an estrogenic steroid. *J Neurosci* 21:6561-6568.

288. Pons, S., J. Sallette, J.P. Bourgeois, A. Taly, J.P. Changeux, and A. Devillers-Thiery. 2004. Critical role of the C-terminal segment in the maturation and export to the cell surface of the homopentameric α7-5HT$_{3A}$ receptor. *Eur J Neurosci* 20:2022-2030.

289. Shen, X.M., K. Ohno, A. Tsujino, J.M. Brengman, M. Gingold, S.M. Sine, and A.G. Engel. 2003. Mutation causing severe myasthenia reveals functional asymmetry of AChR signature cystine loops in agonist binding and gating. *J Clin Invest* 111:497-505.

290. Karlin, A., V. Damle, R. Valderrama, S. Hamilton, D. Wise, and M. McLaughlin. 1978. Interactions among binding sites on acetylcholine receptors in membrane and in detergent solution. *Fed Proc* 37:121-122.

291. Paradiso, K., K. Sabey, A.S. Evers, C.F. Zorumski, D.F. Covey, and J.H. Steinbach. 2000. Steroid inhibition of rat neuronal nicotinic α4β2 receptors expressed in HEK 293 cells. *Mol Pharmacol* 58:341-351.

292. Wang, J.M., L. Zhang, Y. Yao, N. Viroonchatapan, E. Rothe, and Z.Z. Wang. 2002. A transmembrane motif governs the surface trafficking of nicotinic acetylcholine receptors. *Nat Neurosci* 5:963-970.

293. Stevens, T.J., and I.T. Arkin. 2001. Substitution rates in α-helical transmembrane proteins. *Protein Sci* 10:2507-2517.

294. Xu, Y., F.J. Barrantes, X. Luo, K. Chen, J. Shen, and H. Jiang. 2005. Conformational dynamics of the nicotinic acetylcholine receptor channel: a 35-ns molecular dynamics simulation study. *J Am Chem Soc* 127:1291-1299.

295. de Almeida, R.F., L.M. Loura, M. Prieto, A. Watts, A. Fedorov, and F.J. Barrantes. 2004. Cholesterol modulates the organization of the γM4 transmembrane domain of the muscle nicotinic acetylcholine receptor. *Biophys J* 86:2261-2272.

296. Long, S.B., E.B. Campbell, and R. Mackinnon. 2005. Crystal structure of a mammalian voltage-dependent Shaker family K^+ channel. *Science* 309:897-903.

297. Long, S.B., E.B. Campbell, and R. Mackinnon. 2005. Voltage sensor of K_v1.2: structural basis of electromechanical coupling. *Science* 309:903-908.

298. Sparr, E., W.L. Ash, P.V. Nazarov, D.T. Rijkers, M.A. Hemminga, D.P. Tieleman, and J.A. Killian. 2005. Self-association of transmembrane alpha-helices in model membranes: importance of helix orientation and role of hydrophobic mismatch. *J Biol Chem* 280:39324-39331.

299. Jensen, M.O., and O.G. Mouritsen. 2004. Lipids do influence protein function-the hydrophobic matching hypothesis revisited. *Biochim Biophys Acta* 1666:205-226.

300. Syed, A.K. and J.E. Baenziger. Unpublished observation.

301. Lee, A.G. 2004. How lipids affect the activities of integral membrane proteins. *Biochim Biophys Acta* 1666:62-87.

302. Williamson, P.T., G. Zandomeneghi, F.J. Barrantes, A. Watts, and B.H. Meier. 2005. Structural and dynamic studies of the γM4 trans-membrane domain of the nicotinic acetylcholine receptor. *Mol Membr Biol* 22:485-496.

303. Antollini, S.S., Y. Xu, H. Jiang, and F.J. Barrantes. 2005. Fluorescence and molecular dynamics studies of the acetylcholine receptor γM4 transmembrane peptide in reconstituted systems. *Mol Membr Biol* 22:471-483.

304. Attard, G.S., R.H. Templer, W.S. Smith, A.N. Hunt, and S. Jackowski. 2000. Modulation of CTP:phosphocholine cytidylyltransferase by membrane curvature elastic stress. *Proc Natl Acad Sci U S A* 97:9032-9036.

305. Brown, M.F. 1997. Influence of nonlamellar-forming lipids on rhodopsin. *Curr. Top. Membr.* 44:285-356.

306. Demel, R., G. Schiavo, B. de Kruijff, and C. Montecucco. 1991. Lipid interaction of diphtheria toxin and mutants. A study with phospholipid and protein monolayers. *Eur J Biochem* 197:481-486.

307. Ryan, S.E. 2000. An Investigation into the mechanisms by which both membrane lipid composition and local anesthetics modulate the structure and function of the nicotinic acetylcholine receptor. *Ph.D Thesis.* Department of Biochemistry, Microbiology and Immunology, University of Ottawa. 210 pages.

Appendix

Statistical Significance of Difference Spectroscopy Measurements

All presented Carb difference spectra are the average of between 30 and 75 individual difference measurements. Each individual difference measurement is obtained by subtracting a 512 scan spectrum of the nAChR in the absence of agonist, from a 512 scan spectrum of the nAChR in the presence of the agonist carbamylcholine. Individual difference measurements are then averaged in order to (1) improve spectral signal-to-noise ratio, as well as to (2) minimize artifacts from broad baseline distortions (see Figure A.1).

Each averaged difference spectrum (and individual difference measurement) has an internal measure of "significance of difference" called its signal-to-noise ratio. This signal-to-noise ratio can be assessed by examining the "flatness" of a region of the spectrum lacking difference bands (i.e. 1760-1900 cm^{-1} of Figure A.1). Fluctuations in this baseline region give a direct measure of the significance of difference in each averaged difference spectrum. Differences between spectra approaching the signal-to-noise ratio of each spectrum cannot be considered significant.

In addition to directly assessing signal-to-noise ratio, it is also necessary to collect two successive 512 scan spectra of the nAChR in the absence of agonist. As a negative control for agonist induced spectral differences, these two spectra are subtracted (Figure A.1). Because there are no differences in the chemical composition of these two samples (i.e. both are from samples without agonist), there should be no differences between the two spectra (i.e. difference spectrum should yield a flat line). These "control" difference measurements give an indication of the stability of spectral baselines, and are a direct measure of broad baseline shifts and artifacts.

In order to illustrate the relative significance of both baseline shifts and signal-to-noise ratio in dictating uncertainty in averaged difference spectra, it is possible to calculate the standard deviation in spectral intensity amongst a set of individual difference measurements. Figure A.1E shows that most of the variability in measurements can be attributed to large/broad baseline fluctuations (compare standard deviation before (black) and after (red) offset correction of individual difference measurements). If these broad baseline fluctuations affect every point in the spectrum equally (or approximately equally) they can be considered unimportant, since all intensity measurements in difference spectra are relative to baseline. **As a result, as long as control spectra are "flat lines", confidence in difference spectroscopy is ultimately related to the signal-to-noise ratio of each averaged difference spectrum.**

Figure A.1

Measuring the "significance-of-difference" in FTIR difference spectra. **(A)** Overlay of 60 individual difference measurements. **(B)** Overlay of same measurements in **(A)** but after each difference measurement has been offset corrected at 1900 $^{cm-1}$ (red dot). **(C)** Two individual difference measurements, compared to the average **(D)** of all 60 difference measurements showing the improvement in signal-to-noise ratio upon averaging. **(E)** Averaged control measurement (referred to in the text). **(F)** Standard deviation of individual difference measurements relative to baseline (dashed line) before (black line) and after (red line) offset correction, illustrating that most of the standard deviation can be attributed to broad baseline fluctuations.

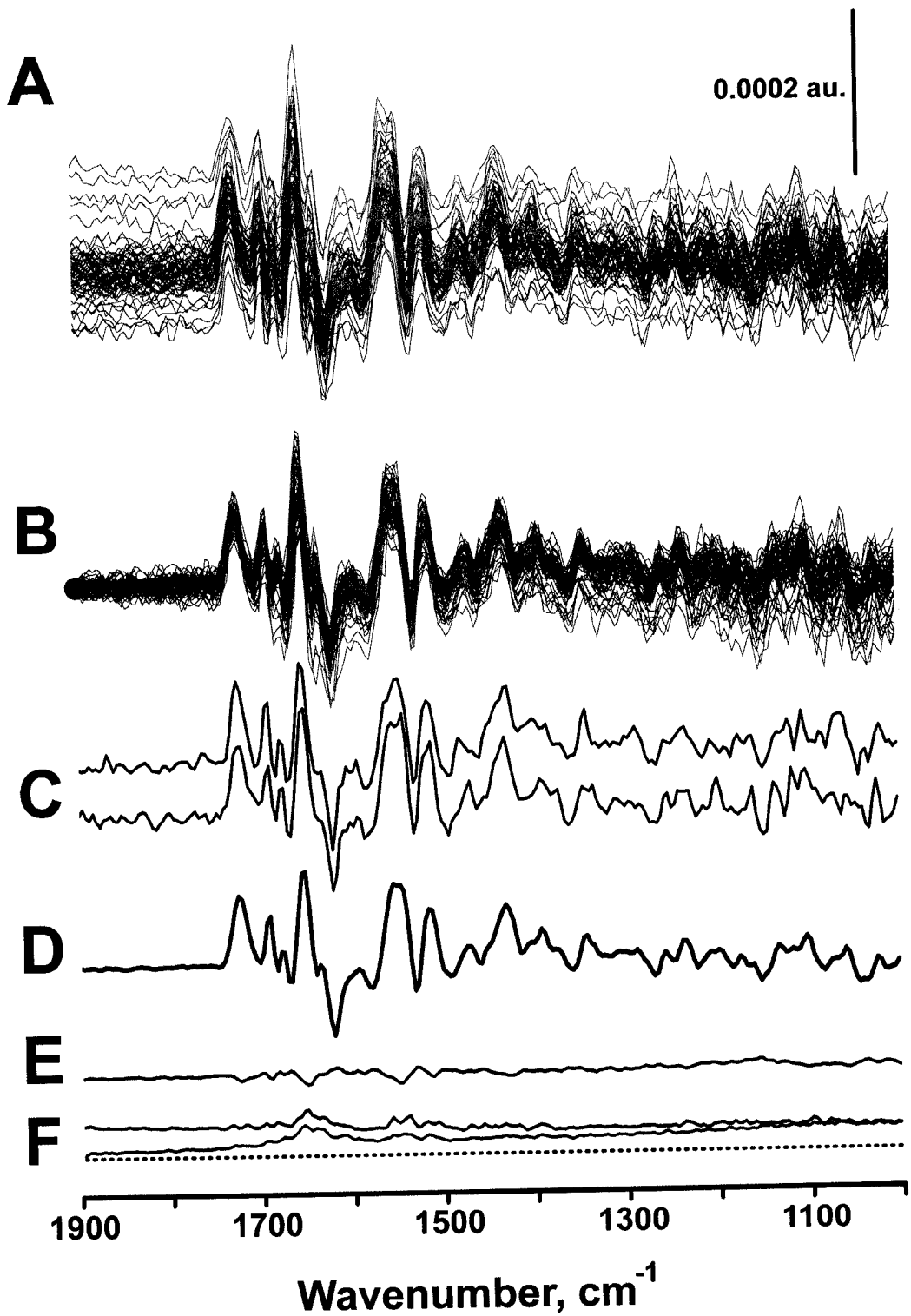
A
0.0002 au.
B
C
D
E
F
1900
1700
1500
1300
1100
Wavenumber, cm-1

CURRICULUM VITAE

NAME:
DACOSTA, Corrie John Bayley, PhD. Candidate
Member of the School of Graduate Studies and Research
University of Ottawa

DEGREES:
B.Sc. (honours), Biochemistry, University of Ottawa, Canada, 2000.

SCHOLARSHIPS:

Canadian Institutes of Health Research, JSPS Summer Research Allowance.
June14th – August 24th, 2005.
($3000)

Japanese Society for the Promotion of Science Summer Scholarship.
June14th – August 24th, 2005.
(592000¥en plus return airfare to Japan)

Canadian Institutes of Health Research, Canadian Graduate Scholarship -
May 2004 – December 2005.
($30000 p.a. with 5000 p.a. research allowance)

University of Ottawa, Excellence Scholarship, *May 2004 – December 2005.*
(Tuition waved for 18 months)

National Sciences and Engineering Research Council of Canada, Post Graduate Scholarship - B, *May 2002-April 2004.*
($38200 over 2 years)

University of Ottawa, Excellence Scholarship, *May 2002.*
($2000)

University of Ottawa, Graduates Admission Scholarship, *May 2002-April 2004.*
(Tuition waved for two years)

Ontario Graduate Scholarship, Government of Ontario, *May 2001-April 2002.* **($15000)**

University of Ottawa, Graduates Admission Scholarship, *Sept 2001-Aug 2002.* **(Tuition waved for one year)**

Strategic Areas of Development Award, University of Ottawa, *Sept 2000-April 2001.* **($6000)**

Department of Biochemistry, Microbiology and Immunology, University of Ottawa, Entrance Program Scholarship, *Sept 2000-Aug 2001.* **($4000)**

University of Ottawa, Graduates Admission Scholarship, *Sept 2000-Aug 2002.* **(Tuition waved for one year)**

University of Ottawa, **Undergraduate Entrance Scholarship**, *Sept 1996-April 1997.* **($1,800, renewable)**

ACHIEVEMENTS:

1. Winner of the **2005 University of Ottawa, Faculty of Medicine – Awards of Excellence** for outstanding achievement in the Biochemistry PhD program.

2. **Japanese Society for the Promotion of Science 2005 Summer Student.** Worked in the Lab of Dr. Yoshinori Fujiyoshi, Department of Biophysics, University of Kyoto. June 14th – August 24th, 2005.

3. Poster presentation at the **49th Annual Biophysical Society Meeting** (refereed) in Long Beach, Calif. U.S.A. Feb, 2005.

4. Selected participant for the **Centre for Membrane Proteomics 2004 Summer School Course** in Frankfurt Germany. September 28th – October 3rd, 2004.

5. Poster presentation at the **48th Annual Biophysical Society Meeting** (refereed) in Baltimore, Maryland. U.S.A. Feb, 2004.

6. 2nd place (Biochemistry Doctoral Student) in Graduate Poster Session, 2003.

7. Poster presentation at the **46th Annual Biophysical Society Meeting** (refereed) in San Francisco, Calif. U.S.A. Feb, 2002.

8. Poster presentation at the **45th Annual Biophysical Society Meeting** (refereed) in Boston Mass. U.S.A. Feb, 2001.

9. Graduated, **Magna Cum Laude**, Honours Biochemistry, University of Ottawa, 2000.

10. University of Ottawa, **Dean's Honour List**, 2000.

11. 2nd place (Biophysics Section) in 4th Year Honours Thesis Poster Presentation, 2000.

12. University of Ottawa, **Dean's Honour List**, 1998.

13. University of Ottawa, **Dean's Honour List**, 1997.

PUBLICATIONS:

Articles published in refereed journals

1. Corrie J.B. daCosta, Daniel E. E. Kaiser, and John E. Baenziger. **Role of glycosylation and membrane environment in nicotinic acetylcholine receptor stability.** (2005). *Biophys J.* **88(3)**, 1755-1764.

2. Corrie J.B. daCosta, Ian D. Wagg, Marlene E. McKay, and John E. Baenziger. **Phosphatidic acid and phosphatidylserine have distinct structural and functional interactions with the nicotinic acetylcholine receptor.** (2004). *J. Biol. Chem.* **279**, 14967-14974.

3. Corrie J.B. daCosta, and John E. Baenziger. **A rapid method for assessing lipid:protein and detergent:protein ratios in membrane-protein crystallization.** (2003). *Acta Cryst.* **D59**, 77-83.

4. Corrie J.B. daCosta, Andrei A. Ogrel, Elizabeth A. McCardy, Michael P. Blanton and John E. Baenziger. **Lipid-protein interactions at the nicotinic acetylcholine receptor: a functional coupling between nicotinic receptors and phosphatidic acid containing lipid bilayers.** (2002). *J. Biol. Chem.* **277**, 201-208.

Refereed abstracts

1. Corrie J.B. daCosta, Suzi Wang, Ian D. Wagg, Giovanni Bonacci, Bridget Thompson and John E. Baenziger. **Expression, purification, reconstitution and preliminary FTIR analysis of the bacterial osmoregulatory protein, ProP.** *Biophysical Journal, Supplement* (2005).

2. Corrie J.B. daCosta, Daniel E. Kaiser and John E. Baenziger. **The effect of deglycosylation and monomerization on reconstituted nicotinic acetylcholine receptor structure and function.** *Biophysical Journal, Supplement* (2004) v86(1) Part 2., Pos-1321.

3. Corrie J.B. daCosta and J.E. Baenziger. **Infrared Spectroscopy as a tool in the three-dimensional crystallization of membrane proteins.** *Biophysical Journal, Supplement* (2002) v82(1) Part 2., Pos-2597.

4. Corrie J.B. daCosta, Andrei A. Ogrel and John E. Baenziger. **Characterization of the physical properties of reconstituted nicotinic acetylcholine receptor membranes by FTIR Spectroscopy.** *Biophysical Journal*, (2001) v80(1) Part 2., Pos-2424.

5. Baenziger J.E., Corrie J.B. daCosta, Andrei A. Ogrel and Harold C. Jarrell. **Protein lipid interactions at the nicotinic acetylcholine receptor.** *Biophysical Journal*, (2001) v80(1) Part 2., 718-Plat.

Non-refereed contributions

1. Corrie J.B. daCosta and Patrick T.T. Wong. **Mechanisms of the side effects of the anti-osteoporosis agent pamidronate using pressure-tuning FTIR** *(Honours Thesis)*.

2. Corrie J.B. daCosta and Patrick T.T. Wong. Poster Presentation (Fourth Year). **Mechanisms of the side effects of the anti-osteoporosis agent pamidronate using pressure-tuning FTIR** *(Honours Thesis)*.

   ***Note:** Initially we had intended to submit this work for publication. However, due to contractual obligations it was not permitted.*

EXTRA CURRICULAR:

1. Executive member of the **Biochemistry, Microbiology and Immunology Graduates Students Association (BMIGSA).** *Summer 2004 – Summer 2005.*

2. Student member of the **Faculty of Medicine Graduate Studies Committee.** *2005.*

3. Elected Executive Member of **The Science Students Association** (undergraduate) of The University of Ottawa, *1998-1999.*